Pressure Transient Analysis for Minifracs/DFIT and Waterflood Induced Fractures

By

Yawar Rizwan

in partial fulfilment of the requirements for the degree of

Master of Science

in Petroleum Engineering

at the Delft University of Technology,

to be defended publicly on Friday September 29, 2017 at 15:00 PM.

Student Number: 4515242

Supervisor: Prof. dr. Paul van den Hoek TU Delft

Thesis committee: Prof. dr. Paul van den Hoek TU Delft

Prof. dr. Denis Voskov TU Delft

Prof. dr. Mike Buxton TU Delft

TU Delft

Supervisor:

Dr. Paul van den Hoek **Senior Research Associate Reservoir Geomechanics**

P.J.vandenHoek@tudelft.nl **Dept. of Geoscience and Engineering**

TU Delft

Thesis Committee:

Dr. Paul van den Hoek **Senior Research Associate Reservoir Geomechanics**

P.J.vandenHoek@tudelft.nl **Dept. of Geoscience and Engineering**

TU Delft

Dr. Denis Voskov **Associate Professor**

D.V.Voskov@tudelft.nl **Dept. of Geoscience and Engineering**

TU Delft

Dr. Mike Buxton **Associate Professor and Head of The Resource Engineering Section**

M.W.N.Buxton@tudelft.nl **Dept. of Geoscience and Engineering**

TU Delft

CONTENTS

Acknowledgement

I would like to express my profound gratitude to my supervisor, Paul van den Hoek. His continuous guidance, assistance and review at all stages of this thesis were very vital and very much appreciated indeed. Without him , this thesis was never possible.

I would also like to thank IHS Markit ©, their technical helpdesk, providing with university license of the FEKETE software without which this work wouldn't be able to finish. In addition, will like to thank Mr. Josef Shaoul and Dr. Hans de Pater at Fenix Consulting Delft for their insights and providing with the required field data to work on. Special thanks to Dr. Paul Branagan of Paul Branagan and Associates for sharing a critical field data which otherwise wasn't available anywhere.

Finally, I would like to thank my family, friends and everyone who added value to the work described in this thesis and gave support at every step of this challenging yet exciting journey so far.

Lastly, in loving memory of Rizwanul Haque (1957-2015), my father, my greatest source of inspiration who always supported and believed in me, but sadly is no longer with me today.

List of Figures

List of Tables

Chapter 1 - Background and Motivation

1.1 Introduction & Problem Recognition

Pressure Transient Analysis (PTA) is commonly used as cheap, quick and reliable way in petroleum industry to estimate parameters such as fracture dimensions (length, height), reservoir permeability and skin of induced (hydraulic) fractures. For wells with artificial fractures, following tests are carried out depending on the requirement and life-stage of the well [(i) Injection/Fall-Off tests, (ii) Minifrac /DFIT tests (iii) Pressure Build-up tests in producer wells with propped fractures)], the fundamental ideas used in identifying different flow regimes and fracture parameters remain similar, however the physics happening during each test isn't similar. We have discussed about the above tests in chapter 3 in detail.
Up until the new methodology proposed exclusively for PTA analysis of Injection Fall-Off tests using "Storage" regime of the log-log diagnostic plot to determine fracture closure, estimate fracture dimensions [Van Den Hoek, 2016], pressure transient tests from fractured water injector wells were done similar to the methodologies used for production after stimulation (propped fracture, Pressure Build Up tests) (Cinco-Ley and Samaniego-V., 1981). Gradually, PTA interpretation methods are now well established for the limiting cases of 'low' fluid leak-off [Minifrac Analysis (MFA) and Diagnostic Fracture Injection Tests (DFIT) of stimulation hydraulic fractures] and 'high' fluid leak-off [Injection Fall-Off (IFO) analysis of waterflood-induced fractures]. However, traditional methodologies used for these two limiting cases as discussed later differ fundamentally and there exists no established approach for intermediate leak-off, in spite of many efforts to date.
Unfortunately, to date no efforts have been published to (numerically) compute the pressure transients following shut-in for a fracture that during pumping was propagating at an arbitrary, not necessarily constant velocity; and to use these computations to systematically understand the physics (type curves) of pressure decline after shut-in for both very rapidly growing and very slowly growing fractures during pumping; and to compare this with (existing or new) PTA analysis methods incorporating fracture closure

Paul van den Hoek came up with a new methodology to address the problem(Van Den Hoek, 2016; 2005). The method enabled to handle the otherwise unaddressed problem of 'fractured' injector wells for both end of the fluid leak off spectrum and associated pressure transient analysis – i.e. for DFIT tests done for very low permeability reservoirs to Minifrac (MF) tests for medium to high permeability reservoirs, up until Injection Fall-off (IFO) tests done as part of waterfloods in low to high permeability reservoirs. A coupled geomechanics simulator was developed that can compute pressure response based on post shut-in reservoir fluid flow in and around the fracture, at any given arbitrary rate and leak-off value. Based on accuracy of numerical model results, an easy to use analytical model was formulated by generalization of IFO model developed for fractured waterflood injectors (high leak-off case)(van den Hoek, 2005). Comparison of analytical results against numerical results showed good coherency for multiple field cases for all scenarios in both Before Closure Analysis (BCA) and After Closure Analysis (ACA) which lead to determination of key reservoir parameters like fracture dimensions, skin, permeability, leak-off coefficient etc.

1.2 Objective of the Work

The primary objectives of this thesis work are:

(1) Compare VdHoek (Van Den Hoek, 2016) method against 'standard method' which in our report is industry wide used well test program FEKETE for a number of hydraulic frac field cases. To identify each methods short comings and advantages. The identified advantages and disadvantages are to be highlighted and used as ready made reference for future work on the subject. Emphasis on the point that reservoir and fracture geometry, leak-off parameters etc. obtained from each of the methodologies used must be in fair agreement with each other.

(2) Summary of hydraulically fractured wells with propped fractures – Pressure Build up tests: (PTA, assumptions, typical flow regimes.)
Summary of Water flood injector wells with high leak-off - Injection Fall Off tests - (PTA, assumptions, typical flow regimes etc.)

(3) Summary of hydraulically fractured wells with low fluid leak off – MiniFrac/DFIT tests
'Standard / Conventional' approach as used in FEKETE.
- Before Closure Analysis (BCA): G – function (Nolte) method, Square root of time method, log-log diagnostic plot method. Some of the parameters obtained are Instantaneous Shut-In Pressure (ISIP), Fracture Closure Pressure (FCP), injection time, injection rate, Fluid Efficiency
- After Closure Analysis (ACA): Two main approaches used (a) Nolte approach (1997) (b) Soliman & Craig approach (2005). Some of the main parameters obtained are fracture dimensions, permeability.

(4) To serve as easy-to-use overview of commonly used existing approaches of artificial/hydraulically fractured wells for both end of spectrum – (low leak off) Minifrac /DFIT and (high leak-off) Injection Fall Off tests. Highlighting the physics involved, fundamental assumptions, and how they differ from each other subtly has been covered.

(5) Summary of the working, physics, assumptions, exhaustive validation of recently proposed (Van Den Hoek, 2016) method i.e. "unified IFO/DFIT method (Analytical and Numerical model) presented by in SPE-181593" using several hydraulic frac field cases.

(6) Brief discussion on 'Fracture Compliance Method', work by (McClure et al., 2016) for BCA analysis.

(7) Development of basic model to determine Permeability from Before Closure Analysis presented by (Lamei and Soliman, 2014). Cross check the permeability value against other existing BCA and ACA methods.

FEKETE, (owned by IHS Markit ©) a well testing software widely used for practical applications in the industry for many kinds of well tests (drawdown, buildup, injection, fall off, minifrac, slug test etc.) has been used on the other hand for comparative analysis of its performance, advantages and short comings. It represents the conventional analysis method used elsewhere too in other softwares in the industry. Some of the standard analysis techniques used are 'Tangent method on a G-function plot' used to identify Fracture Closure point and Nolte, Soliman and Craig proposed methods used for After-Closure Analysis. However the technique is not flaw proof as evident when some field well data analyzed gives erroneous analysis results and in some cases, it is not possible to make an analysis at all. Fracture Closure Point identified in FEKETE may not be closure point at all and can reflect the point where storage ends as highlighted by VdHoek method.

1.3 Methodology

(1) An extensive list of literatures was studied (bibliography)[1] and summary of conclusions was presented in the report

(2) Field cases of frac in very low permeability formation named Example no. 1,2,3 were chosen initially from the low permeability gas field. Then, Gas Research Institute/Department of Energy (U.S.A.) sponsored M-site (B sand) injection well data were analyzed. These field data were considerably clean and versatile with a mix of pump-in, shut-in (long and short duration), flowback and step rate flow. Purpose was to check robustness of the VdHoek unified approach IFO/DFIT model, identify short comings and area of improvement for future work.

(3) Discussion of analysis and results. All the field cases under (2) were analyzed using both, standard methods and method of (Van Den Hoek, 2016). Later an analysis was also done based on recently introduced method of (McClure et al., 2016). Based on the analysis and comparative study of results obtained, final conclusions were made.

(4) Implementation of Lamei and Soliman' Before Closure Model (BCA) in developing a basic working model to determine permeability (K) and cross match it against other model's permeability results.

[1] Refer Bibliography

Chapter 2 - Theory of Transient Well Testing/Pressure Transient Analysis

2.1 Introduction

During a well test, pressure response of a reservoir is monitored by changing production (or injection) rate. Pressure is location and time dependent i.e. P(r, t). Pressure response of a reservoir depends on its formation properties, hence significant reservoir properties (mainly skin factor, average permeability, location of reservoir boundaries from a general production well). For an injection well where induced fracture almost always occurs, in addition to formation properties, fracture dimensions, frac closure pressure etc. can also be estimated.
It is mainly done during the exploration phase to gauge the economic value of the reservoir, but also done during production phase to assess the change in reservoir properties over time with continuous production and/or injection. As part of the field data, well test data contributes in production and/or injector analysis predictive model. They are a convenient means to extract reservoir information, which in turn helps in creating a sound model giving more accurate estimates of production forecast and various strategies for production depending on the life stage of the well.

2.2 What is a Well Test?

Well Testing is based on the concept of sending input signals to the formation around the wellbore in the reservoir and study its response (pressure generally). The data from the output response is used to evaluate the formation condition in terms of reservoir characteristics around the wellbore.
The pressure responses versus time obtained from a well test are matched with the expected pressure response from a chosen physical model. This matching gives an estimate of reservoir parameters.

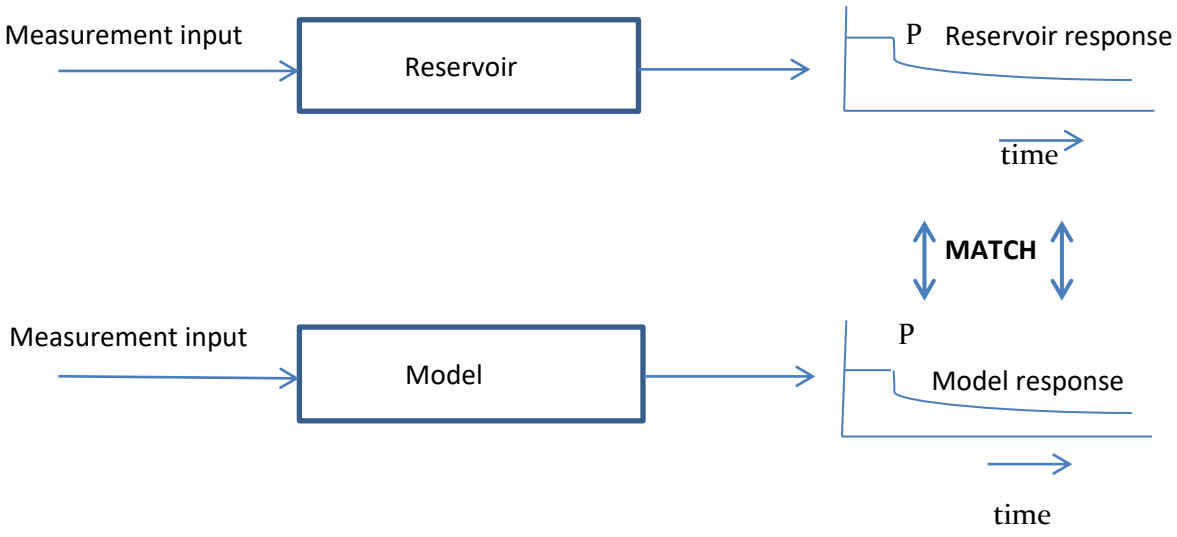

Figure 1 Method of estimating reservoir properties
(Comparing and matching the pressure response obtained from a field well test with the expected pressure response based on a physical model. 'P' is generally taken as the pressure at the top of the well)

2.3 How is it done?

To get this information, the well flow rate is varied and the variation disturbs the existing pressure in the reservoir. Measuring the change in pressure versus time in turn gives detailed reservoir and well characteristics. The pressure can be measured:

- In the well where the flow rate has been changed. Used in most cases
- From another well: Interference test's purpose

The pressure and flow rate can be measured from two locations:

1) At the top of the well i.e. at surface (p_{th})

2) At the bottom of the well (p_{bh})

The measurements are most commonly done at the surface since taking measurements at downhole conditions requires expensive downhole shut in equipment. If the measurement is taken downhole, the wellbore is no longer part of the 'input system', thereby reducing the otherwise challenging 'wellbore storage' problem. In this thesis report and accompanying research, we have considered all measurements done at surface (top of the well) unless stated otherwise.

2.4 Pressure Transient Analysis Test (PTA Test)

It can be simply defined as the measurement of *rate, time and pressure* under *controlled conditions.* PTA is very subjective to the type of tests being conducted and the associated plot changes significantly. For our study, we are only focused on PTA of artificially/hydraulically fractured wells. Accordingly, there are two type of PTA:

1) Conventional Well Tests

Tests like Drawdown, Build Up, and Hydraulic Fracture Stimulation with propped fracture (Pressure Build up tests) can be categorized in this type. It is based on conventional well test theory where fracture is "static" and closure does not occur.

2) Well Tests with closing fracture

MiniFrac Test (MF), Diagnostic Fracture Injection Test (DFIT), Injection Fall Off test (IFO) come under this category. MF and DFIT tests are done prior to the main stimulation, fracture treatment schedule to gauge the critical reservoir parameters like reservoir permeability, skin factor, wellbore storage effect, fracture storage, fracture dimensions etc. Knowledge of these parameters help in planning correct stimulation schedule, in turn providing easy and cheap method to assure that the money and resource involved applied in the stimulation is used optimally for more accurate production forecasts.

Chapter3 - Hydraulically Fractured Wells

Artificial fractures occur in the vicinity of the wellbore caused by the operation carried out in the well. It can occur in both horizontal as well as vertical planes with each having different interpretation methodologies. The first hydraulic fracture treatment was done in 1947 on a gas well by Pan American Petroleum Corporation in the Hugoton filed in Kansas, USA. Since then, hydraulic fracturing or commonly called as Fraccing has been used progressively across all oil and gas fields in world to increase productivity and field efficiency.

Fraccing process consist of the following stages: Planning and Design -> Execution -> Analysis (Pre-frac and Post-frac analysis).The design process consists of determining the fluid type, proppant type, pumping schedule, pumping rate, proppant concentration and every other parameter required to carry out the stimulation efficiently. Importance of various design parameters vary according to the geology of the field. Few key questions taken as reference while planning the frac design are: dimensions (length, width, height) of fracture, fracture propagating speed, fluid efficiency etc. Providing a good estimated input value of reservoir and fraccing parameters, an optimum stimulation can be achieved. This stimulation can be modeled with a simulator to provide wealth of information for planning future field activities.

The scenarios where artificial fractures occur are:

1) **Hydraulic Fracture Stimulation**

   (a) During Job execution: Minifrac/DFIT – This is with a closing fracture.
   Objective: To identify unknown reservoir and fracture parameters before main “propped hydraulic fracturing stimulation”.

   (b) After completion of the job: Pressure Build-Up Test - This is without a closing fracture.(Proppant used to keep the fracture open)
   Objective: To enhance reservoir overall production in cost effective method.

2) **Water flood injector well** – This is with a closing fracture.
   Objective: To maintain reservoir pressure, monitoring fracture growth, Improved oil recovery.

Well Stimulation with propped fracture requires detailed planning with considerable resource and money involved. With such high stakes, an obvious question to ask is "how do we get a preliminary idea of what should be the input values of reservoir and fraccing treatment involving minimum possible risk and costs". To exactly address this question, MiniFrac Tests or DFIT tests were introduced. Waterflood injection wells (Injection Fall-Off tests) on the other hand are mainly done for pressure maintenance of depleting reservoirs or for Improved Oil Recovery (IOR).
At depths greater than 1000 meters, the overburden stress only allows formation of vertical planes and in this work, we have only considered vertical fractures unless stated otherwise. In well test analysis, three main fracture types are commonly considered: (a) finite conductivity fractures (b) infinite conductivity fractures (c) uniform flux fracture

The research work done under this thesis highlights the current industry used methods to identify fracture closure against the recently proposed analytical method in the paper (Van Den Hoek, 2016). However before we dive into the actual problem, let us have a brief preview of What, Why and How of MiniFrac Tests

Description of the fracture: The following description / assumptions stand valid in this entire report

1) The Fracture is vertical, bi-wing, planar

2) It extends over the entire net thickness of reservoir 'h' unless stated otherwise
3) It has a symmetrical wing on each side of the wellbore with half length 'L'

3.1 (A) Propped Fractured Wells

The presence of an artificial non-closing i.e. static fracture changes the flow and in turn pressure transient response of the well significantly. It has been studied extensively over the years with some pioneering work done by H.Cinco Ley (Cinco-Ley et al.,1978, 1981,1986), (Gringarten et al., 1974). Propped fractured wells have generally finite conductivity (i.e. $F_{CD} < 300$)

3.1 Flows around a Propped Fractured Wells & Associated PTA

3.1.1. Wellbore Storage Dominated Flow

A shut-in (pressure buildup or falloff), in which the well is shut in at the surface and the wellbore contains a compressible fluid, may be distorted for a significant portion of the early response by the storage effects of the wellbore. The duration of wellbore storage effects is governed primarily by the volume of the wellbore exposed to the completed reservoir and the compressibility of the fluids contained in the wellbore. Thus, downhole shut-in for pressure buildup can reduce wellbore effects considerably. Pressure drawdown or injection transients may also result in domination of a significant portion of the transient behavior by wellbore storage distortion if the well is opened for production or injected into at the surface and the wellbore contains compressible fluids. The pressure and pressure derivative response of a system with a positive steady-state skin effect and constant wellbore storage is a single unit-slope line. Non-ideal conditions may exist in the system in which the wellbore storage cannot be characterized by a constant value. These conditions are common in wells that simultaneously produce both oil and gas and in which momentum, density and thermal effects result in afterflow and a changing liquid level in the wellbore.

3.1.2. Linear Fracture Flow

This flow exists theoretically at the beginning of the test and most of the fluid injected / produced during this flow is due to the fracture expansion. The flow is linear along the length of the fracture, and the pressure varies with $\sqrt{t}$ of time. It is of very short duration and Cinco ley observed it is almost always undetectable on the log-log diagnostic plot. (van den Hoek, 2005)(Padmakar, 2013)

3.1.3. Bilinear Flow (Finite Conductivity Fracture)

This flow was first described by Cinco Ley et al (H. Cinco-Ley et al., 1978, 1981). It is generally exhibited in the finite conductivity vertical fracture ($F_{CD} < 300$) and is not present in case of high fracture storage capacity and high conductivity fracture (F_{CD}). It occurs as a result of two simultaneous linear flow patterns:

I. Linear flow in the fracture
II. Linear flow in the reservoir

Both I and II flow perpendicular to each other. Bilinear flow exists when most of the fluid entering the wellbore comes from the formation (Cinco-Ley et al., 1978) and lasts as long as the fracture tip effects (end of the fracture) do not influence the transient behavior of the well.

Once the fluid crosses the fracture face and enters into the fracture, the fluid is conducted down the fracture to the wellbore, under essentially incompressible linear flow conditions. Flow patterns in the reservoir and fracture during the bilinear flow regime are presented in Fig.2.

Wellbore pressure transient behavior during the bilinear flow regime is expressed in dimensionless form by:

$$p_{wD} = \frac{\pi}{(\Gamma(1.25)\sqrt{2(k_f w)_D}}\ t_D^{\frac{1}{4}} \tag{1}$$

Or,

$$p_{wD} = \frac{2.45}{\sqrt{(k_f w)_D}}\ (t_D)^{\frac{1}{4}} \tag{2}$$

And in real terms, the expression for pressure drop for oil becomes:

$$\Delta p = \frac{34.97\ qB\mu}{(\ h\ (k_f w)^{\frac{1}{2}}\ (\Phi \mu c_t k)^{\frac{1}{4}}}\ (t)^{\frac{1}{4}} \tag{3}$$

And in real terms, the expression for pressure drop for gas becomes:

$$\Delta m(p) = \frac{24.57\ qT}{(\ h\ (k_f w)^{\frac{1}{2}}\ (\Phi \mu c_t k)^{\frac{1}{4}}}\ (t)^{\frac{1}{4}} \tag{4}$$

Evident from eq. (1), (2), (3), (4) the pressure behavior for the bilinear flow exhibits a straight line whose slope is equal to one fourth. From the equation of slope, fracture permeability, fracture width can be obtained subjected the reservoir parameters are known. It also suggests that the pressure change is inversely proportional to the square root of fracture conductivity and directly proportional to the fourth root of time.

Any attempt to analyze the data over this period with the conventional method of (p vs. $\sqrt{t}$ or p vs log t) will give erroneous results. (Cinco-Ley et al., 1978)

The end of the bilinear flow can be given by following equations for different range (Cinco-Ley et al, 1981):

$$t_{Debf} = \frac{0.1}{(k_f w)_D^2} \quad for\ (k_f w)_D \geq 3 \tag{5}$$

$$t_{Debf} = 0.0205\ \left[(k_f w)_D - 1.5\right]^{-1.53} \quad for\ 1.6 \leq (k_f w)_D \leq 3 \tag{6}$$

$$t_{Debf} = \left[\frac{4.55}{\sqrt{(k_f w)_D}} - 2.5\right]^{-4} \quad for\ \ (k_f w)_D \leq 1.6 \tag{7}$$

Corresponding pressure drop at the end of bilinear flow for the various fracture conductivity given above can be calculated as well from simple mathematical relation.

The transient behavior of a finite-conductivity fracture under bilinear flow is presented in Fig. 3 as a Cartesian graph of Δp versus the fourth root of time. For a finite-conductivity fracture with Fcd > 1.6, the tail of the transient data graph is concave upward. Similarly, for a fracture with a very low dimensionless fracture conductivity (Fcd < 1.6), the transient data tails off concave downward. This quick-look diagnostic feature helps to identify the conductivity range of the fracture.

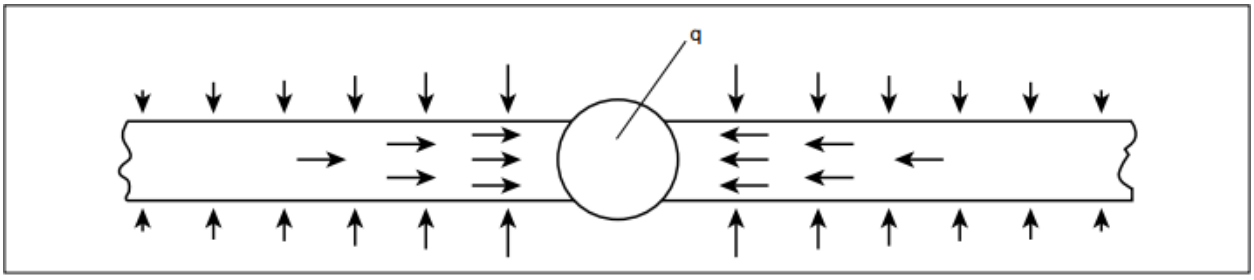

Figure 2 Bilinear flow in a finite-conductivity vertical fracture

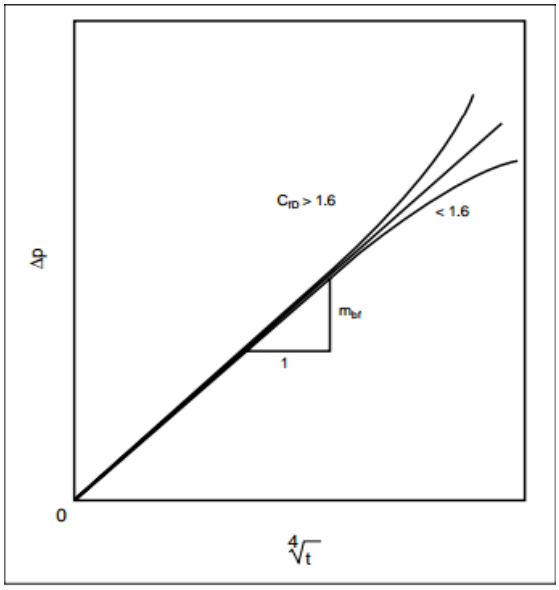

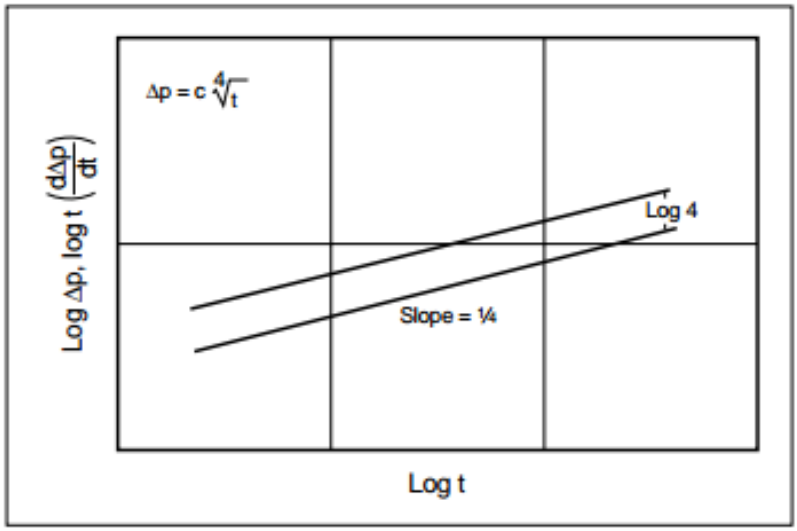

Figure 3 Cartesian graph of bilinear flow regime behavior

Figure 4 Pressure and derivative response of bilinear regime behavior flow regime in log-log coordinates.

Cinco Ley also pointed out that in some cases, straight line corresponding to bilinear flow does not pass through the origin of the coordinates possible due to following reason (Gilles_Bourdarot, 1998) (Page 219 of 342):

- Internal damage of the fracture
- Deviation from the Darcy law in the fracture (gas well)

The wellbore storage value is generally small but can very well mask the bilinear flow, making the interpretation difficult as visible in the figure.

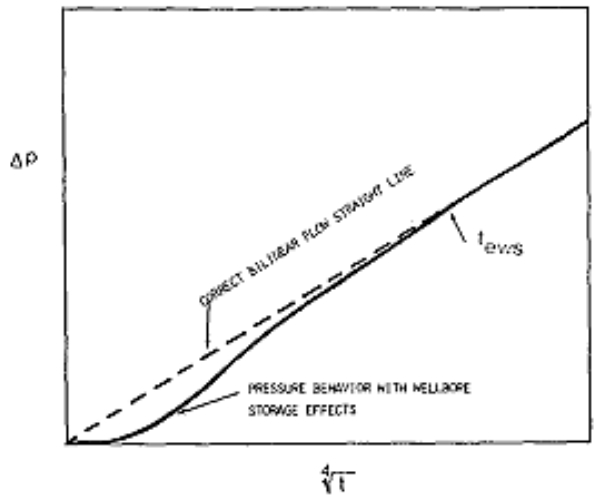

Figure 5 Wellbore storage effect on the bilinear flow on the graph

3.1.4. Formation Linear Flow Period (Infinite Conductivity Fractures or finite conductivity fractures for $t>t_{Debf}$)

This flow is almost always visible during the testing of hydraulically fractured well with propped fractures, being an integral part of conventional well test analysis. During this flow, end of the fracture propagation has reached and fracture dimensions affect the fluid flow behavior.

For finite-conductivity fractures with dimensionless fracture conductivity (F_{CD}) in excess of approximately 100, a second linear flow period may be exhibited in which the fracture conductivity is sufficiently high that the pressure loss caused by flow in the fracture is negligible. In this case, the pressure transient behavior at the well is governed by reservoir compressible linear flow normal to the plane of the fracture. This flow regime is commonly referred to as the formation linear flow regime. The wellbore pressure transient behavior of formation linear flow is governed by (Cinco-Ley et al., 1978; 1981)

In dimensionless form,

$$p_D = \sqrt{\pi t_D} \tag{8}$$

In real terms,

$$p_i - p_{wf} = \frac{qB}{2h\sqrt{\pi}} \sqrt{\frac{\mu}{\phi c_t}} \frac{\sqrt{t}}{L\sqrt{k}} \tag{9}$$

The start of the formation linear flow regime is determined, respectively, by:

$$t_{Dblf} = \frac{100}{\left(k_f w\right)_D^2} \tag{10}$$

The end of the formation linear flow regime is given by:

$$t_{Delf} = 0.016 \tag{11}$$

Equation (8), (9) are only applicable when Fracture conductivity, F_{CD} i.e. $\left(k_f w\right)_D \geq 100$ (Cinco-Ley et al., 1978)

In general, as the fracture conductivity value increases above 100, the more visible ½ characteristic slope of a linear formation flow is on the log-log plot (Gringarten et al., 1974) and other way round, the duration for bilinear flow (slope of ¼) becomes smaller and smaller when F_{CD} value increases.

The flow pattern in the reservoir for a vertical fracture under formation linear flow is presented in Fig. 6. The transient pressure behavior illustrated in Fig. 7 is in log-log coordinates with the derivative offset by the multiple of log 2. The Cartesian representation of the pressure and pressure derivative behavior is in Fig. 8, and the slope determines "L ".

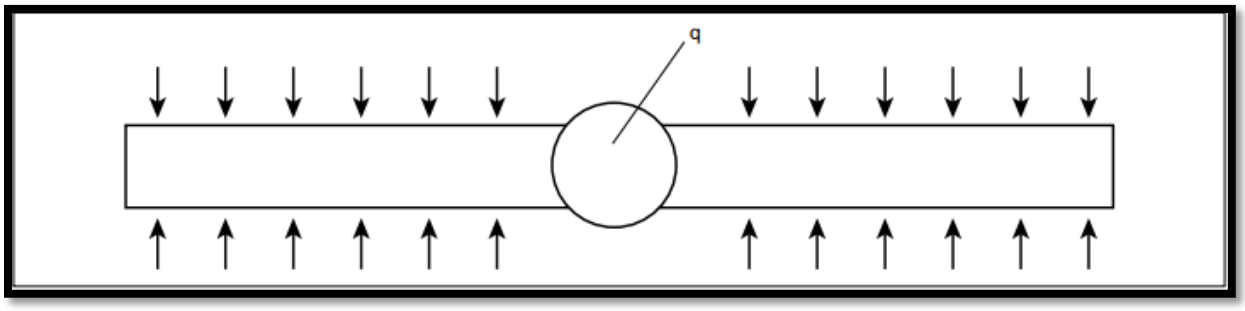

Figure 6 Formation linear flow to the plane of a finite-conductivity vertical fracture.

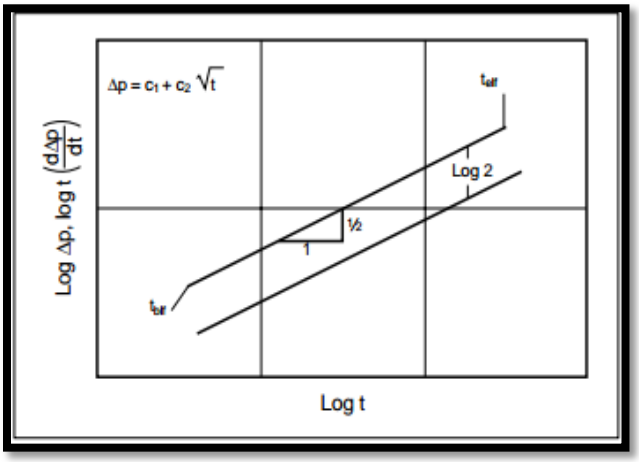

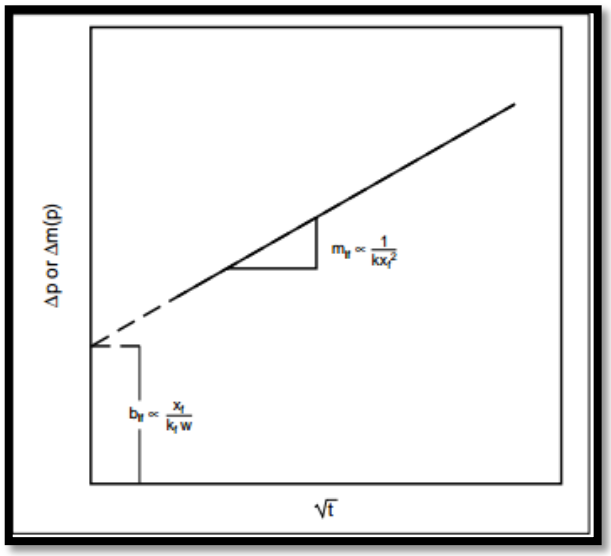

Figure 7 Pressure and derivative response of the formation linear flow regime in log-log coordinate

Figure 8 Cartesian graph of formation linear (If) behavior

3.1.5. Radial Flow

Assuming that the oil zone is of homogeneous, uniform thickness and that the oil well has drilled the entire oil zone, then after opening the well and starting up production, fluid in the reservoir will flow from the perimeter to the bottom hole along radial directions in the horizontal plane. On any horizontal plane perpendicular to the wellbore in the reservoir, the flow lines are always ray beams that converge to the wellbore from all directions; the equal pressure curves on the horizontal plane in the reservoir are all concentric circles and their center is the wellbore axis, as shown in Figure 9. Such flow is called radial flow.

The major characteristics of radial flow on type curves include that the pressure derivative curve segment is a horizontal straight line. Radial flow is a kind of typical transient flow state. As time elapses, the equal pressure curves are changing continuously, even though the flow lines are always ray beams that flow toward the bottom hole directly.

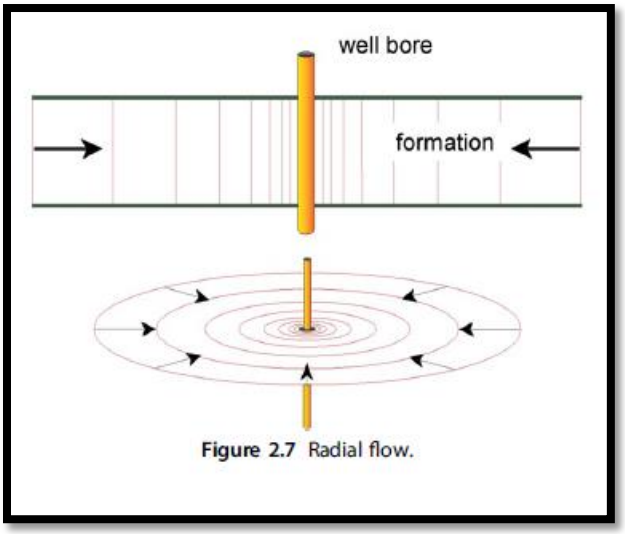

Figure 2.7 Radial flow.

Figure 9 Radial Flow in a production well

The above explanation is based on a production well. For injector well, the same process follows but in reverse order i.e. starting from wellbore storage -> fracture storage -> Bilinear flow (if it occurs) --> linear formation flow -> radial flow.

The flow is characterized by the following dimensionless pressure variations(Gilles_Bourdarot, 1998):

$$p_D = \frac{1}{2}(\ln t_D + 0.81 + 2S_f) \tag{12}$$

In real terms, the expression becomes,

$$p_i - p_{wf} = \frac{0.183qB\mu}{kh} \left(\log t + \log\frac{k}{\emptyset\mu C_t r_w^2} - 0.352 + 0.87\, S_f \right. \tag{13}$$

Where,

S_f = geometrical skin which depends on the length and conductivity of the fracture

Cinco ley gave the beginning of pseudo radial flow at(Gilles_Bourdarot, 1998):

$$t_{Dbrf} = 5\exp\left\{-0.5\left(k_f w\right)^{-0.6}\right\} \tag{14}$$

i.e. for an infinite conductivity fracture, t_{Dbrf} = 5.

An important point to note here is that the time lapse between the end of formation linear flow ($t_{Delf} = 0.016$) and beginning of radial flow, differs by factor of more than 300 indicating that a considerable transition time passes between the end of linear flow period and beginning of radial flow.

Mathieu Function Results:

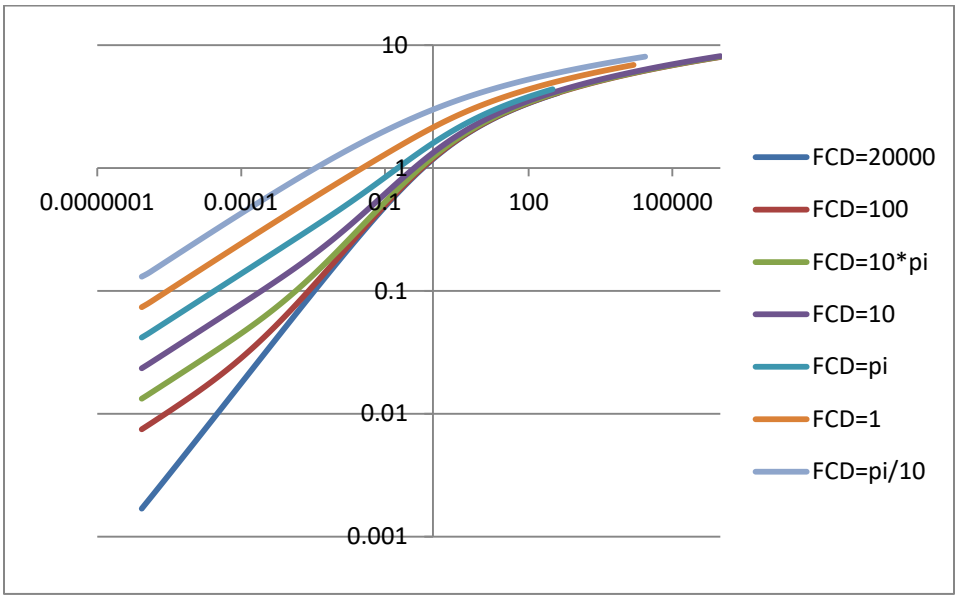

The above figure is obtained from Mathieu function results. This simple plot reiterates the discussion about the dimensionless fracture conductivity (shown here by FCD) and identification of flow regimes.

(i) For FCD>300, (here a value of FCD=20000), no bilinear flow regime exists. Linear flow regime identified by slope=1/2 is visible which translates to radial flow after the transition period.

(ii) FCD=100, the flow regime starts with a brief period of bilinear flow identified with 1/4 slope. Linear flow regime follows and then a radial flow.

(iii) It is observed that as the FCD values reduces, the linear flow regime keeps getting shorter and not visible at all from FCD=10*pi and lower values.

3.2. (B) Waterflood Injector Wells

While extensive research and development work has been done for PTA on wells with propped fractures, mainly led by H.Cinco Ley et al (Cinco-Ley et al., 1978; 1981;1986) and on other side of spectrum, equally good amount of work has been done for PTA during well stimulation (Minifrac tests) by Nolte et al ., very little work has been done for PTA on fractured water injectors. For same reason up until early last decade, PTA for Pressure Build Up tests (wells with propped fracture) methodology was used to help analyze fractured water injectors. However, some quality work has been done in past (Koning, 1988) and (Paul van den Hoek, 2005). One of the main assumptions for waterflood induced fractures is that the fracture propagation velocity during pumping is (much smaller) << fluid leak-off velocity.

One of the main physical processes which happen under IFO is:

(1) Fracture Propagation velocity (v_frac) << Fluid Propagation velocity (v_fluid)
(2) The Fluid leak-off rate is inversely proportional to the "natural log of square root of shut-in time".
(3) $Q_L = Q_{leak\text{-}off}$ (where, Q_L = rate of fluid injection; $Q_{leak\text{-}off}$ = rate of fluid leak-off from fracture face into formation)

3.2.1 Flows around Waterflood Induced Fractures & Associated PTA

The typical flow regime around fracture in a waterflood injector wells in order of appearance is shown below:

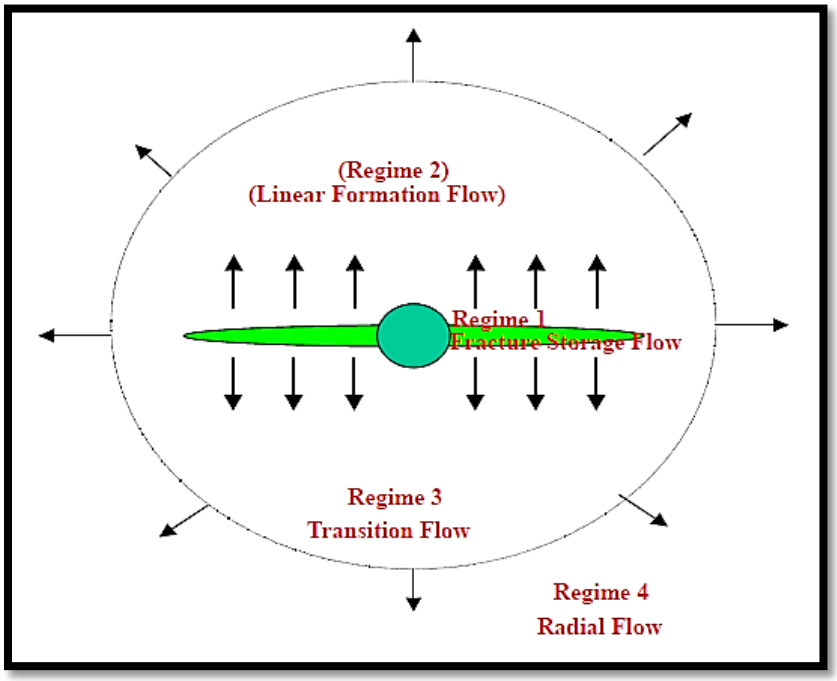

Figure 10 Flow regimes around frac during Pressure Fall-off

Different types of flows seen in standard hydraulically fractured wells were discussed under the heading of 'Propped Fractured Well'. Fracture storage flow which occurs due to the fracture closure is a new phenomenon seen here and only fracture storage flow can give information about fracture containment and in-situ stress contrasts.

From the above, one point which deserves special mention is the presence of Fracture Storage in a closing fracture. The value of Fracture Storage is much higher than of wellbore storage (Van Den Hoek, 2016) . This storage with a slope of 1 on log-log plot masks off the entire early flow period i.e. fracture linear flow, formation

linear flow which in conventional PTA analysis are critical flow regime to determine reservoir parameters. It was also shown that the same reservoir and fracture dimensions determined from the linear flow (slope=1/2) or bilinear flow period (slope=3/4) often gives erroneous results and that the best way is to determine it from the fracture closure induced flow ((Paul van den Hoek, 2005). Subsequent VdHoek model with its detailed working and the problem it solves is discussed in detail later.

Some of the key points worth highlighting are (Paul van den Hoek, 2005):

(1) There is a sudden increase in pressure and pressure derivative change on a log-log diagnostic plot which marks as easy reference to identify fracture closure point. Indicates 'Hinge' type of closure but more often the fracture closes as mix of 'hinge' followed by 'zipper' type fracture closure.

This sudden increase in pressure change following fracture closure becomes less pronounced for fractures with low dimensionless fracture compliance. This applies for long, contained fractures and/or stiff formations. Hence absence of sudden spike in pressure and derivative plot is a good indication of a long, contained induced fracture. It shouldn't be mistaken for absence of fracture.

(2) For all practical cases of pressure fall-off tests, contribution of transient flow within finite conductivity fracture can be neglected.

(3) The impact of 'true' wellbore storage on the pressure profile can be neglected for induced fracture whose length > 5 – 10 meter. But for length less than 5-10 meter, true wellbore storage dominates masking off the early transient pressure response on the log-log plot.

The fundamental differences between propped fractures and fractured water injectors can be summed up as shown in Table 1.

Table 1 Propped Fracture vs. Fractured water injectors

	Propped Fractures	Fractured Water Injectors
Type of Fracture	Static (non-shrinking)	Non-Static (non-shrinking)
Fracture Closure Occurs?	No	Yes
Proppant Used?	Yes	No
Key parameters obtained	Conductivity, Fracture Face Skin	Fracture Length and Height
Fracture Storage occurs?	No	Yes
Type of conductivity (infinite or finite?)	Finite Conductivity (F_{CD} < 300)	Infinite during injection (F_{CD} >300). Can become finite during shut-in
Fracture induced – intention or accidental?	Intentional	Mostly induced as by product of process
Type of PTA used	Pressure Build-Up type	Injection Fall-Off type
Closure Induced Flow which affects PTA?	Not observed in this case	Strongly observed in this case every time

3.2.2. Impact of Storage & Skin

We briefly mentioned about impact of storage (mainly Fracture Storage) during an IFO test. For definition and equation of wellbore, fracture and total storage, please refer to Appendix (A). Following discussion sheds more insights about it.

I. Impact of High Storage when Skin, S=0

Fig.11. When skin is not present, evident from the figure above, storage masks off the entire formation linear flow period. So after the end of storage flow regime identified by slope of 1, the transition zone is straight followed by the radial flow regime (slope = 0)

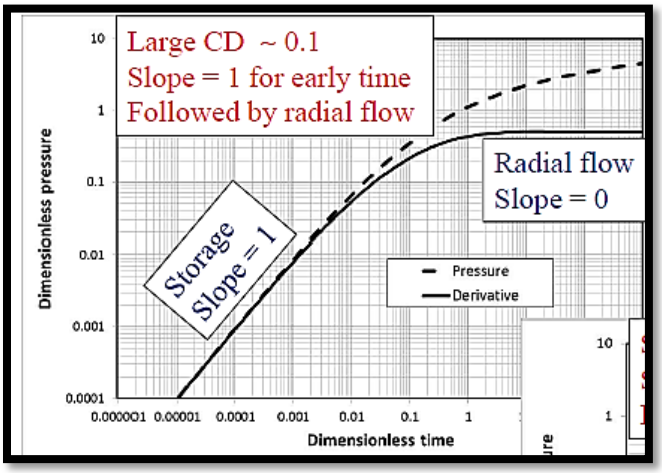

Figure 11 Case I – Impact of High Storage when skin = 0

II. Impact of low Storage when Skin, S=0

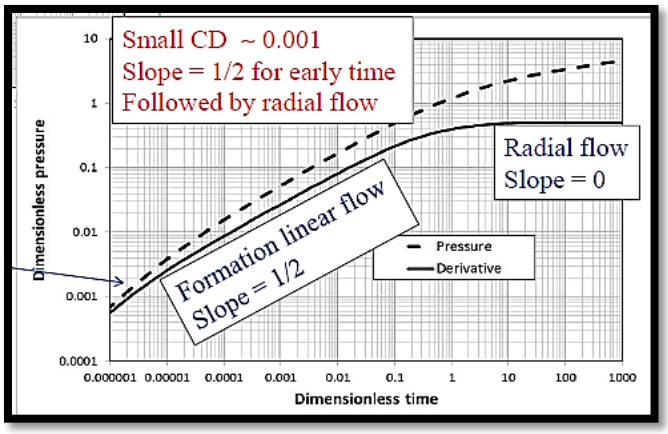

Figure 12 Case II – Impact of low storage when skin=0

Fig.12. In case of low storage, as expected the storage flow regime period ends quite early which doesn't masks off the otherwise hidden formation linear flow period. A prominent long formation linear flow period is visible before the transition period kicks in, led by radial flow.

III. Impact of Storage (High to Low values) in presence of Skin (S=2)

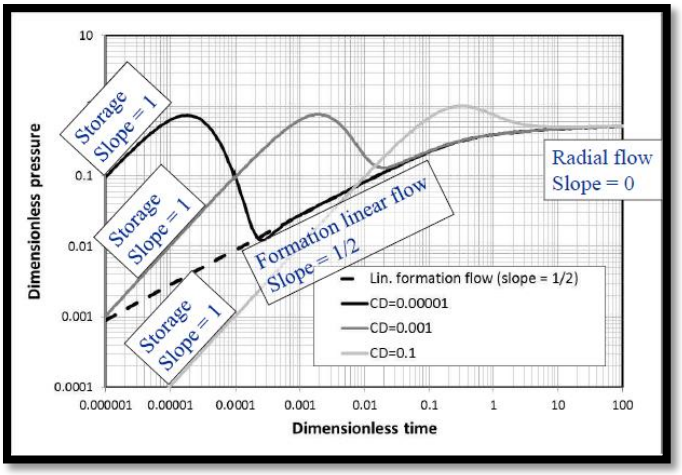

Figure 13 – Impact od Storage (High to low) with skin=2

Fig.13 shows three cases:

Case (1) **Black Line** – Low Dimensionless compliance (C_D = 0.00001) with Skin, S=2

For low value of fracture storage, the unity slope ends very early followed by a steep slope decline and then a good period of formation linear flow marked by slope=1/2. Longest formation linear flow regime zone exists of all the three cases discussed. In short, Skin effect is prominently visible.

Case (2) **Dark Grey Line** – Medium Dimensionless compliance (C_D = 0.001) with Skin, S=2

For medium value of fracture storage, the unity slope lasts much longer than for case (1) discussed above. A lesser steep slope follows it before entering a short formation linear flow period. Skin effect is still largely visible but not as much as in case (1).

Case(3) **Light Grey Line** – High Dimensionless compliance (C_D= 0.1) with Skin, S=2

For high values of dimensionless compliance, storage flow regime basically dominates the early flow period with a long storage flow regime period. Skin effect despite a value of 2 is largely masked by storage flow regime and is only visible as smooth short decline gradually entering the radial flow regime. Linear formation flow period is not visible for the case.

Conclusion: For all three cases it is evident that the formation linear flow regime (slope =1/2) is always masked in presence of fracture compliance (storage). Fracture face skin causes a drop in pressure slope after unit slope of storage with most prominent in case of low dimensionless compliance.

3.2.3. Practical Issues in Injection Fall-Off Operation and Analysis

Like every other tests conducted in a field, IFO tests have to deal with some practical challenges too. Some of the main one is:

(a) Short Shut-in time required to enable analysis of early-time (when flow is storage-dominated)

Care should be taken that the shut-in time is not very slow i.e. greater than 30 seconds. Downhole shut-in tools may be slow as well. A “slam” shut-in often leads to period of waterhammer, however analysis during and after waterhammer can still be done. In our report, a clearly observable waterhammer after shut-in was observed in various field cases like Example1,2 field data.

(b) Deciding for the “Right Choice of shut-in moment” from the pressure data

Rate and pressure data may not always be synchronized which leads to erroneous log-log pressure plot. As a general rule, pressure and derivative data have to overly each other during early time which is storage dominated flow period.

(c) Liquid Level drop during IFO in depleted reservoirs

Liquid level drop is seen as an increase in storage and mostly takes place in strongly depleted reservoir. More detail discussion about it has been done under ‘Concepts and Definition’ heading in Appendix A.

Chapter 4 Literature Review

Literature study was done with an aim to understand the underlying concepts, common analysis techniques for PTA tests on both ends of the spectrum i.e. Injection/Fall-Off tests ($t_{pump} \gg t_{shut-in}$) and Fracture Calibration tests also known as minifrac and diagnostic fracture injection tests (DFIT) ($t_{pump} \ll t_{shut-in}$), and pressure-transient tests during production after stimulation [i.e., "pressure buildup" (PBU) tests; see (Gringarten et al., 1974; Cinco-Ley et al.,1981, 1986)

SPE – 107877, 162779,169539, ARMA/USRMS 05-658 (Barree et al., 2007, 2014; Ewens et al., 2012)

For minifrac tests, Nolte (1979) presented his pioneer work in determining the closure pressure under Carter Leak-off assumption. This formed the basis for introduction of now popular G-time function, which has dominated the analysis for years now. Difficulties in selecting departure from straight line which marks fracture closure pressure in a plot of Pressure vs. G time is addressed in the work of Barree and Mukherjee(1996). In their work, special derivative functions were introduced to overcome the subjectiveness of picking the fracture closure pressure. The normal derivative of pressure (dP/dG), the semi-log derivative of pressure with respect to G-function (G*dP/dG), along with the usual pressure plot of pressure vs. G time constitute a combination plot which has been widely used in the industry and forms part of "standard text-book methodologies" to identify fracture closure point. They also gave possible explanation for the challenges associated with various fracture geometries such as presence of natural fractures, fissures and leak-off dependency to stress. For After-Closure analysis (ACA), in addition to Nolte's technique, (Soliman et al., 2005) presented their ACA technique which was based on "constant rate injection and fall-off sequence" and unlike Nolte approach (based on "impulse injection"), considers the finite injection period along with the shut-in period. The ACA technique helps to estimate reservoir permeability, reservoir pressure and flow regimes with fair accuracy evident from numerous case studies.

(Barree et al., 2007) presented a holistic fracture diagnostic approach where other types of fracture geometries such as fracture tip extension, height recession etc. during the shut-in period were discussed. The shape of the various curves in the combination plot vs. G time gives insight about fracture geometry and leak-offs. In addition to G-function derived pressure plot, square root of time plot and a log-log plot were also used in conjunction to validate the results.

SPE-7490 (Cinco-Ley and Samaniego-V., 1981)

For PTA during production after stimulation (Pressure Build Up), Cinco Ley et al proposed a new interpretation technique for early time pressure data based on "bilinear flow theory" which considers transient linear flow in both formation and the fracture, mutually perpendicular to each other. This flow type was a new addition to pre-identified fracture linear flow, formation linear flow and radial flow. He underlined the difference between an infinite conductivity fracture ($F_{CD} > 300$) and finite conductivity fractures stating all such cases with long or poorly conductive fractures must be analyzed by considering a finite conductivity fracture model. Further work in this area was done by (Gringarten et al., 1974)(Wong et al., 1986)

SPE-179725,170956 (McClure et al., 2014,2016)

McClure et al challenged the existing standard methodology used and advocated by many in the industry. He stated that the concave up or down behavior of semi-log derivative of G-function can be explained in simpler way than using complicated processes like height recession or transverse storage etc. (Barree et al., 2007) in his holistic approach considers Compliance is considered constant but McClure pointed out that these interpretations neglect changing fracture compliance during closure. A curve of G*dP/dG that constantly

increases during the shut-in period may be caused by wellbore storage rather than the "fracture tip extension". The specific shape of the G*dP/dG curve is controlled by factors that affect fracture compliance before and after closure. These factors include fracture height, fracture stiffness and the residual aperture.

In all cases, as long as a single planar fracture has formed, the best pick for minimum principal stress is at the deviation from linearity on the G*dP/dG plot whether or not this departure is concave up or concave down. Closure pick via tangent method (Barree et al., 2007, Castillo, n.d) may significantly underestimate the minimum principal stress. The fact that an extremely sharp upward trend in G*dP/dG is generally not observed in DFIT tests suggest the actual geometry of the created fracture is rougher and more complex than is typically assumed by standard models.

SPE-181593 (Van Den Hoek, 2016)

On the other end of the leak-off spectrum, PTA from fractured water injection wells [called "Injection Fall-Off tests"] was done using methodologies built for Pressure Build Up tests until (van den Hoek, 2005; Van den Hoek et al., 2012) came up with a dedicated method using "storage" of the closing fracture to estimate the fracture dimensions, interpret and analyze an IFO tests, which is now routinely used as part of "injector surveillance". In recent years, several groups have attempted to extend PTA methodologies to be used for minifrac analysis involving mix of G-concept + specialized PTA derivative concepts as developed by Bourdet and Agarwal in 80's(Bourdet et al., 1989). No efforts before Paul's paper were made to numerically compute the pressure transients following shut-in when during pumping the fracture propagated at a random, not necessarily a constant velocity. The type curves obtained were then used to systematically understand the physics of very fast and very slow propagating fractures, thus covering both limits of the fracture propagation mode.

To achieve the objective, a coupled geomechanics- reservoir simulator was developed which captured the pressure response during injection and after shut-in. The growing fracture was modeled as moving reservoir boundary with "fracture growth rate and leak-off rate" given as "user input" to avoid the otherwise tedious problem of modeling fracture propagation phenomenon. Simple bi-wing fracture which was created during one preceding injection cycle with constant injection rate in one formation layer were the basic assumptions. Fracture growth rate was given by fracture propagating Power Law with Carter leak-off assumptions.

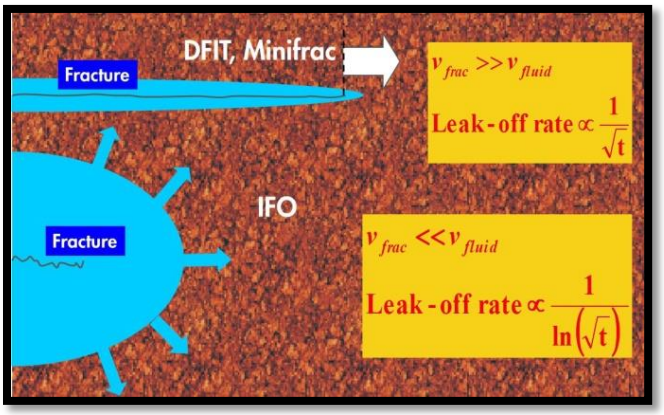

Figure 14 Different leak-off regimes around the fracture

Main findings were:

Fracture Compliance is several orders of magnitude higher than wellbore compliance and dominates the early pressure transient after shut-in. Wellbore compliance only starts once fracture compliance period is over.

Early time pressure and derivative curves is linear with time (with slope of 1 on log-log plot) irrespective of pumping durations, hence the early time period is independent of the test type. In presence of moderate storage and skin, formation linear flow period is almost masked by the storage flow period.

The next section discussed about the type curve behavior and associated physics for a hinge type vs. zipper type fracture closure method. The plots associated with hinge closure is almost never seen in real field data; rather plots which can be associated with a mix of hinge vs. zipper having moderate compliance and skin closure mechanism are seen. Some authors also call this mode of fracture closure mechanism as Progressive Fracture Closure. p_D^0 is a dimensionless pressure value at which zipper closure starts. Higher value of p_D^0 is associated with higher net pressure, in turn implying wide fracture tip area which takes longer time for hinge closure. For fractures with medium to high residual conductivity, there is a sharp increase in pressure derivative with fracture closure which can be explained by reducing stiffness with length recession while the fracture leak-off surface remaining almost constant. However, for low residual conductivity fractures where fracture leak-off surface also reduces, the derivative follows simpler, normal curve similar to plots obtained from field data. Possible explanation is the reducing fracture stiffness due to length recession is more or less compensated by a decreasing fracture leak-off surface area. The net result of this effect is that even though fracture is closing, it will be invisible on the pressure decline plot, hence end of storage-dominated flow period doesn't necessarily marks end of fracture closure.

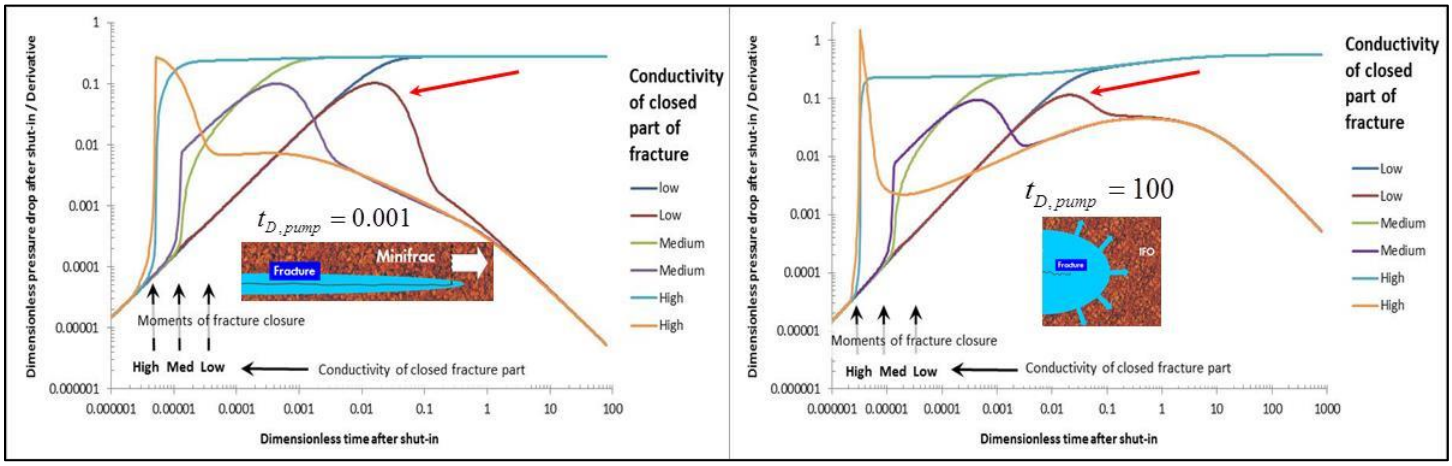

Figure 15 Computed pressure decline curves and corresponding derivatives for a *propagating* fracture during pumping, which closes after shut-in. Shown are 'zipper-closure' cases with low/mid/high conductivity of the residual (closed part of the) fracture.

Black vertical arrows indicate the time of complete fracture closure; red arrows indicate the type of derivative curve ("smooth") that we generally observe in the field. Fracture with "moderate" dimensionless fracture compliance C_{fD} of 0.07 and skin S of 0.2.

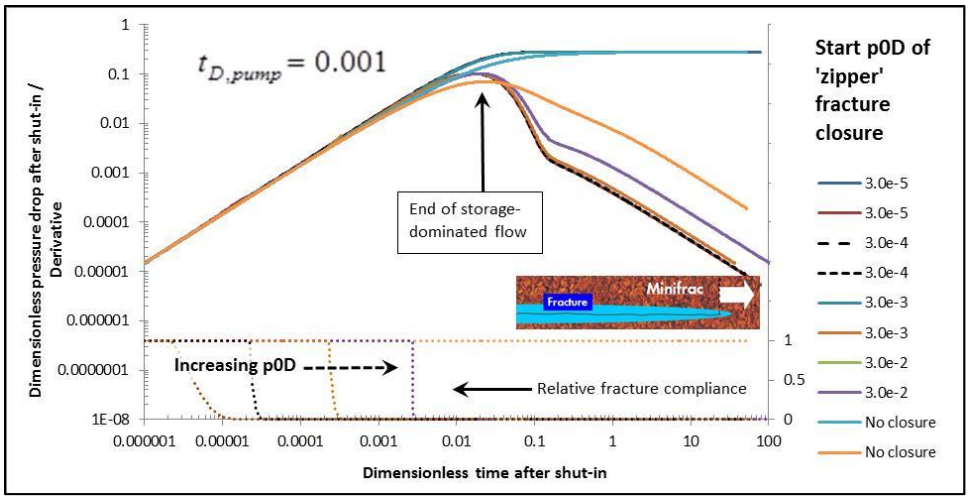

Figure 16 Computed pressure decline curves and corresponding derivatives for a *propagating* fracture during pumping, which closes after shut-in. Shown is a mixture of 'hinge-closure' and 'zipper-closure' [see Eq. (6)], in which the pressure p_D^o at which zipper closure starts is varied.

The process of fracture closure is indicated by the relative fracture compliance curves (1=fully open, 0=fully closed). Fracture with "moderate" dimensionless fracture compliance C_{fD} of 0.07 and skin S of 0.2. Low conductivity of residual fracture.

For IFO analysis as part of waterflood operations, a simple IFO model was proposed by VdHoek (2005) based on an approximate solution to the elliptical diffusivity equation for transient fluid flow around a static hydraulic fracture. Such a model is valid to use here since in waterfloods, fracture propagates very slowly. A suitable generalization to incorporate minifrac, DFIT (where shut-in time is equal or bigger than the injection times) was made by using Duhamel's superposition principle using constant terminal rate solution p_{CR}. The resulting modified analytical solution was compared against numerical model and other conventional standard method like G-function analysis. Results were similar between numerical and analytical model while superior in some cases to G-functions. It was also demonstrated that 'Agarwal time' function can be used correctly to identify correct flow regime only if a correct radial reservoir flow has developed, which often isn't developed in short dimensionless pump times.

At end, three field examples of three different leak-off types (very low leak-off for gas well, moderate leak-off for frac-packing of oil well (minifrac, DFIT) and high leak-off for water flood induced fracturing) was analyzed with the generalized IFO methodology highlighting its simplicity and generality.

Chapter 5- Results and Discussions

This section is arranged as follows for each field data analyzed:

Brief introduction about the field (critical information, geology etc.) ---> followed by Before Closure Analysis (also known as Pre-Closure Analysis/Diagnostics) of the results. BCA analysis is done using G-function plot, Square root of time plot and log-log delta pressure and derivative plots. (Please refer to Appendix D for brief summary of these topics) ---> Then comparative After-Closure Analysis of Nolte approach vs. Soliman-Craig approach is done. The BCA and ACA analysis were done using well testing software FEKETE which follows standard interpretation method used in industry. ---> The discussion then moves to the results obtained from VdHoek's IFO analytical model ---> Later, comparison between IFO model vs. FEKETE in form of table and brief discussion is shown ---> Finally, the summary of above analyses is discussed in Conclusion section.

The datasets taken to achieve the objectives of this work comprised a variety of Hydraulic Fracturing tests for example, pump-in- shut-in; pump-in-flowback, step-rate tests etc. Purpose of choosing different kind of tests was to demonstrate the working robustness of FEKETE and IFO model.

Few important points for considerations:

(1) Field data were chosen to validate VdHoek's analytical model's robustness in handling both ends of injection/shut-in periods and associated physical mechanisms i.e. (Injection/Fall-Off to Mini-Frac/DFIT tests).

Example 1, 2, 3, (2B, 5B, 6B – from M-site injection) = Minifrac/ DFIT tests

NIMR field data, BP field data = Injection/ Fall-Off tests

(1) To calculate the reservoir fluid properties, following correlations, equations of state are used as 'default' in FEKETE unless changed otherwise:

(i) P.V.T Correlation = Benedict-Webb-Rubin table

(ii) Viscosity Correlation= Carr et al correlation

(2) Some of the parameter values used as input in IFO model such as (t_{inj}), Total Compressibility (c_t) etc. are automatically calculated as output parameters in FEKETE model, but it is worth mentioning that the values obtained from both bear close resemblance in magnitude with each other.

(3) For gas reservoir fluids, pressure (p) is replaced with Pseudopressure (Ψ) and time with pseudo/adjusted time (t_a). For reading convenience in discussion of field data from gas-reservoir fluids, pseudo-pressure is written as 'pressure' unless stated otherwise.

(i) Pseudo-pressure is a mathematical pressure function that accounts for the variable compressibility and viscosity of gas with respect to pressure.

(ii) Pseudo-time t_a is a mathematical time function that accounts for the variable compressibility (c_t) and viscosity (μ_g) of gas, as well as the variable total (formation) porosity ($\emptyset$) with respect to time and pressure.

The equation for the flow of gas in the reservoir is very similar to that of liquid flow. In particular, four assumptions are very important: (1) Total system compressibility c_t is constant (2) Gas viscosity μ_g is constant (3) Total porosity ($\emptyset$) is constant (4) Fluid saturation (S_w andS_g) is constant, if S_{wi} (initial water saturation) is not equal to 0.

For liquids, these assumptions are reasonable, since liquid compressibility and viscosity do not vary significantly with pressure but for gas, the assumptions listed above are no longer valid, since gas compressibility (c_g) and thus the gas compressibility factor (z) can vary significantly with pressure. To deal with these changing gas properties, the concept of pseudo-pressure (Ψ) was developed by Al-Hussainy et al. (1966).

(4) The pressure derivative, $t\frac{dP}{dt}$ used in log-log plot of vanden Hoek model and semi-log derivative represented in FEKETE $\Delta t\frac{dP}{d\Delta t}$ are same. The parameter, t = Δt = shut-in time in both cases.

(5) Example 1, 2, 3 data set was provided by FenixConsulting © from different gas formations in Europe. Example 2 and 3 comes from same reservoir field. Except the must-have input parameter to carry out the analysis provided by them, very little information was available about field geology and reservoir due to the confidentiality agreement.

(6) A tolerance range of 10-15 % is accepted when matching "output parameter" values derived from different techniques, models except for pressure where a 10% deviation can be quite high.

(7) The delta time (Δt) and closure time (t_c) are calculated differently in FEKETE.

(a) t_c: Closure time. Calculated from the time the fluid starts propagating into the formation (where the red line marking "Start of Injection" is placed) to the point where closure is believed to have happened.

(b) Δt: shut-in time. Calculated from ISIP point to the point where closure is believed to have happened.

5.1 - Example 1: Low Permeability, Gas Well

This data set comes from a vertical well at perforation depth of 3692 m TVDSS from a Gas-Condensate reservoir. Brine was used as injection fluid. The formation height is bounded by impermeable shale layers above and below. The pressure gauge recorded data every second providing better information about the associated pressure transient during analysis.

Injection History

Fig. 17 is a plot of bottomhole pressure (bar) on primary axis, injection rate (slurry flow rate) on secondary y-axis against the time (seconds) on x-axis representing the complete pump-in/shut-in history of the field data set named "Example 1". The first spike in pressure colored with green is noted without any significant injection rate. This period is associated with the time when the pre-test pressure equipment testing is conducted and they do not contribute to any real data. Following this, two short periods of injection followed by shut-in period was observed shown in Table 2

Table 2 Pump-in and shut-in period details - Example 1

Period	Starts at (sec)	Ends at (sec)	Pump-in (seconds)
1st Period (Pump-in)	560	1000	440 = (7.3 minutes)
1st Period (Shut-in)	1000	4000	3000 = (50 minutes)
2nd Period (Pump-in)	4000	4475	475 = (7.9 minutes)
2nd Period (Shut-in)	4476	7393	2917 = (48.6 minutes)

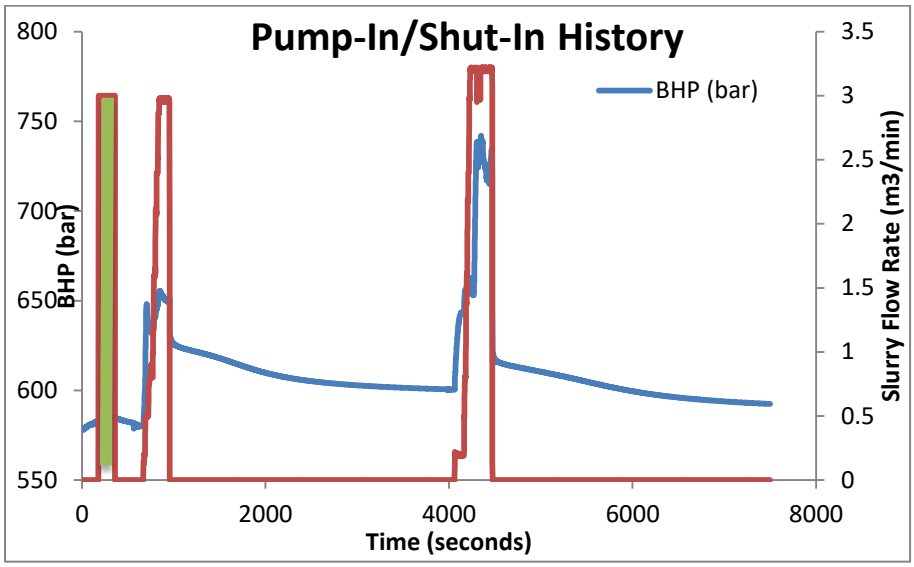

Figure 17 Injection/Shut-in History for Example 1 field data

Fig.18 is a plot of pressure [bar] against shut-in time showing there was a clear water hammer period right after shut-in time , which resulted in distorting early pressure data (identified by the area within green circle). Shut-in point for both FEKETE (Fig.20) and VdHoek model analysis (fig. 18) was taken at the point when water hammer period ended. The pressure and slurry flow rate data for both the period was clean, with short injection period and a longer shut-in time.

Care should be taken while identifying the shut-in point since it directly affects the pressure difference curve ($\Delta P = P_{shut-in} - P_{fo}$) where $P_{fo} = pressure\ after\ shut - in(fall\ off period$).Incorrect identification of shut-in moment leads to erroneous pressure difference curve in the log-log diagnostic plot which affects flow regime identification, closure point etc. which in turn affects the estimated reservoir parameters values.

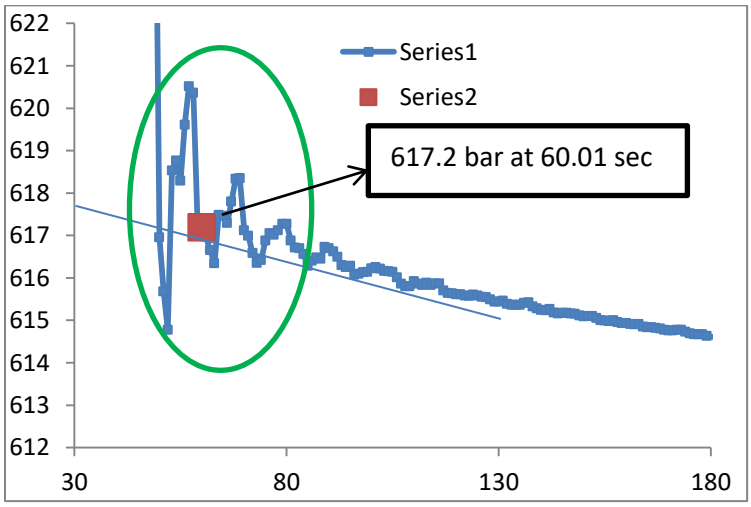

Figure 18 Water Hammer during early shut-in time – Example 1

Although the point of shut-in in both is roughly same, corresponding pressure values are different. This is because in FEKETE, pressure adjustment was calculated and adjusted in the data to account for the difference between "gauge depth=3368.3 m" and datum depth=3692 m using a fluid gradient of 10 kPa (a)/m (brine water). The net adjusted pressure was 3237 kPa (a).

Analysis using FEKETE:

Second period of pump-in and shut-in was chosen for analysis.

Table 3 Input parameters for FEKETE – Example 1

Parameters	Values	Unit
Initial Reservoir Pressure (P_i)	60500	KPa (a)(a)
Reservoir Temperature	108	°C
Net Pay/ Height of Formation	45	m
Wellbore Radius	0.107	m
Porosity	17	%
Initial Gas Saturation	68	%
Initial Water Saturation	32	%

With the aid of 'inbuilt correlations selected as *default*' in FEKETE for calculating other reservoir fluid parameters, a list of necessary parameters is obtained mentioned in Table 4.

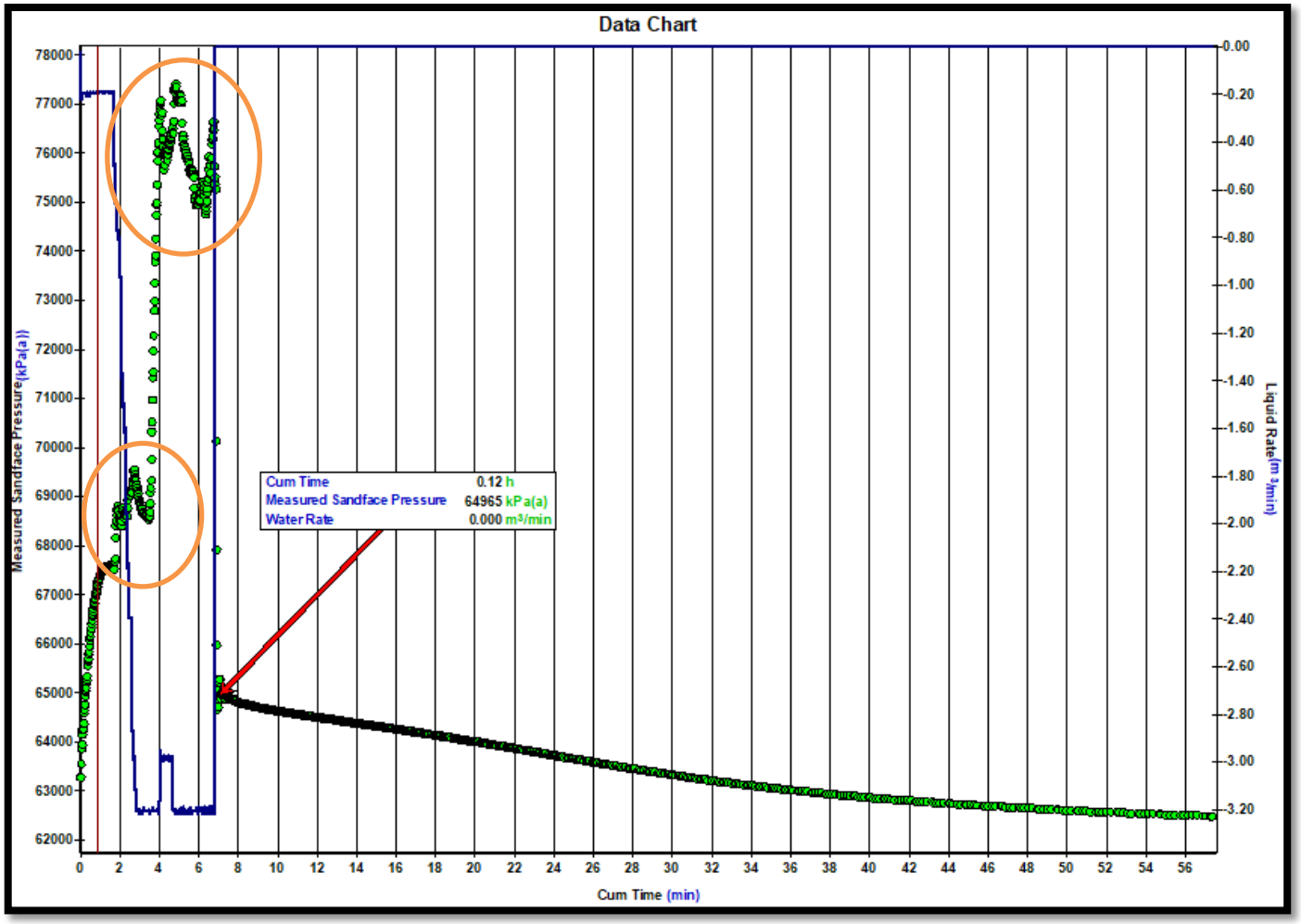

Figure.19 Injection/Shut-In details for period 2 – Example 1

Fig. 19 is a plot of measured bottomhole pressure (kPa (a)) (on primary y-axis) and injection rate (m^3/min) (on the secondary y-axis) against the time (x-axis) showing the pump-in/shut-in history of period 2. The red vertical line in the above plot marks the start of actual injection into the formation at time 0.9 minutes. Volume injected before it was used in filling wellbore volume giving rise to the wellbore storage. The red arrow annotation in fig.19 shows the point of instantaneous shut-in pressure (zoomed version is fig.20). The analyzed portion of the minifrac test consisted of 14.801 m^3 of brine water, applied at average injection rate of -3 to -3.2m^3/minutes Three occasions of sharp pressure drop is observed (shown by orange circles) which shows formation breakdown. The first break down for period 2 of pump-in/shut-in was established at approximate injection rate of -2.4 m^3/min at measured sandface pressure (bottomhole pressure) of ~69541 kPa (a)(a), following stable fracture propagation period with approx. injection rate of -3.2 m^3/minutes The last two pressure drop occurred (between 4-7 minutes) during the stable fracture propagation rate. The well was then shut-in to monitor pressure fall-off.

Table 4 Value of calculated parameters from FEKETE – Example 1

	Parameters	**Values**	**Unit**
	Separator Gas Gravity	0.650	
Critical Properties	**Critical Temperature**	206.3	K
	Critical Pressure	4603.7	KPa (a) (a)
Properties at Initial conditions	**Gas Compressibility Factor (Deviation Factor)**	1.307	---
	Gas Formation Volume Factor (B_{gl})	2.89e-03	$m^{3/}$ m^3
	Gas Compressibility (Z_I)	7.43e-06	1/kPa (a)
	Gas Viscosity (μ_{gl})	0.0330	mPa.s
	Gas Density (ρ_{gl})	275.1	Kg/m^3
	Formation Compressibility (c_{fl})	5.66e-07	1/kPa (a)
	Initial Total Compressibility (c_{tl})	5.75e-06	1/kPa (a)

(A) Before Closure Analysis (Pre-Closure Analysis):

Total injection time (t_{inj}) (also called as pumping time t_{pump}) is 6.22 minutes with an injected volume of 14.801 m^3. Previously mentioned total pump time for 2nd period as mentioned in table is 7.91 minutes. The difference of 1.85 min can be attributed to the wellbore filling time.

Fig.20 is a Cartesian plot of pressure (kPa (a)) vs. time (minutes). Instantaneous shut-in pressure occurred at 64965 kPa (a), identified by placing a straight line on the early fall off portion of the fall data. After shut-in the friction decreases rapidly which appears to cause a steep drop in pressure (noticed as a brief linear trend in the data) in Fig 20. ISIP (marked by green circle) was chosen few pressure points later once the shut-in pressure stabilized. This point is basically the final injection point after adjusting the shut-in induced frictional pressure losses.

The “expected" shut-in point would be just at the start of stabilized fall-off pressure and not some time later, however doing so was leading to incorrect pressure difference curve where the initial storage flow of unity slope was not matching for pressure difference and derivative curve. This is a good example to demonstrate that care

should be taken while identifying the correct shut-in point because ISIP point directly affects the pressure difference curve in a log-log plot.

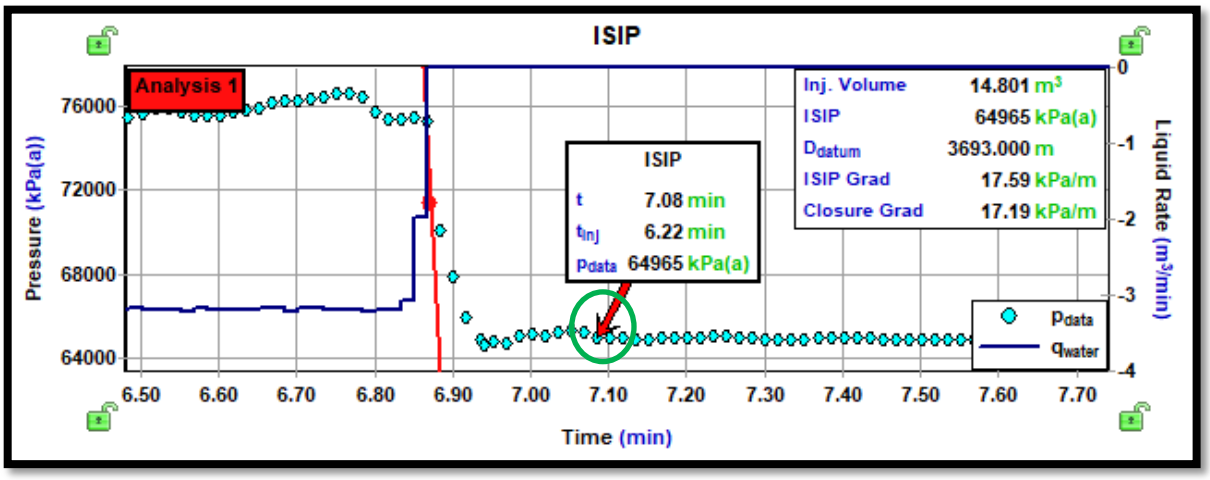

Figure 20 ISIP plot – Example 1

Figure 21 is a plot of Derivative (G*dP/dG) (primary y-axis), pressure (P) and first derivative (dP/dG) on secondary y-axis against G-function time. After a very brief period of short linear increase of the semi-log pressure derivative against G-time (please refer Appendix D for definition), a mild bend can be noticed followed by another long linear line until G-time=3 (it can also be viewed as going concave-up after the linear trend until G-time =0.8). Few concepts as proposed by respective authors explaining the physics behind are discussed below, however it must be noted that all these explanations are speculative and never quantified for this field data given the limited field information available:

(i) Barree et al proposed idea of Transverse Storage and Height Recession discussed in (i) and (ii).

At shut-in there is large volume of fluid stored in the fracture (V_{inj} = 14.801 m^3) relative to the expected surface area of the fracture for a normal planar bi-wing fracture model. Leak-off rate relative to the stored volume must be small; hence rate of pressure decline is likewise small. It is visible from the relation $\frac{dP}{dt} = -\frac{q_{leakoff}}{(c_f.V_{wl}+\frac{A}{S_f})}$ - (McClure et al., 2016) (where fracture compliance C_f expressed here as A/S_f can also be expressed for elliptical shape fracture model as proposed by (van den Hoek, 2005,2016). Please refer Appendix (B), (C)

It was noted from the injection/shut-in history plot Fig.19 that possible natural secondary fractures, fissures were encountered during fracture propagation period (in orange circle). Possible explanation is a secondary fracture set was opened when the fluid injection pressure exceeded the critical fissure-opening pressure. As the secondary fracture dilates, it creates a storage volume for fluid which is taken from the primary hydraulic fractures. While the fracture storage volume increases, the leak-off rate can also be accelerated; this acts as a quick indication of the formation's permeability. Fig21 shows the pressure decline rate decreases which give a first indication that it was low permeability reservoir.

At shut-in the secondary fractures will close before the primary fractures because they are held open against a stress higher than the minimum in-site horizontal stress. As they close, fluid will be expelled from the additionally created storage volume back into the main fracture decreasing the normal rate of pressure decline (shown roughly between G-time= 0-1). Once the fluids are back in main fracture, they have less storage area leading to relatively higher rate of leak-off. The end of storage period is

followed by a constant area, constant matrix permeability dominated leak-off as evident by the linear slope which starts at G-time~3.

(ii) The other possible and equally valid explanation can be that leak-off occurs only through a thin permeable bed and that the fracture extends in height to cover impermeable strata with no leak off (shale layer). At shut-in, there is a large volume of fluid stored in the fracture and the leak-off rate relative to the stored volume is small, hence the rate of pressure decline is likewise small. The energy which otherwise is dissipated due to normal leak off is mostly conserved here due to the low leak-off rate. This facilitates a higher fracture propagation energy (net pressure = 1486 kPa (a)) to penetrate the impermeable shales. As the fracture empties gradually, the fracture face opened in impermeable shales is closed first. Afterwards, normal leak-off occurs with accelerated rate in the formation height and pressure declines more rapidly until the fracture closes completely. This phenomenon is commonly called as "Height Recession".

The discussed physical phenomena in (i) and (ii) require excess stored volume of fluid at shut-in that must be leaked off to reach fracture closure than what is generally expected for a normal bi-wing constant height fracture.

(iii) The third explanation came from Mark W.McClure. He presented the Fracture-Compliance method, a technique for estimating the closure pressure from diagnostic fracture injection tests (DFIT's) assuming variable fracture compliance. The method is based on the observation that fracture retains finite aperture after asperities come into contact (mechanical closure).His main idea was "fracture closure increases fracture stiffness (reducing storage/compliance), which in low-permeability formations leads to increase in the pressure derivative". On basis of these findings, he proposed the method which consists of picking closure at the first point of deviation from linearity on a plot of pressure or G x dP/dG vs. G-time (after the end of the very-early transient associated with wellbore and near-wellbore friction and fracture tip extension).

A.1. - G-function analysis:

Fig21. The characteristic G-function derivative signature is a "belly" below the diagnostic straight line (cyan color) through the origin and tangent to the semi-log derivative of P vs. G at the point of fracture closure. It indicates that fracture closure occurred after 20.4 minutes of the shut-in time at a fracture closure pressure of 63479 kPa (a). It is also worth noting that a small period of (Δt= 0.34 – 0.29= 0.05 hrs. = 3 minutes) normal leak-off follows the storage related leak-off.

The value of fracture closure pressure and time ($P_c and\ t_c$) was obtained using standard "Tangent method" in a G-function plot which states that an ideal DFIT with normal leak-off has a G*dP/dG curve that is a straight line until closure, at which time the curve bends, decreasing in slope; eventually the curve crests then turns downwards.

Net Pressure value (ISIP – FCP) is 1486 kPa (a), a measure of total reserve energy available with the fracture, above the closure pressure to facilitate its propagation. The magnitude is fairly high, giving more energy for the fracture to propagate farther in low permeability surroundings.

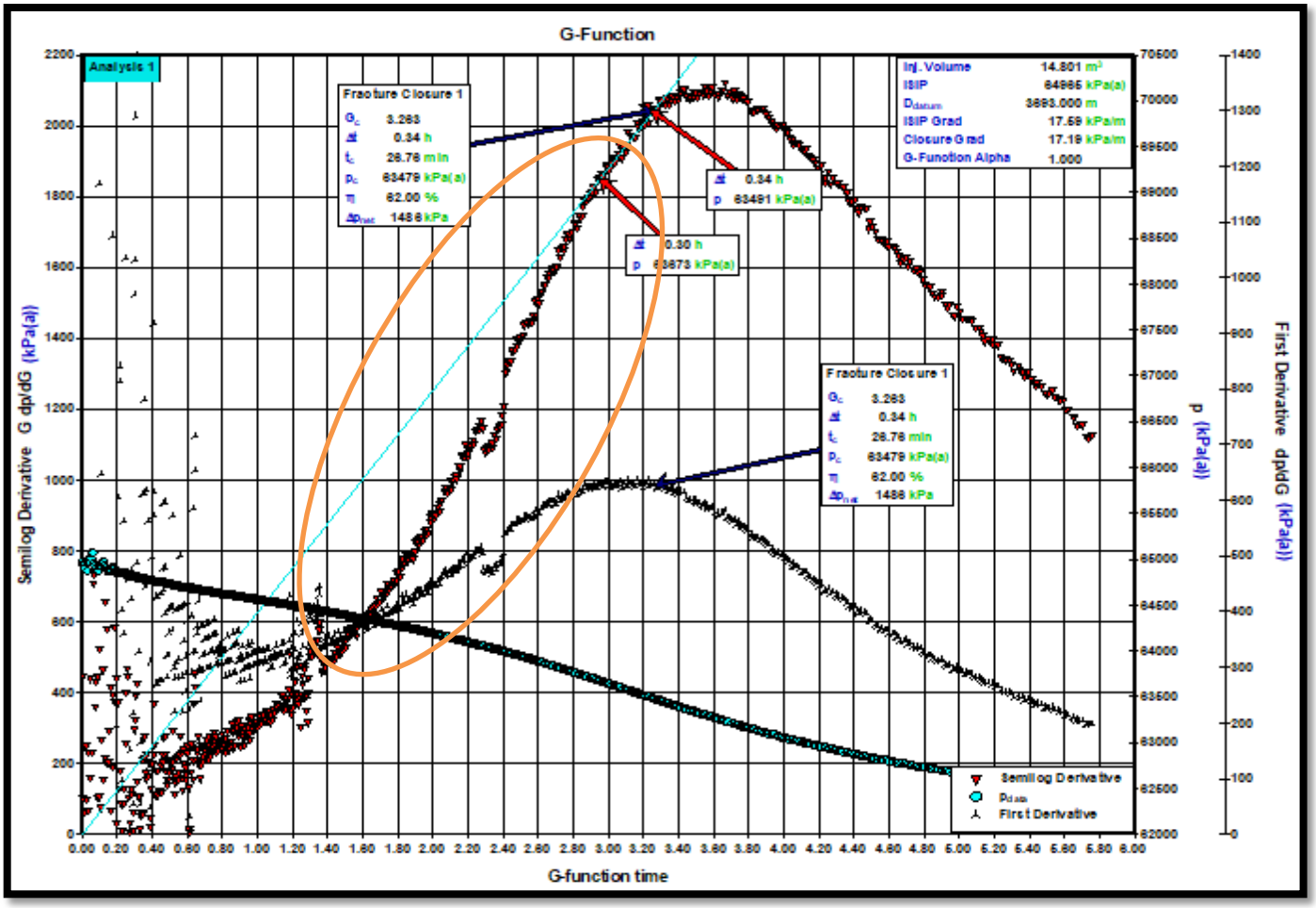

Figure 21 Pressure, First derivative and semi-log derivative of G-function curve against G-time – Example 1

A.2. - Sqrt(t) Analysis:

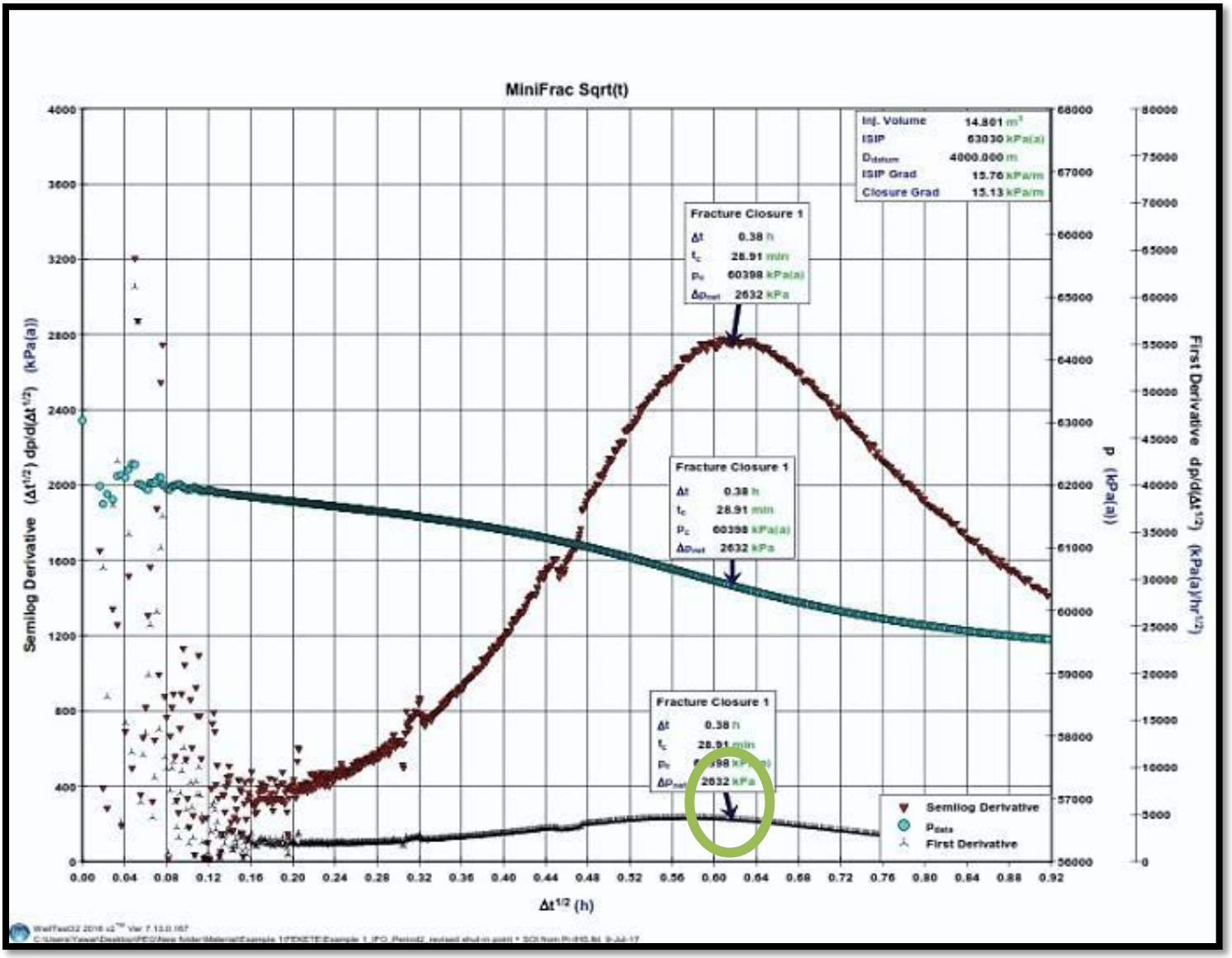

Figure 22 Pressure, First derivative and semi-log derivative of Sqrt(t) function curve against Square root of time – Example 1

The correct indication of closure is the inflection point on plot of pressure, first derivative and semi-log derivative vs. square root of time. The best way to find the inflection point is to plot the first derivative $dP/d\Delta t^{\frac{1}{2}}$ and find the point of maximum amplitude of the derivative. For this case, the sqrt (t) plot (Fig.22) shows a clear indication of closure based on both the first-derivative inflection point (highlighted with green circle) and the semi-log derivative curve. Picking closure in field cases where "Storage phenomenon" is observed is generally not a problem.

A.3. - Pre-Closure Log-Log Pressure Derivative plot:

Fig.23 shows the log-log plot of pressure difference and semi-log derivative (y-axis) against the shut-in time (x-axis).

The accurate storage flow identified with slope 1 is for very short time (Δt = 0.15 – 0.07 = 0.08 hrs. = 4.8 minutes). The radial flow characterized by a slope= -1 starts developing at Δt = 0.48 hrs. and ends at 0.70 hrs. lasting for 0.21 hrs. = 12.6 minutes when the test was terminated. The radial flow time range is too short to make any reliable

estimation of reservoir transmissibility and pore pressure and at best, can only give an indication of upper limit of those parameters.

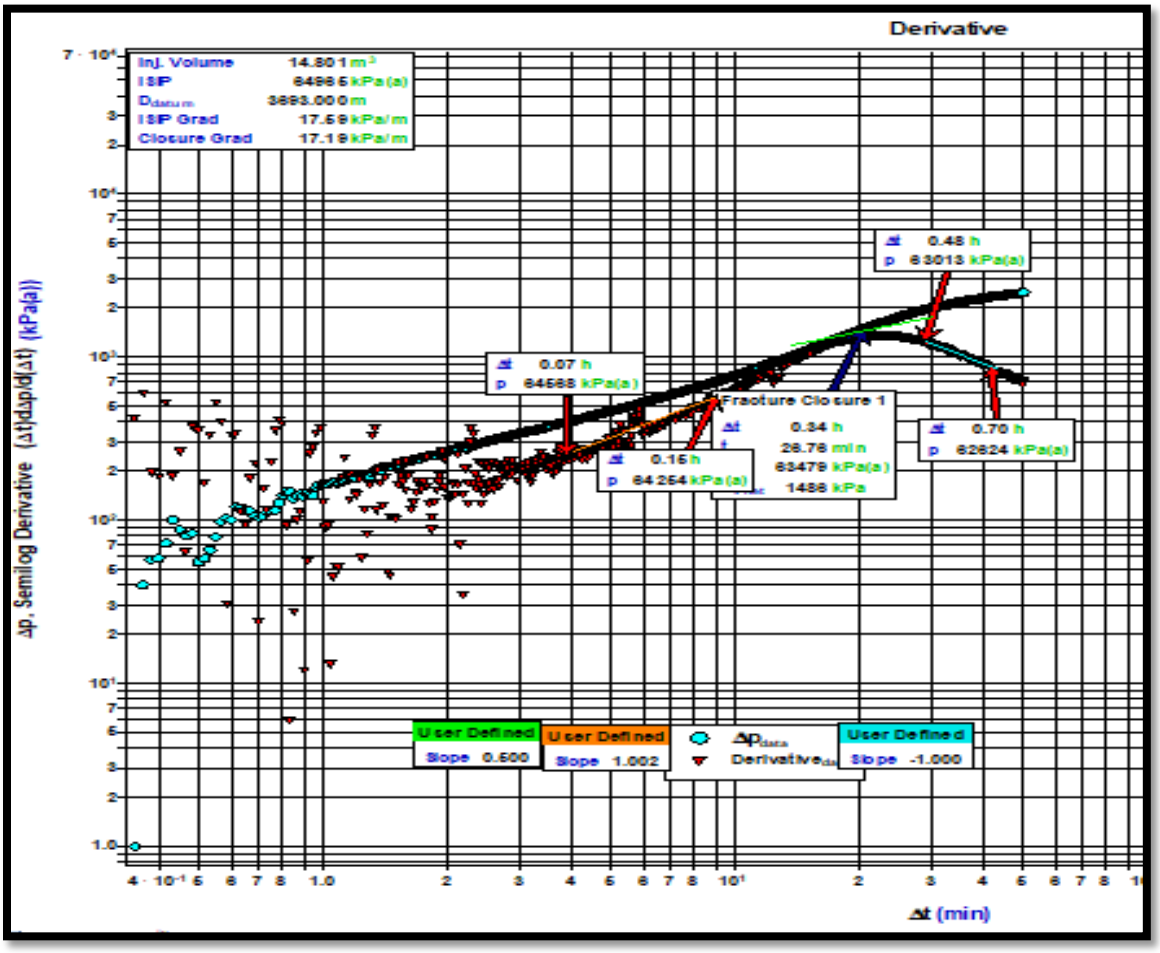

Figure 23 log-log plot of pressure difference and semi-log derivative

"As a rule of thumb (Barree et al 2009, 2015) states that on a log-log plot of pressure change and its derivative vs. Shut-in time, a safe and realistic lag time is one-half of a log cycle in time after closure, which means roughly that no data should be analyzed for any reservoir-flow regime, including pseudo-linear flow, until three times the closure time has elapsed." For this case, the closure time occurs at Δt=0.34 hrs. , the data set ends at 0.85 hrs. Three times the closure time is 1.02 hrs. but the data set terminates long before that happens.

Paul van den Hoek stated that unlike the established trend of taking end of linear storage line or deviation from first linear line as point of fracture closure, the real point of fracture closure cannot be confirmed with absolute certainty by above methods (Van Den Hoek, 2016). Point of fracture closure may or may not agree with the standard methods proposed by Barree et al (Barree et al., 2007) or McClure et al (McClure et al., 2016). To validate his idea, more discussion follows under "Numerical Model plots" section.

(B) After Closure Analysis (ACA):

The ACA technique is based on the method of type curve matching in order to obtain a representative value of the formation transmissibility (kh/μ), reservoir pore pressure (p*) , spurt loss coefficients (if value assumed is not

negligible), by identifying the presence of pseudolinear and pseudoradial flow after complete fracture closure. Once completed, this approach provides a reasonable accurate estimate of reservoir/fracture parameters.
The first approach for after-closure analysis (ACA) was developed by Nolte et al (1997). In this approach, ACA model was developed by assuming a constant injection pressure followed by shut-in. The solution of this problem can be found in the classical heat conduction problems in solids. Manipulating the solution to account for closure time, the fall off equation was developed. The basic weakness of this approach is that one has to assume the prevailing flow regime during after closure period. In this approach, two models were developed for pseudo-linear and pseudo-radial flow conditions.

It is to be noted here that for fractured injection, both rate and pressure are constant during injection.

B.1. Soliman and Craig Analysis

The second approach developed by (Soliman et al., 2005) is grounded in conventional well-test analysis and is similar to an approach that had been developed earlier for analysis of well data when the producing time is short . Rather than considering the test as a constant pressure injection as proposed by Nolte et al. the test here is considered to be a constant rate test. This is actually a more realistic approach because most of those injection tests are done at constant rate. Even if the rate is not exactly constant, Soliman et al. demonstrated that it has very minor effects on the results.

Following section involves mathematical expressions for different flow regimes based on Soliman and Craig approach:

Radial flow regime

Eq. (15) describes pressure data during the after-closure period when the created fracture is short and little to no residue fracture conductivity remains. In this case, the pressure follows a radial flow behavior. Eq. (16), (17), (18) gives the log, semi-log and impulse derivative forms of eq. (15)

Equations 15 to 18 represent Radial flow regime in Field units:

$$p_{fo} - p_i = \frac{(1694.4)\, V_{inj}\, \mu}{kh} \cdot \frac{1}{(t_p + \Delta t)} \tag{15}$$

$$\log(p_{fo} - p_i) = \log(\frac{(1694.4) V_{inj}\, \mu}{kh}) - \log\frac{1}{(t_p + \Delta t)} \tag{16}$$

$$\log\left(t\frac{\partial p_{fo}}{\partial t}\right) = \log(\frac{(1694.4) V_{inj}\, \mu}{kh}) - \log\frac{1}{(t_p + \Delta t)} \tag{17}$$

$$\log\left(t^2\frac{\partial p_{fo}}{\partial t}\right) = \log(\frac{(1694.4) V_{inj}\, \mu}{kh}) \tag{18}$$

Equation 19 to 22 represent Radial flow regime of in SI units:

$$p_{fo} - p_i = \frac{(0.000014\frac{\pi}{2}) V_{inj}\, \mu}{kh} \cdot \frac{1}{(t_p + \Delta t)} \tag{19}$$

$$\log(p_{fo} - p_i) = \log(\frac{(0.000014\frac{\pi}{2})V_{inj}\mu}{kh}) - \log\frac{1}{(t_p + \Delta t)} \quad (20)$$

$$\log\left(t\frac{\partial p_{fo}}{\partial t}\right) = \log(\frac{(0.000014\frac{\pi}{2})V_{inj}\mu}{kh}) - \log\frac{1}{(t_p + \Delta t)} \quad (21)$$

$$\log\left(t^2\frac{\partial p_{fo}}{\partial t}\right) = \log(\frac{(0.000014\frac{\pi}{2})V_{inj}\,\mu}{kh}) \quad (22)$$

Eq. (15) indicates that if a radial flow regime dominates the reservoir plotting, the left hand side of the equation vs. total time on a log-log plot will eventually yield a straight line with slope of -1.0. Eq. (17) is independent of initial reservoir pressure, the plot is only a function of observed pressure and time making it an ideal technique to determine flow regime. Eq. (18) also called as Impulse Derivative is variation of eq. (17) that may be used for the same purpose; however it would produce a straight line whose slope is zero i.e. a horizontal line. Once the flow regime is determined to be radial, a plot of pressure and time data (according to eq. (15)) would yield reservoir pressure. Formation permeability can be calculated from any of the eq. (15) to (18), but it is recommended to use eq. (16) as it is straightforward quick calculation

Bilinear Flow Regime:

If the created fracture is long, or if it did not completely close and some residual conductivity was maintained, it is possible that we will observe a bilinear flow regime. The presence of bilinear flow indicates that the flow is controlled by the pressure drop caused by the linear flow inside the fracture as well as the pressure drop caused by the linear flow in the formation just surrounding the fracture, perpendicular to the fracture linear flow. Similar to eq. (15) to (18), corresponding equations for bilinear flow are:

Equations 23 to 26 represent bilinear flow regime of in Field units:

$$p_{fo} - p_i = (264.6)\frac{V_{inj}}{h}\,\mu^{0.75}\left(\frac{1}{\emptyset\, c_t k}\right)^{0.25}\frac{1}{\sqrt{k_f.w_f}}\left(\frac{1}{(t_p + \Delta t)}\right)^{0.75} \quad (23)$$

$$\log p_{fo} - p_i = \log\left((264.6)\frac{V_{inj}}{h}.\mu^{0.75}\left(\frac{1}{\emptyset\, c_t k}\right)^{0.25}\frac{1}{\sqrt{k_f.w_f}}\right) - 0.75\log(t_p + \Delta t) \quad (24)$$

$$\log\left(t\frac{\partial p_{fo}}{\partial t}\right) = log\left((264.6)\frac{V_{inj}}{h}\,\mu^{0.75}\left(\frac{1}{\emptyset\, c_t k}\right)^{0.25}\frac{1}{\sqrt{k_f.w_f}}\right) - 0.75\log(t_p + \Delta t) \quad (25)$$

$$log\left(t^2\frac{\partial p_{fo}}{\partial t}\right) = \log\left(\left((264.6)\frac{V_{inj}}{h}.\mu^{0.75}\left(\frac{1}{\emptyset\, c_t k}\right)^{0.25}\frac{1}{\sqrt{k_f.w_f}}\right) + 0.25\log(\left(t_p + \Delta t\right)\right) \quad (26)$$

The plot coming from eq. (25) would yield a straight line with a slope of -0.75. The equivalent impulse derivative graph from Eq. (26) would yield a slope of 0.25. Formation permeability can be calculated using eq. (24).

Equations 27 to 30 represent bilinear flow regime of in SI units:

$$p_{fo} - p_i = (0.000135\frac{\pi}{2})\frac{V_{inj}}{h}\ \mu^{0.75}\left(\frac{1}{\emptyset\ c_t k}\right)^{0.25}\frac{1}{\sqrt{k_f . w_f}}\left(\frac{1}{(t_p + \Delta t)}\right)^{0.75} \quad (27)$$

$$\log p_{fo} - p_i = \log\left((0.000135\frac{\pi}{2})\frac{V_{inj}}{h}.\mu^{0.75}\left(\frac{1}{\emptyset\ c_t k}\right)^{0.25}\frac{1}{\sqrt{k_f . w_f}}\right) - 0.75\log(t_p + \Delta t) \quad (28)$$

$$\log\left(t\frac{\partial p_{fo}}{\partial t}\right) = log\left((0.000135\frac{\pi}{2})\frac{V_{inj}}{h}\ \mu^{0.75}\left(\frac{1}{\emptyset\ c_t k}\right)^{0.25}\frac{1}{\sqrt{k_f . w_f}}\right) - 0.75\log(t_p + \Delta t) \quad (29)$$

$$log\left(t^2\frac{\partial p_{fo}}{\partial t}\right) = \log(\left((0.000135\frac{\pi}{2})\frac{V_{inj}}{h}.\mu^{0.75}\left(\frac{1}{\emptyset\ c_t k}\right)^{0.25}\frac{1}{\sqrt{k_f . w_f}}\right) + 0.25\log(\left(t_p + \Delta t\right) \quad (30)$$

Linear Flow Regime

If the fracture is fairly long and it stays open with high dimensionless conductivity, a linear flow region may be observed. This generally happens in either of the two conditions: (i) if formation permeability is low and the minifrac test conducted with fluid-containing proppant. (ii) When the fracture staying open for a fairly long time

Corresponding equations similar to radial and bilinear flow regime are given below in <u>field units</u>:

$$p_{fo} - p_i = 31.05\ \frac{V_{inj}}{h}\ \left(\frac{\mu}{\emptyset c_t k\ L^2}\right)^{0.5}.\left(\frac{1}{t_p + \Delta t}\right)^{0.5} \quad (31)$$

$$\log(p_{fo} - p_i) = log\left[31.05\ \frac{V_{inj}}{h}\ \left(\frac{\mu}{\emptyset c_t k. L^2}\right)^{0.5}\right] - 0.5\log t_p + \Delta t) \quad (32)$$

$$\log\left(t\frac{\partial p_{fo}}{\partial t}\right) = \log[\ 31.05\ \frac{V_{inj}}{h}\ \left(\frac{\mu}{\emptyset c_t k L^2}\right)^{0.5}\ ]\ - 0.5\log t_p + \Delta t) \quad (33)$$

$$log\left(t^2\frac{\partial p_{fo}}{\partial t}\right) = \log\left[31.05\ \frac{V_{inj}}{h}\ \left(\frac{\mu}{\emptyset c_t k L^2}\right)^{0.5}\right] + 0.5\log t_p + \Delta t) \quad (34)$$

Where, p_{fo} = fall-off pressure (kPa (a)); p_i = initial reservoir pressure (KPa (a)); V_{inj} = Injected volume (m^3); h = net pay thickness (meter); L= fracture half length; t_p = pumping time; Δt = shut-in time; k = formation permeability (m^2)

Equations 35 to 38 represent linear flow regime of in <u>SI units</u>:

$$p_{fo} - p_i = (0.00424\frac{\sqrt{\pi}}{2})\frac{V_{inj}}{h}\ \left(\frac{\mu}{\emptyset c_t k\ L^2}\right)^{0.5}.\left(\frac{1}{t_p + \Delta t}\right)^{0.5} \quad (35)$$

$$\log(p_{fo} - p_i) = log\left[(0.00424\frac{\sqrt{\pi}}{2})\ \frac{V_{inj}}{h}\ \left(\frac{\mu}{\emptyset c_t k.L^2}\right)^{0.5}\right] - 0.5\log t_p + \Delta t) \quad (36)$$

$$\log\left(t\frac{\partial p_{fo}}{\partial t}\right) = \log[(0.00424\frac{\sqrt{\pi}}{2})\ \frac{V_{inj}}{h}\ \left(\frac{\mu}{\emptyset c_t kL^2}\right)^{0.5}]\ - 0.5\log t_p + \Delta t) \quad (37)$$

$$log\left(t^2\frac{\partial p_{fo}}{\partial t}\right) = \log\left[(0.00424\frac{\sqrt{\pi}}{2})\ \frac{V_{inj}}{h}\ \left(\frac{\mu}{\emptyset c_t kL^2}\right)^{0.5}\right] + 0.5\log t_p + \Delta t) \quad (38)$$

The detailed information and mathematical expressions associated with the analysis are discussed in Appendix (D).

The analysis done from after-closure analysis data using Soliman and Craig approach can be summarized as:

1. Derivative plot: Fig.24 shows impulse derivative ($\Delta t_a(t_p + \Delta t_a)\, d\Psi/dt_a$) is plotted on a log-log plot against 'adjusted time (Δt_a)' showing the after-closure pressure derivative plot. This plot is used to identify flow regimes with the radial flow identified by slope = 0 and linear flow by slope of 1/2, given from the general equation (18) and (34). General form can be expressed as Linear flow = $-\frac{t^2\partial\Delta p_w}{\partial t} = \frac{C_{pl}}{2}\ t^{\frac{1}{2}}$; Radial Flow = $-\frac{t^2\partial\Delta p_w}{\partial t} = \frac{C_{pr}}{2}\ t^0$ where C_{pl} and C_{pr} are constant terms. Pressure is pseudo pressure (Ψ) as reservoir fluid is gas, time is adjusted/pseudo time, t_a.

   The impulse derivative is calculated by multiplying the after-closure derivatives with product of pseudo/adjusted time Δt_a and time$(t_p + \Delta t_a)$. They are used, instead of the semi-log derivative$(t_p + \Delta t_a)\, d\Psi/d(t_p + \Delta t_a)$, to produce diagnostic plots with straight lines in which the flow regimes have characteristic slopes identical to those noted in conventional well test interpretation (SPE-107877, Equations summarized above). By eyeball estimate, radial flow lasts only for Δt=0.06 hrs. i.e. 3.6 minutes and linear flow lasts short too as shown in fig.25, implying that the neither of the flow regime was developed enough to give reliable estimate of unknown fracture and reservoir parameters. The presence of radial flow (though a short duration here) is an indication that either the fracture is short or that it had completely closed with no residual conductivity, since radial flow only occurs when the fluid is deep in the formation well beyond the near well-bore damage influencing zone.

2. Impulse Linear and Radial flow plot: Fig. 25 and 26 are the Cartesian plots of pseudo-pressure (Ψ) vs. $\frac{1}{t_p+\Delta t}$ for radial flow and $\left(\frac{1}{t_p+\Delta t}\right)^{0.5}$ for linear flow respectively. Since radial flow is short developed, late time extrapolations on specialized radial and linear plots are included to give an upper limit of reservoir permeability, fracture dimensions etc. If linear flow is identified, fracture half-length (L) can be estimated using Eq. 31 or 32. Evident from the equation (31 or 32) is that estimated value of fracture half-length (L) is inversely proportional to the value of square root of permeability (k) used.

   If a long radial flow is observed, permeability value determined is of high confidence which in turn gives a reliable estimate of half-length. However, like for our case where the radial flow is barely developed (Fig.24) using (Eq. 15 or 16) can be reformulated to give $m_{R1} = \frac{(1694.4).V_{inj}.\mu}{kh}$, (all required values of variable were taken from Table 3 and 4), the value obtained from radial Cartesian plot at best gives an upper limit of permeability (k=3.21*10^{-16} m^2) which in turn gives an incorrect half-length value or worst can predict a value which is way off from the true value.

3. *Erroneous value of permeability leads to erroneous value of fracture half-length. This can be demonstrated from a simple exercise. For a permeability value of k= 3.21*10^{-16} m², the half-length value obtained is 3.55 m using (Eq.31). We know from the VdHoek model's derived results and confirmed by FenixConsulting Delft © expert's analysis, that the permeability value is of order 10^{-17} m² and fracture half-length is between 11 and 18 m. When k=3.2*10^{-16} m² was changed manually to k=3.2*10^{-17} m² in the 'parameter box', the half–length calculated came to be 11.23 m, which is in the accepted value range.*

4. The history matching and associated plot hasn't been discussed here because, with the limited radial flow regime observed, results weren't accurate. The permeability value obtained from history matching plot was k= 5.3*10^{-16} m², one order higher than the true permeability.

5. Extrapolated pressure (p*) obtained from Radial flow was 58773 kPa (a) and from linear flow was 57202 kPa (a).The true reservoir pressure value is 60500 kPa (a). Sensitivity analysis taking the lower estimate of reservoir pressure i.e. 57202 against the true reservoir pressure gives a deviation of 5.4% which was still under the acceptable error/tolerance range.

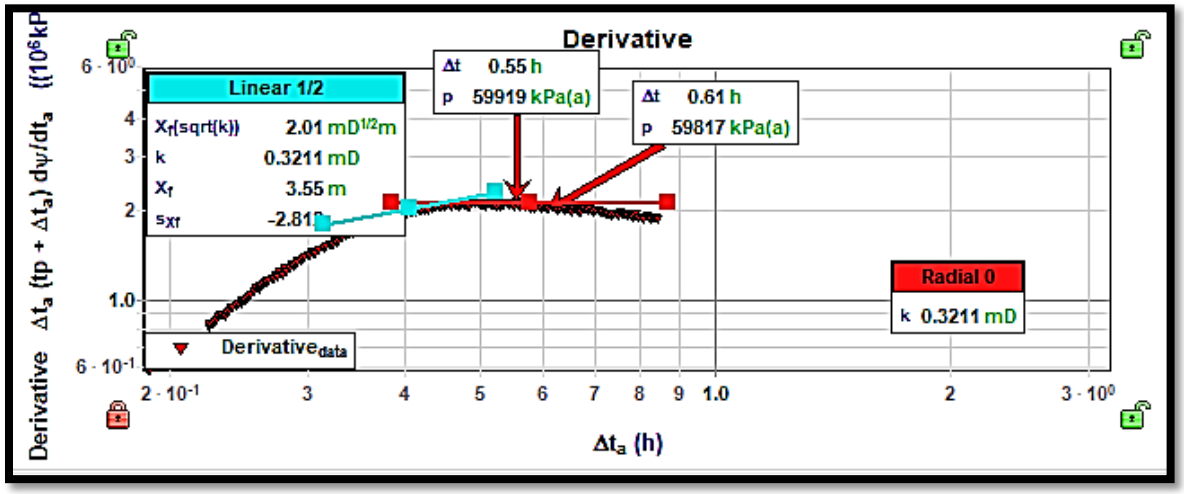

Figure 24 Soliman-Craig Log-log plot of Impulse derivative vs. adjusted shut-in time (hrs.)

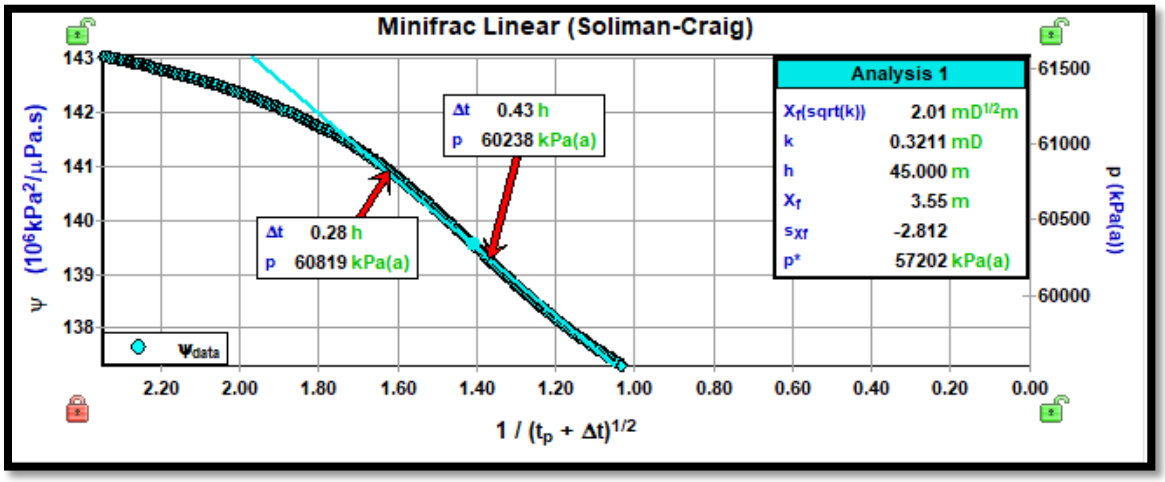

Figure 25 Soliman-Craig Cartesian plot linear flow plot of pseudo pressure vs. (1/(t_p+delta t))^0.5

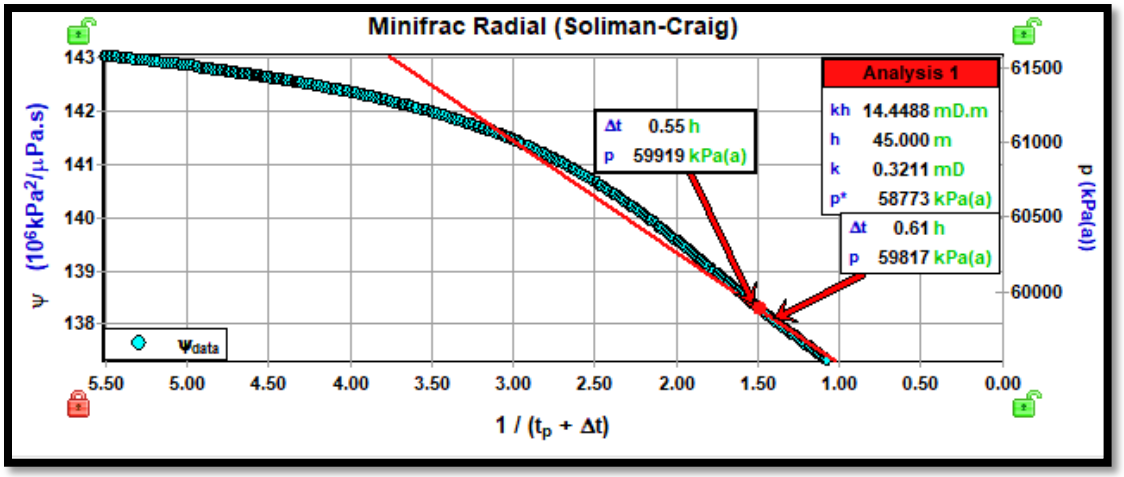

Figure 26 Soliman-Craig Cartesian radial flow plot of pseudo pressure vs. (1/(t_p+delta_t))

(B.2.) Nolte ACA analysis:

All mathematical expression and associated discussion can be found in more detail in Appendix (D) "Nolte ACA section". As quick recap, key formulas and other important concepts are mentioned before the analysis for the data is started. Fig. 27 shows pressure difference (dΨ) (which equals pressure fall-off – reservoir pressure) and semi-log derivative (X* dY/dX)of the pressure difference curve vs. square of the Linear Nolte-time function (F_L^2) representing the derivative plot. There can be two Minifrac Nolte After-Closure Analysis (ACA) linear time function. F_{L1} is an approximation of F_{L2} and the two time function converge quickly. F_R is the Nolte Radial flow time function.

$$F_{L1} = \frac{2}{\pi}\sin_1\frac{(t_c)}{t} \tag{39}$$

$$F_{L2} = \sqrt{1} + \frac{\sqrt{(t-t_c)}}{\sqrt{\frac{16}{\pi^2 t_c}}} \tag{40}$$

$$F_R(t,t_c) = \frac{1}{4}\ln\left(1+\frac{\chi t_c}{t-t_c}\right) \quad ; \chi = \frac{16}{\pi^2} \approx 1.6 \tag{41}$$

Nolte Linear Flow:

In Field Units:

$$\Delta p_{Total} = \ p_{fo} - p_i = 477.C_T\sqrt{\frac{\pi\mu}{k\emptyset c_t}}\ \ F_{L1} \tag{42}$$

And fluid loss coefficients obtained from eq. 42 are given as:

$$C_R = \frac{\Delta P_{total}}{477}.\frac{\sqrt{k\emptyset c_t}}{\pi\mu} \ \ where\ \Delta P_{total} = P_c - P_i \tag{43}$$

$P@t_c$ is the extrapolation of the linear flow line at closure time t_c. $F_{L(1\ or\ 2)} = 1.0\ at\ t_c$

$$C_T = \frac{\Delta P_{reservoir}}{477}.\frac{\sqrt{k\emptyset c_t}}{\pi\mu} \quad where\ \Delta P_{reservoir} = P@t_c - P_i \tag{44}$$

Nolte Linear Flow (Eq. 42) when represented in SI units is:

$$\Delta p_{Total} = \ p_{fo} - p_i =. C_T \sqrt{\frac{\pi\mu}{k\emptyset c_t}} \ \ F_{L1} \tag{45}$$

Radial Flow:

$$\Delta p_{Total} = \ p_{fo} - p_i = 251000\ Q_t \frac{\mu}{kht_c}\ F_{R1} \tag{46}$$

The slope of the line on the minifrac radial plot is m_{R1}, and eq.46 can be rearranged to calculate permeability as follows:

$$m_{(R1)} = 251{,}000.\frac{Q_t \mu}{kht_c} \tag{47}$$

Where, Q_t $\left(\frac{m^3}{\min}\right)$ =total flow rate (total injected volume/ time of injection), μ(Pa.s) = viscosity of the reservoir fluid , k (m^2)= permeability , h (m) = height of formation (net pay) , t_c = closure time

Nolte Radial Flow when represented in SI unit is:

$$\Delta p_{Total} = \ p_{fo} - p_i = (\frac{\pi}{2} 0.082)\ Q_t \frac{\mu}{kht_c}\ F_{R1} \tag{48}$$

The analysis done is as follows:

1. Both time functions (F_L and F_R) are bounded by 1.0 (at early shut-in time) signifying the time of closure, and 0.0 (at late time) representing an infinite shut-in time.
2. Derivative plot: The first graph to look at is the log-log derivative graph (Fig.27) to identify the developed flow regime. Once the flow regime is well identified, possible information can be extracted about unknown fracture and reservoir parameters with confidence.

   If radial flow is identified, p* (extrapolated pressure) and permeability can be estimated using Eq. (46).p* is estimated from extrapolation of linear line to F_{R1}=0. F_{R1}=1 represents early shut-in time i.e. the time of fracture closure and F_{R1}=0 represents infinite shut-in time. Radial flow portion of after-closure data will have a straight line trend on pressure vs. F_{R1} plot
3. It is important to note here that the guess of the reservoir pressure, p_i used in construction of the flow regime plot severely affects the slope and magnitude of the pressure difference curve. However, the pressure derivative, because of the difference function used to generate it, is not affected by the initial guess of reservoir pressure.

4. While the log-log plot of pressure difference and its semi-log derivative for Soliman and Craig ACA technique (Fig.24) shows extremely short radial flow period, on other hand in Nolte derivative plot (Fig.27), slope of the derivative and corrected pressure difference ($\Delta\Psi$) curve coincide at slope of -1. This is a standard identification technique for cases where pseudo radial flow is developed. For this field data, however the radial flow wasn't well developed which was confirmed from pre-closure log-log plot (Fig.23) and Soliman, Craig analysis plots (Fig.24,26).This exercise demonstrates that Nolte analysis is less reliable for such cases and it is always recommended to double confirm the findings using other approaches.

5. Cartesian plot of pseudo pressure (Ψ) against Linear Nolte time function F_L(Fig.28) and Radial Nolte Time function F_R (Fig. 29) is used here only to get an extrapolated pore pressure (p*) using Eq. 42 and 46 which at best only serves as the upper limit of unknown reservoir/fracture parameter's value. The method to identify extrapolated pressure (p*) is discussed under (2) and the values estimated is 58135 kPa (a) and 58868 kPa (a).

6. Linear flow analysis helps in determining Leak-off coefficients (Total Leak-off coefficient,C_t and Reservoir Leak-off coefficient, C_R) with values of $1.12 * 10^{-3}\, m/\min^{\frac{1}{2}}$ and $8.33 * 10^{-4} m/\min^{\frac{1}{2}}$ using Eq.(43),(44). Value of permeability (k) is taken from Nolte Radial flow plot $=0.45 * 10^{-15} m^2, \emptyset = 0.17$, initial total compressiblity $c_t = 5.75 * 10^{-6}\,(1/kPa)$ and μ = 0.03 cP. $\Delta p_{Total} = p_c - p_i$ where p_i is taken as the extrapolated initial pressure = 58135 kPa (a). The resulting leak-off coefficient values come in accordance with the values obtained from IFO analytical model as discussed under the heading of "Comparison".

7. Extrapolated pressure obtained from Radial flow was 58868 kPa (a) and from linear flow was 58135 kPa (a).The true reservoir pressure value is 60500 kPa (a). Doing sensitivity analysis taking the lower estimate of reservoir i.e. 58135 against the true reservoir pressure gives a deviation of 4.06% which is still acceptable to get working numbers of the field.

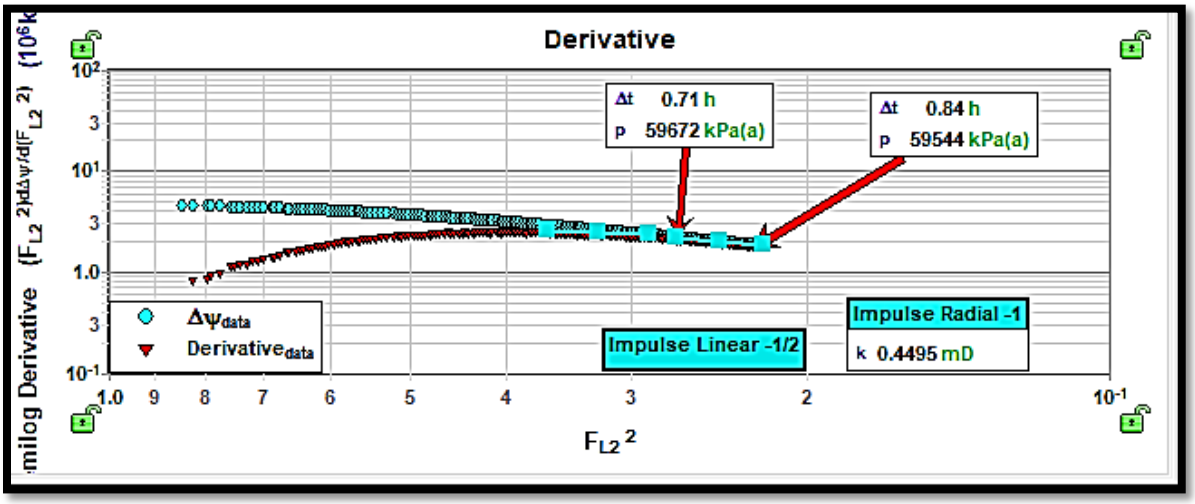

Figure 27 Log-lot plot of pressure difference and semi-log derivative vs. F_L^2

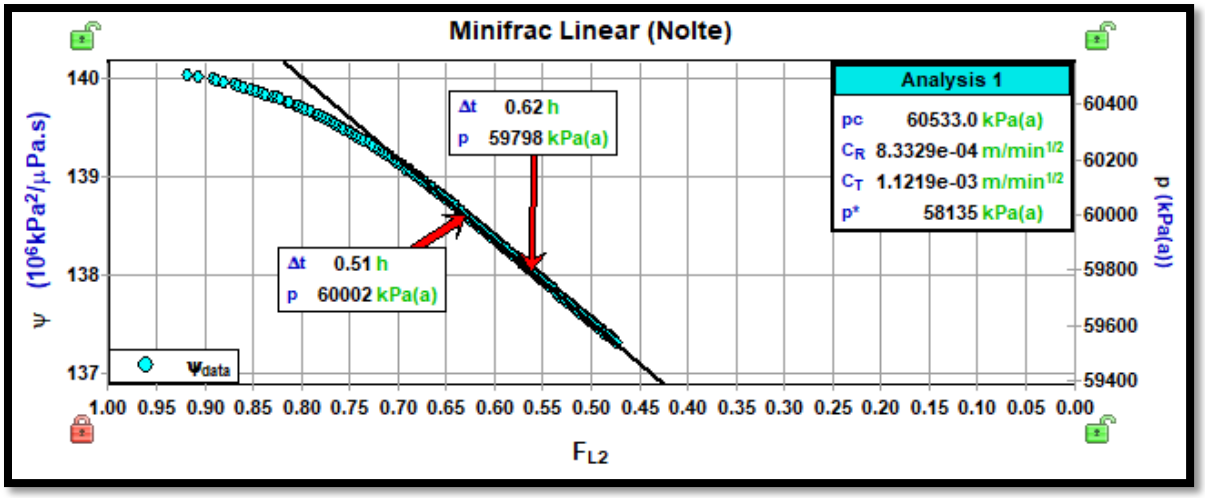

Figure 28 Cartesian Linear plot of pseudo pressure against Nolte Linear time (F_L)

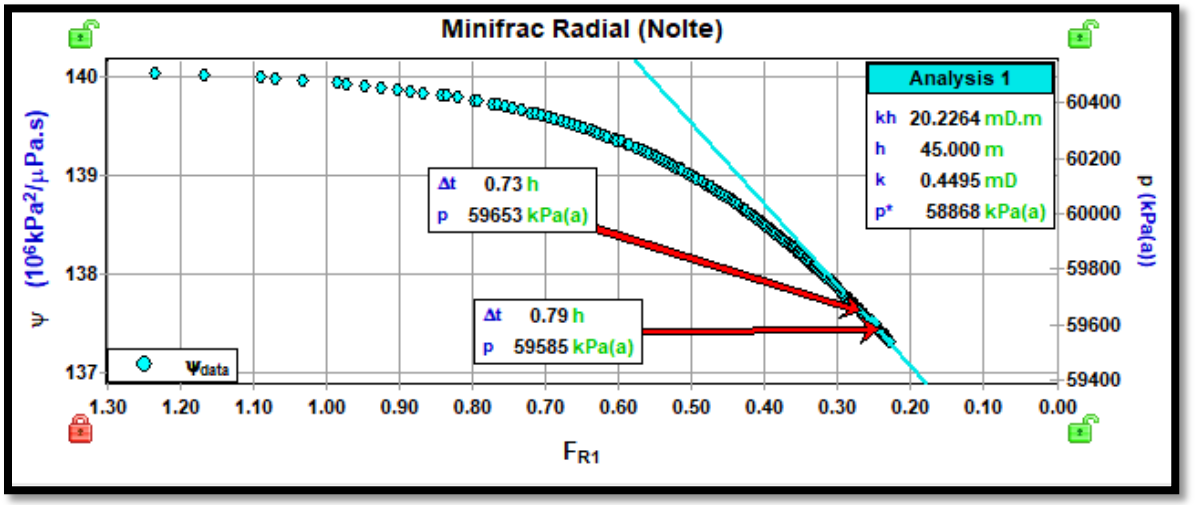

Figure 29 Cartesian Radial plot of pseudo pressure against Nolte Radial time (F_R)

(C) - VdHoek Analytical Model:

Table 5 Input parameters for VdHoek analytical model – Example 1

Porosity	0.17	[-]
Fluid Compressibility	1.67e-08	Pa^{-1}
Reservoir fluid viscosity	0.00002	Pa*s
Injection fluid viscosity	0.0003516	Pa*s
Young's modulus	6.89	GPa
Net pressure	20 (estimate)	Bar
Fracture height	50	m
Injection rate	0.0361	m^3/sec
t_{pump}	6.91	min

Fig.30 shows a log-log diagnostic plot of delta pressure and derivative against shut-in time obtained from the Analytical model. The analysis was done till shut-in time of 0.35 hrs. (highlighted by a green vertical line), which is the fracture closure point, same value as obtained from BCA log-log derivative plot in FEKETE. While the accurate closure point cannot be yet calculated from the analytical model, applying the standard accepted rule that the "point where delta and derivative of pressure starts to deviate after initial storage flow period of slope 1 is the fracture closure point" seems to agree in the plot.

Due to low permeability (in nanodarcy range), fracture shows a storage dominated growth. The estimated leak-off rate $Q_l\,(t_{pump})$ is done under the assumption that during pumping, leak-off rate is one-dimensional (following Carter's leak-off assumptions). Hence under Carter's assumptions, for storage dominated flow, leak-off rate is calculated from (Nolte, 1986) as

$$Q_l(t_{pump}) = \frac{|Slope| * V_{inj}}{\frac{2}{3} * |Slope| * t_{pump} + (\text{Net Pressure})} \qquad (49)$$

Where, $|Slope|$ is the absolute value of pressure decline slope at shut-in, V_{inj} is the cumulative injected volume at the end of pumping period, and the net pressure = ISIP -FCP

Series of equations as developed in Appendix (B) (VdHoek's analytical model) are used here to calculate necessary parameters. From fig.30, it is visible that the early time flow is fracture storage dominated with slope=1, but the duration of the flow is relatively short (0.01 –0.3 hrs.).This period can still be used to estimate fracture compliance C_f by using eq. 61 (Refer appendix B), which in combination with the input data given in Table 5, fracture half-length value of 14.5 m was obtained. Subsequently, formation permeability (k = 0.2*10^{-17} m^2) and fracture face skin (S) [$S = \left(\frac{k}{k_{filtercake}}\right) * \left(\frac{d}{L}\right)$, where d is filtercake thickness on the fracture face] respectively was calculated when a best possible fit between the field data and model was obtained up to the point of "fracture closure". Here, the fracture dimension results comes in good agreement with the specialized technique plots as used in FEKETE but any disparity in dimensions can be attributed to the different fracture geometry models (PKN/GDK or radial model vs. elliptical used here)

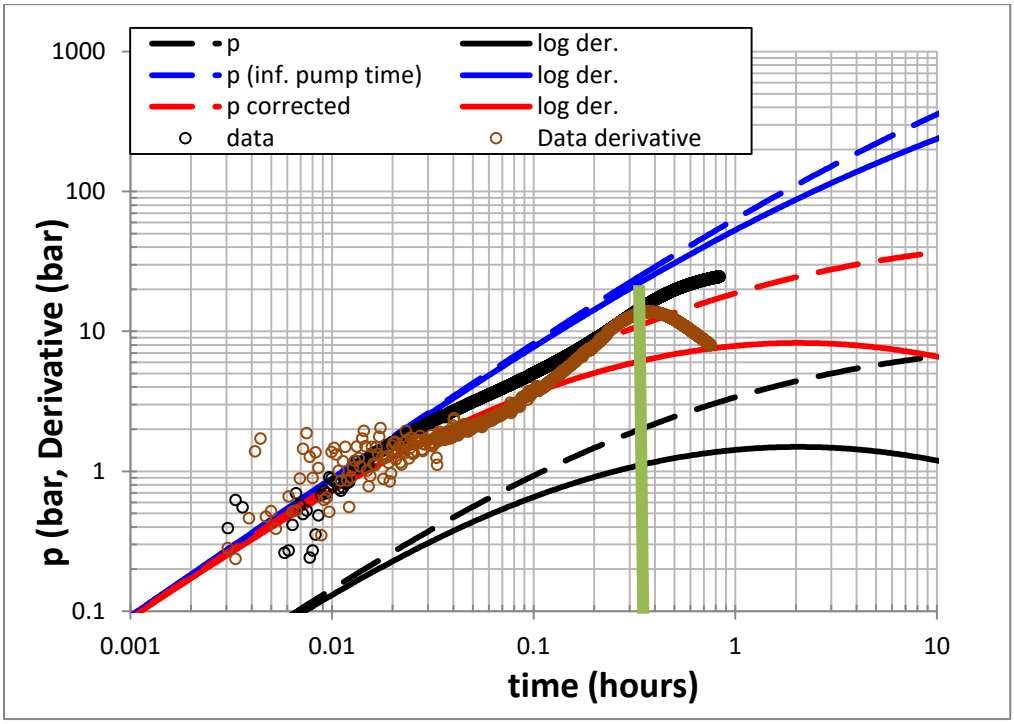

Figure 30 Log-Log pressure difference and derivative diagnostic plot (VdHoek Analytical model)

(D) - Comparison between FEKETE (Specialized Plot) vs. VdHoek Model

Table 6 Comparison between FEKETE vs. VdHoek model – Example 1

Parameters	Unit	Plot from where value came in FEKETE analysis ***	FEKETE (***)	VdHoek Analytical Model
Volume Injected	m^3	NA	14.801	14.89
Injection rate	m^3/sec	NA	0.040	0.0361
Injection time	min	NA	6.06	6.9
Fracture Half-length	meter	* Frac Boundary model	16.455	14.5
Fracture height	meter	NA	50	45
Permeability	m^2	* Frac Boundary model	$3.2 * 10^{-16}$	$0.2 * 10^{-17}$
Net Pressure	kPa (a) (a)	BCA – G-function, Sqrt(t) plot	2497	2000 (estimate)
Skin (Frac Face Damage)			0	0.007
Total Leak-Off coefficient	(m/sqrt(sec))	Nolte ACA Linear plot	1.56e-04	1.08e-04
Initial Total Compressibility (c_{tl})	Pa^{-1}	NA	5.75e-09	1.79e-08
Time to Fracture Closure	min	BCA – G-function, Sqrt(t) plot	26.76	Cannot be determined
Pressure at fracture closure time	kPa (a) (a)	BCA – G-function, Sqrt(t) plot	60533	Cannot be determined

* Frac Boundary model - based on Soliman and Craig ACA method
**NA = Not Applicable
*** = For reason, please see pt. (9) and (10) of 'Conclusion' section
= Value given as input in VdHoek analytical model
= Value given as input (an initial estimate) but it self-optimizes when model simulates
= Value determined as output in VdHoek analytical model
Please note the same color scheme is used in comparison table of all further field analyzed data

While a detailed discussion about the values estimated from both models is mentioned in "Conclusion" section, a quick preview shows that values of unknown parameters are in same order range.

Determined permeability value from pre-closure analysis by FenixConsulting © in-house analysis yielded result of $0.2 * 10^{-17} m^2$. This values matches *exactly* with the permeability value obtained from VdHoek analytical model (k= $0.2 * 10^{-17}\ m^2$). The value obtained using FEKETE is one order higher.

(E) - Numerical Model plot

Fracture closure occurs with a mix of "hinge-closure and zipper-closure" and the details have been discussed in detail in Chapter 3 (Literature Review) section. It states that until a point, p^o depending on fracture effective toughness, fracture closure occurs by Hinge closure mode. Once that point is crossed, the fracture length recession starts by "zipper-closure". The physical meaning of the value of p^o at which "zipper closure" starts is related to the well-known issue of high net pressure in propagation fracture, implying that increasing p^o can be associated with increasing high net pressure/ effective fracture toughness during propagation. *Thus higher the p^o value is, higher is the duration of "hinge closure" associated time.*

Figure 31 to 36 shows the (dimensionless) pressure decline and derivative curves for a propagating fracture during pumping, which closes after shut-in (assuming low-conductivity of residual fracture). Shown is a mixture of 'hinge-closure' and 'zipper-closure' [see Eq. 65) in Literature review – Chapter 3], in which the pressure p^o at which zipper closure starts is varied, from very small value of 0.1 bar till value of ∞ demonstrating its effect on the plot . The process of fracture closure is indicated by the curves of relative fracture compliance (1=fully open, 0=fully closed) as a function of time.

The abbreviation for the various plots in the figures is described below:

1) **Light blue color** (solid and dashed line) = Analytical model (closed fracture)
2) **Dark blue color** (solid and dashed line) = Analytical model (open fracture)
3) Series 9 and 10 = Field data
4) **Green Color** (solid and dashed line) = Numerical model plot

Following observations can be deduced from these plots as follows:

(a) Fracture closure pressure cannot be observed from the pressure transient and derivative plot. Situations can happen when fracture length recession leads to reduction of both fracture compliance and effective fracture leak-off surface so that the net rate of pressure decline remains almost same with no significant change in magnitude. For such cases, deviation of pressure transient from linear dependency of time as can be seen in figures 31 till 36 are only indicative of end of storage flow period and not of fracture closure point. Fig.31 to 36 also show various possible points of fracture closure depending on relative fracture compliance's value.

Hence, end of storage-dominated flow period isn't necessarily mark fracture closure point.

(b) For po = 0.1 and 1 bar where zipper closure starts early, the late time derivative curve($t_{shut-in} \gg t_{pump}$) of Numerical model (green color) and AfterClosure Analytical model (light blue color) coincides showing a good agreement between numerical model and analytical model results. As the po value starts increasing from 5,10 till infinity bar so that hinge closure duration lasts longer, it was seen that the numerical derivative plot changes gradually from steep declining curve (signature of closed fracture as visible in po=0.1 bar) and at infinity, it is parallel to the "analytical model- open fracture" curve. This can also be used as evidence to demonstrate that the real point of fracture closure cannot be taken at "end of bump marking end of storage flow period" with certainty.

If fracture closure always occurred at end of storage period as mentioned in standard methodologies, the late time derivative curve for higher po wouldn't be parallel to the "analytical model- open fracture" derivative curve.

(i) po=0.1 bar

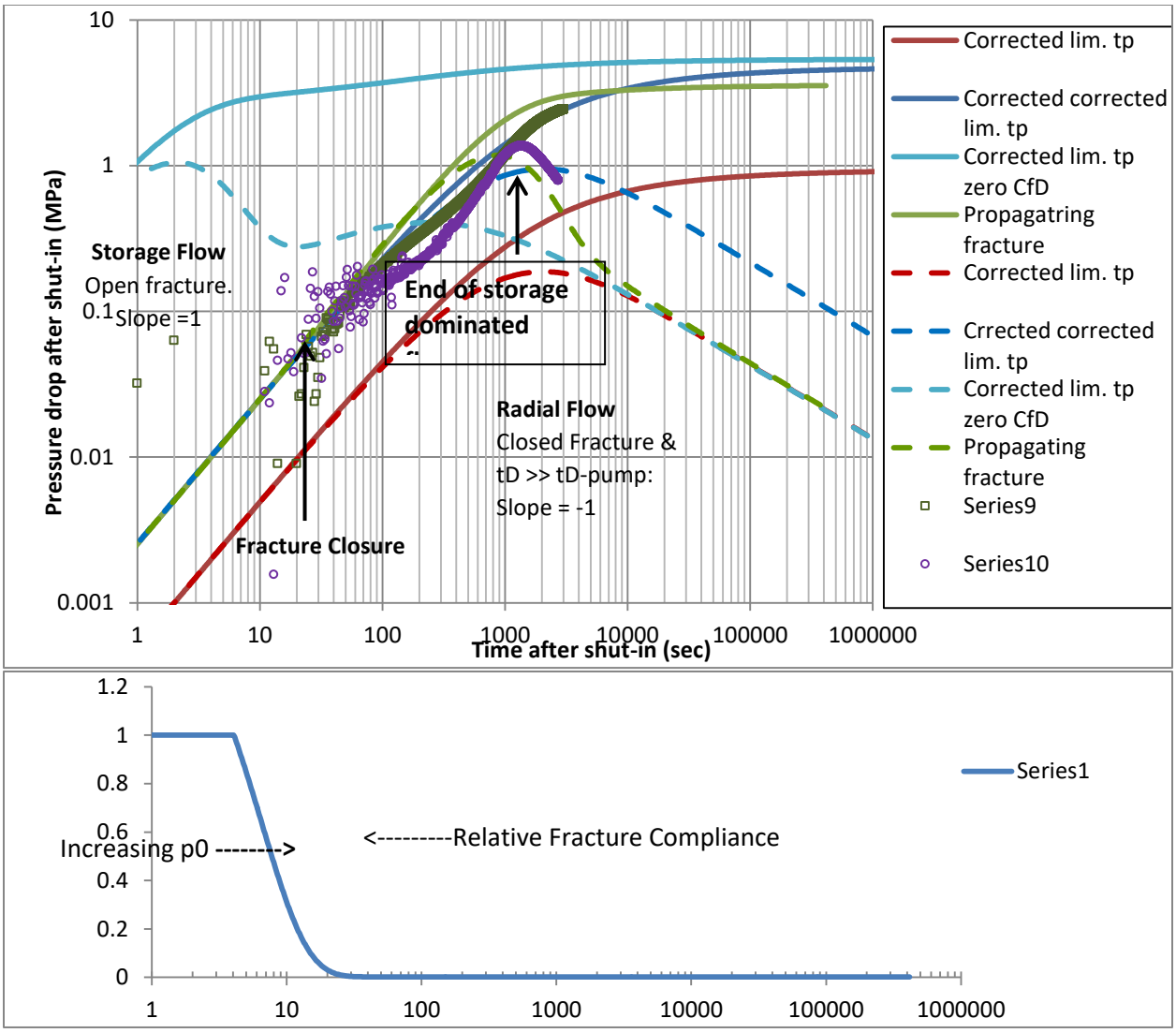

Figure 31-36 Computed pressure decline and derivative curves matched with field data for a propagating fracture during pumping, which closes after shut-in (assuming low-conductivity of residual fracture).Comparison with analytical results. Short dimensionless pump times. Low po=0.1 bar at which zipper closure starts

(ii) po= 1 bar

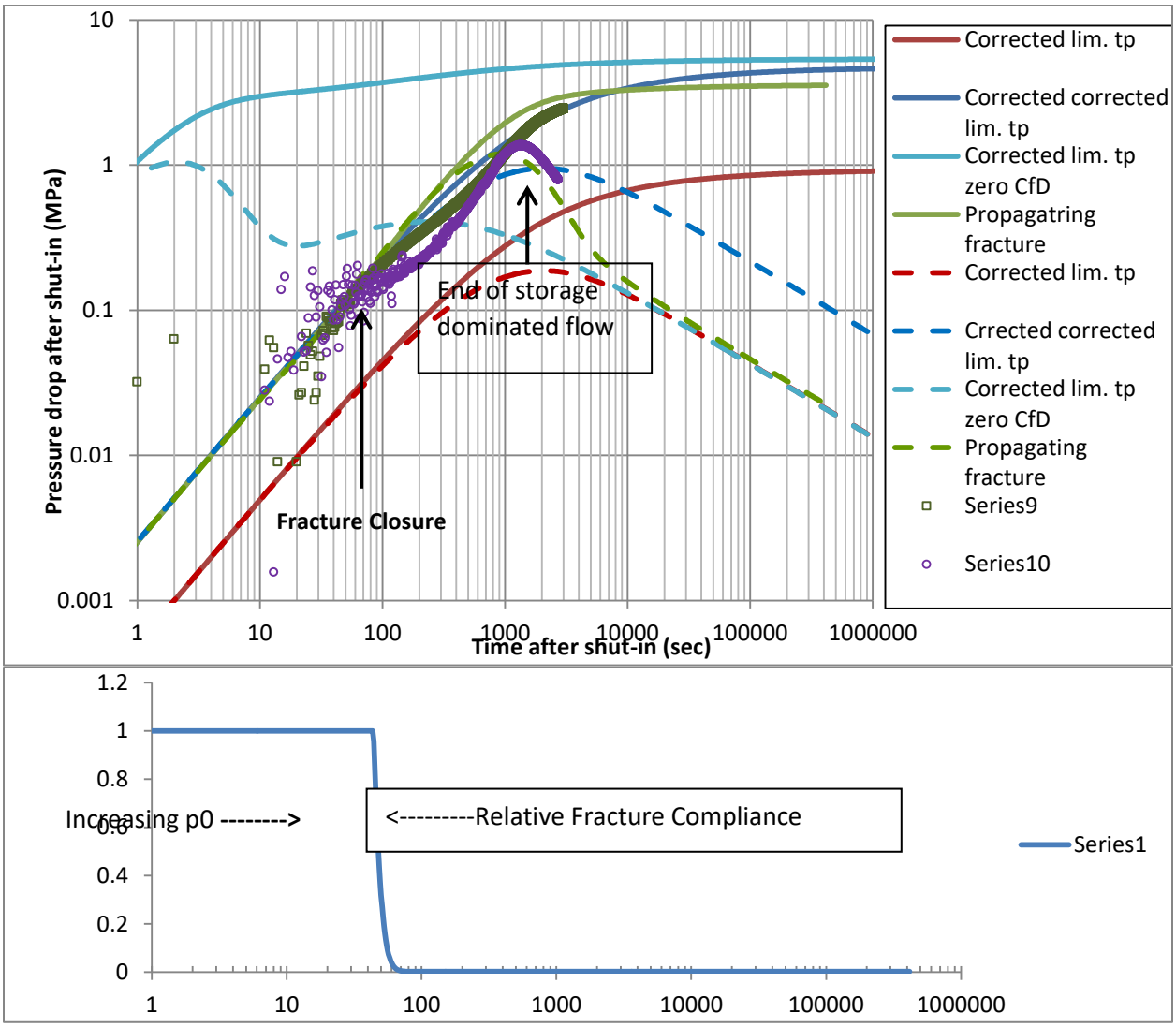

Figure 32 Low po =1 bar at which zipper closure starts

(iii) po= 5 bar

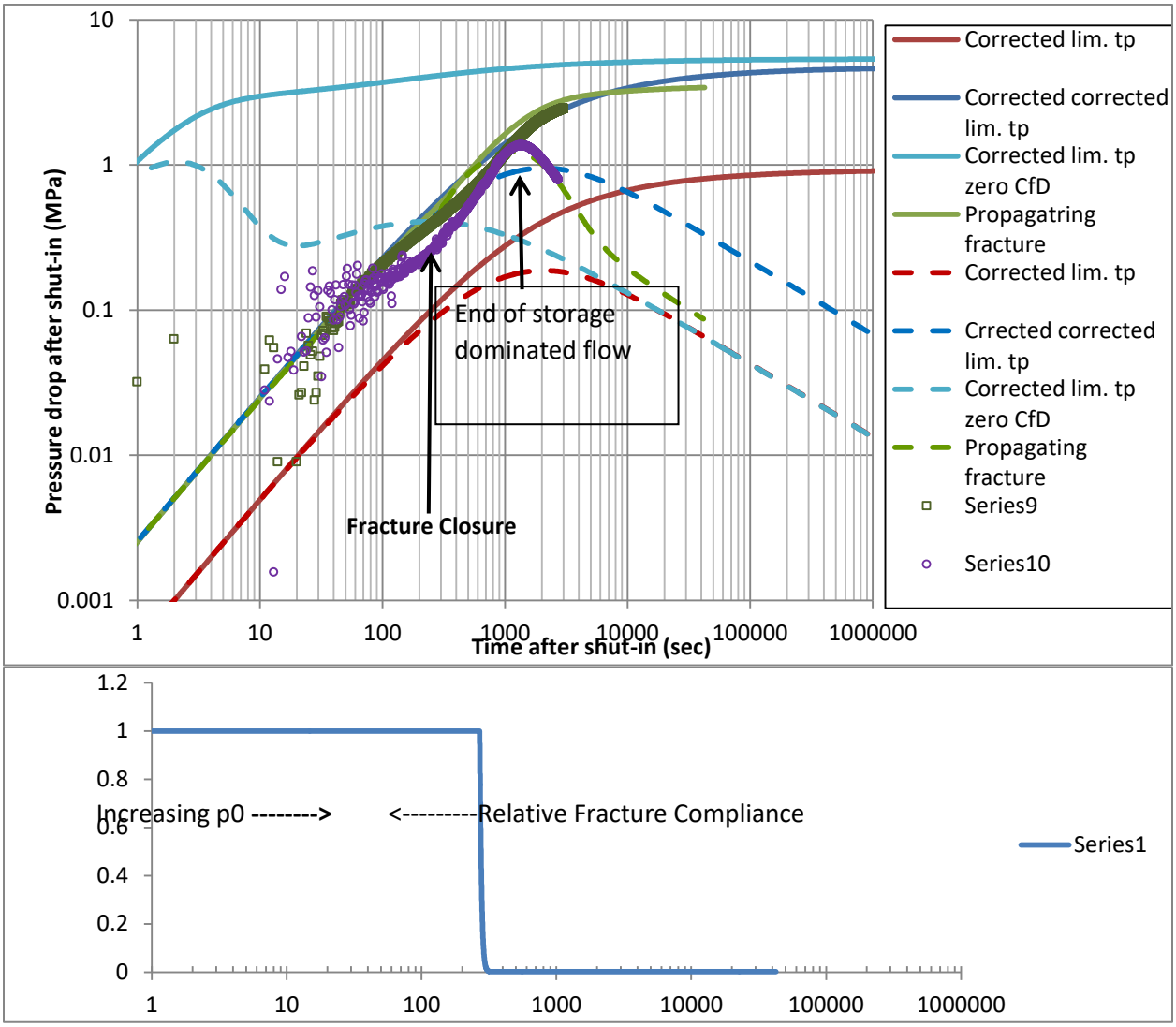

Figure 33 Low po = 5 bar at which zipper closure starts

(iv) po=10 bar

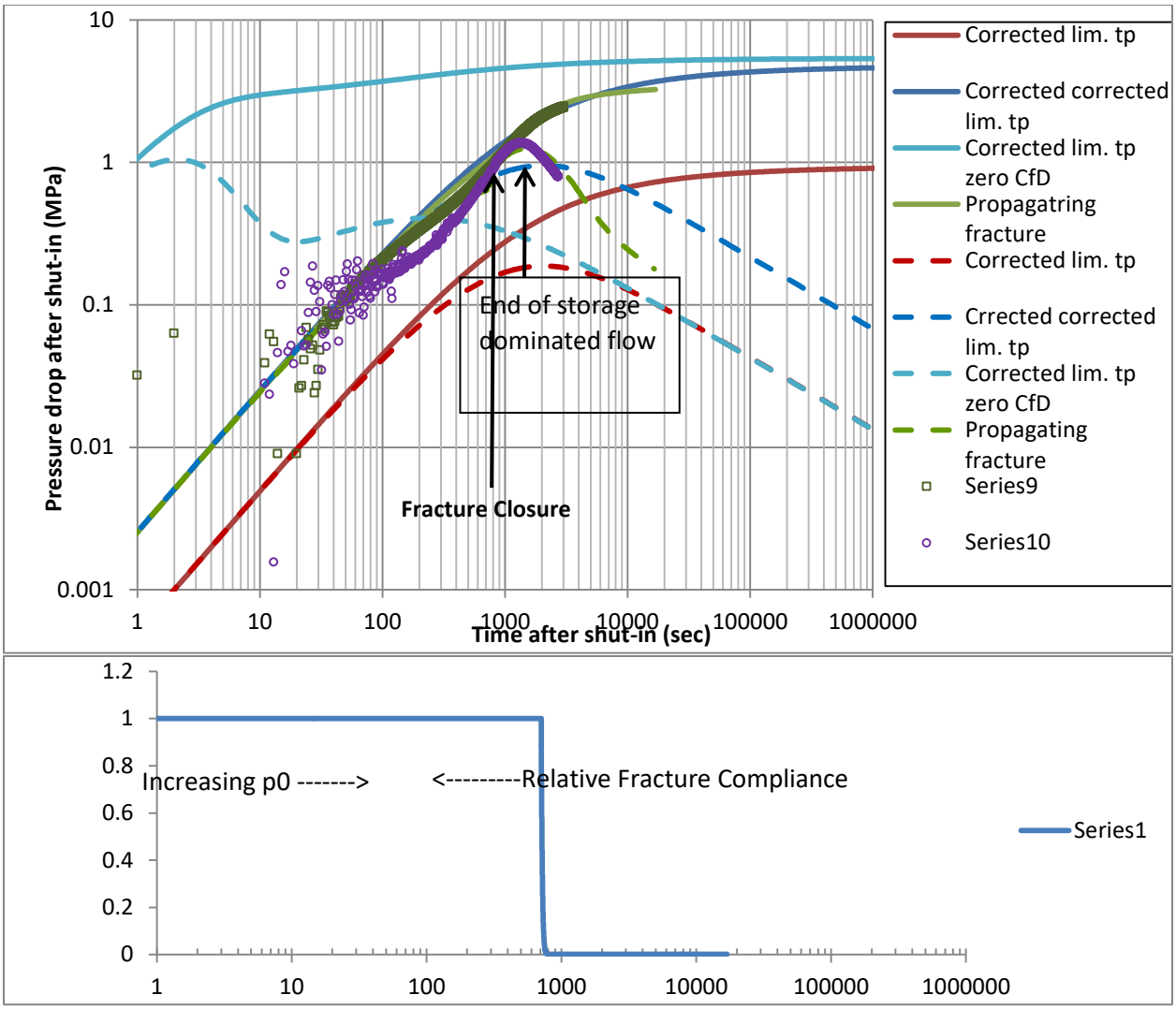

Figure 34 Medium po = 10 bar at which zipper closure starts

(v) po=20 bar

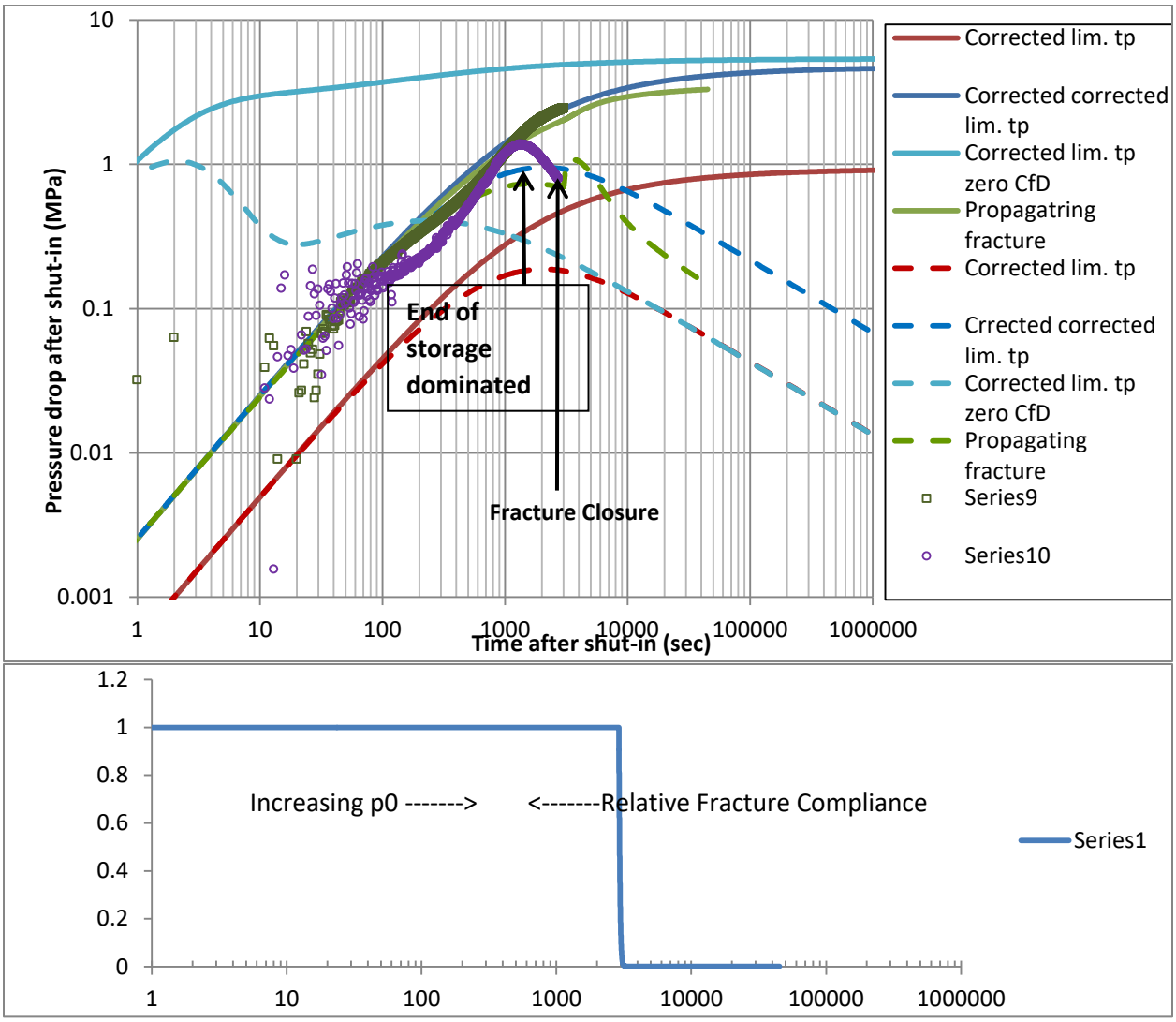

Figure 35 High po = 20 bar at which zipper closure starts

(vi) po = infinity

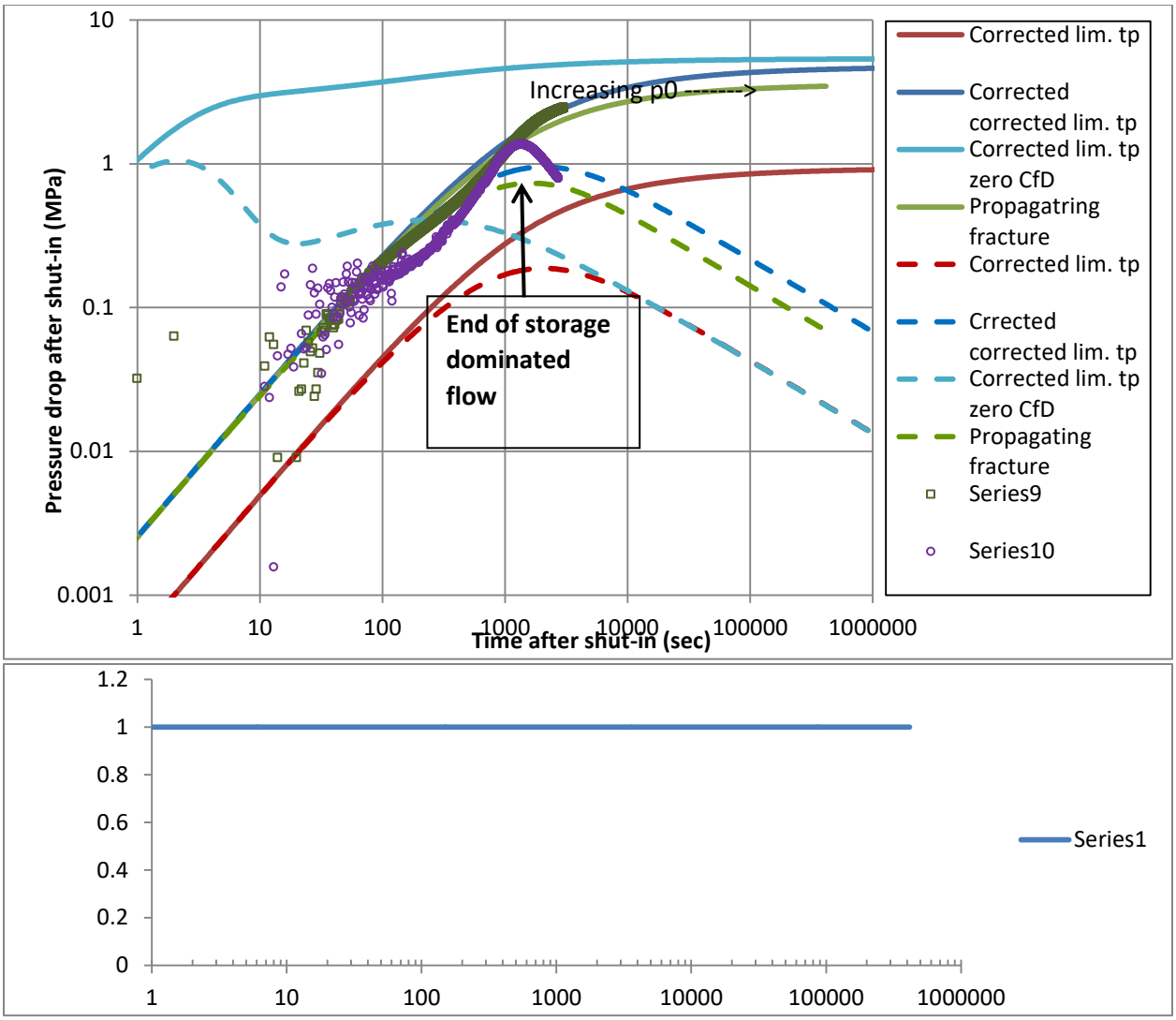

Figure 36 High po = infinity bar at which zipper closure starts

(F) - McClure's Analysis:

Fig. 37 is a zoomed version of early part of the plot from Fig.22 to identify the first sharp point of deviation from linearity on a plot of pressure or G * dP/dG vs. G-time.

Fig. 22: Example 1 - Pressure or G * dP/dG vs. G-time

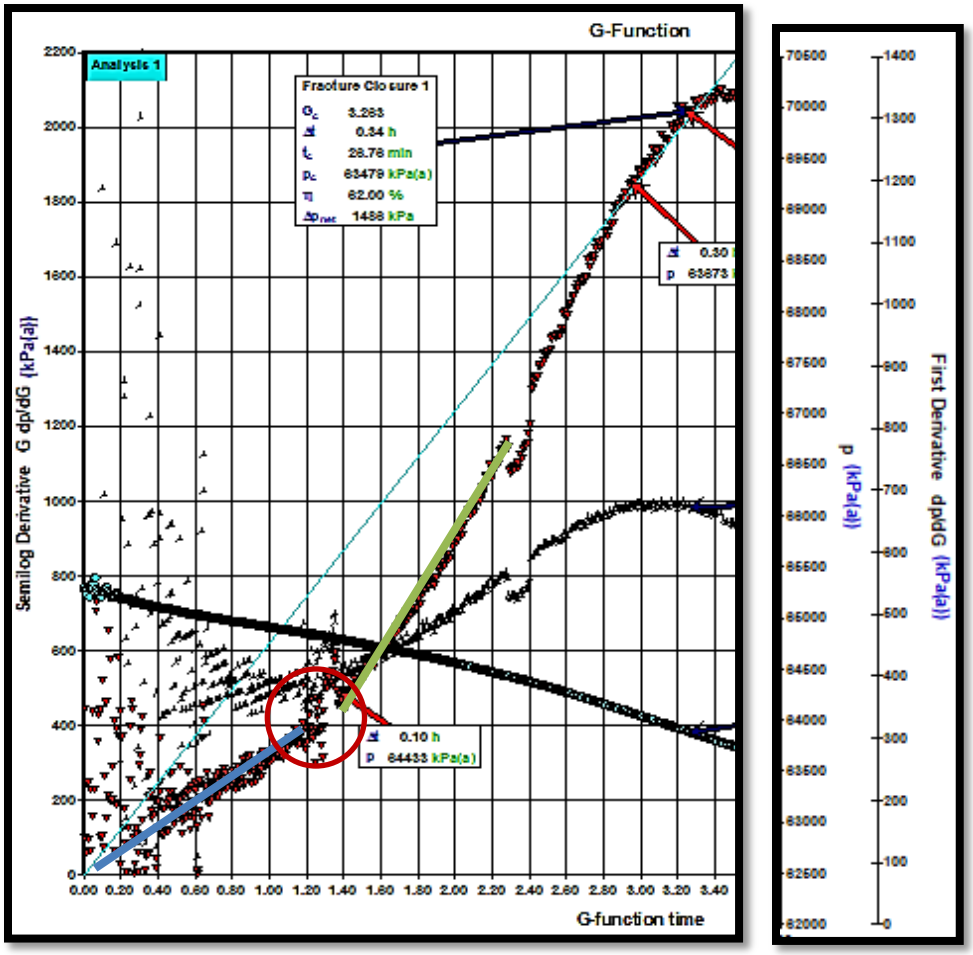

Figure 37 Zoomed in plot of early portion of Example 1 - Pressure or G * dP/dG vs. G-time

In this case, it is less clear where to pick closure because the upward deviation caused by (McClure's proposed) closure is less sharp and too much of noise in early data set. The best estimate of deviation point from linearity here is taken at G-time of 1.30 ~ 1.40 (encircled with red arrow). The corresponding closure pressure is 64433 kPa (a)(a). This closure pressure value is higher by roughly 10000 kPa (a). Couple of possible explanations is:

(i) There can be presence of high-residual aperture. Because the walls begin to come in contact while there is still a significant amount of residual aperture, the backstress on the fracture has not returned entirely to zero (which would only occur with full closure if the fracture aperture returned to zero). This helps to prevent an abrupt drop in compliance when closure occurred and can be one possible reason for a less sharp, curvier G*dP/dG plot. Since we do not know more geomechanics details of this reservoir, it could not be confirmed.

This backstress usually causes closure to begin at a pressure of 0-10000 kPa (a) higher than the original closure pressure. The closure pressure identified from Tangent method using FEKETE and FRACPRO(used by FenixConsulting©) comes to ~63400 kPa (a)(a) respectively. The value obtained from Fracture Compliance Method (~64400 kPa (a) (a)) comes in fair agreement with them for this field data.

(ii) Magnitude of closure pressure directly affects the pressure plots. A lower closure stress implies fracture has higher compliance when closure begins and as a result the G*dP/dG curve increases less abruptly. A closure stress value of ~ 630 bars fits well in low closure stress value range. On the other hand for high closure stress (for instance, 900 – 1000 bar), compliance at closure is very low, leading to an extreme contrast in compliance at closure, causing a very abrupt increase in the G*dP/dG curve

(G) - Conclusion:

1. From Table 6, values of all key parameters (fracture dimensions, permeability etc.) are in close match with each other.

2. Both Nolte, Soliman and Craig radial plot shows that the radial flow has just begun to develop when the data terminates. As a result. The permeability is too high.

   Subtle difference in results between different methods can be attributed to:

   - Constant Pressure (Nolte) vs. Constant Rate assumptions (Soliman)
   - Time function used.
   - The Shut-in point. Nolte assumed fluid movement continues until fracture closure, whereas Soliman assumed it stops at shut-in
   - Exact duration of linear and radial flow may vary depending on the manual interpretation as well as the different mathematical expressions of "time functions" used, but the essence remains that both the after-closure flow regimes were underdeveloped to give any reliable estimate. At best, the obtained parameters value can be taken as 'upper limit'.

3. IFO analytical model ((Van Den Hoek, 2016)) demonstrates the relative magnitude difference between a much larger fracture compliance /storage against well-bore compliance/storage while it isn't visible in FEKETE analysis. This crucial piece of information is almost always overlooked in current industry practice.

4. The methodology of the VdHoek's IFO analytical model is very different from the established industry method as used in FEKETE but the results are similar. This demonstrates that the VdHoek's analytical model when applied for mini-frac analysis even when the after closure flow regime are not well developed can give reliable estimates on par with established methods.

5. Comparison of the plots from VdHoek analytical model with the numerical plot shows that in the BCA and ACA time periods, there is good agreement.

6. Since the after closure reservoir flow regime was barely developed, it can be said that the permeability estimates obtained from either of the models maybe in fluctuation range of one order of magnitude too high.

7. The VdHoek analytical model for the *open* fracture gives a good representation of the pressure transient and its derivative prior to fracture closure. Therefore, this model can be used for Before Closure Analysis (BCA), from which one can obtain fracture compliance C_f(and from that fracture dimensions - length, height), fracture face skin, formation permeability (and from those: leak-off coefficient).

8. Any methodology where deviation of the pressure transient from linear behavior as a function of time (like in G-function, square root of time function) is interpreted as the point of fracture closure should be viewed with caution and definitely cross checked against independent tests for example, with inclinometer test.

9. The analysis done with FEKETE comprise of different approaches depending on Before closure time or After closure time. For example, before closure analysis is based on G-function, square root of time and pre-closure log-log diagnostic plots while for After-Closure, separate Nolte and Soliman - Craig approach was used. The analysis and results obtained from these distinct methods can be validated using "History Matching" against various 'in built analytical or numerical models' available for different well types, conditions and orientation (vertical or horizontal, with fracture or without fracture, conductivity of fractures, faults or no faults etc.)

   While a reasonable match between all these parts can be made for clean data sets when a long after-closure radial flow is developed however for cases like Example 1 where the radial flow was very small, interpretation can be a tricky affair requiring an analytical mindset and prior experience of working on similar data.

10. FEKETE gives the option of doing multiple analyses based on different widely used approaches conveniently. It's visible by above analysis that not all parameters obtained from a single analysis method give fool-proof results, like the estimated reservoir pressure obtained from ACA is although in close range to each other but still are four different pressure values. In such case, parameters should be chosen as best pick from different analysis plots using the analyst's expertise and matched against data obtained from other independent tests carried for same or analogous field. We have followed similar approach here.

11. Fracture Face Skin is very small because proppant free, brine water without any significant pollutant particulates was injected.

12. Care should be taken while identifying the shut-in point since it directly affects the pressure difference curve ($\Delta P = P_{shut-in} - P_{fo}$) where $P_{fo} = pressure\ after\ shut - in(fall\ off period\ )$.Incorrect identification of shut-in moment leads to erroneous pressure difference curve in the log-log diagnostic plot which affects flow regime identification, closure point etc. which in turn affects the estimated reservoir parameters values.

13. Using McClure's Fracture Compliance Method, the closure pressure value comes higher by 10000 kPa (a) against the value obtained from Tangent method, however it isn't the case more often than not as will be shown in later data sets. Residual fracture width is often overlooked during analysis in field condition's limited time, which is a potential reason of lower recorded closure stress.

5.2 - Example 2: Low Permeability Gas Well

Injection History

Example 2 and the next data set (Example 3) were taken from same reservoir. This data set comes from a vertical well at perforation depth of 2577 m from a dry-gas reservoir. Brine was used as fluid for injection. The formation height (net pay) was bounded by impermeable shale layers above and below. The pressure gauge recorded data per second providing detailed information about the associated pressure transient during analysis.

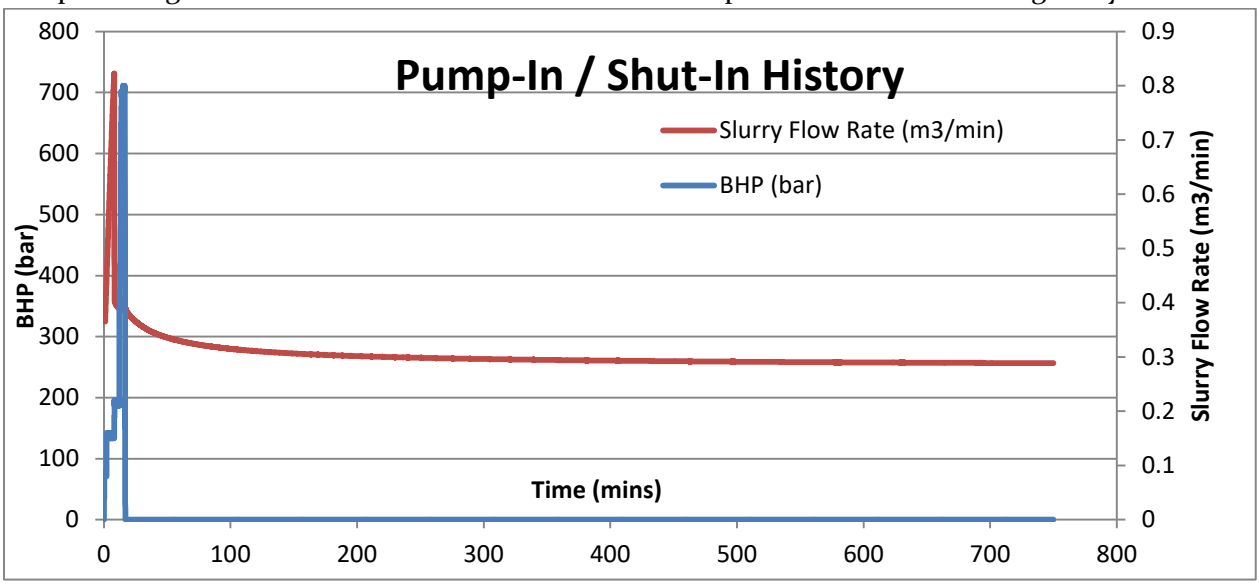

Figure 38 Injection/Shut-in History for Example 2 field data

Fig38. is a plot of bottomhole pressure (bar) on primary axis, injection rate (slurry flow rate) on secondary y-axis against the time (minutes) on x-axis representing the complete pump-in/shut-in history of the field data set named "Example 2". The plot shows that only one period of injection/ pump-in occurred lasting for 16.83 minutes (~0.28 hrs.), followed by considerably long shut-in time of 733.27 minutes (~12.2 hours).The shut-in period was 43.5 times than the injection period, which should give a good case of long developed radial flow as shown later.Fig.39 demonstrates a distinct water hammer period right after shut-in (highlighted with green circle). The shut-in point for analysis in both VdHoek model (Fig.39) and FEKETE (Fig. 41) was identified at approx. same point.

Difference in pressure value between the two models (344.2 bar vs. 351.77 bar) is because "pressure adjustment" was done in FEKETE to account for pressure difference between "Gauge depth=2450.90 m against Datum depth= 2577 m for the given fluid gradient=6kPa (a)/m". This led to adjusted pressure difference of 7.57 bars. Except water hammer period, the entire data recorded was clean with minimal noise.

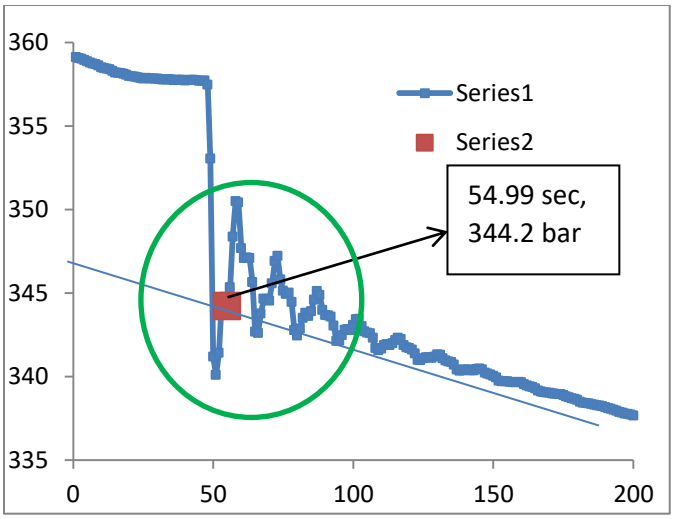

Figure 39 Water Hammer during early shut-in time – Example 2

Analysis using FEKETE:

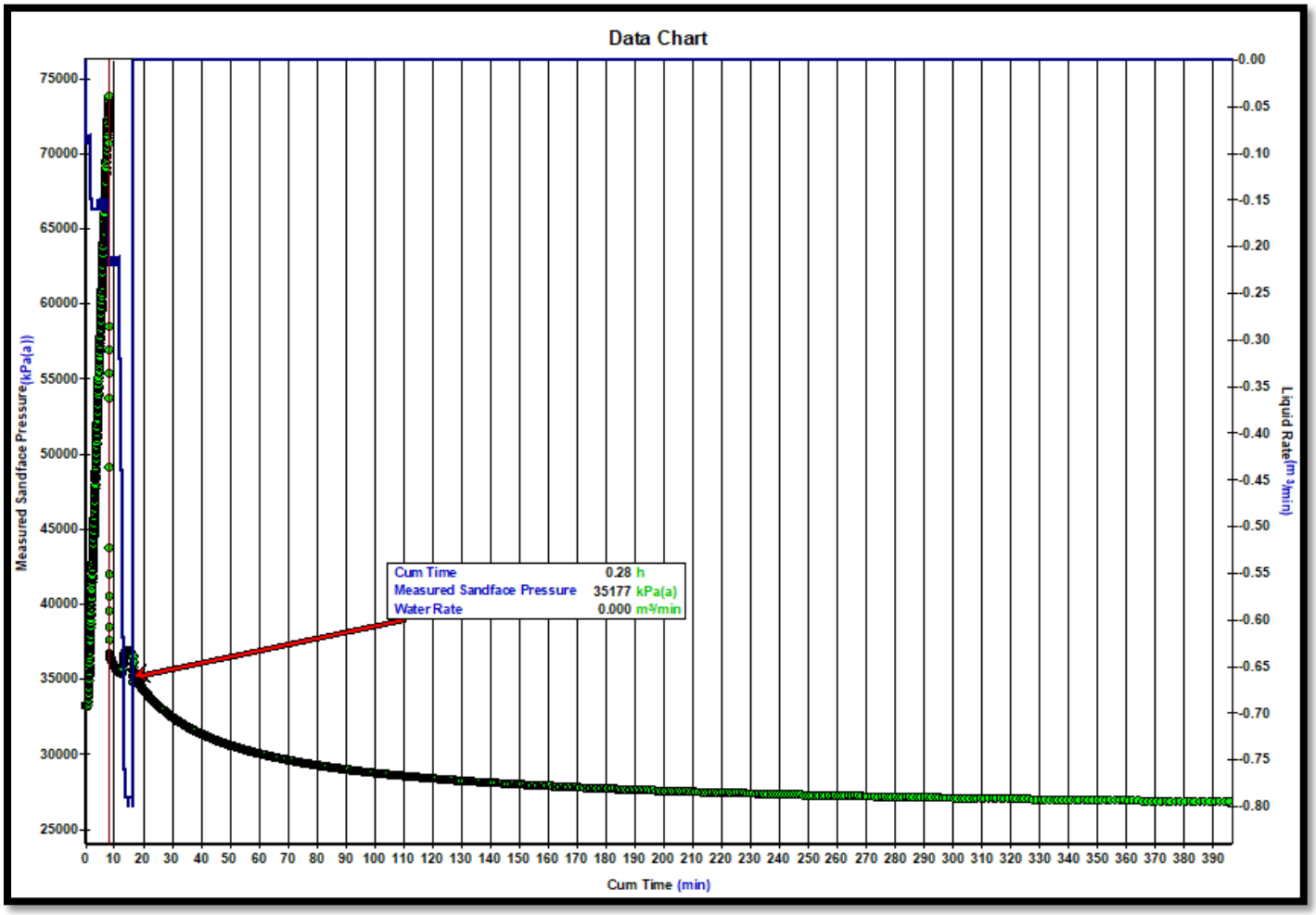

Figure 40 Injection / Fall off history

Fig 40 is a zoomed in version of early part of Fig.38. The red vertical line in it marks the start of actual injection into the formation at time 8.05 minutes Red annotation arrow is showing the shut-in point. Volume injected before it shown by a steady increase in linear pressure was used in filling wellbore volume giving rise to the wellbore storage. The analyzed portion of the minifrac test consisted of 3.945 m^3 of brine water, applied at

average injection rate of (-0.15 to -0.22) m^3/minutes The break down point identified by sudden drop in pressure (just where Start of Injection line is placed) was established at approximate injection rate of -0.15 m^3/min at measured sandface pressure (bottomhole pressure) of 73500 kPa(a), following short, stable fracture propagation period with approx. injection rate of -0.22 m^3/minutes The well was then shut-in to monitor pressure fall-off.

Table 7 Input parameters for FEKETE – Example 2

Parameters	Values	Unit
Initial Reservoir Pressure (P_i)	26500	KPa (a)(a)
Reservoir Temperature	85	°C
Net Pay/ Height of Formation	55	m
Wellbore Radius	0.107	m
Porosity	12	%
Initial Gas Saturation	65	%
Initial Water Saturation	35	%

With the aid of 'inbuilt correlations selected as *default*' in FEKETE for calculating other reservoir fluid parameters, a list of necessary parameters is obtained mentioned in Table 8.

Table 8 Value of calculated parameters from FEKETE – Example 2

	Parameters	Values	Unit
	Separator Gas Gravity	0.650	
Critical Properties	**Critical Temperature**	207.8	K
	Critical Pressure	4625.7	KPa (a) (a)
Properties at Initial conditions	**Gas Compressibility Factor (Deviation Factor)**	0.919	---
	Gas Formation Volume Factor (B_{gl})	4.37e-03	$m^{3/}$ m^3
	Gas Compressibility (Z_I)	2.9e-05	1/kPa (a)
	Gas Viscosity (μ_{gl})	0.0216	mPa.s
	Gas Density (ρ_{gl})	182.4	Kg/m^3
	Formation Compressibility (c_{fl})	6.54e-07	1/kPa (a)
	Initial Total Compressibility (c_t)	1.96e-05	1/kPa (a)

(A) Before Closure Analysis (Pre-Closure Analysis):

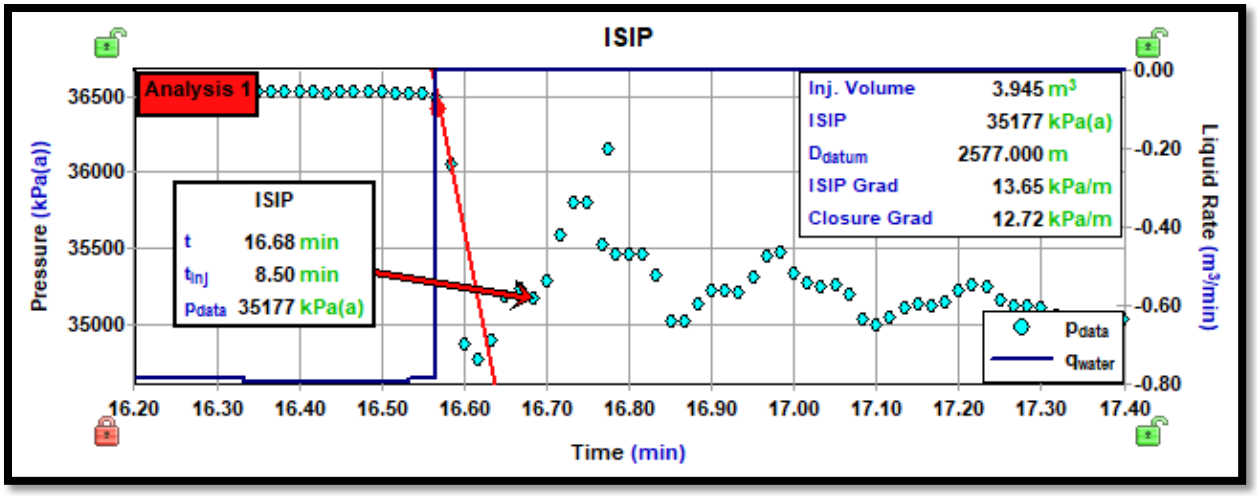

Figure 41 ISIP plot – Example 2

Total injection time (t_{inj}) (also called as pumping time,t_{pump}) is 8.54 minutes with an injected volume of 3.95 m^3.Fig. 41 is a Cartesian plot of pressure (kPa (a)) vs. time (minutes).Instantaneous shut-in pressure occurred at 35177 kPa (a), identified by placing a straight line on the early fall off portion of the fall data. The identified ISIP point is basically the shut-in point after adjusting the shut-in induced frictional pressure losses. Unlike Example 1, it can be noticed that the well experienced more friction immediately post shut-in visible by more scattered pressure points

Figure 42 is a plot of semi-log derivative (G*dP/dG) (primary y-axis), pressure (P) and first derivative (dP/dG) on secondary y-axis against G-function time. Unlike Fig.22 G-plot of example 1 where we saw clear concave up (*or a small linear trend->kink-> longer linear trend*), here we see a single linear line trend. The possible physical explanations (which are only speculative and were never confirmed on field) are as follows:

(i) Barree et al explanation: The plot shows behavior of "normal leak-off mechanism". Normal leak-off is observed when the composite reservoir system permeability is constant. The reservoir may exhibit only secondary natural fracture or fissure overprint in which the flow capacity of the secondary fracture system does not change with pore pressure or net stress. After shut-in the fracture is assumed to stop propagating and fracture surface area open to leak-off remains constant during closure.

At shut-in there is small volume of fluid stored in the fracture (V_{inj} = 3.95 m^3).Equation (96-please Refer Appendix C) shows that the pressure decline rate is directly proportional to the leak-off rate and inversely to the total storage/compliance. Pressure decline rate linearly increases with increase of leak-off rate (called as Normal Leak-off) until the point where fracture compliance term reduces to its minimal value with minimum surface area. This point of minimal storage/compliance corresponds to the fracture closure point.

(ii) McClure et al explanation: A clear sharp linear line is hard to identify in this case. Please refer to the later section "McClure's Analysis" for detailed discussion.

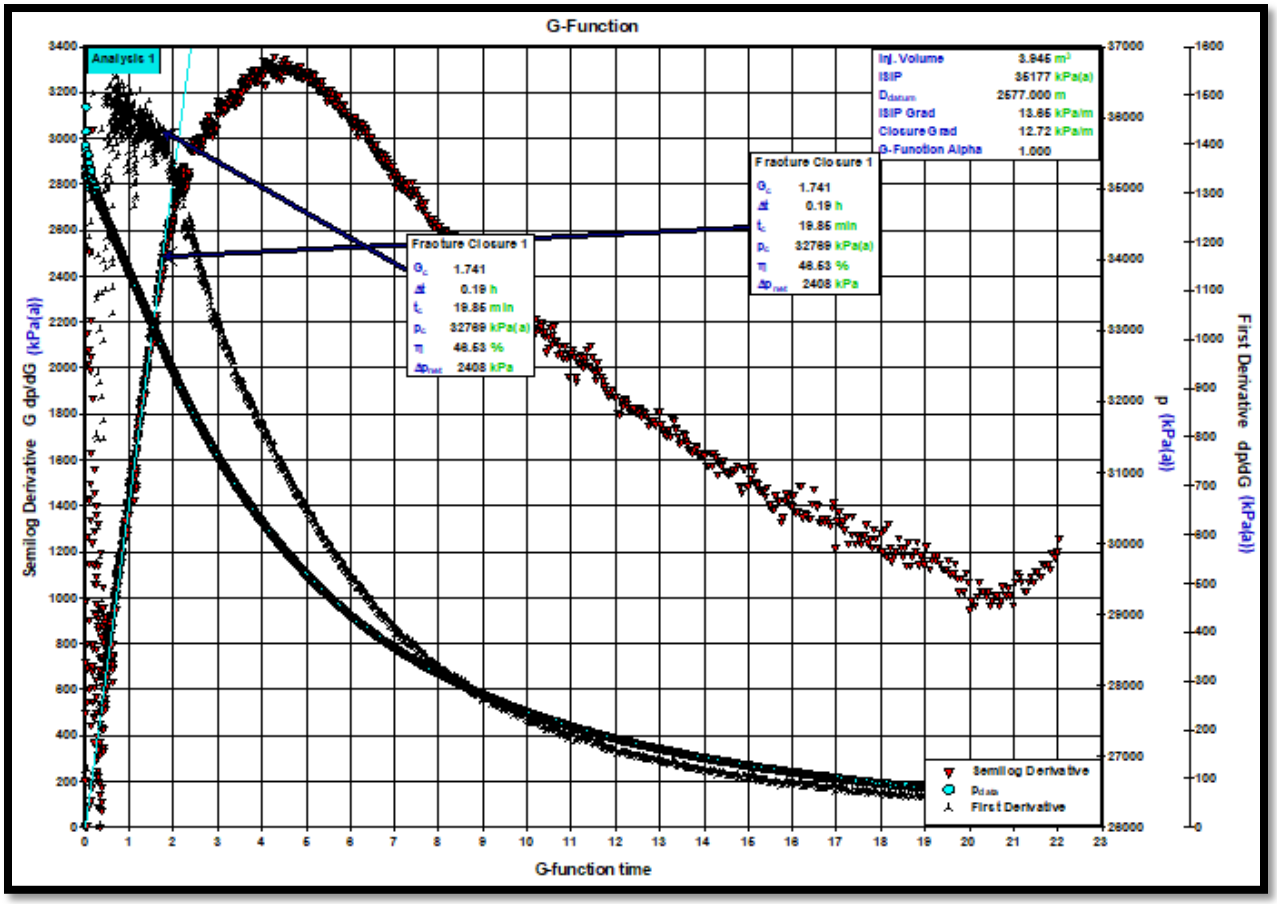

Figure 42 Pressure, First derivative and semi-log derivative of G-function curve against G-time – Example 2

A.1. - G-function analysis:

Fig42. The characteristic G-function derivative signature is a straight-line through the origin (Barree 1998). Fracture closure is identified by the departure of the semi-log derivative of pressure with respect to G-function (G*dP/dG) from the straight line through the origin. During normal leak-off, with constant fracture surface area and constant permeability, the first derivative (dP/dG) should also be constant. It indicates that fracture closure occurred after 10.42 minutes of the shut-in time at a fracture closure pressure of 32769 kPa (a). The value of fracture closure pressure and time (P_C and t_C) was obtained using standard "Tangent method"

Net Pressure value (ISIP – FCP) is 2408 kPa (a)(a). The magnitude is high, giving more energy for the fracture to propagate farther in low permeability surroundings which is confirmed later with a fracture height of 28 meters.

A.2. - Sqrt(t) Analysis:

The correct indication of closure is the maximum inflection point on plot of first derivative of pressure (p) vs. square root of time (sqrt(t)). The plot in fig. 43 shows that slope of the pressure derivative curve starts low, and then increases to reach a maximum rate of decline at the inflection point, decreases again after closure. Semi-log derivative of the pressure curve is also shown in the sqrt(t) plot. Identification of closure pressure based on departure of data from semi-log derivative straight line trend similar to the way G-function closure is picked is incorrect method and leads to a late closure pressure.

For this case, the sqrt (t) plot (Fig.43) shows a clear indication of closure based on the first-derivative inflection point (highlighted with green circle).

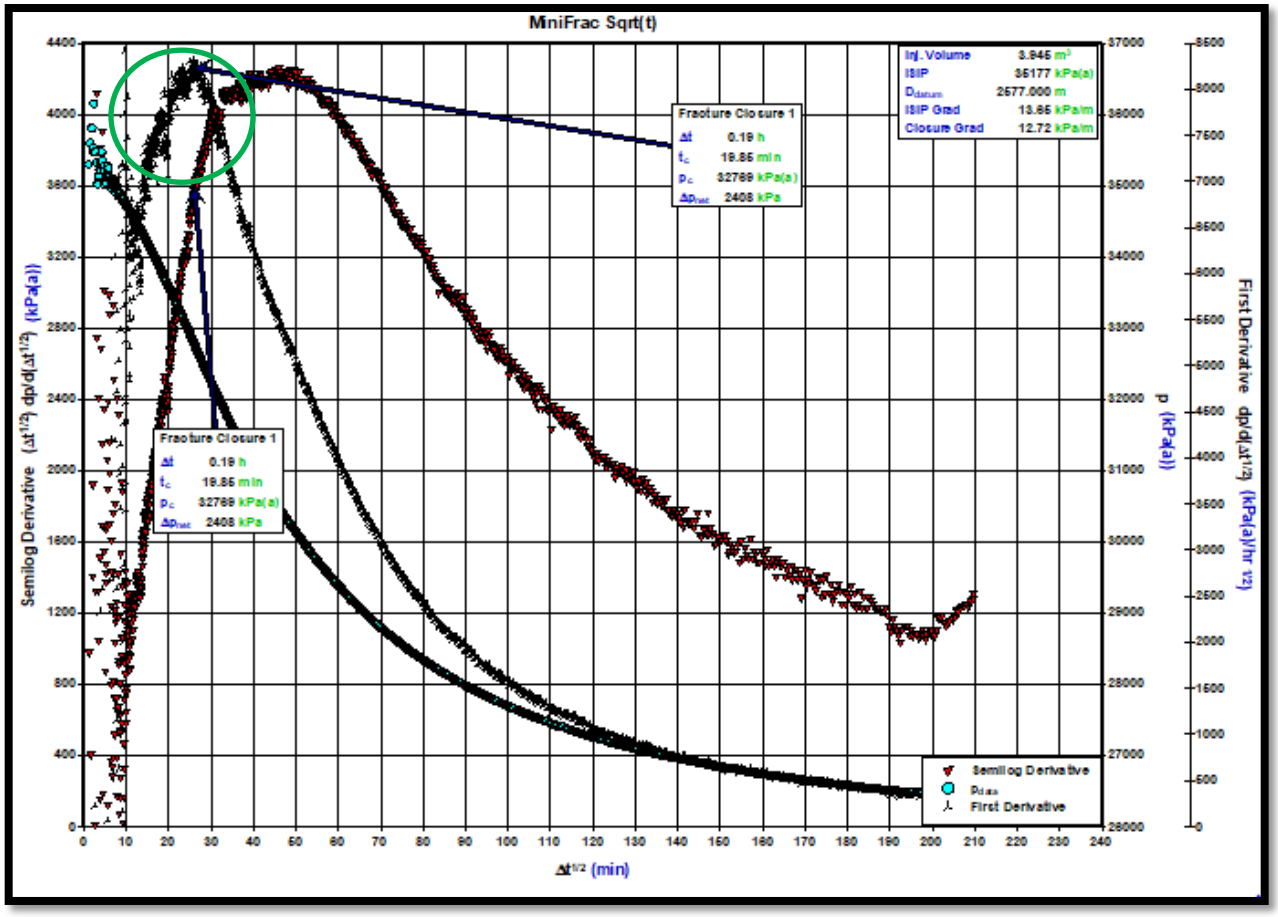

Figure 43 Pressure, First derivative and semi-log derivative of Sqrt(t) function curve against Square root of time – Example 2

A.3. - Pre-Closure Log-Log Pressure Derivative plot:

The log-log plot of pressure difference (green curve) and semi-log derivative (red curve) (on y-axis) against the shut-in time (x-axis) is shown in fig.44. Prior to closure here, we see a short storage flow regime (slope=1) followed by a fracture linear flow regime (slope= 0.5). Fracture linear flow regime is rarely noticed in field though.

The accurate storage flow identified with slope 1 is for very short time (Δt = 0.01 – 0.08 = 0.07 hrs. = 4.1 minutes) followed by fracture linear flow period time (Δt = 0.25 – 0.13 = 0.12 hrs. = 7.3 minutes). Using Barree's rule of thumb that no data should be analyzed until three times the closure time has passed. This condition is easily satisfied here as closure time is Δt=0.19 hrs. while the data sets terminate only at Δt= 11 hrs. Three times the closure time is 0.57 hrs. The data extends roughly 21 times post that time period.

Following closure, formation linear flow period is visible for long duration of (Δt=5.16hrs - Δt=1.29 hrs= 3.87 hrs= 232 minutes).The radial flow characterized by a slope= -1 starts developing at Δt = 7.67 hrs. ends at 10.62 hrs. lasting for 2.95 hrs.=177 minutes when the test was terminated. Formation linear and Radial flow period are well developed for this case which results in giving a reliable estimate of reservoir pressure, permeability and fracture dimensions as demonstrated later.

Paul van den Hoek (Van Den Hoek, 2016) suggested that unlike the established trend of taking end of linear storage line or deviation from first linear line as point of fracture closure, the real point of fracture closure cannot be confirmed with absolute certainty by above methods. Point of fracture closure may or may not agree with the standard methods proposed by Barree et al or McClure et al. To validate it, more discussion follows under "Numerical Model plots" section of Example 1

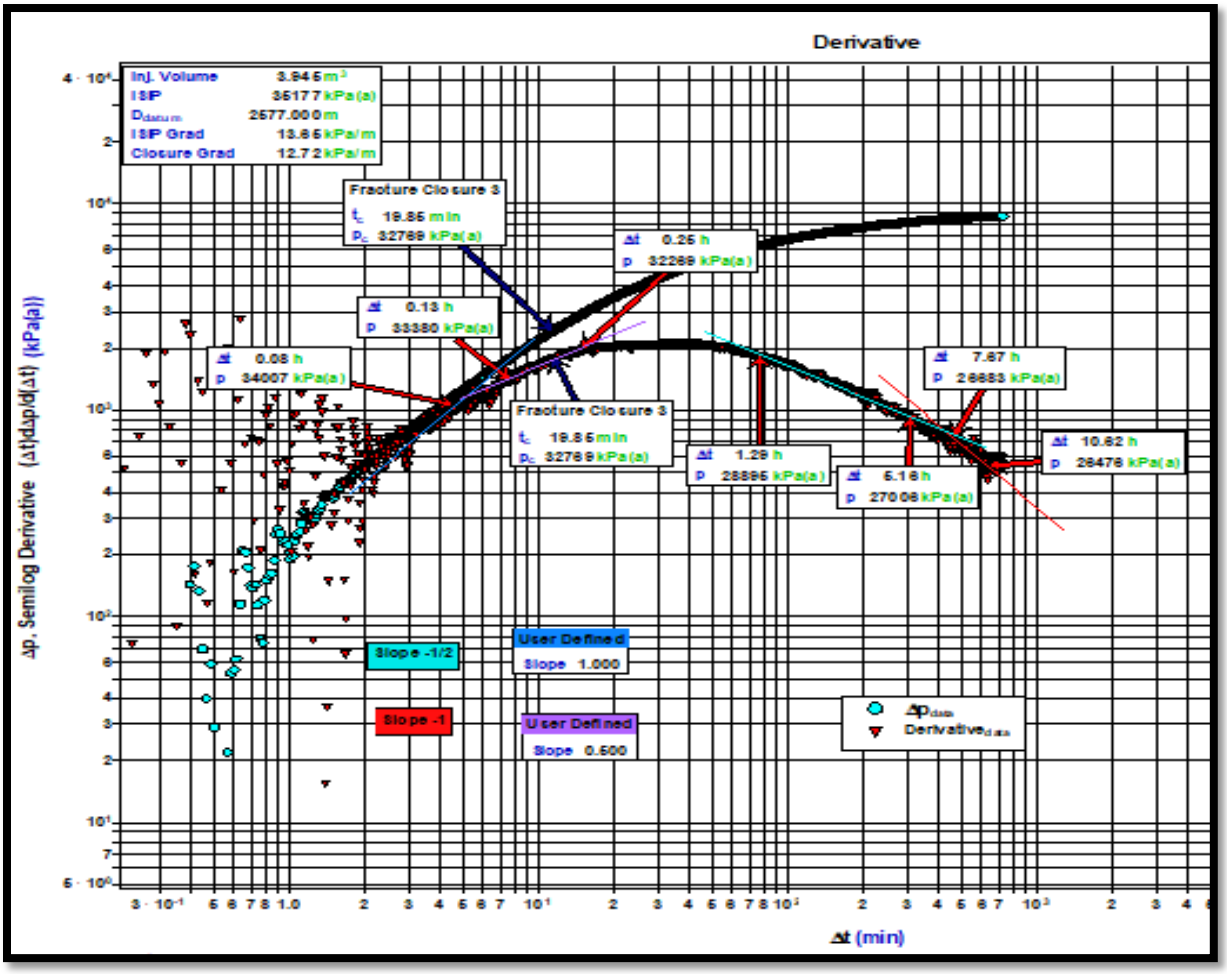

Figure 44 log-log plot of pressure difference and semi-log derivative – Example 2

(B) After Closure Analysis (ACA):

The after-closure analysis will serve to validate the finding from Before Closure Analysis and confirm if the reservoir and fracture estimates are reliable.

B.1. - Nolte ACA analysis:

Fig. 45 shows analysis plots done using Nolte method. Top Left is a Cartesian plot of pressure vs. Nolte Linear time function used in establishing formation linear flow. Top right is Cartesian plot of pressure against Nolte radial function used in establishing/identifying formation radial flow. Fig46 is the pressure difference and derivative against square of nolte time on log-log diagnostic plot.

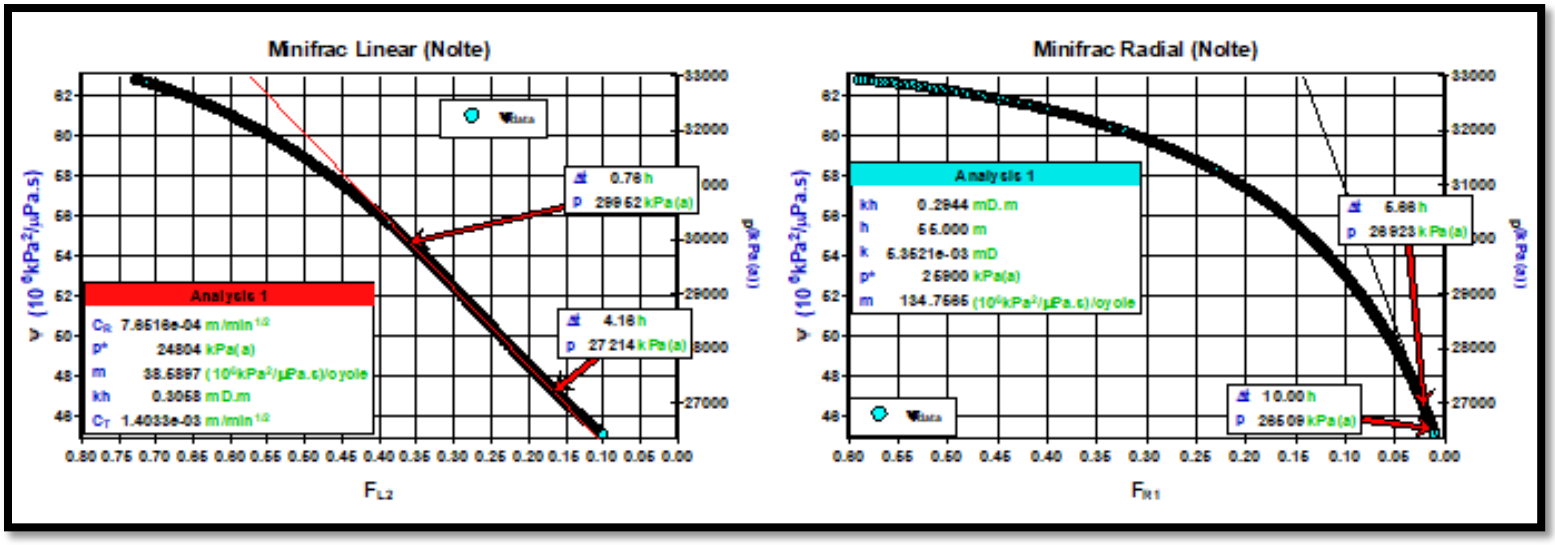

Figure 45 Nolte Analysis – (Left = Cartesian Linear plot of pseudo pressure against Nolte Linear time (F_L) ; Right = Cartesian Radial plot of pseudo pressure against Nolte Radial time (F_R)

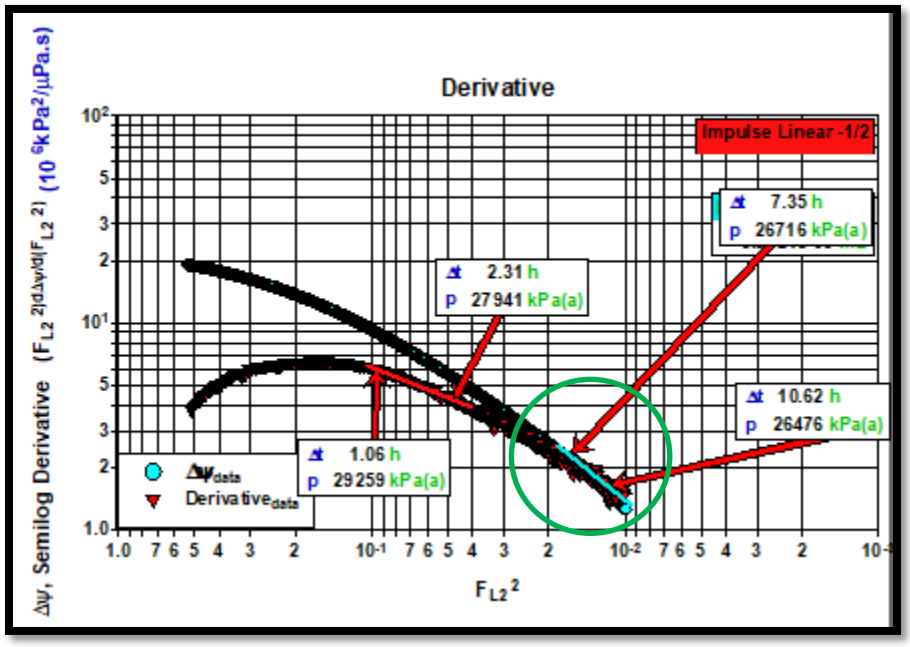

Figure 46 Log-log plot of pressure difference and semi-log derivative vs. F_L^2)

1. Here, linear flow (identified with slope=-1/2) and radial flow are well identified. Radial flow is identified when the pressure difference and pressure derivative coincide on same line with slope=-1 on the derivative plot. (highlighted with green circle)

   Since radial flow is properly developed here visible for atleast four hours (Δt_radial = 4.24 hrs.) after formation linear flow regimes end, p* (extrapolated pressure) and permeability was estimated using Eq.46. The permeability calculated 5.35 x 10^{-18} m^2. Extrapolated pressure (p*) was estimated from extrapolation of linear line to F_{R1}=0. Radial flow portion of after-closure data has a straight line trend on pressure vs. F_{R1} - Cartesian plot (Fig.45 - right) with estimated post-closure radial flow time of 4.24 hrs.

2. With a long linear flow period of 3.4 hrs. (Fig.45 - left plot), using Eq.42, reservoir leak-off coefficient, C_R and total leak-off coefficient, C_T is 7.6 e-04 m/$min^{1/2}$ and 1.4 e-03 m/$min^{1/2}$ respectively. Permeability (k) is taken from Nolte Radial flow plot = 5.35 * $10^{-15} m^2$, $\emptyset$ = 0.12, initial total compressiblity c_t= 1.96e-05

(1/kPa (a)) and μ = 0.021cP. $\Delta p_{Total} = p_c - p_i$ where p_i is taken as the extrapolated initial pressure = 24804 kPa (a). This is done only when permeability from radial flow and closure pressure (P_c) from before closure analysis is known.

Leak-off coefficient values obtained here comes in good match with the values obtained from IFO analytical model.

3. Extrapolated pressure value has different value for linear (24804kPa (a)) and radial flow plots (25900kPa (a)). Comparing with the known original reservoir pressure of 26500 kPa (a), the maximum deviation comes to be at 8.1 % which is in the accepted tolerance range.

B.2. - Soliman and Craig ACA Analysis:

Fig. 47 is a pressure difference and impulse derivative against adjusted shut-in time (Δt_a) log-log diagnostic plot. Fig. 47,48 shows all analysis plots obtained using Soliman and Craig method. Fig. 48 Left is a Cartesian plot of pressure vs. $\left(\frac{1}{t_p+\Delta t}\right)^{0.5}$ used in establishing formation linear flow. Fig. 48 Right is Cartesian plot of pressure against $\left(\frac{1}{t_p+\Delta t}\right)$ used in establishing/identifying formation radial flow.

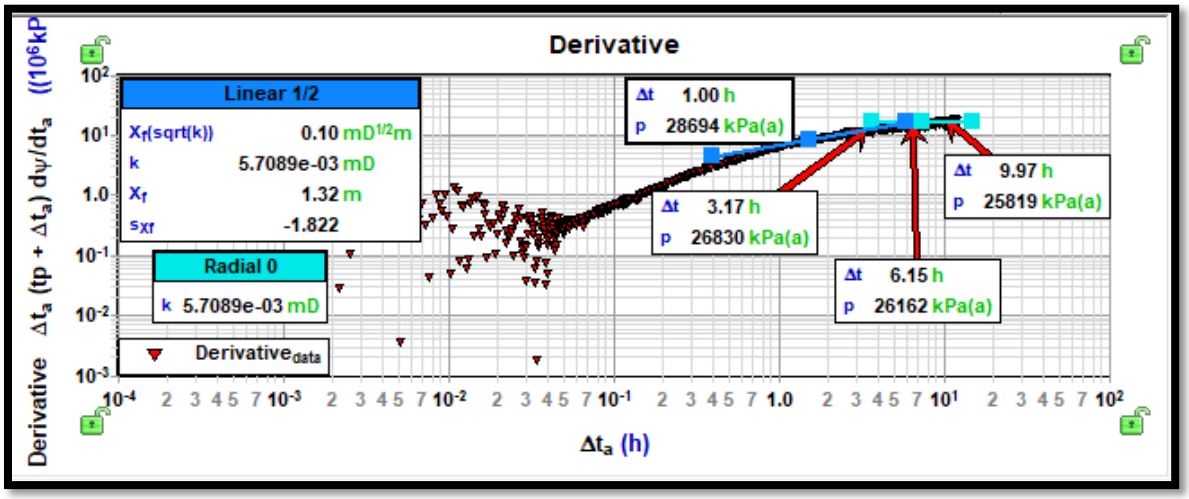

Figure 47 Soliman-Craig Log-log plot of Impulse derivative vs. adjusted shut-in time (hrs.)

The analysis done with these figures are as follows:

(i) Impulse Derivative plot: The derivative plot identifies a well-developed formation radial flow period with an approx. duration 3.34 hrs. Using eq. (22) on radial flow plot of fig. 48, pressure against time gives a slope $m_{R_1} = \frac{(0.000014\frac{\pi}{2})V_{inj}\,\mu}{kh}$. With inbuilt feature of auto calculation of slope (m_{R_1} = 16.89 ($\frac{10^6 kPa^2}{(\mu Pa.s)}$ / *cycle*), and using input values from Table 7 and 8 (h=55m, V_{inj}= 3.945 m^3, viscosity of the reservoir fluid = 0.021 cP), the value of permeability (k) estimated is 5.41*10^{-18}m ^{2}. This value of permeability in microdarcy range (10^{-18}) falls in line with the estimated value from other analysis methods and models.

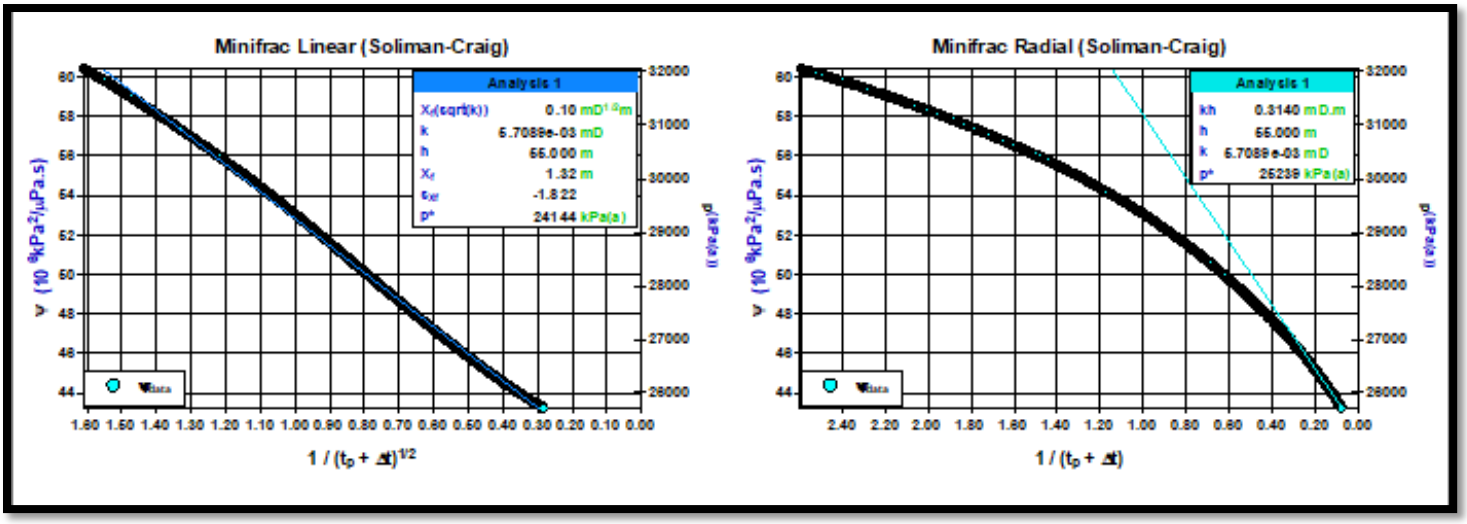

Figure 48 Left Soliman-Craig cartesian plot of pseudo pressure vs. (1/(t_p+delta_t))^0.5 ; Right = Soliman-Craig cartesian radial flow

(ii) Impulse Linear Flow plot: Formation Linear flow period continued for decently long time (1.93 hrs.) evident from the derivative plot. It is a reasonable time frame to calculate reliable fracture half length. Using eq. 35 on fig. 48 (left) such that for a plot of pressure vs. time gives the slope $m_L = (0.00424\frac{\sqrt{\pi}}{2})\frac{V_{inj}}{h}\left(\frac{\mu}{\emptyset c_t k L^2}\right)^{0.5}$. The input parameters are taken from table 7 and 8. Resulting half-length value (L) is estimated to be 1.32 m.

(iii) Extrapolated pressure value from the Cartesian linear and radial flow plot comes out to be 24853 kPa (a) and 25919 kPa (a). Estimating the deviation factor against the original value of p=26500 kPa (a), the deviation measure is 8.8% and 4.7 % respectively. This range comes under the accepted tolerance limit.

(C) - History Matching

Since the formation flows are well-developed here, a good history match was expected. For achieving it, an inbuilt model of "Fracture with boundaries" was adopted. The input parameters used are same i.e. taken from table 7 and 8.

This model simulates the pressure response in a vertical well intercepted by an infinite-conductivity vertical fracture within a rectangular-shaped reservoir with homogeneous or dual porosity characteristics (see figure 49). This well may be at any location within the reservoir and the model supports infinite, no-flow, and constant pressure boundaries. Thus, classical configurations like a well near a sealing fault, or a constant pressure boundary near intersecting faults can be easily modeled.

For our case, we have neglected complex phenomena like dual porosity feature and considered "no flow" boundaries since the net pay height is surrounded by impermeable shale layers above and below.

At very early times, the cylindrical source solution is used, which is followed by Green's function solutions. The Green's function solution, as developed by Thompson et al. (1991) with slight modifications, is used to simulate an infinite-conductivity vertical fracture. No-flow boundaries are modeled using the method of images. The result is superposed in time based on the rate history provided.

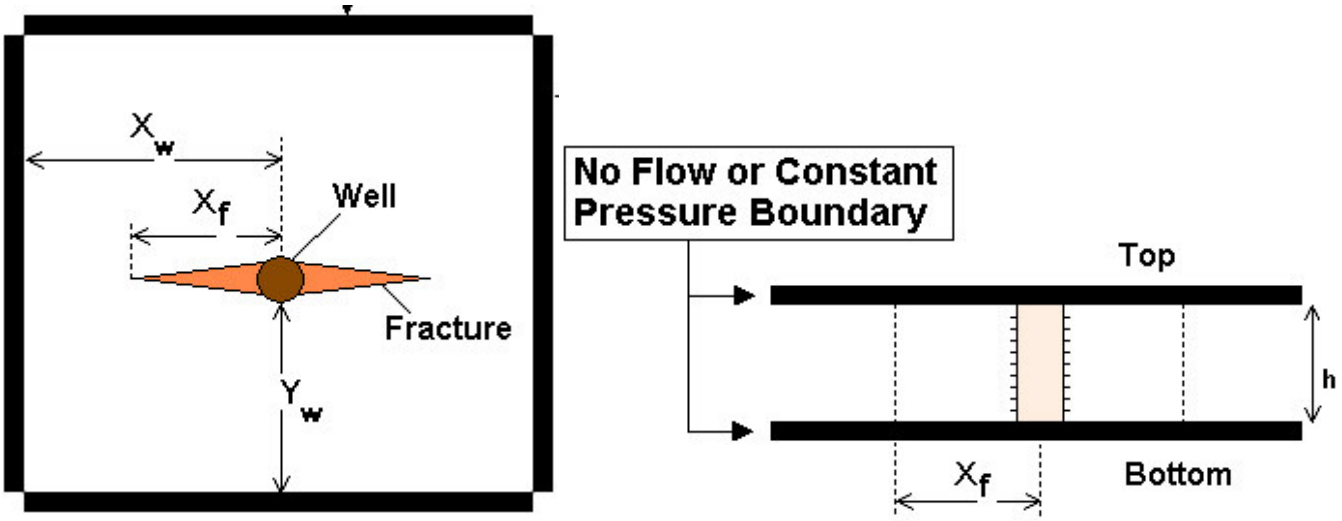

Figure 49 (Note that L = fracture half –length = L in nomenclature used in other parts of this report)

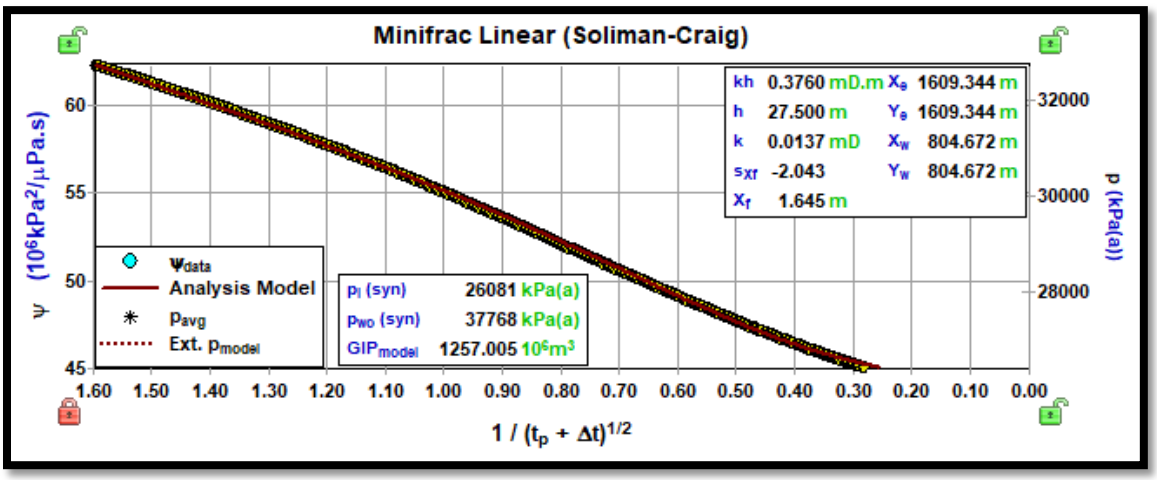

Figure 50 Pressure vs. time (based on Soliman and Craig method) – History matching plot

Fig. 50 and 51 are linear and radial flow plots; fig.52 is history matching while the fig.53 is impulse derivative log-log diagnostic plot. A good match is identified from a long superposition of synthetic data (red line) of analysis model against the field data (green circles) in both plots. Permeability values obtained is in nanodarcy (10^{-18} m^2) while the fracture half-length is 2.24 meters. Synthetically identified pressure value is 26081 kPa (a), which is only 1.58 % deviation from the original initial reservoir pressure value of 26500 kPa (a). Fig. 53 is a match between derivative_data and derivative_model with a good superposition of data between the two models from the shut-in time of 0.15 hrs. – 10 hrs. The general idea of using history matching plot using any particular model against the field data is to understand how well and long the field data matches/superpose over model's synthetic data. The values obtained using "Fracture with boundaries model" is in good confidence comparing the value obtained from VdHoek analytical model as will be discussed later in the "Comparison between model" section.

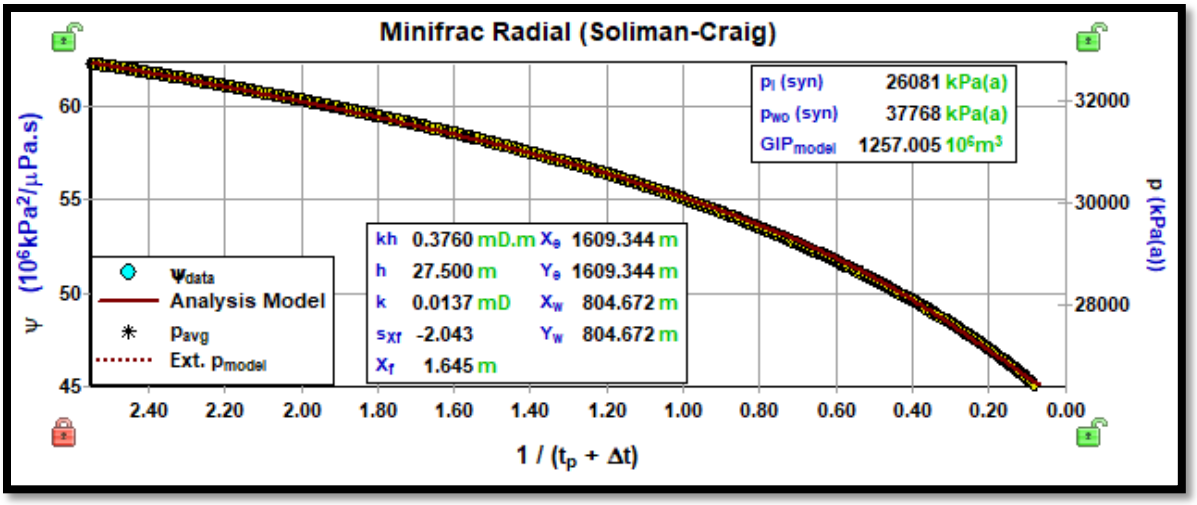

Figure 51 Soliman and Craig Radial flow – History Matching plot

Fig.52 is history matching plot of field vs. model pressure data (kPa (a)) (primary y-axis), (%error on secondary y-axis) against post shut-in time (hrs.) showing the error percentage between the two. As can be seen, the error margin is less than 0.5% indicating a good match with high confidence.

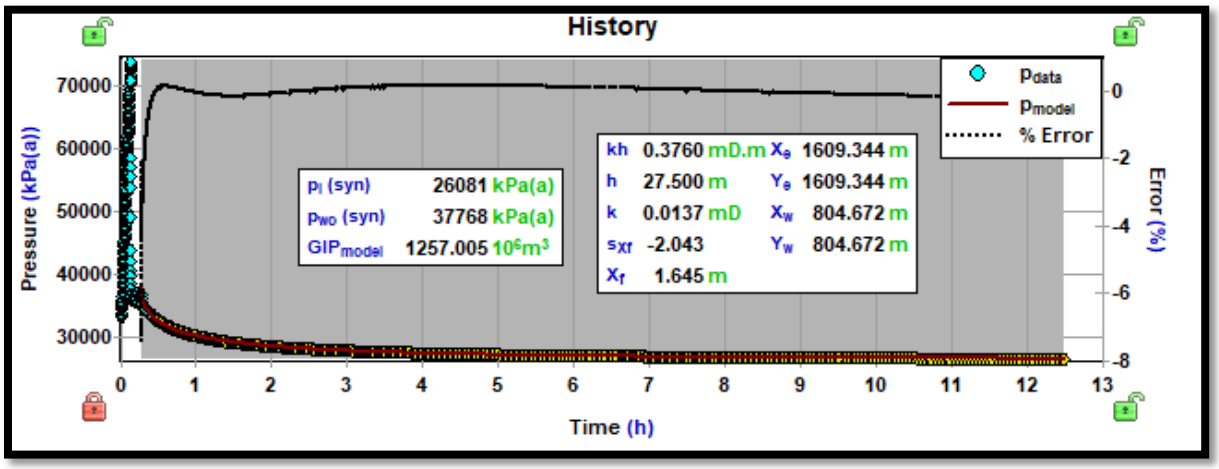

Figure 52 Soliman and Craig Pressure vs. time – After shut-in history matching plot

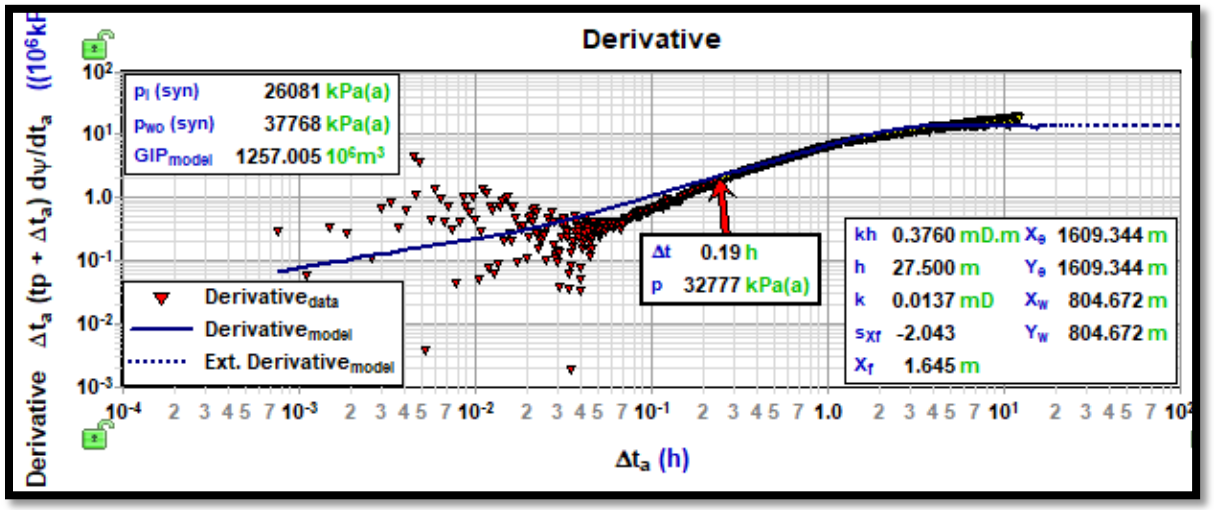

Figure 53 Soliman and Craig derivative vs. time – History Matching plot

(D) - VdHoek Analytical Model:

In order to provide a good comparison with 'specialized plot' methodology, we estimated the fracture and reservoir unknown parameters using the analytical model as mentioned in Appendix (B).

Table 9 Input parameters for VdHoek analytical model – Example 2

Porosity	0.12	[-]
Fluid Compressibility	3.13 E-08	Pa^{-1}
Reservoir fluid viscosity	0.00002	Pa*s
Injection fluid viscosity	0.0003516	Pa*s
Young's modulus	6.89	GPa
Net pressure	170	Bar
Fracture height	43.5	m
Injection rate	0.01316	m^3/sec
t_{pump}	6.484	min

Fig.54 shows a log-log diagnostic plot of delta pressure and derivative against shut-in time obtained from the vanden Hoek's analytical model. The maximum analysis time was chosen as 10 hrs. Δt = 0.19 hrs. was the closure time (highlighted by a green vertical line) identified from FEKETE BCA plot. In "standard methodology", it is common for the pressure difference and derivative curves to be parallel or coincide on same line of slope=1 from early time until before closure. The slope of these parallel/coinciding lines is diagnostic of the flow regime established. Using this approach, we do see that the pressure difference and derivative plot starts deviating from each other roughly at 0.17 hrs. which affirms that the closure pressure should occur at that point if "standard methodologies rule" are followed.

As demonstrated in example1 VdHoek numerical model plots, it is entirely possible that what are observed as the fracture closure point in every analysis technique using standard methodologies can just be a point where storage/compliance ends and not a definite proof of the fracture closure point.

Table 10 contains values of all output fracture and reservoir parameters estimated using the analytical model. The permeability value is in microdarcy, implying a low permeability reservoir. This low permeability of the formation rocks leads to the fracture showing a storage dominated growth where the leak-off rate is very low (0.00557554 m^3/sec). The estimated leak-off rate $Q_l(t_{pump})$ is done under the assumption that during pumping, leak-off rate is one-dimensional (following Carter's leak-off assumptions). Hence under Carter's assumptions, for storage dominated flow, leak-off rate is calculated from Nolte (1986) from eq.49 where, $|Slope|$ is the absolute value of pressure decline slope at shut-in, V_{inj} is the cumulative injected volume at the end of pumping period, and the net pressure = ISIP -FCP

From fig.54, it is visible that the early time flow is fracture storage dominated with slope=1, but the duration of the flow is relatively short (0.01 –0.17 hrs). With the obtained value of C_f using expression 61) for an elliptical fracture (mentioned in Appendix B) in combination with the input data given in Table 9, fracture half-length value of 6.37 m was obtained. Subsequently, formation permeability (k = $2.42*10^{-18}$ m^2) and fracture face skin (S = 0.036) respectively was calculated. A good fit was obtained between the field data and model up until the very

end of field data. This good fit is in contrast to the fit obtained for Example 1 plot (Fig.30) stressing the fact that a long post closure flow period is critical for reliable estimates of parameters. Here, the fracture dimension results comes in good agreement with the specialized technique plots as used in FEKETE but any disparity if any, in dimensions can be attributed to the different fracture geometry models (PKN or Radial for Specialized plot vs. elliptical used here)

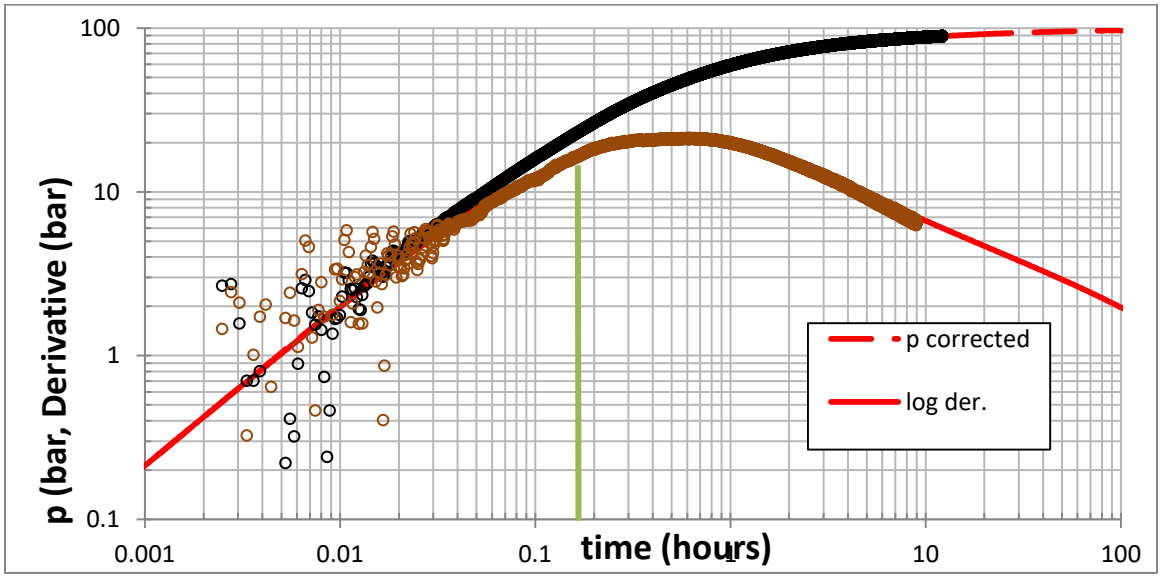

Figure 54 Log-Log pressure difference and derivative diagnostic plot (VdHoek Analytical model)

(E) - Comparison between FEKETE (Specialized Plot) vs. VdHoek's Analytical Model

Table 10 shows the value obtained from standard analysis methods of BCA and ACA using FEKETE vs. the value obtained from VdHoek analytical model:

Table 10 Comparison between FEKETE vs. VdHoek model – Example 2

Parameters	Unit	Plot from where value came in FEKETE analysis ***	FEKETE	VdHoek Analytical Model
Volume Injected	m^3	NA	3.945	5.12
Injection rate	m^3/sec	NA	0.0076	0.01316
Injection time	min	NA	8.54	6.484
Fracture Half-length	meter	Frac Boundary model	2.236	6.37
Fracture height	meter	NA	55	43.5
Permeability	m^2	Frac Boundary model	$2.31*10^{-18}$	$2.4*10^{-18}$
Net Pressure	kPa (a) (a)	BCA – G-function, Sqrt(t) plot	2655	2000 (estimate)
Skin (Frac Face Damage)			0	0.036
Total Leak-Off coefficient	(m/sqrt(sec))	Nolte ACA Linear plot	$1.8\ *10^{-4}$	$0.24\ *10^{-4}$
Initial Total	Pa^{-1}	Properties Tab	$1.96*10^{-8}$	$3.30\ *10^{-8}$

Compressibility (c_{tl})				
Time to Fracture Closure	min	BCA – G-function, Sqrt(t) plot	18.79	Cannot be estimated
Pressure at fracture closure time	kPa (a) (a)	BCA – G-function, Sqrt(t) plot		Cannot be estimated
Instantaneous Shut-In pressure (ISIP)	kPa (a) (a)	BCA – G-function, Sqrt(t) plot		Cannot be estimated

* Frac Boundary model - based on Soliman and Craig ACA method
**NA = Not Applicable
*** = For reason, please see pt. (9) and (10) of 'Conclusion' section of Example 1

A detailed discussion about the values estimated from both models is mentioned in "Conclusion" section, a quick preview shows that values of unknown parameters are in same order range.

Determined permeability value from pre-closure analysis by FenixConsulting © in-house analysis yielded result of $14 * 10^{-18}\ m^2$. This values matches strongly against the permeability value obtained from VdHoek analytical model (k= $2.4 * 10^{-18}\ m^2$) and the value obtained using FEKETE $2.31 * 10^{-18}\ m^2$ highlighting the fact that well-developed after closure flow regimes is crucial to get reliable estimate of unknown parameters since later these parameters are used as input for much expensive procedure of fracture treatment design and stimulation.

(F) - McClure's Analysis:

Fig. 55 is a zoomed version of early part of the plot from Fig.42 to identify the first sharp point of deviation from linearity on a plot of pressure or G * dP/dG vs. G-time. As per McClure's recommendation to identify fracture closure, the first linear line occurs at very early time leading to a higher closure pressure value than the value obtained from G-function plot. A sharp break point between two linear lines is however very difficult to see in field data, attributed to complex fracture geometry. Here as well, a clear sharp line isn't easily identifiable. There were possible two spots: (i) one at yellow circle (ii) second one at red circle

Point (i) wasn't a good choice (although we notice a small breakage between two possible linear lines) because data are highly scattered there with high noise.

Point (ii) was a better choice. A small break (red circle) was noticed between two lines. Beginning of the second line was a better bet for fracture closure point at 33581 kPa (a) (a). This fracture closure pressure value is ~ 7800 kPa (a) (a) higher than Tangent method. Verification of the result couldn't be done since the closure value given by FenixConsulting(c) was done using Tangent method, with no other independent source to confirm.

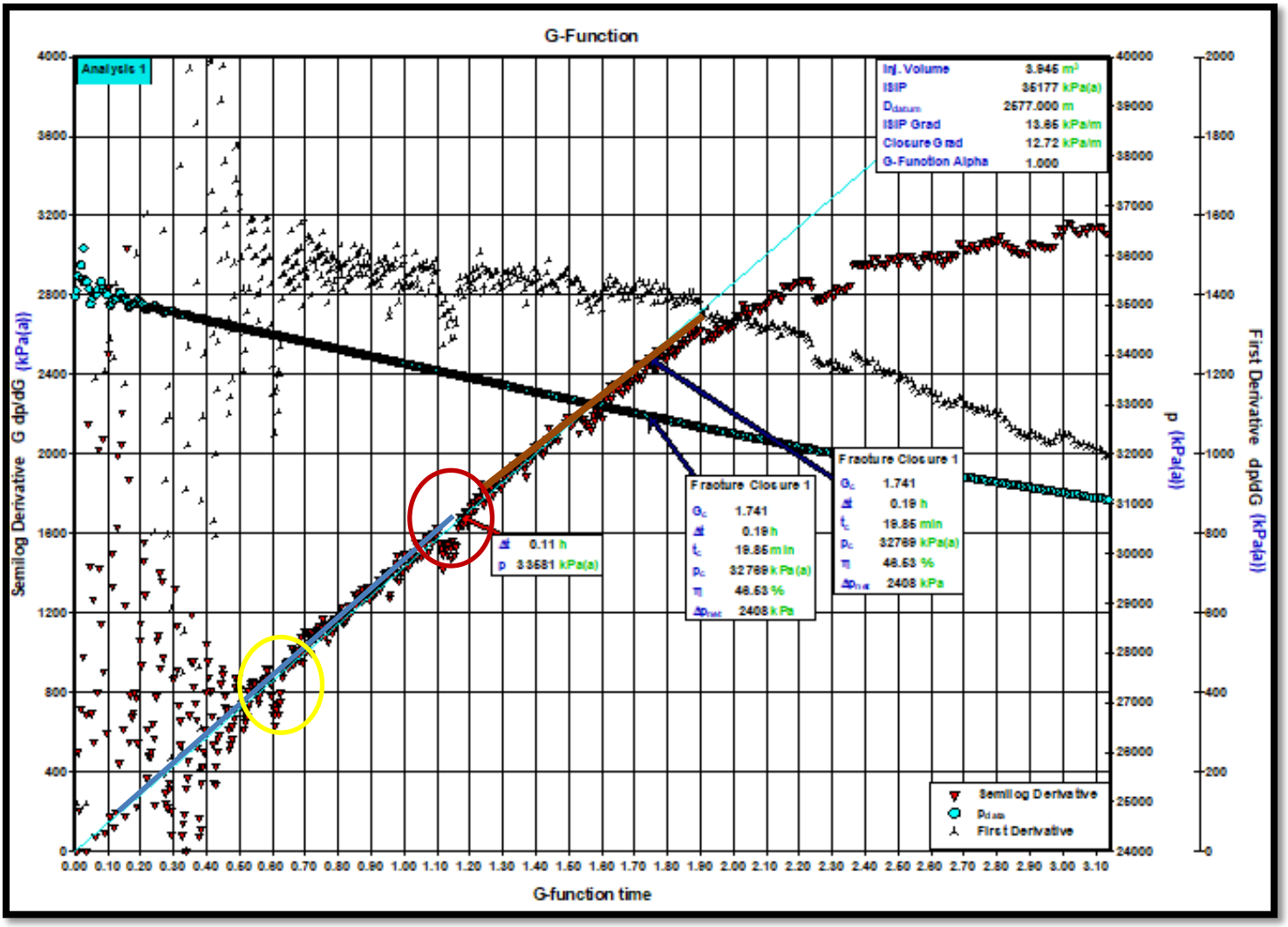

Figure 55 Zoomed in plot of early portion of Example 2 - Pressure or G * dP/dG vs. G-time

(G) - Conclusion:

1. From Table 10, values of all key parameters (fracture dimensions, permeability etc.) are in close match with each other.
2. Both Nolte, Soliman and Craig linear and radial plot show a well-developed after closure flow regime. This flow regime helps in correct estimation of fracture dimensions (length and height), permeability, reservoir and total leak-off coefficient
3. VdHoek analytical model demonstrates the relative magnitude difference between a much larger fracture compliance/storage against well-bore compliance/storage while it cannot be demonstrated using standard (FEKETE) analysis.
4. VdHoek analytical model results are in same range with the results obtained from standard (FEKETE) analysis (see Table 10). This demonstrates that the VdHoek's analytical model when applied for mini-frac analysis for a suitably long after closure flow regime gives reliable estimates on par with established methods. A match of ACA and BCA plots using Numerical model of analytical model was desirable but due to limited time, it could not be performed.

5. Fracture closure point may or may not be at 328 bars as estimated from standard approaches, indicating it may only indicate end of storage regime. To validate, further research work using VdHoek Numerical model and other independent tests should be carried out in future.

6. Care should be taken not to identify closure pressure from semi-log derivative of sqrt (t) plot using Tangent method. This leads to lower valued wrong closure pressure.

7. Since the field data here is long enough to highlight all possible flow regimes, it was a good candidate for "History matching" using independent models to validate the results. The analysis done and results obtained using standard analysis technique employed in FEKETE are validated here against "History matching" using an in-built "Fracture with boundaries model". The match between synthetic data, automatic estimated parameters (APE) using "Marquardt-Levenberg (QR Factorization) is in excellent agreement with the values derived from standard BCA/ACA techniques.

   This is in contrast against the history matching plot for example 1 where a lesser confidence limit for the values was observed between the standard analyses derived vs. model derived values

8. Fracture Face Skin is very small because proppant free, brine water without any significant pollutant particulates was injected.

9. Using McClure's Fracture Compliance Method, the closure pressure value was determined at 33581 kkPa (a)(a).While the McClure approach offers a new perspective to identify closure pressure, but evident from analysis of example 2 and 3 data sets (shown later) it is hard to implement it on field data, since field data are never perfect, contains noises and scattered especially at early times. A sharp linear rise after a small linear line is also not seen on field data which shows that the fracture geometry is much more complex than the general assumption we take in our studies of a "simple bi-wing planar fracture"

5.3- Example 3: Low Permeability Gas Well

Injection History

The brief introduction about this field data is covered in Example 2 introduction section as both these data come from same reservoir.

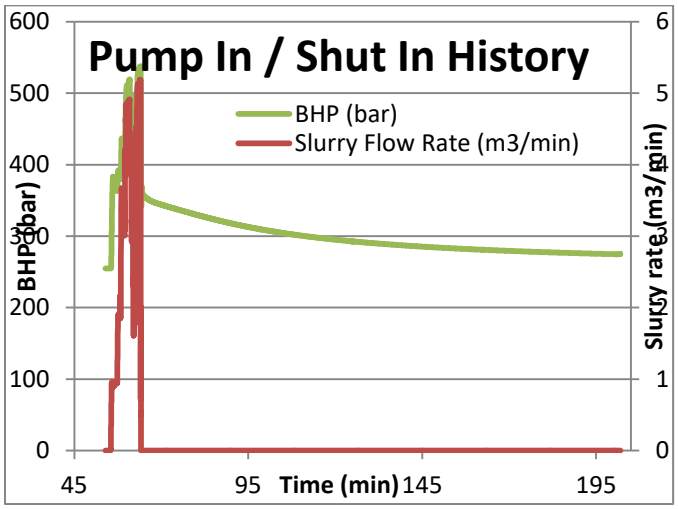

Figure 56 Total Injection/Shut-in History for Example 3 field data

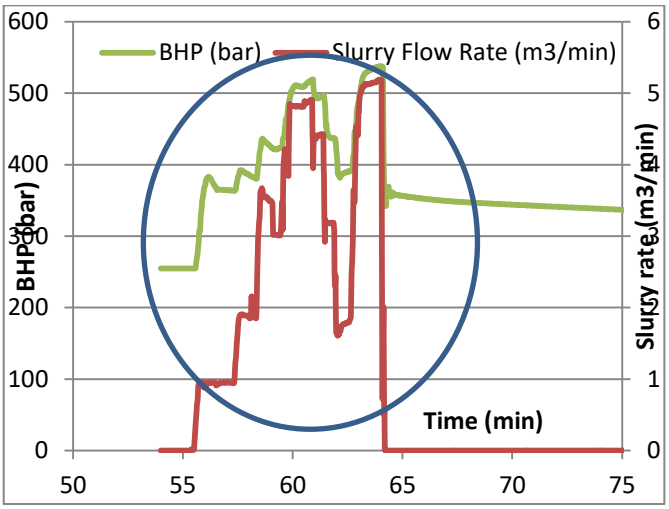

Figure 57 Zoomed in plot of injection period for Example 3 field data

Fig.56 is a plot of bottomhole pressure (bar) on primary axis, injection rate (slurry flow rate) on secondary y-axis against the time (minutes) on x-axis representing the complete pump-in/shut-in history of the field data set named "Example 3". Fig. 57 shows the zoomed view of injection period. Even though the test was conducted on same well as Example 2, injection type is different. Fig. 56 shows the test conducted was similar to a step-rate test where flow rate was increased in small incremental steps (highlighted by blue circle), possibly to identify a closure stress value.

Cumulative of multiple small injections lasted for 8.817 minutes (0.147 hrs.), followed by shut-in time of 137.78 minutes (2.29 hours). The shut-in period was 15.6 times than the injection period, which is less than ideally desired shut-in period but doing its analysis will shed some interesting conclusions later for the reliability of such data. A distinct short period of water hammer was observed here too and excluding this period, entire data recorded was quite clean with minimal noise.

Analysis using FEKETE:

Fig. 58 shows zoomed view obtained from FEKETE (equivalent of Fig.57) of early part of Fig.56. The red vertical line in it marks the start of actual injection into the formation at time 0.78 minutes Volume injected before it shown by a steady increase in linear pressure was used in filling wellbore volume giving rise to the wellbore storage. The analyzed portion of the minifrac test consisted of 25.096 m^3 of brine water which is 8 times higher than the injection done in Example 2 (3.945 m^3) on same well, applied at average injection rate of (~- 2 to -3) m^3/minutes The first break down point identified by sudden drop in pressure (where Start of Injection line is placed) was established at an approximate injection rate of 0.92 m^3/min at measured sandface pressure (bottomhole pressure) of 38800 kPa (a). A series of short injection followed by short shut-in followed before the well was finally shut-in to monitor pressure fall-off.

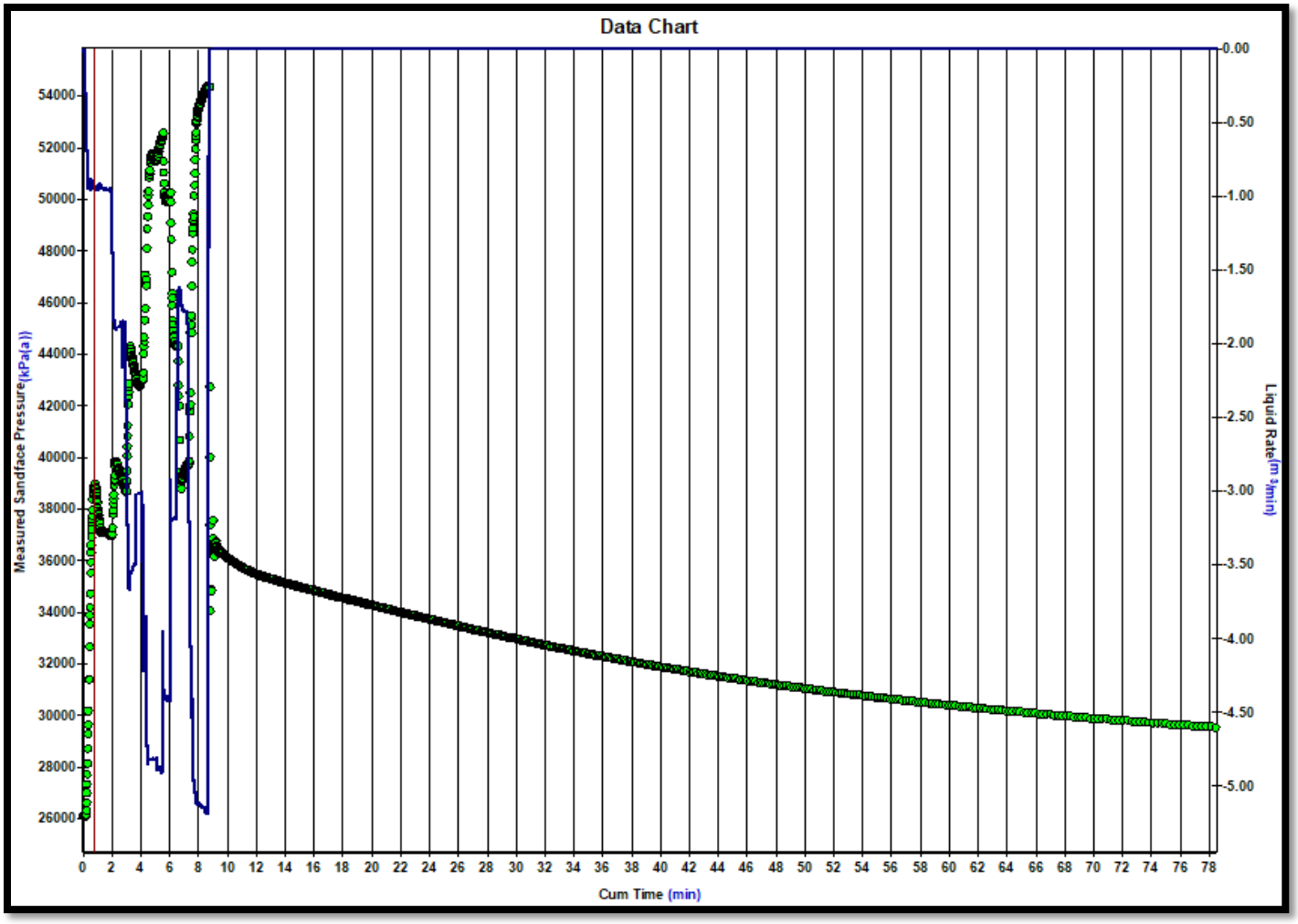

Figure 58 Zoomed in plot of injection period highlighting start of injection line

The parameters used as input to derive the results were same as Table 7. With the aid of 'inbuilt correlations selected as *default*' in FEKETE for calculating other reservoir fluid parameters, a list of necessary parameters was obtained, same as mentioned in Table 8.

(A) - Before Closure Analysis (Pre-Closure Analysis):

Total injection time (t_{inj}) (also called as pumping time (t_{pump}) is 8.82 minutes with high volume (25.096 m^3) of brine water injected. Fig. 59 is a Cartesian plot of pressure (kPa (a)) vs. time (minutes).Instantaneous shut-in pressure occurred at 36647 kPa (a), generally identified by placing a straight line on the early fall off portion of the fall data. Unlike Example 2, it can be noticed that the well experienced less friction immediately post shut-in visible by more scattered pressure points

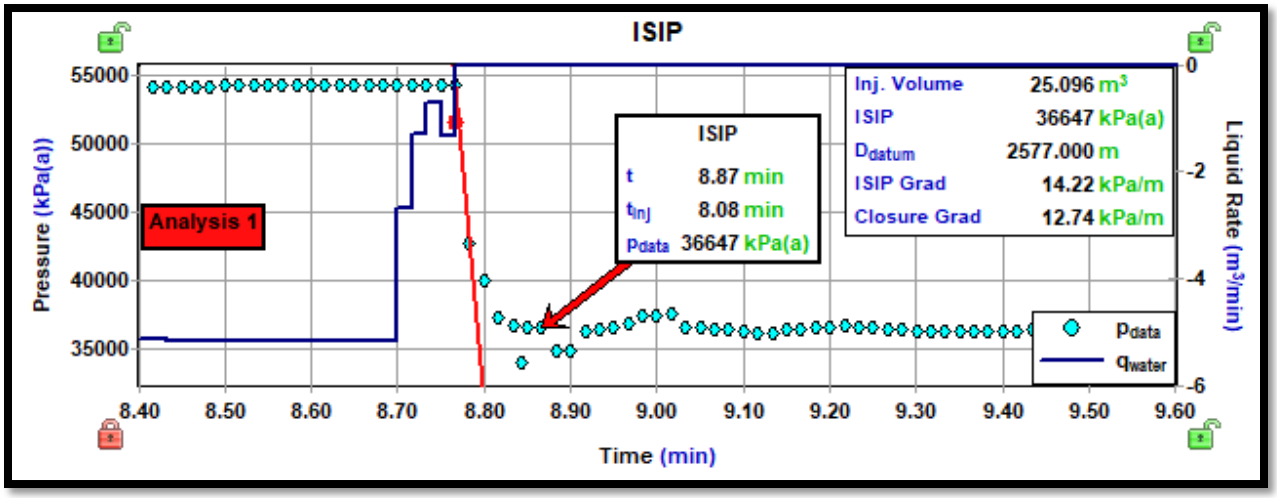

Figure 59 ISIP plot – Example 2

Figure 60 is a plot of semi-log derivative (G*dP/dG) (primary y-axis), pressure (P) and first derivative (dP/dG) on secondary y-axis against G-function time. After a very brief period of short linear increase (G-time=0.5) of the semi-log pressure derivative against G-time, a short stable period (0.3) can be noticed followed by another long non-linear line until G-time of 2.4. (it can also be viewed as going concave-up after G-time =0.8). It can be physically explained using the distinct concepts proposed by Barree et al and McClure et al, however it must be noted that all these explanations are speculative and could not be confirmed during our work due to limited field information.

(i) Barree et al proposed idea of Transverse Storage and Height Recession discussed below.

The behavior of the first derivative (dP/dG) and semi-log derivative (G*dP/dG) is similar to Example 1 plot, hence the underlying physical explanation discussed earlier holds valid here as well.

At shut-in there was a large volume of fluid stored in the fracture (V_{inj} = 25.096 m^3) relative to the expected surface area of the fracture for a normal planar bi-wing fracture model. Even though this volume is much higher than of Example 1 (14.801 m^3), going by the physics discussed before, an interesting observation was made here against Fig.21 (Example 1). The underlying "belly" of the concave up portion is smaller here. This means leak-off rate relative to the stored volume was comparatively higher implying a higher formation permeability value or greater "net pay area= 55 m in this case (reason given below)"; hence rate of pressure decline is likewise faster. This observation was confirmed by the permeability (k) value obtained from FenixConsulting © = $0.1 * 10^{-15} m^2$ against Example 1 permeability (k) value of $0.2 * 10^{-17} m^2$ (source: FenixConsulting © expert analysis)

Another interesting observation was made if we consider vertical fracture propagation phenomenon. FenixConsulting © provided additional piece of information that the fracture formed here penetrated the entire formation height of 55 m against 28 m penetrated during injection of Example 2, though both are done on same field. This can be attributed to the higher net pressure value of Example 3 (3809 kPa (a) against ~ 2408 kPa (a) in Example 2). Chances of fracture breaking into upper and below impermeable shale was low here possibly because of high formation permeability which dissipates substantial energy before it can exceed the value of "stress contrast between layers"

(ii) McClure analysis is covered in detail in later separate section

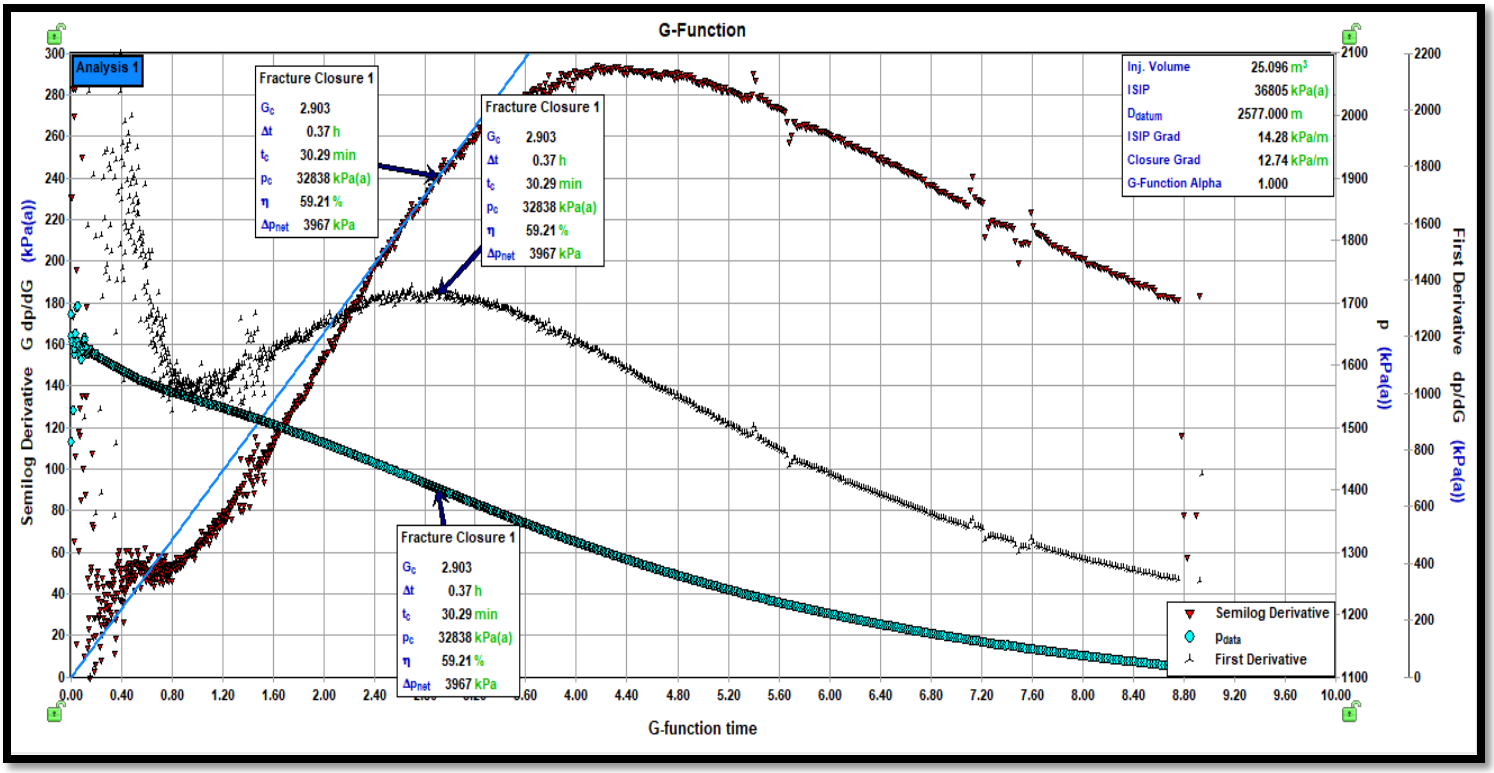

Figure 60 Pressure, First derivative and semi-log derivative of G-function curve against G-time – Example 3

A.1. - G-function analysis:

Fig.60. The characteristic G-function derivative signature is a "small belly" below the diagnostic straight line through the origin and tangent to the semi-log derivative of P vs. G at the point of fracture closure. It indicates that fracture closure occurred after 22.42 minutes of the shut-in time at a fracture closure pressure of 32838 kPa (a) (a). It is also worth noting that a small period of G-time= 2.4 – 2.9= 0.5, "normal leak-off" follows the storage related leak-off.

The value of fracture closure pressure and time (P_c and t_c) was obtained using standard "Tangent method" in a G-function plot. . Fracture closure pressure value is same as the value obtained by FenixConsulting's (c) analysis (32800 kPa (a)).

Net Pressure value (ISIP – FCP) is 3809 kPa (a)(a).The magnitude is high, giving more energy for the fracture to penetrate the entire net pay height of 55 m as discussed before.

A.2. - Sqrt(t) Analysis:

Fig.61. The best way to find the inflection point is to plot the first derivative $dP/d\Delta t^{\frac{1}{2}}$ and find the point of maximum amplitude of the derivative. This approach has been extensively advocated by engineer and scientists who follow "conventional standard approach" however unlike in Example 1 and 2, for this case, the sqrt (t) plot (Fig.61) does not show a clear inflection point (highlighted with green circle). This further strengthens the existing argument that value of fracture closure obtained from one method should always be cross validated against as many other possible methods. All method should agree on one fracture closure value and only then one can say with certainty that the closure point identified is correct.

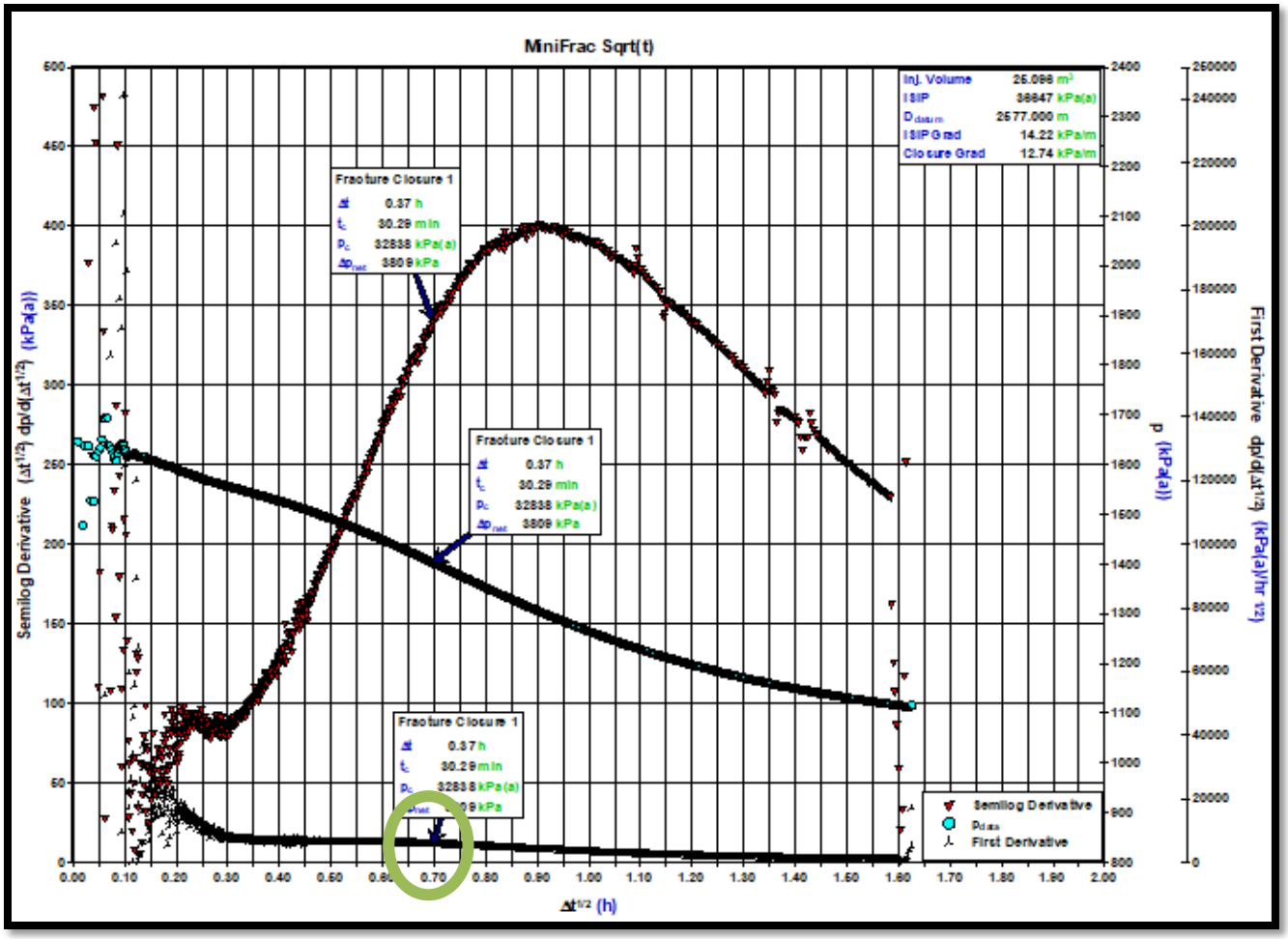

Figure 61 Pressure, First derivative and semi-log derivative of Sqrt(t) function curve against Square root of time – Example 3

A.3. - Pre-Closure Log-Log Pressure Derivative plot:

The log-log plot of pressure difference (green curve) and semi-log derivative (red curve) (on y-axis) against the shut-in time (x-axis) is shown in fig.62. Prior to closure here, we see a short storage flow regime (slope=1) followed by fracture linear flow regime (slope= 0.5). Fracture linear flow regime is rarely noticed in field though.

The accurate storage flow identified with slope 1 is for very short time (Δt = 17.2 – 8.06 = 9.14 minutes) followed by fracture linear flow period time (Δt = 37.5 – 28.5=9 min). Using Barree's rule of thumb that "no data should be analyzed until three times the closure time has passed", the unanalyzable time comes till 90.87 minutes From figure 62, we see that this is the time when formation linear flow (identified by slope=-1/2) just ends and a short radial flow regime started thereafter. Hence, the focus of analysis will be the radial flow regime here.

Following closure, formation linear flow period is visible for 26 minutes (Δt=97 min - Δt=71 min).The radial flow characterized by a slope= -1 starts developing at Δt = 1.73 hrs. ends at 1.97 hrs. lasting 14.4 min when the test was terminated.

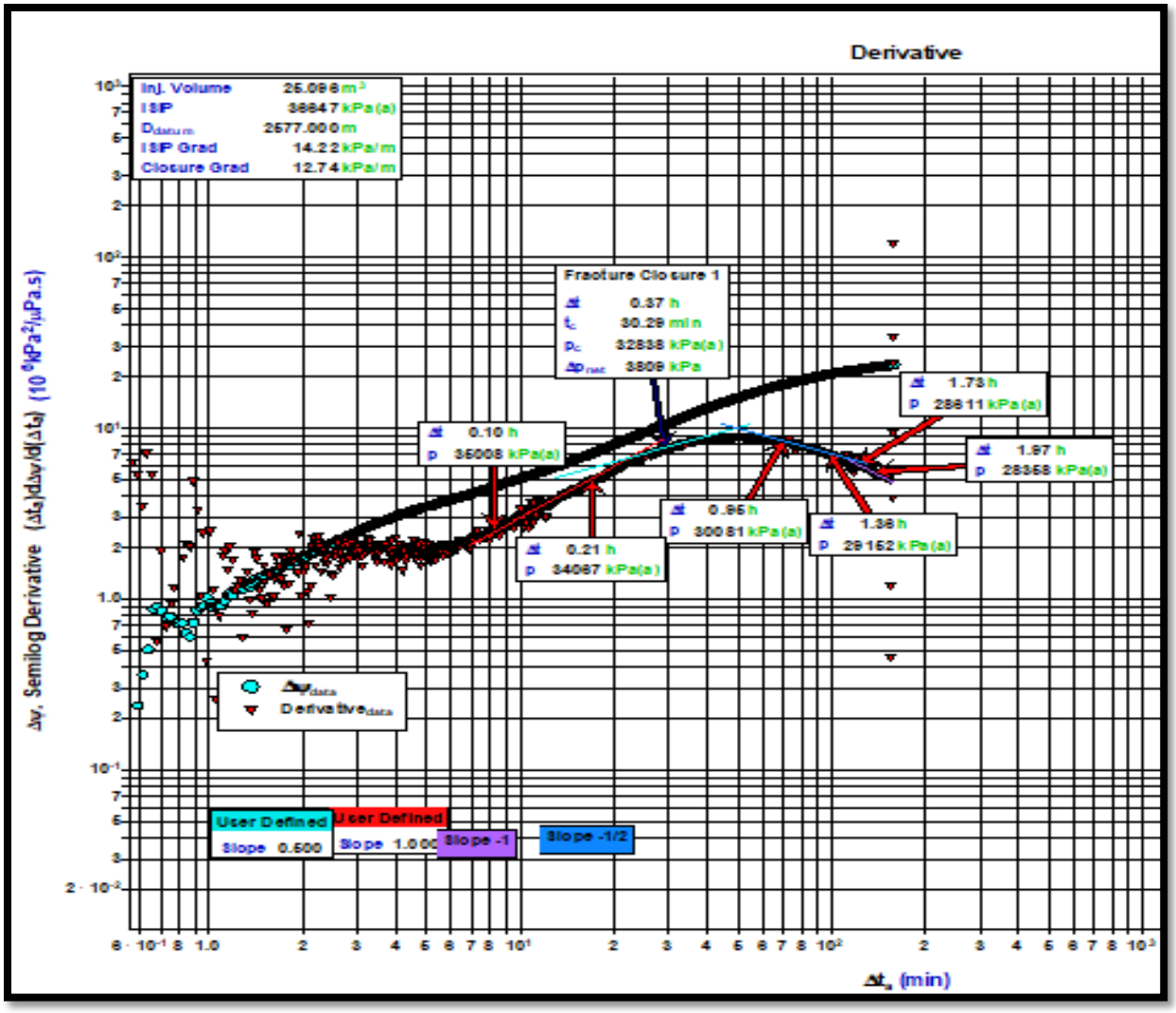

Figure 62 log-log plot of pressure difference and semi-log derivative – Example 3

(B) - After Closure Analysis (ACA):

The after-closure analysis will serve to validate the finding from Before Closure Analysis and confirm if the reservoir and fracture estimated are reliable.

B.1. - Nolte ACA analysis:

Fig. 63, 64 shows analysis plots done using Nolte method. Fig. 63 (Left) is a Cartesian plot of pressure vs. Nolte Linear time function used in establishing formation linear flow. Fig. 63 (Right) is Cartesian plot of pressure against Nolte radial function used in establishing/identifying formation radial flow. Fig. 64 is pressure difference and derivative against time log-log diagnostic plot.

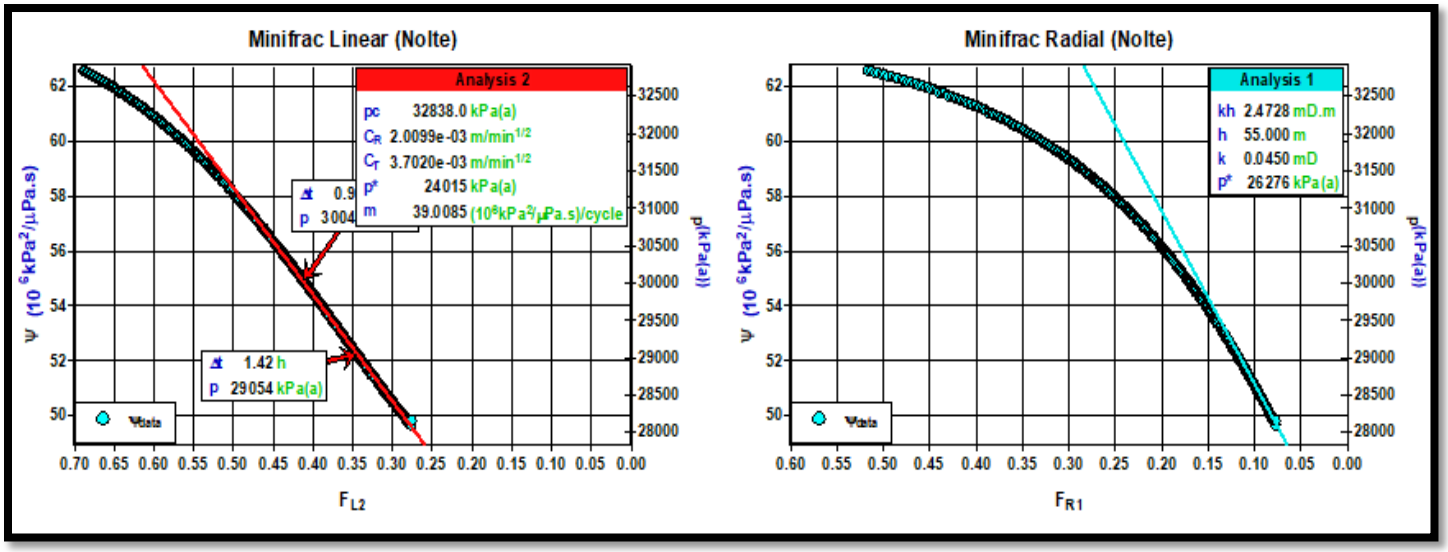

Figure 63 Nolte Analysis – (Top Left = Cartesian Linear plot of pseudo pressure against Nolte Linear time (F_L) ; Top Right = Cartesian Radial plot of pseudo pressure against Nolte Radial time (F_R)

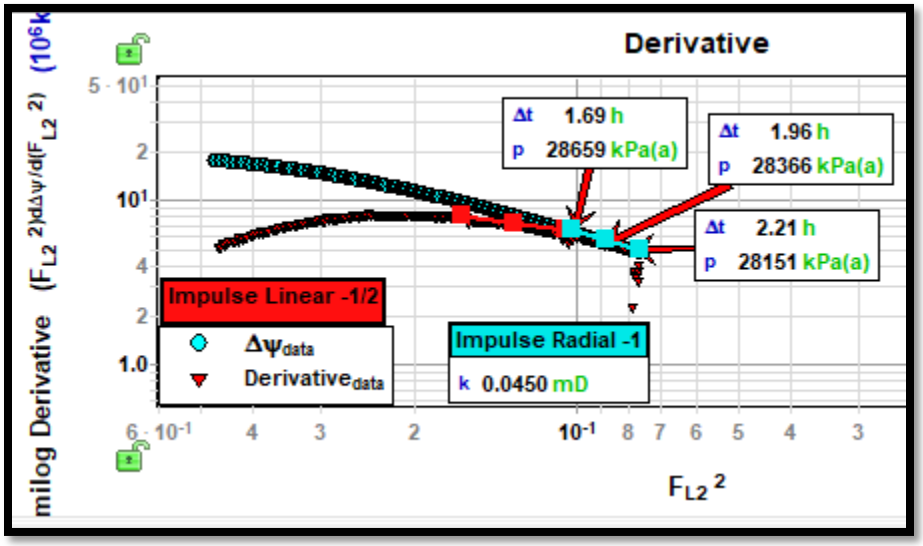

Figure 64 Log-lot plot of pressure difference and semi-log derivative vs. F_L^2

The analysis and observation shown in Fig.63 and 64 can be summarized as follows:

(i) Derivative plot: As mentioned before, the first analysis is done on the derivative plot to identify the flow regimes. Fig. 64 shows that linear flow regime (slope=-1/2) is short-lived. If impulse radial flow is identified, the pressure data overlay the derivative data which happens here albeit lasts only for a short duration of Δt=0.25 hrs.=15 minutes.

(ii) Impulse radial flow plot: Correct estimate of extrapolated pressure (p*) and permeability (k) is estimated. As discussed in detail in Example 1 section, value of extrapolated pressure is obtained from extrapolation of linear line to $F_{R1} = 0$ (which represents an infinite shut-in time). This value comes out to be p* = 26280 kPa (a) which is very close to the correct initial reservoir pressure value 26500 kPa (a), hence giving more confidence that the radial flow is the correct regime to focus and can be used to extract other required fracture and reservoir parameters.

With slope $m_{R1} = 63.50 \left(10^6 \frac{kPa^2}{\mu Pa.s}\right)$ per cycle and all other input parameter value known from Table 7 and 8, permeability value was $4.5 * 10^{-17} m^2$. This value matches well against the permeability value confirmed by FenixConsulting © ($10 * 10^{-17}\ m^2$), Soliman Craig analysis (shown later as $4.38 * 10^{-17} m^2$) but VdHoek analytical model permeability value is one order higher at, $2.6 * 10^{-18} m^2$).

(iii) Impulse linear Flow plot: Once closure pressure (from Pre-closure diagnostics) and permeability (from impulse radial flow plot-discussion) are specified, impulse linear line plot was used to calculate fluid loss coefficients (Reservoir leak-off coefficient (C_R) and Total Leak-off coefficient (C_T) using eq. 45 with aid of (left) plot in Fig. 63. Values came out to be$(C_R) = 2.0099 * 10^{-3} m/\sqrt{min}$ and $(C_T) = 3.70 * 10^{-03}\ m/\sqrt{min}$. Seen later, these values do not come in close match with VdHoek's model result because linear flow regime was still under the period where data generally shouldn't be analyzed as per Barree's thumb rule.

(iv) Although the Linear flow period is not completely fit for analysis purpose, the extrapolated pressure (p*) value obtained was 24015 kPa (a) , with an error range of 9.38 % against the correct value of 26500 kPa (a). This shows that the unanalyzable period can still be used to get an idea of the "working numbers" on the field.

B.2. - Soliman and Craig ACA Analysis:

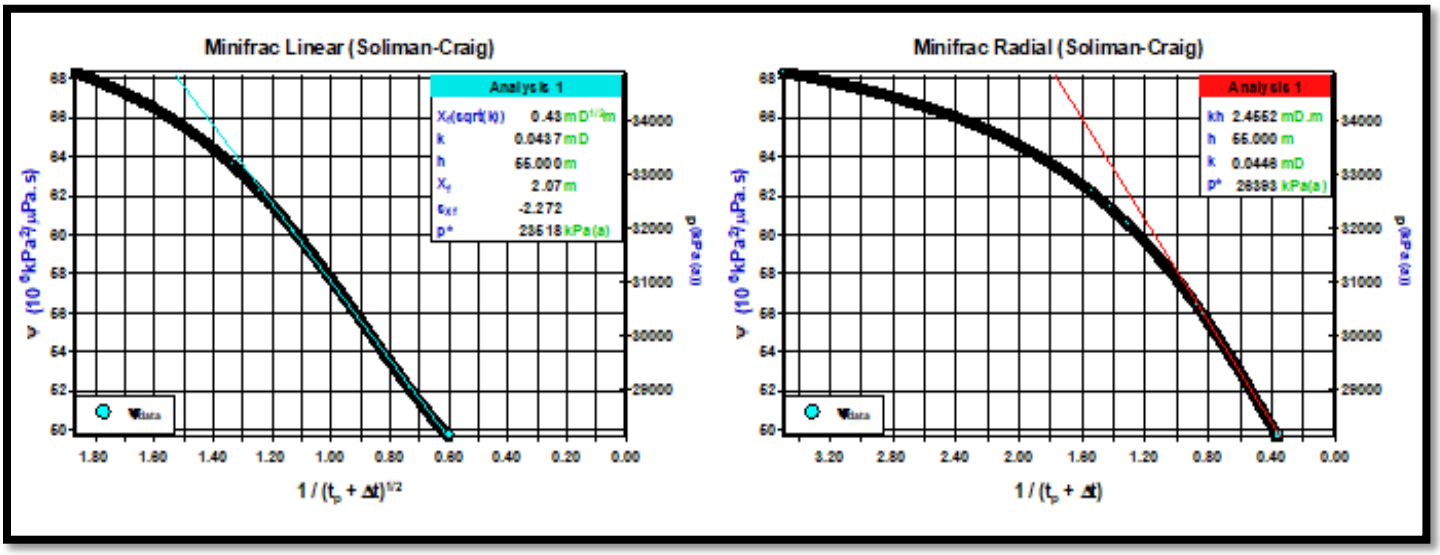

Figure 65 Left Soliman-Craig Cartesian plot of pseudo pressure vs. (1/(t_p + delta_t))^0.5 ; Right = Soliman-Craig Cartesian radial flow plot of pseudo pressure vs. (1/(t_p+ delta_t))

The analysis and observations made are as follows:

(i) Derivative plot: Fig.66. The derivative plot shows linear flow period (slope=1/2) of 17.5 min and radial flow period (slope=1) of ~14 min on a plot of impulse derivative against adjusted shut-in time (Δt_a). These values are similar to Nolte analysis obtained values.

(ii) Impulse Radial Flow: Shown in fig.39 (right plot), the extrapolated pressure (p*) value is 26341 kPa (a), which is only couple of hundreds psi shorter than the correct initial reservoir pressure (26500 kPa (a)). p* is the extrapolation of the radial line to the time of 0 (red straight line in fig. 39) , which corresponds to an infinite shut-in time. Using eq. 15 and representing it in term of slope, $m_{R2} = \frac{(0.000014\frac{\pi}{2})V_{inj}\mu}{kh}$. With value of

$m_{R2} = 13.28\ \left(10^6 \frac{kPa^2}{\mu Pa.s}\right)$ per cycle, and other input parameters value already given as input (please refer Table 7 and 8), permeability (k) comes to $4.38 * 10^{-17} m^2$.

There is an agreement in permeability value between Soliman Craig and Nolte analysis

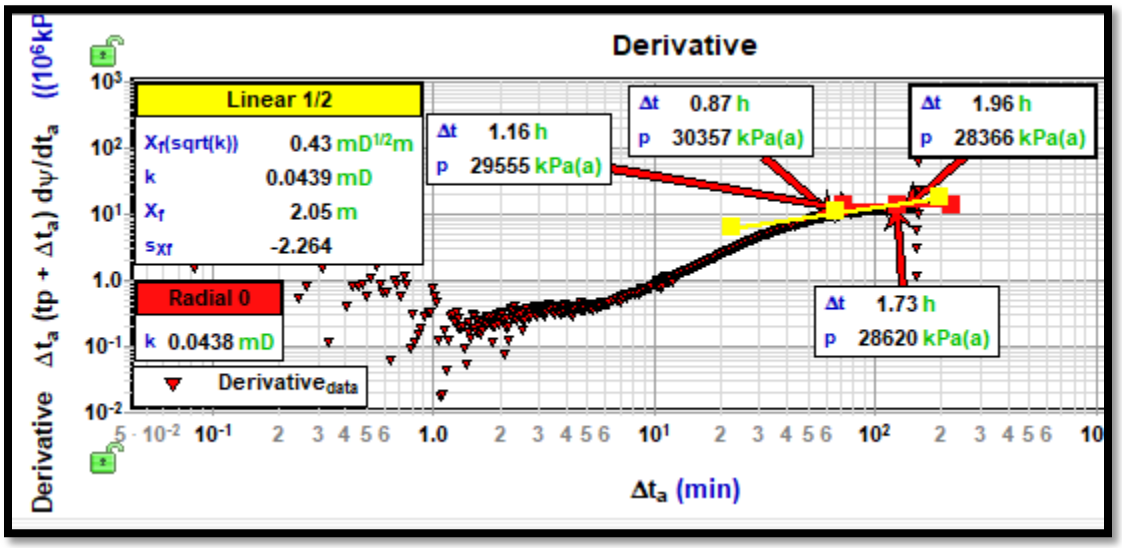

Figure 66 Soliman-Craig Log-log plot of Impulse derivative vs. adjusted shut-in time (min)

(iii) Impulse Linear Flow: Shown in fig. 65 (left plot) Formation Linear flow period continued for short time ((Δt= 1.16-0.96)hrs. = 0.29 hrs.=17 minutes) evident from the derivative plot (fig.66). It is a limited time to calculate reliable fracture half length. Using eq. 35 on fig. 65 (left) such that for a plot of pressure vs. time gives the slope $m_L = 0.00424 \frac{\sqrt{\pi}}{2} \frac{V_{inj}}{h} \left(\frac{\mu}{\emptyset c_t k L^2}\right)^{0.5}$. The input parameters are taken from table 7 and 8. Resulting half-length value (L) is estimated to be 2.05 m.

(iv) Extrapolated pressure value from the Cartesian linear and radial flow plot comes out to be 23496 kPa (a) and 26341 kPa (a). Stated before using Barree's thumb rule that the linear flow regime shouldn't be ideally analyzed and only radial flow happens after thrice the closure time visible in log-log diagnostic plot, hence the pressure value (p*) during radial flow is more accurate and close to the correct initial reservoir pressure.

(C) - History Matching

Although the radial flow was short developed yet it occurred at a much later time after closure, so it was decided to do its history matching. *Purpose was to gauge the accuracy of history match for such data where the radial flow isn't well developed yet it falls in "analyzable zone" i.e. 1.5 log cycles after closure*. To realize it, an inbuilt model of "Fracture with boundaries" was adopted. The input parameters used were taken from Table 7 and 8.

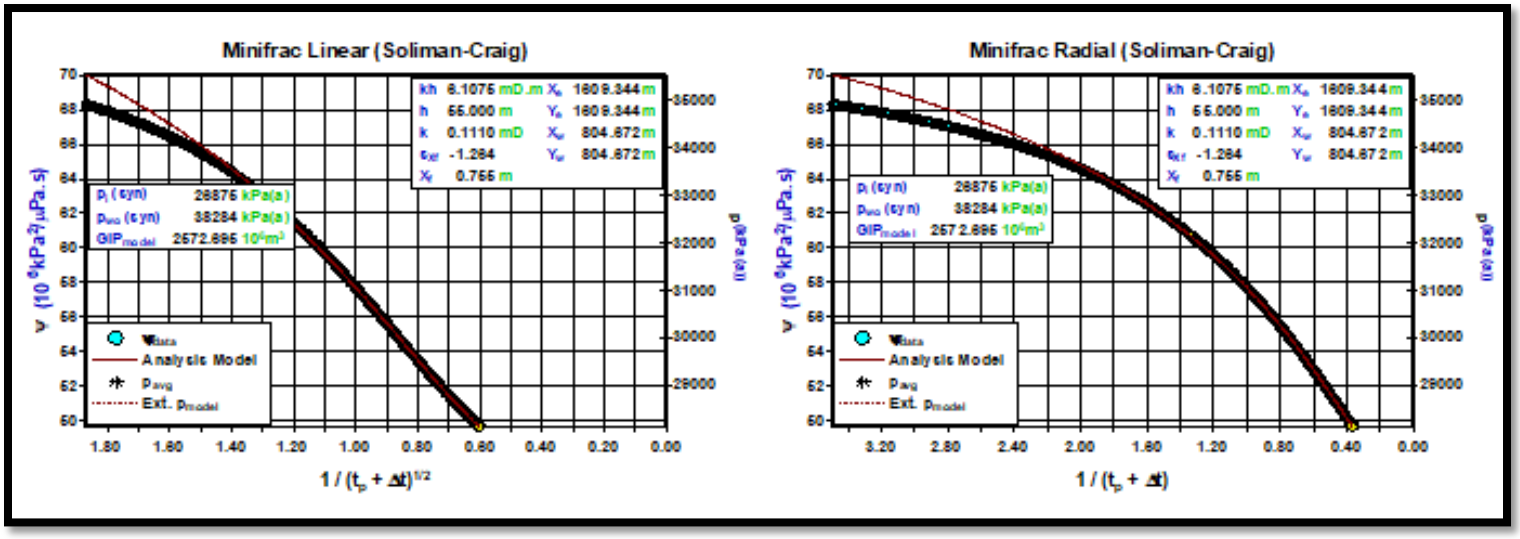

Figure 67 Soliman and Craig Linear flow (Right plot) and Radial flow (left plot) – History Matching plot

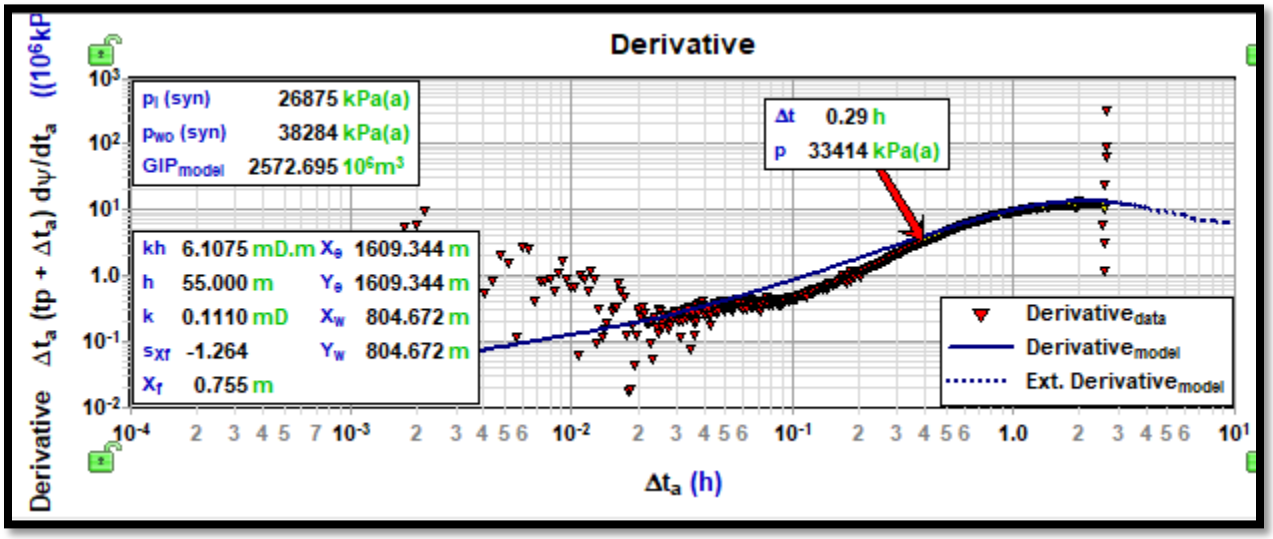

Figure 68 Soliman and Craig derivative vs. time – History Matching plot

Fig. 67 (left) and (right) are linear and radial flow plots, Fig. 68 shows impulse derivative log-log diagnostic plot. A decent match is identified from a good superposition of synthetic data (blue line) of analysis model against the field data (red inverted triangles) covering most part of post shut-in duration.

Permeability values obtained is in $11.1 * 10^{-17} m^2$which is of same order as obtained from other analysis method (Soliman Craig, Nolte, FenixConsulting ©) while the fracture half-length is only of 0.755 meters. Synthetically identified pressure value is 26875 kPa (a), which is almost same as the original initial reservoir pressure value of 26500 kPa (a).

(D) - VdHoek Analytical Model:

In order to provide a good comparison with 'specialized plot' methodology, we estimated the fracture and reservoir unknown parameters using the analytical model mentioned in Appendix (B). Input data are provided in Table 11

Table 11 Input parameters for VdHoek analytical model – Example 3

Porosity	0.12	[-]
Fluid Compressibility	$3.13 * 10^{-8}$	Pa^{-1}
Reservoir fluid viscosity	0.00002	Pa*s
Injection fluid viscosity	0.0003516	Pa*s
Young's modulus	6.89	GPa
Net pressure	170	Bar
Fracture height	43.5	m
Injection rate	0.01316	m^3/sec
t_{pump}	6.484	min

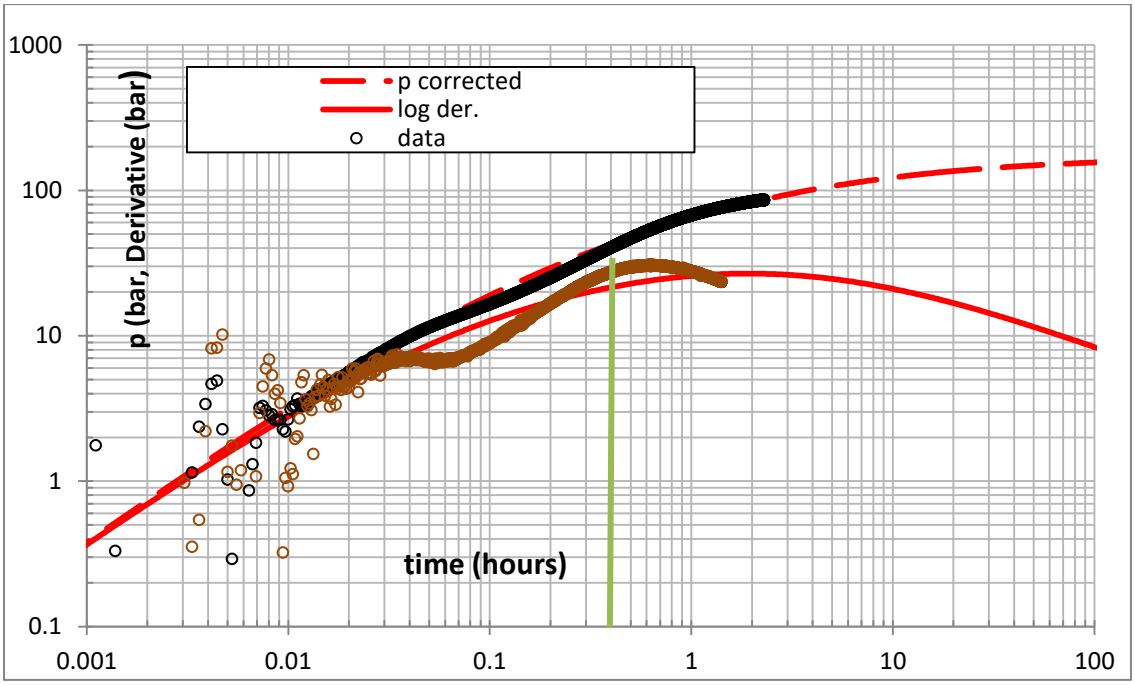

Figure 69 Log-Log pressure difference and derivative diagnostic plot (VdHoek Analytical model) – Example 3

Fig.69 shows a log-log diagnostic plot of delta pressure and derivative against shut-in time obtained from the VdHoek's analytical model. The maximum analysis time was chosen as 0.5 hrs. Δt = 0.36 hrs. was the closure time (highlighted by a green vertical line) identified from FEKETE BCA plot. In "standard methodology", it is common for the pressure difference and derivative curves to be parallel or coincide on same line of slope=1 from early time until before closure. The slope of these parallel/coinciding lines is diagnostic of the flow regime established. Using this approach, we do see that the pressure difference and derivative plot starts deviating from each other roughly at 0.36 hrs. which affirms the closure pressure rule if "standard methodologies" are followed.

Demonstrated in the case of example1 VdHoek numerical model plots, it is entirely possible that what was observed as the fracture closure point in every analysis technique using standard methodologies, in reality can just be a point where fracture storage/compliance ends and not a definite proof of the fracture closure point.

Table 12 contains values of output fracture and reservoir parameters estimated using the VdHoek's analytical model. It's a low permeability reservoir. This low permeability of the formation rocks leads to the fracture showing a storage dominated growth where the leak-off rate is very low (0.034 m^3/sec). The estimated leak-off rate $Q_l(t_{pump})$ is done under the assumption that during pumping, leak-off rate is one-dimensional (following Carter's leak-off assumptions). Hence under Carter's assumptions, for storage dominated flow, leak-off rate is calculated from Nolte (1986) from Eq.49 where, $|Slope|$ is the absolute value of pressure decline slope at shut-in, V_{inj} is the cumulative injected volume at the end of pumping period, and the net pressure = ISIP -FCP

From fig.69, it is visible that the early time flow is fracture storage dominated with slope=1, but the duration of the flow is relatively short (6.6 min). With the obtained value of C_f in combination with the input data given in Table 11, fracture half-length value of 10.90 m was obtained which is very high against the fracture value obtained from FEKETE. The most likely explanation can be the usage of different fracture geometry models (PKN, GDK or Radial vs. Elliptical).

An optimum fit wasn't obtained between the field data and model data in contrast to the fit obtained for Example 2 plot (Fig.54) stressing the fact that a long post closure flow period is critical for reliable estimates of parameters.

(E) - Comparison between FEKETE (Specialized Plot) vs. VdHoek analytical Model

Table 12 Comparison between FEKETE vs. VdHoek model – Example 3

Parameters	**Unit**	**Plot from where value came in FEKETE analysis** ***	**FEKETE**	**Analytical Model**
Volume Injected	m^3	NA	25.096	25
Injection rate	m^3/sec	NA	0.052	0.0833
Injection time	min	NA	8.03	5
Fracture Half-length	meter	Frac Boundary model	2.06	10.90
Fracture height	meter	NA	55	51.83
Permeability	m^2	Frac Boundary model	$4.5 * 10^{-17}$	$1.02 * 10^{-18}$
Net Pressure	kPa (a)	BCA – G-function, Sqrt(t) plot	3967	2000 (estimate)
Skin (Frac Face Damage)			0	0
Total Leak-Off coefficient	(m/sqrt(sec))	Nolte ACA Linear plot	$4.77 * 10^{-04}$	$1.48 * 10^{-04}$
Initial Total Compressibility (c_{tl})	Pa^{-1}	Properties Tab	$1.96 * 10^{-08}$	$3.3 * 10^{-8}$
Time to Fracture Closure	min	BCA – G-function, Sqrt(t) plot	30.29	Cannot be estimated

Pressure at fracture closure time	kPa (a) (a)	BCA – G-function, Sqrt(t) plot	32838	Cannot be estimated
Instantaneous Shut-In pressure (ISIP)	kPa (a) (a)	BCA – G-function, Sqrt(t) plot	36805	Cannot be estimated

* Frac Boundary model - based on Soliman and Craig ACA method
**NA = Not Applicable
*** = For reason, please see pt. (4) and (5) of 'Conclusion' section of Example 1

While a detailed discussion about the values estimated from both models is mentioned in "Conclusion" section, a quick preview shows that values of unknown parameters are in same order range.

(F) - McClure's Analysis:

Fig. 70 is a zoomed version of early part of the plot from Fig.60 to identify the first sharp point of deviation from linearity on a plot of pressure or G * dP/dG vs. G-time. Like the previous data sets, Example 3 also doesn't show a sharp spike of increase in semi-log derivative plot, highlighting the real fracture geometry is way more complex than assumption of simple bi-wing planar fracture. The earlier short linear line can be attributed with the early time before shut-in period. The likeliest point visible where a sharp linear line starts is at G-time of 0.80, at closure pressure of 35368 kPa (a). This closure value is higher by 2600 kPa (a) when compared with values obtained of "Tangent method".

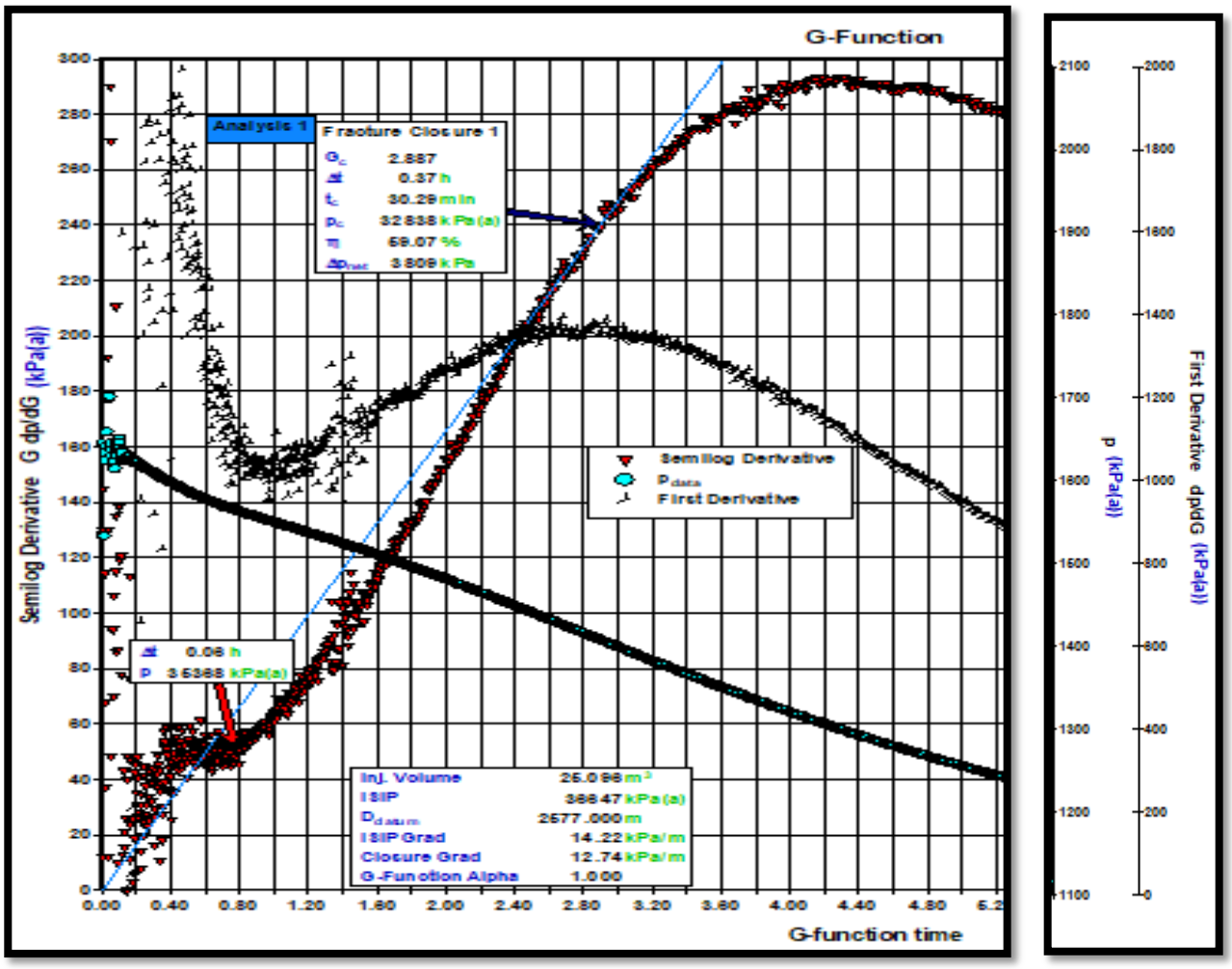

Figure 70 Zoomed in plot of early portion of Example 3 - Pressure or G * dP/dG vs. G-time

(G) - Conclusion

1. An interesting observation from results obtained of "History matching in FEKETE", permeability and initial reservoir pressure can be predicted fairly accurately despite the small radial flow developed if the flow regime comes after "1.5 times of log-cycle after closure".

2. Results match between VdHoek analytical model and FEKETE are in close match with each other.

3. Example 3 was tested in the same formation in the same well as Example 2 where the abnormal leak-off behaviors are clear. This abnormal leak-off was highly likely due to the higher injection rate (also injection pressure and net pressure) and large volume (25 m^3). The formation thickness (net pay=55m) was bounded by shale layers both above and below, this thickness was safe for a small injection volume in Example 2, but might be not for the larger injection volume of 25 m^3 used in Example 3. This large injection volume could have possible result in height recession. Transverse storage was also a possibility if natural fractures were present.
   An observation worth noticing is the final closure is almost same for either of these scenarios using Tangent method, which was at ~ 32838kPa. Using Tangent method, the difference between closure pressure of Example 2 and 3 is 69 kPa or 10 psi, which is almost similar closure stress value. On the other hand, the reasoning for inapplicability of Variable Fracture Compliance method here is that the closure value obtained is at 35368 kPa, or 2600 kPa (377 psi) higher than Example 2 value.

4. The injection pressure and injection volume was much higher than example 2, causing abnormal leak-off behavior visible from the G-function plot. dP/dG curve decreases and then increases and decreases again. Reason for each behavior can be :
   <u>First decrease of dP/dG</u> = Due to large injection volume and injection rate, there was possibly height recession or transverse storage, thus giving more surface area than fluid leak-off. Stiffness remains constant at this time, and due to more surface area created relative to the fluid, the rate of leak-off decreases till the point fracture keeps on extending and creating more surface area for the fracture.
   <u>Increase of dP/dG</u> = Once the fracture stops propagating (thus stop creating new surface area) and starts to close again, rate of leak-off paces up and starts increasing linearly until fracture closure (lesser surface area and more liquid to leak-off).
   <u>Decrease of dP/dG</u> = The moment fracture closure occurs, stiffness becomes very high and the rate of leak-off rate decreases due to low fluid volume and surface area for the fluid to leak – off.

5.4 - M-Site: Low Permeability (Tight Gas Reservoirs)

Brief Overview

Seven injections were performed in the B Sand in the Upper interval of the Mesa verde group as a part of GRI/DOE multi-site project located in the Piceance Basin, NorthWest Colorado. The various fracture diagnostics techniques provided information on fracture growth and total extent. Microseismics and inclinometer data indicated that fracture(s) propagated in Injections 2-B through 6-B. These injections used relatively simple fluids in volumes ranging from 27 to 400 bbl, rapidly attained their total length extent (maximum of approximately 400-ft. wing length) and had only limited out-of-zone height growth (total height approximately 65 ft.). Inclinometer data further suggested the possibility that the unpropped fractures retained some residual fracture width. Fracture modeling results approximated the microseismically measured fracture lengths, but model-predicted fracture heights were greater than those mapped microseismically. (Warpinski et al., 1996)
Intersection Well 1B was subsequently drilled and 11 hydraulic fractures in the B Sand were recovered in core at a point 126 ft. from the MWX-2 treatment well. The fractures occurred over a 2.6-ft. horizontal interval. Several independent techniques (including observations of pressure transients down the fracture(s), radioactive anomaly in the Intersection Well 1B, and recovery of colored proppant included in Injection 7-B) confirmed that the fractures recovered were hydraulically induced through B-Sand injections. Well-to-well testing of the propped and unpropped hydraulic fractures indicated that system conductivity was 650 md-ft.

The B-Sand experiments involved a series of field operations designed to extend fracture mapping capabilities and hydraulic fracturing technology beyond that which had been developed in the A Sand. It made full use of the fracture mapping capabilities made possible by the Monitor Well No. 1 comprehensive instrument arrays and wireline retrievable arrays in MWX-3.

Geological Setting

The B Sand represents the uppermost sand body deposited in the 1600-ft-thick fluvial subdivision of the Mesa Verde Formation in the Piceance Basin (Lorenz, 1983). The basic stratigraphic column for the southern Piceance Basin is illustrated in Figure 71. Most of the sandstones which characterize this interval were laid down as point bars in association with meandering stream systems. The other lithologies in this fluvial interval are primarily mudstones and carbonaceous mudstones and siltstones deposited as overbank and levee sediments.

Gamma ray (GR) log character from several closely spaced wellbore penetrations, as was shown in Figure 2.2, indicates that the B Sand is consistently thick (e.g., 60 ft. in Monitor Well No. 1) and continuous over well-to-well distances of several hundred feet. The log character also clearly illustrates that the B Sand has sharp contact at the base of the unit and gradational, fining-upward upper sequence. Core descriptions of the B Sand (Peterson et al., 1995) confirm the fining upward sequence and that the main B Sand is composed of fine- to medium-grained, cemented sand with low-angle planar cross beds.

Both core and log character support a point bar depositional setting for the B Sand. On the basis of the locally consistent log character and typical point bar dimensional morphology, it was anticipated that B-Sand thickness would be relatively constant over the 300- to 400-ft distances anticipated to be contacted by the B-Sand hydraulic fractures to either side of MWX-2.

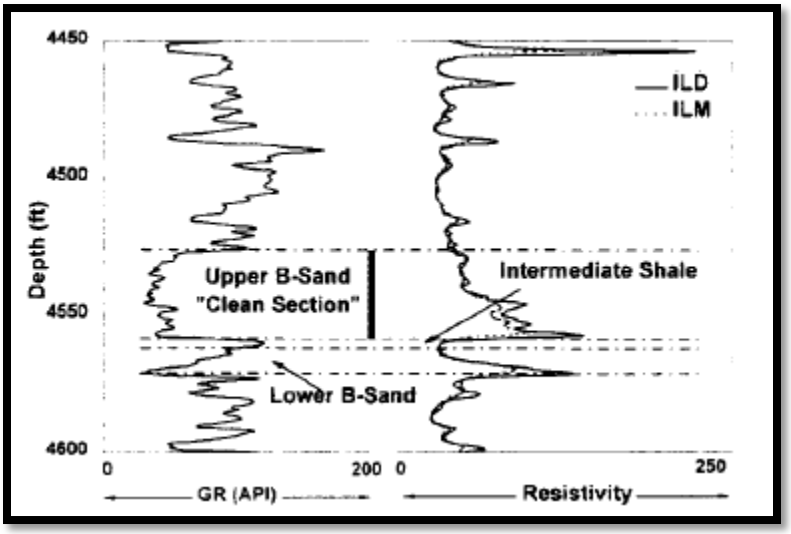

Figure 71 Relevant logs for the B-sand

5.4.1 - Analysis – 5B Results and Discussion – Low Permeability Gas Well

We chose this field data because unlike the other field data on which the analysis were done (Example 1,2,3, NIMR field), extensive multiple independent tests (like inclinometer test, microseismic survey, colored proppant etc.) were done here for estimating unknown fracture and reservoir parameters like permeability, fracture dimensions, closure pressure etc. These results serve as benchmark values to compare the results obtained with FEKETE and VdHoek model with confidence.
Thorough analysis was done for test no: 5B, 6B and 2B with FEKETE and VdHoek Unified model.5B and 6B had same volume and injection rate. One of the primary design objective in doing so was to observe the effect of duplicate fractures on data from microseismic or inclinometer diagnostics (for example, would the reopening of an existing fracture originally created by yield the same response in diagnostic as obtained from 5-B.)

The shut-in transient was unusual (showing no clear indication of closure pressure at any pressure), was the fifth and sixth injection into the interval and uses a much larger volume than is typically used in a DFIT. Therefore the result from 6-B test is not presented but 5-B will be briefly discussed.

Table 13 is a main chart showing the input and output parameters obtained from various studies using microseismic surveys, modeling, inclinometer test etc. Results shown here were used to tally results obtained from our analysis.

Table 13 Main Table showing all parameters from various independent tests - M-site (B-sand injection)

		INJECTION 2B	INJECTION 3B	INJECTION 4B	INJECTION 5B	INJECTION 6B	SOURCE
TEST TYPE		Step-rate/flowback	Pump-in/flowback	Pump-in/Shut-In/flowback	Pump-in/shut-in	Pump-in/shut-in	SPE-38575
	Type	2% KCl	2% KCl	2% KCl	4793 kg/m3linear gel	4793 kg/m3linear gel	SPE-38575

Fluid	**Rheology@ 170 sec^-1 / Viscosity**	Newtonian, μ = 0.001 Pa.s	Newtonian, μ = 0.001 Pa.s	Newtonian, μ = 0.001 Pa.s	μ =0.041 Pa.s	μ =0.041 Pa.s	**SPE-38575**
(GPa)	**Young's Modulus**	31.5	31.5	31.5	31.5	31.5	**SPE-38575**
--	**Poisson Ratio**	0.2	0.2	0.2	0.2	0.2	**SPE-38575**
1/Pa	**Fluid Compressibility**	NA	NA	NA	4.93 E-08	4.93 E-08	**SPE-38575**
1/Pa	**Total Compressibility**	NA	NA	NA	NA	NA	
Length (m)	**Re-Analysis @ SPE-38575**	NA	NA	NA	105.1	97.8	**SPE-38575**
	Tip-to-tip microseismics	53.34	91.44	106.68	76.2(l) / 149.35 (r)	88.4(l)/134.1(r)	**SPE-38575**
	Warpinski et al				106.7	99.06	**SPE-38575**
Height (m)	**Re-Analysis @ SPE-38575**	NA	NA	NA	12.2(t)/16.5(b)=28.7 (t)	10.05(t)/13.10(b)=23.15 (tot)	**SPE-38575**
	Tip-to-tip microseismics	NA	NA	NA	15.5(t)/16.8(b)=32.3(t)	12.2(t)/14.6(b)=26.8(t ot)	**SPE-38575/36451**
	Warpinski et al	NA	NA	NA	24.4	22.9	**SPE-38575**
	2D Model used in the paper	9.8-12.8	18.3	18.9	NA	NA	**SPE-36451**
kPa (a)	**Net Fracture Pressure = ISIP - FCP**	4823	6201	6201	8957	8957	**SPE 39950**
m3/min	**Injection Rate**	0.08 - 0.48	1.6	1.6	3.5	3.5	**SPE 39950**
m3	**Injected**	4.3	15.9	33.4	63.6	63.6	**SPE 39950**

	Volume						
%	**Porosity**	6-8%	6-8%	6-8%	6-8%	6-8%	**SPE-38575**
	Reservoir Fluid type	Gas	Gas	Gas	Gas	Gas	**GRI/DOE - 96550**
Pa.s	**Reservoir Fluid Viscosity**	NA	NA	NA	NA	NA	
Pa	**Reservoir Pressure**	13435.5	13435.5	13435.5	13435.5	13435.5	**SPE-38575**
Celsius	**Reservoir Temperature**	60	60	60	60	60	**SPE-38575**

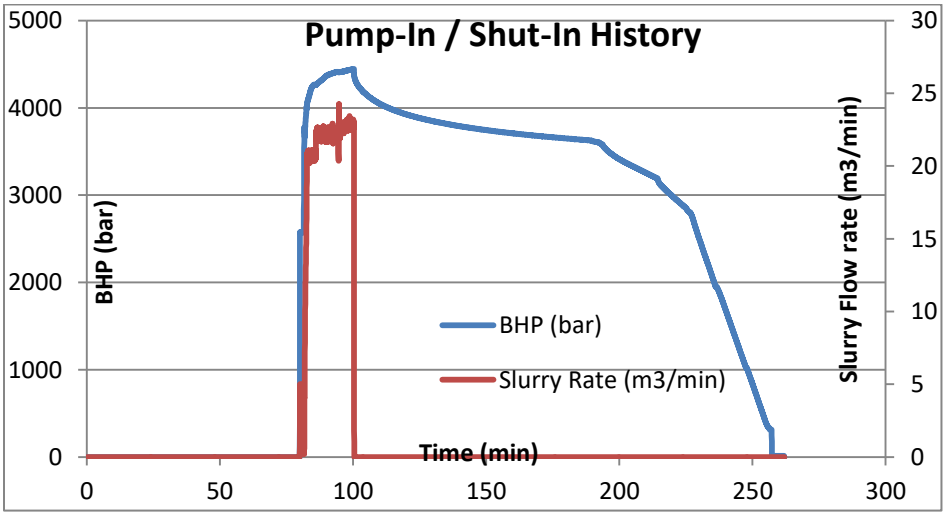

Figure 72 Total Injection/Shut-in History for Injection 5b- M-site injection

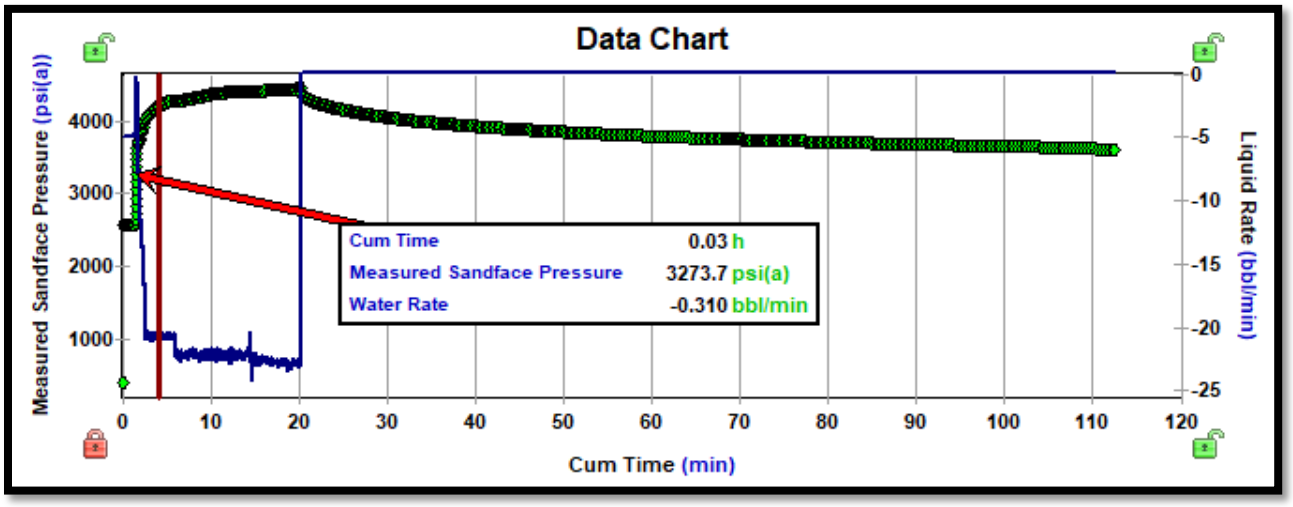

Figure 73 Injection/Shut-in considered for analysis - Injection 5b- M-site injection

Fig72. is a plot of bottomhole pressure (bar) on primary axis, injection rate (slurry flow rate) on secondary y-axis against the time (minutes) on x-axis representing the complete pump-in/shut-in +flowback history of the injection 5b. Data after flowback is not useful; hence it was trimmed out of the final production history plot shown in fig.73. The injection consisted of 63.6 m3 of 4793 kg/m3linear gel at a constant injection rate of 3.5 m3/minutes Injection (5-B and 6-B) were the two linear gel minifracs as a prelude to the larger propped fracture of Injection 7-B.

Analysis Using Fekete:

(A) - Before Closure Analysis (Pre-Closure Analysis):

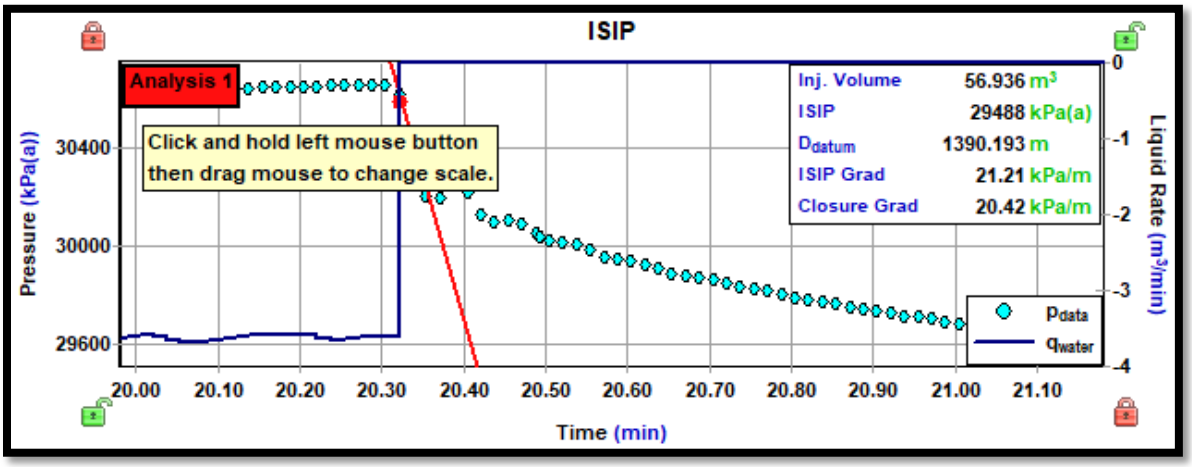

Figure 74 ISIP plot – Injection 5-B

Injected volume was estimated at 59.94 m^3 against the original 63.6m^3. Remaining 3.6 $m^3$was used for wellbore filling.

(A.1,2,3) - G-function analysis, Sqrt(t) analysis and Pre-Closure Log-Log Pressure Derivative plot:

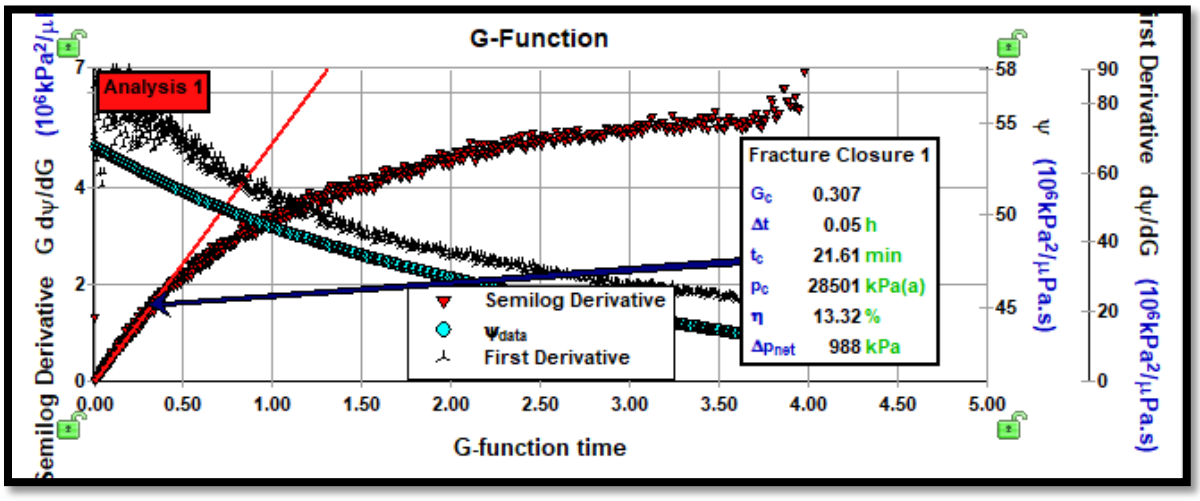

Figure 75 Pressure, First derivative and semi-log derivative of G-function curve against G-time – Injection 5B

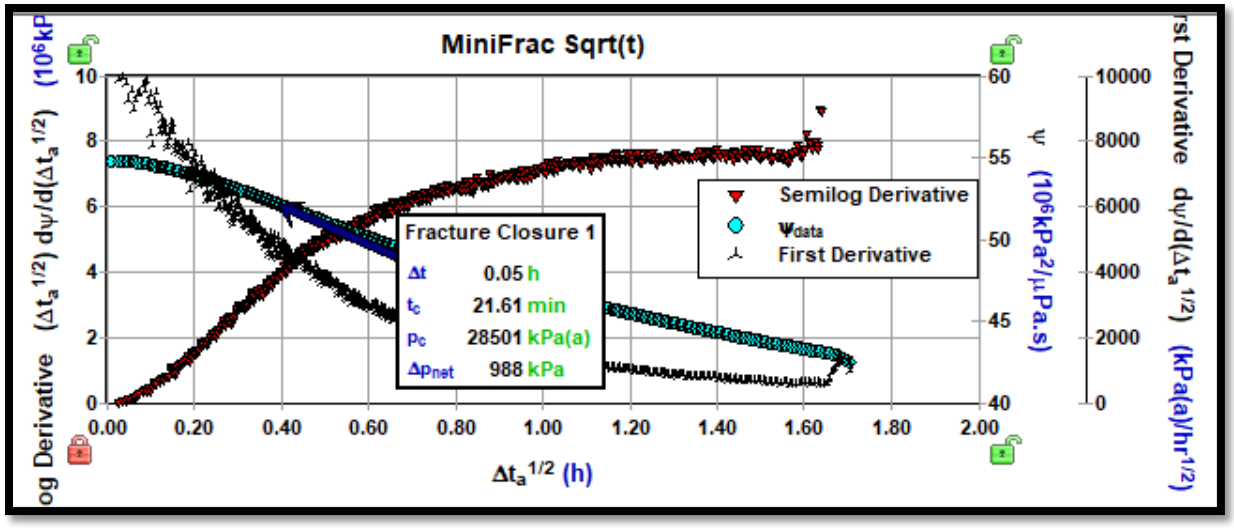

Figure 76 Pressure, First derivative and semi-log derivative of Sqrt(t) function curve against Square root of time – Injection 5B

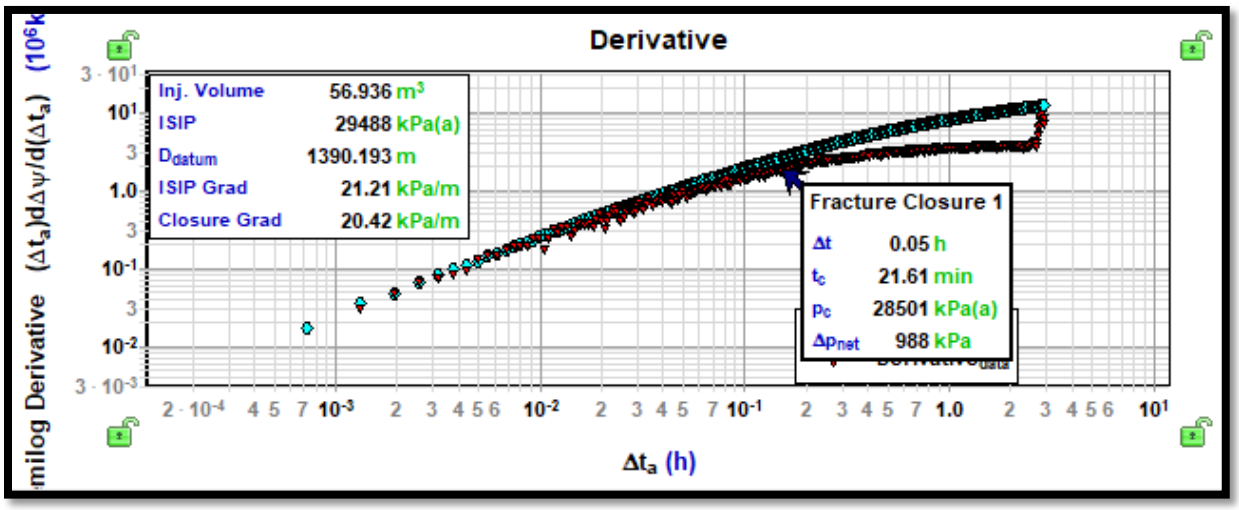

Figure 77 log-log plot of pressure difference and semi-log derivative – Injection 5B

Fig. 75, 76 and 77 are the three standard ways to do Pre-Closure Diagnostics explained in previous examples. The semi-log derivative (G*dp/dG) curve is still increasing at the final data point. However going by the "Tangent method" of identifying closure pressure, the values comes to be: closure at shut-in of Δt= 0.05 hrs = 3 min, closure pressure of 28501 kPa (a), efficiency of 13.32 % and net fracture propagating pressure of only 988 kPa (a).

From the established source – ("SPE-38575-MS.pdf,"; BRANAGAN et al., 1997; Warpinski et al., 1998,), we know that the closure was not observed during injection test 5-B and 6-B. It is also easily visible from the G-function and Sqrt(t) plot where the semi-log derivative curve keeps on increasing while it should gradually decrease post-closure, seen in previous field examples. The formation is a tight gas reservoir with permeability in range of micro Darcy or higher, the net efficiency must be much higher (60% or above). Net fracture pressure from independent sources ("SPE-38575-MS.pdf,"; BRANAGAN et al., 1997; Warpinski et al., 1998, n.d.) is 8957 kPa (a) while with FEKETE, it's only 988 kPa (a) which is clearly a wrong figure. Similarly, After-Closure Analysis results and plots done were inaccurate.

One way of explaining the non-decreasing pressure and derivative plot is that due to very low permeability reservoir, leak-off rate was extremely minimal. The near-well pressure decreases as the fracture closes, which results in a decrease of fracture width at the well. The closing of the fracture volumetrically displaces fluid to the

tip of the fracture, causing continued extension of fracture length. (Barree et al). This mechanism is called Fracture Tip Extension and often extends into the adjacent layers. Here, as well similar observation was seen where the fracture length propagated past B-sand layer (confirmed by microseismic survey and tiltmeter tests) (BRANAGAN et al., 1997)

Since no fracture closure was observed for injection 5-B and 6-B, no after-closure analysis could be conducted.

(B) - VdHoek Analytical Model:

The values in our case shown in Table 14 are taken from Table 13 (with the Source literature mentioned)

Table 14 Input parameters for VdHoek analytical model – Injection 5-B

Porosity	0.08	[-]
Fluid Compressibility	$4.93 * 10^{-08}$	Pa^{-1}
Reservoir fluid viscosity	0.00002	Pa*s
Injection fluid viscosity	0.041	Pa*s
Young's modulus	31.5	GPa
Net pressure	89.6	Bar
Fracture height	30	m
Injection rate	0.0583	m^3/sec
t_{pump}	18.18	min

Fig.78 shows a log-log diagnostic plot of delta pressure and derivative against shut-in time obtained from the VdHoek's analytical model. Couple of important observations was:

(1) Following "standard methodology" where a deviation between pressure change and derivative lines after an early period of storage with slope =1 is considered as an indicator of "fracture closure point" even though no fracture closure was observed (as confirmed from independent tests ("SPE-38575-MS.pdf," n.d.; BRANAGAN et al., 1997; Warpinski et al., 1998, n.d.). We demonstrated same observation with the help of VdHoek numerical model plots for Example 1 that end of storage line may or may not represent a fracture closure point. Analysis of injection 5-B data adds further evidence to VdHoek conclusion from the paper SPE-181593 (Van Den Hoek, 2016)

(2) In fig. 78, pressure derivative departs from the early unit slope (storage) and establishes a (1/4) slope during fracture tip extension. 1/4 slope line is diagnostic of bilinear flow representing a continued dissipation of the linear pressure transient along the fracture length and some linear flow driving the minimal leak-off. As long as the 1/4 parallel slope trend continues between the pressure difference and derivative, the fracture has not closed and is still in the process of extending.

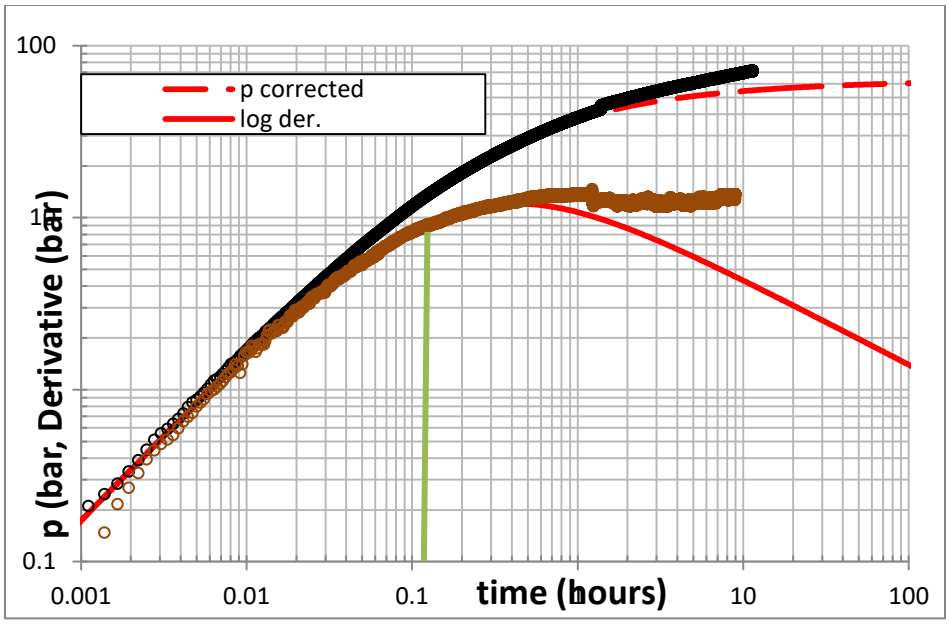

Figure 78 Log-Log pressure difference and derivative diagnostic plot (VdHoek Analytical model) – Injection 5-B

(C) - Comparison between FEKETE (Specialized Plot) vs. Analytical Model

Table 15 Comparison between FEKETE vs. VdHoek model – Injection- 5-B (M-site)

Parameters	Unit	Plot from where value came in FEKETE analysis ***	FEKETE	Analytical Model
Volume Injected	m^3	NA	56.94	63.6
Injection rate	m^3/sec	NA	3.05	3.5
Injection time	min	NA	18.69	18.18
Fracture Half-length	meter	Frac Boundary model	Cannot be determined as no closure occurred	86 ****
Fracture height	meter	NA	Cannot be determined as no closure occurred	30 ****
Permeability	m^2	Frac Boundary model	Cannot be determined as no closure occurred	$1.18 * 10^{-18}$
Net Pressure	kPa (a)	BCA – G-function, Sqrt(t) plot	Erroneous value	8961.8 ****

Total Leak-Off coefficient	(m/sqrt(sec))	Nolte ACA Linear plot	Cannot be determined as no closure occurred	$3.04 * 10^{-06}$
Initial Total Compressibility (c_{tl})	Pa^{-1}	Properties Tab	$5.24 * 10^{-8}$	$5 * 10^{-8}$
Time to Fracture Closure	min	BCA – G-function, Sqrt(t) plot	Cannot be determined as no closure occurred	Cannot be estimated
Pressure at fracture closure time	Bar	BCA – G-function, Sqrt(t) plot	Cannot be determined as no closure occurred	Cannot be estimated
Instantaneous Shut-In pressure (ISIP)	Bar	BCA – G-function, Sqrt(t) plot	Cannot be determined as no closure occurred	Cannot be estimated

* Frac Boundary model - based on Soliman and Craig ACA method
**NA = Not Applicable
*** = For reason, please see pt. (9) and (10) of 'Conclusion' section of Example 1
**** = Source – GRI/DOE 96/ 0225. Initial value taken from obtained, and optimized by the analytical model.

(D) - McClure's Analysis

McClure explains this characteristic of curve on the basis of "well-bore storage" phenomenon, without involving more complex terms like Fracture Tip extension, the explanation of which is mentioned in the preceding section. We decided not to elaborate on the explanation based on wellbore storage here as it wasn't relevant to the scope of this report. Please refer to (McClure et al., 2014)

(E) - Conclusion

Some of the conclusions from injection 5-B data are:

1) Point of deviation between pressure change and derivative data after early storage period cannot be taken as a fool proof method to identify Fracture closure point. Fig. 78 shows a deviation after early storage period which should be taken as closure point but we know from independent sources that no closure occurred at all. Corresponding values of closure pressure point, fluid efficiency, net pressure etc. interpreted were wrong.

   This analysis further cements VdHoek's idea to be cautious of identifying closure point in a log-log pressure derivative plot, and that results from standard methods should always be cross checked against independent methods.

2) Tangent method as used in G-function plot of FEKETE gives erroneous answers. However the plot with non-decreasing semi-log derivative (G*dP/dG) viewed with an expert eyes is sufficient to say that the fracture was still propagating when data terminated.

5.4.2 - M-Site: Injection 2-B (Step-Rate test) – Low Permeability Gas well

Injection (2-B) was performed a day after injection 1-B and consisted of total 4.3 m3 of KCl water pumped down casing at rates starting from 0.08 m3/min to 4.8 m3/minutes. It was designed in part to assess the sensitivity and time response of the inclinometer (which in turn provides a reliable source of fracture closure value). Data was acquired per second.

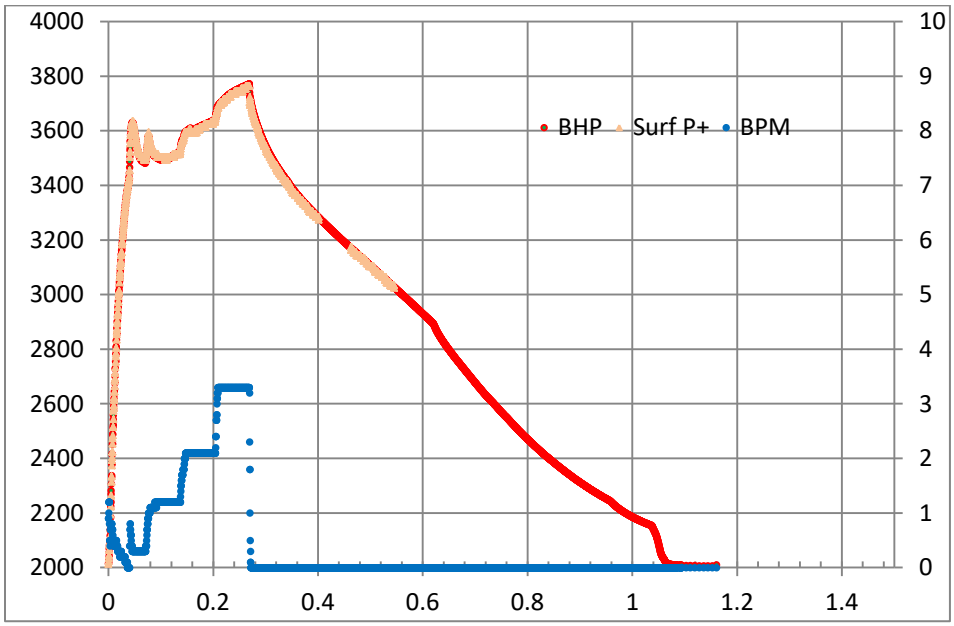

Figure 79 Injection/Shut-in history of Injection 2-B

The brakes in surface P+ [= surface pressure + static head value of 1984 (psi)] between ~ 0.4 – 0.46 hrs. was due to loss of link and later while retrieving those gauges. The obvious change after ~0.62 hrs. was due to the service companies retrieving their high pressure frac lines, valves etc. which probably created a loss of pressure or a leak , hence data beyond that point is no flowback nor is it a result of anything going on in the fractured interval

Analysis using FEKETE:

Total injection time (t_{inj}) is 13.62 minutes with high volume (4.15 m^3) of brine water injected. Fig. 80 is a Cartesian plot of pressure (kPa (a)) vs. time (minutes).Instantaneous shut-in pressure was identified at 25535 kPa (a) (a) by eyeball accuracy. Similar to injection 5-B, it can be noticed that the friction immediately post shut-in was minimal as there weren't enough scattered pressure points visible.

(A) - Before Closure Analysis (Pre-Closure Analysis):

Fig.81 shows a unique behavior of semi-log derivative (G*dP/dG) unseen in field data analyzed before. There is a unique "hump" above the analysis line till G-time = 0.8, after which the analysis line is linear with the curve from 0.8 - ~ 1.15 G-time. There after the semi-log derivative plot increases again until the end of data. Possible reasons can be:

(i) Barree et al explained such behavior is indicative of "pressure dependent leak-off system" which occurs when the fluid loss rate changes with pore pressure or net effective stress in the rock surrounding the fracture. The pressure dependence referred to here is a change in the transmissibility

of the reservoir fissure or fracture system that dominates the fluid loss rate. It only occurs when there is substantial stress dependent permeability in a composite permeability reservoir.

Geology of the formation is indeed multi-layered, lenticular type fracture, a possible suspect for stress dependent permeability.

(ii) McClure explanation – Please refer the McClure analysis section later.

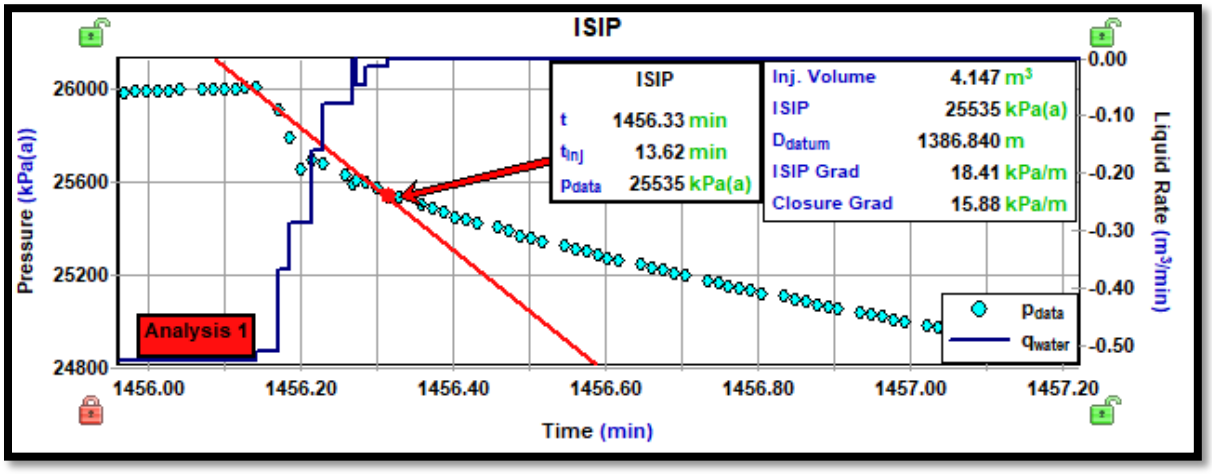

Figure 80 ISIP plot – Injection 2-B

A.1. - G-function analysis:

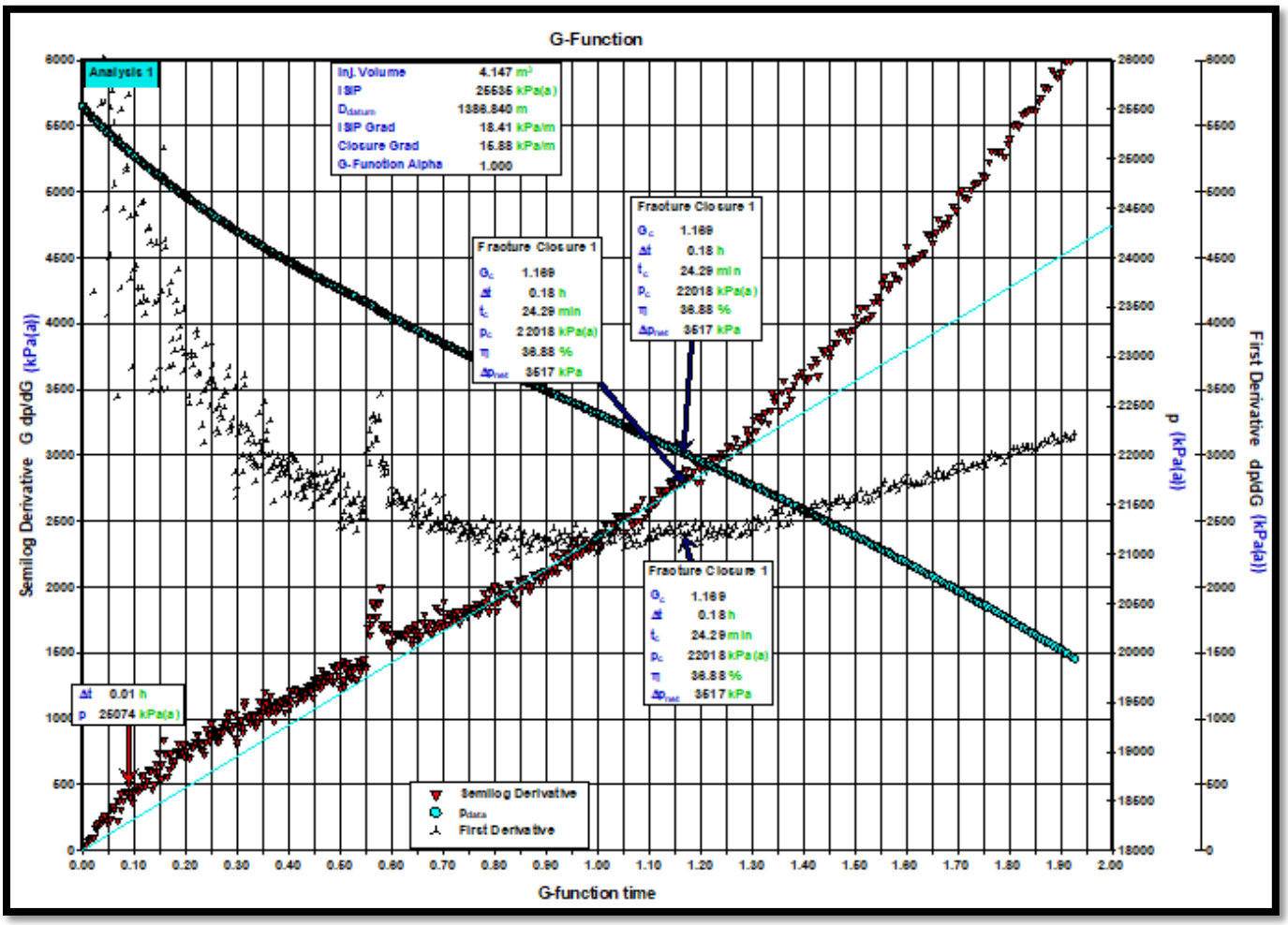

Figure 81 Pressure, First derivative and semi-log derivative of G-function curve against G-time – Injection 2-B

The primary p_data vs. G curve is mildly concave upward and curved while PDL persists. The semi-log derivative exhibits the characteristics "hump" above the straight line extrapolated to the derivative origin. The end of pressure dependent leak-off and the critical fissure opening pressure corresponds to the end of the "hump" and beginning of the straight line representing matrix dominated leak-off. Fracture closure is still shown by the departure of the semi-log derivative from the straight line through origin

A.2. - Sqrt(t) Analysis:

Fig.82. Picking of closure from the most prominent inflection point on the first derivative plot can lead erroneous results in this case. Considering "pressure dependent leak-off phenomenon", the maximum derivative is caused by the changing leak-off associated with PDL and does not indicate fracture closure.
In fact one look at the figure is sufficient to say that till the end of data, the first derivative is still increasing, hence identifying most prominent derivative wasn't possible. The other method to identify closure point from "tangent method" of semi-log derivative curve yields similar result, however its authenticity remains in question. It is like validating what's already there using a different version of same technique.

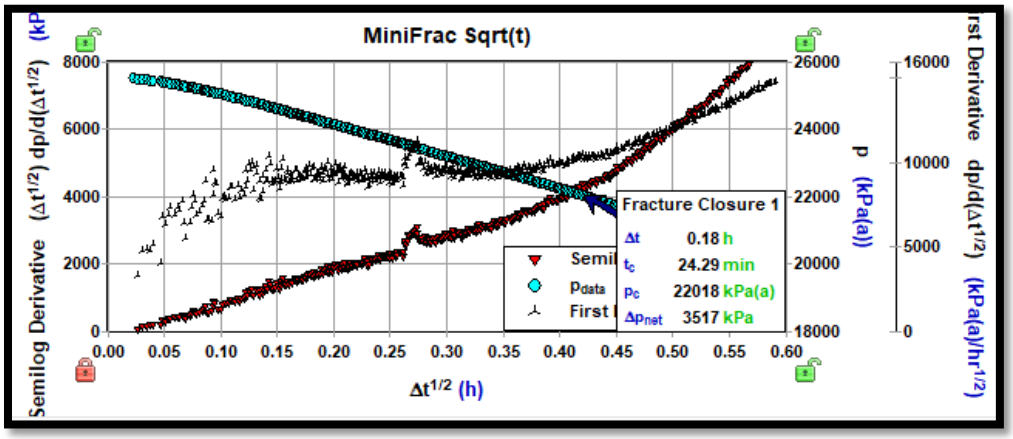

Figure 82 Pressure, First derivative and semi-log derivative of Sqrt(t) function curve against Square root of time – (Injection 2-B)

A.3. - Pre-Closure Log-Log Pressure Derivative plot:

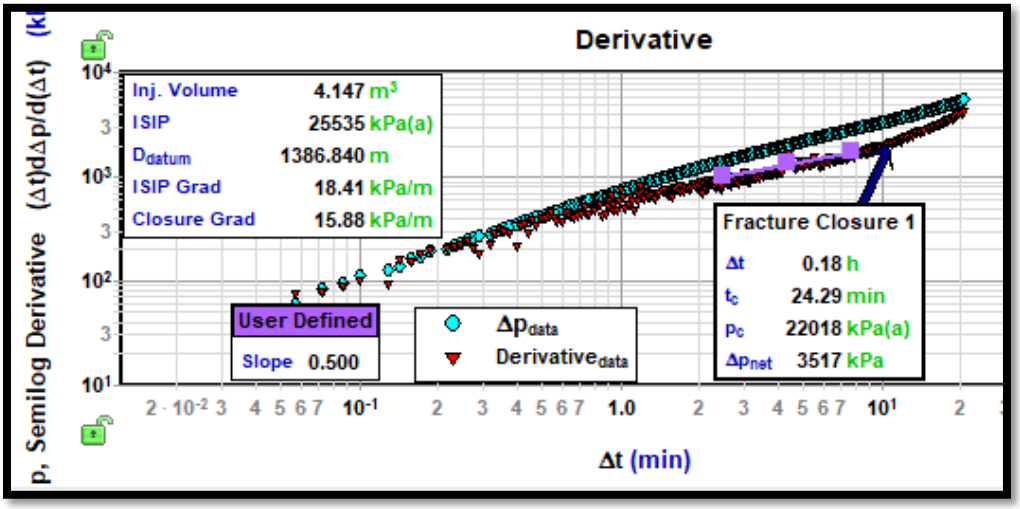

Figure 83 Log – Log plot of pressure difference and derivative curve – (Injection 2-B)

Figure 83 shows the log-log plot for the injection 2-B with the fracture closure point determined from the Tangent method. A slope of ½ indicative of formation linear flow is visible. This period appears following the end of PDL. Although the closure as shown, pressure difference and derivative curve after it are increasing. Discussion about the value of closure pressure being higher than the determined 21029 kPa(a) value is covered in "Conclusion" section.

(B) - After Closure Analysis (ACA):

Fig. 84 and 85 shows the Nolte derivative plot and Soliman and Craig derivative plot. Purpose of showing the plots is to highlight the point that the plots aren't developed showing no reliable indication of any flow regime developed at all. Given such limitation, no constructive interpretation could be carried out. It highlights the importance of a long radial regime to assess the field data reliably and also to understand that not all field data can always be assessed with these ACA techniques, requiring other interpretation methods.

B.1. - Nolte ACA analysis:

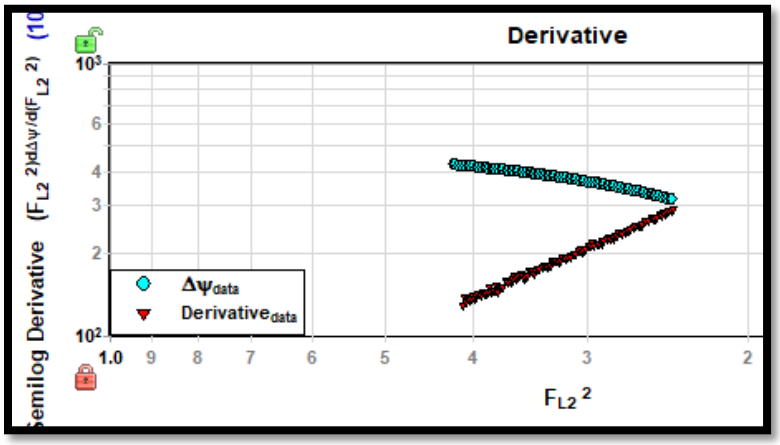

Figure 84 Log-lot plot of pressure difference and semi-log derivative vs. F_L^2

B.2. - Soliman and Craig ACA Analysis:

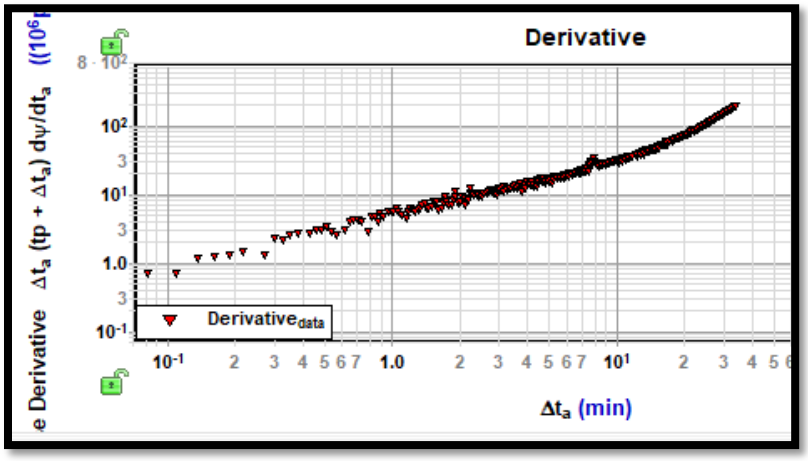

Figure 85 Soliman-Craig Log-log plot of Impulse derivative vs. adjusted shut-in time (min)

(C) - VdHoek Analytical Model:

Table 16 Input parameters for VdHoek analytical model – Injection 2-B

Porosity	0.08	[-]
Fluid Compressibility	$5.80 * 10^{-08}$	Pa^{-1}
Reservoir fluid viscosity	0.00002	Pa*s
Injection fluid viscosity	0.001	Pa*s
Young's modulus	31.5042051	GPa
Net pressure	41.36	Bar
Fracture height	15.17	m
Injection rate	0.00848	m^3/sec
t_{pump}	14	min

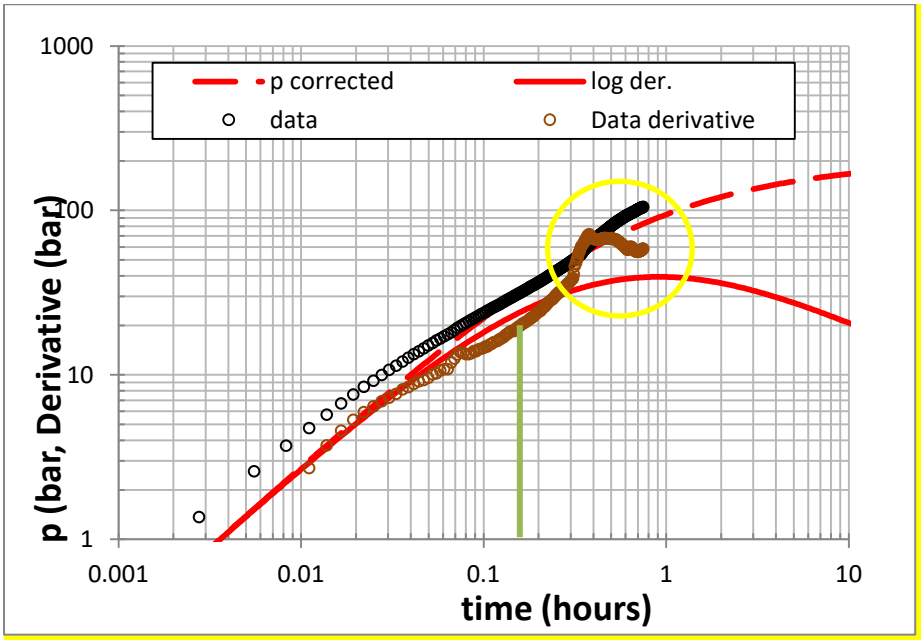

Figure 86 Log-Log pressure difference and derivative diagnostic plot (VdHoek Analytical model) – Injection 2-B

Fig. 86 shows log-log diagnostic plot obtained from VdHoek analytical model. The methodology to obtain the fracture parameters are described in detail in previous field data's discussion. We notice here that the data plot doesn't match well with the model data. The reason is the limited available data set for injection 2-B. The green vertical line reflects the closure point as identified by "Tangent" method in FEKETE, which is almost impossible to pin-point independently from fig. 86.

(D) - Comparison between FEKETE (Specialized Plot) vs. Analytical Model

Table 17 Comparison between FEKETE vs. VdHoek model – Injection- 2-B (M-site)

Parameters	Unit	Plot from where value came in FEKETE analysis ***	FEKETE	Analytical Model
Volume Injected	m^3	NA	4.147	7.12
Injection rate	m^3/sec	NA	0.00507	0.00848
Injection time	min	NA	13.62	14
Fracture Half-length	meter	Frac Boundary model	Cannot be determined	42.7 ****
Fracture height	meter	NA	Cannot be determined	15.2 ****
Permeability	m^2	Frac Boundary model	$2.3 * 10^{-17}$	$22.6 * 10^{-18}$
Net Pressure	Bar	BCA – G-function, Sqrt(t) plot	35.17	41.36
Total Leak-Off coefficient	(m/sqrt(sec)	Nolte ACA Linear plot	Cannot be determined	$5.07 * 10^{-6}$
Initial Total Compressibility c_t	Pa^{-1}	Properties Tab	$6.81 * 10^{-8}$	$5.87 * 10^{-8}$
Time to Fracture Closure	min	BCA – G-function, Sqrt(t) plot	24.29	Cannot be estimated
Pressure at fracture closure time	Bar	BCA – G-function, Sqrt(t) plot	22018	Cannot be estimated
Instantaneous Shut-In pressure (ISIP)	Bar	BCA – G-function, Sqrt(t) plot	25535	Cannot be estimated

* Frac Boundary model - based on Soliman and Craig ACA method
**NA = Not Applicable
*** = For reason, please see pt. (9) and (10) of 'Conclusion' section of Example 1
**** = Source – GRI/DOE 96/ 0225.Initial value taken from obtained, and optimized by the analytical model.

Some observations from the Comparison table are:

1) Total injection time for VdHoek model is almost double (7 minutes) than FEKETE (4 min). This is because data where the "service companies started pulling back their equipment leading to pressure loss – highlighted with yellow circle in fig.86" was filtered in FEKETE whereas it wasn't in VdHoek model, hence one can also see the plot for some time more.

2) Fracture dimensions could not be calculated from FEKETE due to limited after-closure data. This demonstrates a drawback of FEKETE that unless decently long after closure data is available, no ACA analysis can be done.
3) In comparison to point (2) above, although the fracture parameter data are given as input (taken from independent test results), the model works well highlighting the point that VdHoek can be used to validate results from other analysis.
4) Permeability differs by an order of magnitude here between the two models. Likely reason being the limited after closure period as well as the complicated geometry of B-sand injection

(E) - Independent Closure Test measurement using Inclinometer

Fig. 87 shows the normalized tiltmeter response plotted against wellbore pressure during injection 2-B, the test immediately after the breakdown test (step-rate test discussed before). Each tiltmeter response is normalized by dividing the maximum tilt measured at that instrument during the test. The tiltmeter began to demonstrate that the fracture began opening at approximately 23900 KPa, very close to the pressure identified by Fracture Compliance Method from the shut-in transient after the breakdown injection (which immediately preceded the 2-B injection). At 23900 kPa the derivative of tilt with respect to pressure becomes much greater, indicating an abrupt drop in fracture compliance at that pressure corresponding to reopening.
The above figure shows only the data during injection, not shut-in. The shut-in tiltmeter response is much smoother and shows a gradual relationship between tilt and wellbore pressure. This difference is caused by the contribution to the tiltmeter response from the poroelastic effect of the fluid leaked off into the formation. During injection, the amount of leak-off is relatively minimal, which is why the tiltmeter response during injection (reopening) is more appropriate for estimating the minimum principal stress.(McClure et al., 2016)

(Branagan et al., 1996) report substantial residual deformation (20% of the maximum deflection) many weeks after the first four injections into the B-sand, which they interpret as suggesting that the fracture retained significant residual aperture after closure.

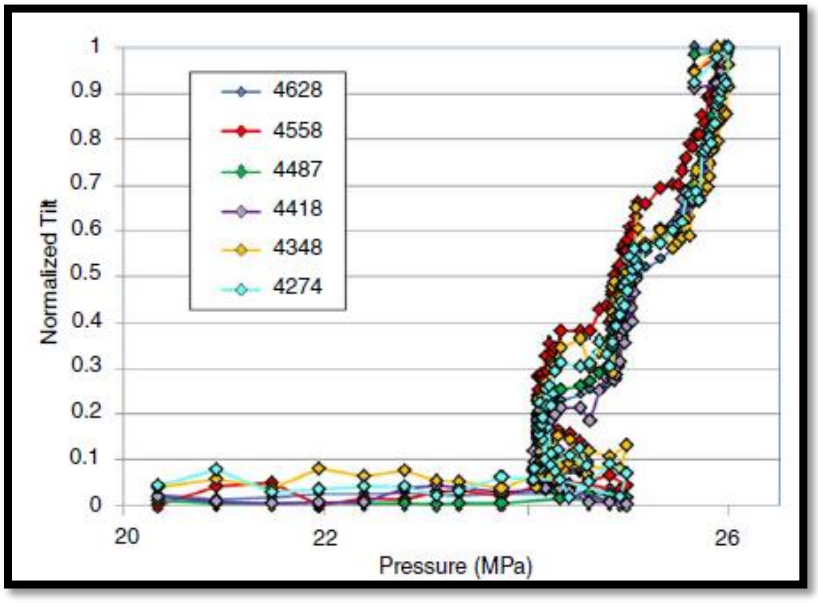

Figure 87 Normalized tiltmeter/inclinometer data from injection 2-B from the GRI/DOE M-site. (SPE -179725 – Data courtesy of Norm Warpinski)

(F) - McClure's Analysis

Fig. 88 is the plot obtained from McClure et al paper. The plot of Pressure and its G-function based semi-log derivative is until G-time of 12 where shown in Fig.81, the data for same injection 2-B obtained from Branagan & Associates only extends until G-time=2. This extended time plot gives a much clear picture of the entire phenomenon.

"The G-function plot shows a period of early fracture tip extension at early time which terminates at G-time ~ 1. Afterwards, the G*dP/dG curve flattens out before beginning to increase sharply after approximately G-time of 3.5 (indicated by orange arrows). According to the fracture compliance method, this increase in the G*dP/dG curve represents closure, and so the minimum principal stress should be picked from the pressure corresponding to G-time of 3.5, which is 24.3 MPa. The tangent method yielded closure point at approximately G-time=9.5, corresponding to pressure of 22750 KPa (blue arrow)" - (McClure et al., 2016)

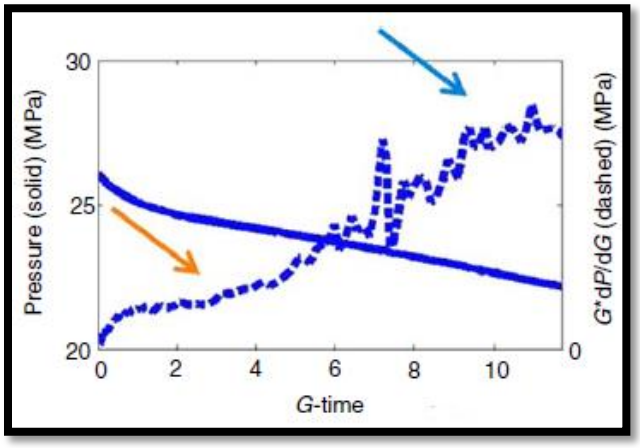

Figure 88 Pressure and G-function based semi-log derivative against G-time (source: McClure et al – SPE-179725)

(G) - Discussion about the Closure Pressure

Although identification of fracture closure point was one of the key focus of the extensive tests done on B-sand over few years, yet different authors who worked on this project have different opinions about closure value.(Branagan et al., 1996) estimated closure value at 21029 kPa, (Gulrajani et al., 2001) at 23787 kPa. Later McClure using his Fracture Compliance method (McClure et al., 2016) also concluded the closure pressure at 23787 kPa.
Stress log that included the sonic log assessment of stress, along with the in-situ stress test data from all 3 M-site wells (MWX-1,2,3) and the perforated interval shows that the stress variation just within the B-sand perforated interval vary from about 21029 kPa to 25510 kPa. Most of that perforated interval lies within a somewhat smaller several hundred kPa zone.

The vertical imaging of the microseismics from the 2B injection and shut down periods indicate that the fracture probably didn't grow much higher than the perforated interval and incidentally continued to create events well after shutdown. Thus the bulk of the fracture was propagating within that not so terribly complex stress zone, say between 21029-23787 kPa.

Fracture opening (or more specifically, reopening) pressure was observable with the inclinometers. Because the rate of pressure increase during fracturing was high, correlating the exact point at which the inclinometers began to respond yields a pressure range of about 4757 kPa. Fracture closure on the other hand was obscure for several reasons. Although complete mechanical frac closure may never really be totally achieved due to asperities, spalled rock debris, shear slippage and other mechanical issues, the effects of fracture fluids should be minimized

for these simple water fractures. Closure, even during flowback, was not a readily definable parameter for the inclinometers. This may be due in part to pore pressure increase resulting from leak-off in the area near the frac faces. Leakoff increases poroelastic effects and accordingly masks mechanical closure, even if not perfect. Another reason for this seeming lack of observed closure was the method used to assess the process. Because each of these water fractures was small, they were executed relatively quickly. Although each injection was followed by a shut-in period, flowback occurred within hours and thus researchers expected the inclinometers to return to very near their original pre-injection baseline after several hours. However, this phenomenon was not observed. While the tilt rate for the inclinometers appeared to go to zero resulting in a flat line, it was considerably above baseline.

Rephrasing Mr. Paul Branagan's word on closure: " Demonstrated by Injection 2-B with confirm residual aperture width, real hydraulic fractures have much more complicated features with branching, non-planarity, and termination against natural fractures (BRANAGAN et al., 1997) as visible from B-sand injection study. All of these features tend to decrease fracture compliance. If fluid is actually distributed into a larger number of smaller fractures, the overall system compliance will be lower because compliance scales with fracture size. The backstress on each fracture would tend to increase normal stress on adjacent fractures, further decreasing system compliance.

Non-planar fracture formation may result in the normal stress not being homogenous along the newly formed fractures. As a result closure could occur more gradually, because the fracture(s) must close against a distribution of different closure stresses. Stress heterogeneity may also exist because of prior geological loading or heterogeneity in elastic properties in the formation. Stress heterogeneity would tend to smear out closure in the pressure transient response by causing closure to occur across a distribution of normal stress along the fracture faces. All of these behaviors may manifest themselves as an effectively "rougher" fracture. "

5.5 - NIMR Field – Water Flooding induced fractures – Medium permeability Gas well

This data set was obtained from NIMR field, Oman and is the only data in our study where waterflooding induced fracturing case occurred. This formation is a fairly homogeneous, medium-permeability (approx. 300mD), medium-strength sandstone with a thickness of several hundreds of meters.
Analysis using FEKETE wasn't done for this case since the injection/fall off test option does not include fracturing feature.

(A) - VdHoek Analytical Model:

Table 18 Input parameters for VdHoek analytical model – NIMR field waterflooding

Porosity	0.25	[-]
Fluid Compressibility	0.0000000005	Pa^{-1}
Reservoir fluid viscosity	0.0005	Pa*s
Injection fluid viscosity	0.001	Pa*s
Young's modulus	5	GPa
Net pressure	27.5	Bar
Fracture height	30.06	m
Injection rate	0.057	m^3/sec
t_{pump}	6000	min

Fig. 89 shows pressure and derivative log-log diagnostic plot for the input parameters given in table 18. The data available was of only of 63 minutes which is extremely short duration for an injection fall off test to do any reliable analysis. Resulting we see from the plot as well that a good match between the field data and model data couldn't be achieved with the optimized fracture length and height value obtained as 18 m and 30 m respectively. This value is far away from the values obtained with HIT test results and PLT test results (46 m each) mentioned in (Hoek et al., 2000).
Since this model has provided reliable estimate for multiple waterflooding field data cases in past, inability to match fracture dimensions here is attributed to very limited test data.

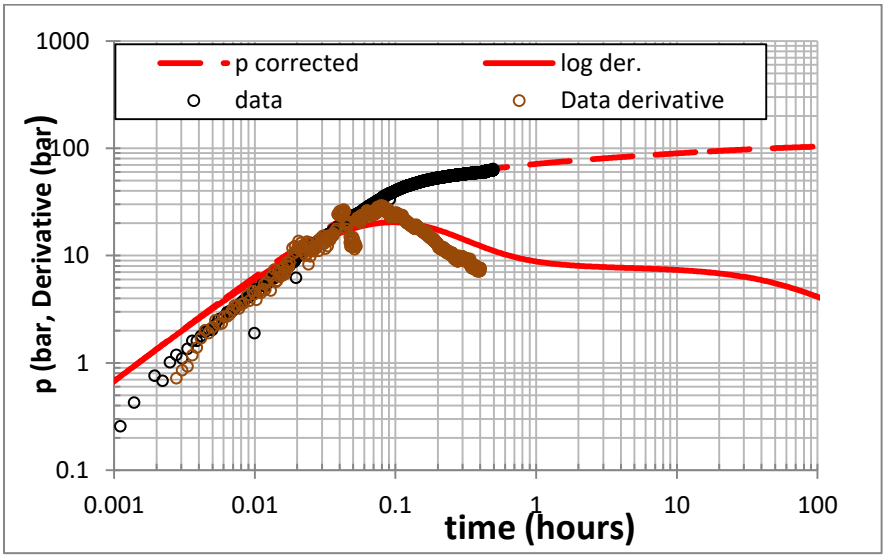

Figure 89 Log-Log pressure difference and derivative diagnostic plot (VdHoek Analytical model) – NIMR field

Chapter 6- Permeability (K) estimation from Before Closure Analysis (BCA)

In the (Lamei and Soliman, 2014) paper, a new method was proposed to identify permeability (K) from Before Closure Analysis. They stated that while a number of models to analyze After-Closure-Regime were developed over years, not much work has been done on BCA. Hence, they introduced a new BCA model based on rigorous treatment of the fluid flow equation in the fracture and the formations, with the main assumptions of linear leak-off and short injection time.
The final form for the new BCA model is:

$$1.05114\,\frac{r_p\,\Delta p_{inj} c_{Df} t_i}{c_f}\left(\frac{\emptyset K c_t}{\mu}\right)^{\frac{1}{2}}\left(\frac{1}{\sqrt{t_n}}-\frac{1}{\sqrt{t_i}}\right)+P_i=P_n \quad \text{------ (a-1)}$$

Rearranging equation a-1 such that permeability (K), the unknown comes at L.H.S. while every known parameter comes to R.H.S:

$$\sqrt{K}=\left(\frac{P_n-P_i}{\frac{1}{\sqrt{t_n}}-\frac{1}{\sqrt{t_i}}}\right)*c_f*\frac{1}{(1.051114\ r_p\Delta p_{inj} c_{Df} t_i)*\sqrt{\emptyset c_t}} \quad \text{--------- (a-2)}$$

Where,

r_p = ratio of permeable to fracture area; Δp_{inj}= P_inj – P_initial; c_{Df}= dimensionless before closure fracture storage;

t_i= time at end of injection; ∅= porosity; μ= viscosity; t_n = time at the end of step “n”; P_n= pressure at end of step “n”; n = time step index (Here “n” is any time step after injection time and before closure time); L= length of fracture; h=height of fracture; E’ = plain strain modulus; c_t = total compressibility (1/Pa)

Implementing equation a-2 in MATLAB where fracture compliance value, dimensionless before closure fracture storage were calculated for different fracture geometries (PKN, GDK, Radial) separately, we obtained following plots for field data Example1,2,3. NIMR data set was waterflood injection, hence no closure was studied. M-site Injection 5-B,6-B also didn’t show a fracture closure and Injection 2-B field data was excluded from this section because the closure pressure range identified was quite high (20684 kPa – 25510 kPa).

Note that: Radial fracture geometry length values are only estimates and not calculated in particular for this study.

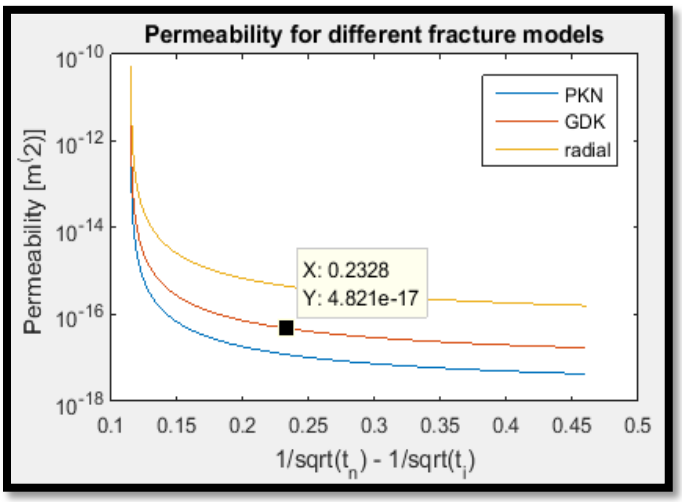

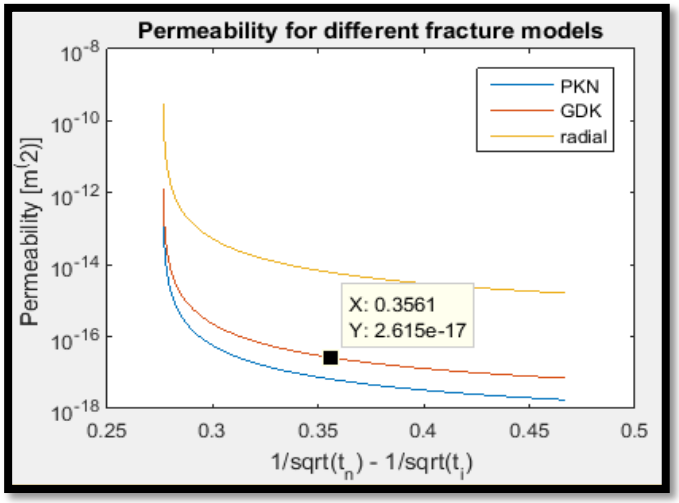

(i) Example 1 (ii) Example 2

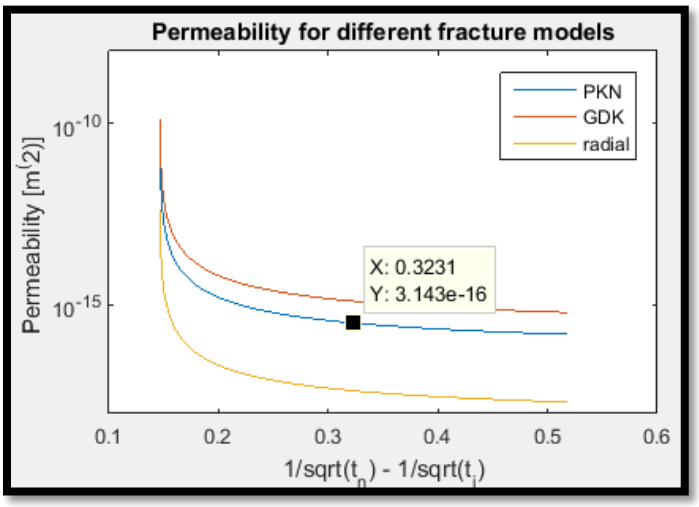

(ii) Example 3

Figure 90 Permeability from Lamei-Soliman BCA model

Figure 90 shows three different plots (i), (ii) and (iii) of permeability against reciprocal of square root of time difference giving permeability value obtained from BCA of Example 1, 2 and 3 respectively.

Following table is a comparison of permeability obtained from VdHoek Model vs. FEKETE vs. FenixConsulting analysis from their BCA approach vs. Lamei and Soliman BCA model

Table 19 Permeability comparison obtained from different models

Field Data		Model type			
	Unit	VdHoek analytical model	FEKETE (ACA)	Fenix Consulting (BCA)	Lamei and Soliman (BCA)
Example 1	m^2	0.2 E-17	3.2 E-16	7E-17	4.8 E-17
Example 2	m^2	2.4 E-18	2.3 E-18	14E-18	26e-18
Example 3	m^2	1.02E-18	4.5 E-17	10E-17	31.4 E-17

A look at Table 19 shows that permeability value obtained from all the four models are in same or similar order of magnitude irrespective of After closure or Before Closure period. Example 2 with a long well developed radial flow has consistent permeability value across all four models. This exercise also helps in pin pointing a particular fracture geometry of the given formation. Thus, it gives more confidence in VdHoek model's working as its results are matching against three different unique models, both with BCA and ACA approach.

Chapter 7 - Summary of Conclusions

1) One of the objectives of the thesis was to provide consistent interpretation that helps to give the most useful information available from the minifrac/DFIT tests. The prescribed diagnostic for post shut-in pressure transient analysis includes a suite of analytical techniques through which bottomhole pressures and delta-pressures are plotted against different time scales. More than one method was used to identify the fracture closure and permeability. Instead of picking any individual diagnostic plots for interpretation, it is important to look at the whole suite of plots in order to gain a more comprehensive understanding of what information (closure pressure, closure mechanism, fracture dimensions etc.) the test data is conveying.

2) VdHoek unified analytical model works good (without making any significant changes) with both waterflooding and minifrac/DFIT tests in estimating correct values of permeability, fracture dimensions etc., hence providing an easy, effective way to confirm / validate the results of fracture and reservoir engineering parameters obtained from other independent tests. This is the only model which can handle arbitrary fracture propagation and leak-off rate between the two ends of spectrum. On other hand, in FEKETE, the methodology to analyze minifrac vs. waterflooding is different (separate BCA and ACA, excluding the closure process) and needs training and expertise to make a reasonable analysis.

3) Fracture Closure point as identified in log-log plot by deviation from linear slope line should be viewed with caution. It may or may not be the closure point (Van Den Hoek, 2016). It was demonstrated in Example 1 using numerical model plot, and injection 5-B against value obtained from independent sources.

4) Jointly Example 1, 2, 3 field data presented three unique post closure cases: Example 1 – short radial flow (but ends before the analyzable time period starts). Example 2 – long well developed radial flow. Example 3 – (short radial flow but it lies in the analyzable time period.) For each of these cases, VdHoek analytical model performs in line with industry used software giving a good match of output parameters. Results were similar to the results obtained from "FEKETE" using standard methodology.

5) When detailed analysis is not possible due to absence of sufficient after closure flow data, the estimated permeability will most likely deviate by an order compared to the true permeability values. See, e.g. Example 1 and 3, NIMR Field data. Thus to determine a reliable estimate of permeability, a well-developed long radial flow regime is critical.

6) After-Closure Analysis (ACA) was done using two methods: (i) Nolte method (ii) Soliman and Craig method.
Nolte's method uses a plot of pressure vs. a specialized function called "the linear flow time function (F_L)". From the experience of working on different data sets, it appears that F_L plots are more complex and comparable interpretation is achieved using simpler plots.
Nolte linear time function, F_L is generally defined as $F_L\left(\frac{t}{t_c}\right) \approx \frac{2}{\pi}\left(\sqrt{\frac{t_c}{t}}\right)$ where t is the shut-in time and t_c is the time to closure, assuming "the shut-in time is more than three times the t_c". As we see, F_L is roughly equal to one over square root of time; it behaves similar to Soliman and Craig time function.

Nolte's approach has several shortcomings. He suggested estimating permeability from early post-closure linear flow period. However, we know that in typical DFIT tests, shut-in time lasts long enough so a post-closure linear-flow regime (slope=-1/2) is always visible. Second, pre knowledge of "closure time, t_c" is

required, the value of which is always a subject of debate/uncertainty in early part of formation testing. Last point is Nolte's derivations were based on "zero fluid presence at closure in the fracture" assumption. It is well established by multiple field observations and lab experiments that fracture walls always are rough, facilitating fluid storage even after fracture walls come into contact. Hence, it is debatable to use Nolte time function for estimating permeability from the postclosure linear period.
Similarly, identifying permeability from radial flow doesn't offer any advantage over simpler one divided by shut-in time method as proposed by Soliman and Craig.

7) To sum up the above discussion in (6), diagnostic plot using F_L or 1/ F_L are used to diagnose postclosure regimes in the same way as standard log-log derivative plot. Nolte's method can be used as a validation technique for the parameters obtained from other techniques, but it is not recommended to use it solely as it make things complicated which can be solved by other simpler method (Soliman and Craig ACA technique in our case).

8) At times, new models are developed and validated against narrow range of selected data to prove they work better against the previous existing models. For such models, multiple introduced quantities (that increases complexity and uncertainty) will provide higher degree of freedom for tuning as the "changeable "quantities are higher. More often than not these models prove unsatisfactory in capturing the underlying physical phenomenon.
For VdHoek model, to prove the point that no "deliberately selected data" were taken and instead data covering both ends of the leak-off spectrum were used; same data was run with another industry wide used model i.e. using FEKETE. The resulting plots from both were similar giving similar output values, thus giving more confidence in VdHoek unified model.

Chapter 8 - Recommendations for Future Work

1) Incorporate option of different Fracture geometry model (PKN or GDK or radial flow model) in the VdHoek analytical model. Different fracture model gives different permeability results. By matching the permeability value obtained from different fracture models against independent sources / other test (like FEKETE), one can easily confirm the actual fracture geometry developed in the formation.

2) VdHoek Numerical model is a promising work to demonstrate that end of storage flow period isn't necessarily fracture closure point, mapping of fracture closure process post shut-in. Further detail analysis using numerical model against field data covering both end of fluid leak-off spectrum should be carried out to validate the robustness of the model and to prove standard methodologies way of identifying fracture closure should be viewed with caution.

   Numerical model simulator is still not very user-friendly. It can be a potential work for a Master's Thesis project with main tasks including: validating the model against variety of field data sets to identify its short coming, optimizing it, making it more user-friendly so that it can be commercialized in near future.

3) Include fracture closure identification feature in VdHoek's Analytical model. Do quality checking against more waterflood cases as in our project, we only could do on one such data (NIMR) and the results weren't very satisfactory. Make it more user-friendly so it may be commercialized in future.

4) Until now, permeability is generally estimated from After Closure Analysis with very limited work done in area of "estimating permeability from Before Closure Analysis" in past. Lamei and Soliman (Lamei and Soliman, 2014) developed a new model to estimate permeability from BCA which they demonstrate in their paper to show matching results against other ACA based techniques. A potential master's thesis topic can be implementing the mathematics used to develop the model as referred in paper to develop a working simulator and do cross validation of their study with new field data sets.

References

1. Barree, R. D., V. L. Barree, A. Llc, and D. P. Craig, 2007, Holistic Fracture Diagnostics: SPE Rocky oil & gas technology symposium, doi:10.2118/107877-PA.
2. Barree, R. D., J. Miskimins, and J. Gilbert, 2014, Diagnostic Fracture Injection Tests: Common Mistakes, Misfires, and Misdiagnoses: SPE Production & Operations, v. Preprint, no. Preprint, p. Preprint, doi:10.2118/169539-PA.
3. Bourdet, D., J. A. Ayoub, and Y. M. Pirard, 1989, Use of Pressure Derivative in Well Test Interpretation: SPE Formation Evaluation, v. 4, no. 2, p. 293–302, doi:10.2118/12777-PA.
4. Branagan, P. T., R. E. Peterson, N. R. Warpinski, and T. B. Wright, 1996, Characterization of a Remotely Intersected Set of Hydraulic Intersection Well No. 1-B, GRVDOE Multi-Site Project: SPE Annual Technical Conference, no. 1, p. 351–361.
5. BRANAGAN, P., R. PETERSON, N. WARPINSKI, T. WRIGHT, B. & ASSOCIATES, S. N. LABS, and R. E. SYSTEMS, 1997, Results of the Multi-Site Project Experimentation in the B-Sand Interval: Fracture Diagnostics and Hydraulic Fracture Intersection: Topical Report: Gas Res. Inst. Rep. No.Gri-96/0225 (Doe/Mc/30070-5218), no. 200036.
6. Cinco-Ley, H., and F. Samaniego-V., 1981, Transient pressure analysis for fractured wells: Journal of Petroleum Technology, v. 33, no. 9, p. 1749–1766, doi:10.2118/7490-PA.
7. Cinco-Ley, H., V. Samaniego, and A. Dominguez, 1978, Transient Pressure Behavior for a Well With a Finite-Conductivity Vertical Fracture: SPE Journal, v. 18, no. 4, p. 253–264, doi:10.2118/6014-PA.
8. Van Everdingen, A. F., and W. Hurst, 1949, The Application of the Laplace Transformation to Flow Problems in Reservoirs: Petroleum Transactions, AIME, no. December, p. 305–324, doi:10.2118/949305-G.
9. Ewens, S., E. Idorenyin, P. O'Donnell, F. Brunner, and M. Santo, 2012, Executing Minifrac Tests and Interpreting After-Closure Data for Determining Reservoir Characteristics in Unconventional Reservoirs: Proceedings of SPE Canadian Unconventional Resources Conference, doi:10.2118/162779-MS.
10. Gilles_Bourdarot, 1998, Well_Testing_Interpretation.
11. Gringarten, A. C., H. J. Ramey, and R. Raghavan, 1974, Unsteady-State Pressure Distributions Created by a Well With a Single Infinite-Conductivity Vertical Fracture: Society of Petroleum Engineers Journal, v. 14, no. 4, p. 347–360, doi:10.2118/4051-PA.
12. Gulrajani, S. N., K. G. Nolte, and J. Romero, 2001, Evaluation of the M-Site B-sand fracture experiments: Evolution of a pressure analysis methodology: Spe Production & Facilities, v. 16, no. 1, p. 30–41, doi:10.2118/69206-PA.
13. van den Hoek, P. J., 2005, Dimensions and Degree of Containment of Waterflood-Induced Fractures from Pressure Transient Analysis: SPE Reservoir Evaluation & Engineering, v. 8, no. 5, p. 377–387, doi:10.2118/84289-PA.
14. Van Den Hoek, P., 2016, SPE-181593-MS A Simple Unified Pressure Transient Analysis Method for Fractured Waterflood Injectors and Minifracs in Hydraulic Fracture Stimulation: p. 1–24.
15. Van den Hoek, P., H. Mahani, T. Sorop, D. Brooks, M. Zwaan, S. Sen, K. Shuaili, and F. Saadi, 2012, Application of Injection Fall-Off Analysis in Polymer flooding: SPE Europec/EAGE Annual Conference, p. 1–10, doi:10.2118/154376-MS.
16. Hoek, P. J. Van Den, G. Sommerauer, L. Nnabuihe, and D. Munro, 2000, Large-Scale Produced Water Re-Injection Under Fracturing Conditions in Oman: doi:10.2118/87267-MS.
17. Koning, E., 1988, Waterflooding under fracturing conditions: p. 251.
18. Lamei, H., and M. Y. Soliman, 2014, New Before Closure Analysis Model for Unconventional Reservoirs: Spe, no. February, p. 25–27.
19. Mayerhofer, M. J., and M. J. Economides, 1997, Fracture-Injection-Test Interpretation: Leakoff Coefficient vs. Permeability: SPE Production & Facilities, v. 12, no. 4, p. 231–236, doi:10.2118/28562-PA.
20. McClure, M. W., C. A. J. Blyton, H. Jung, and M. M. Sharma, 2014, The Effect of Changing Fracture Compliance on Pressure Transient Behavior During Diagnostic Fracture Injection Tests: SPE Annual Technical Conference and Exhibition, doi:10.2118/170956-MS.
21. McClure, M. W., H. Jung, D. D. Cramer, and M. M. Sharma, 2016, The Fracture-Compliance Method for

Picking Closure Pressure From Diagnostic Fracture-Injection Tests: SPE Journal, no. August 2014, p. 1–19, doi:10.2118/179725-PA.

22. Nolte, K. G., 1986, Determination of Proppant and Fluid Schedules From Fracturing-Pressure Decline: SPE Production Engineering, v. 1, no. 4, p. 255–265, doi:10.2118/13278-PA.
23. Nolte, K. G., J. L. Maniere, and K. a. Owens, 1997, After-Closure Analysis of Fracture Calibration Tests: Proceedings of SPE Annual Technical Conference and Exhibition, p. 1–17, doi:10.2523/38676-MS.
24. Padmakar, A. S., 2013, Geomechanics Coupled Reservoir Flow Simulation For Diagnostic Fracture Injection Test Design And Interpretation In Shale Reservoirs: SPE Annual Technical Conference and Exhibition, doi:10.2118/166201-MS.
25. Pater, C. J. De, J. Desroches, and L. Weijers, 1996, Physical and Numerical Modeling of Hydraulic Fracture Closure EXPERIMENTS: v. i, no. May.
26. Soliman, M. Y., D. Craig, K. Bartko, Z. Rahim, and D. Adams, 2005, After-closure analysis to determine formation permeability, reservoir pressure, and residual fracture properties: SPE Middle East Oil and Gas Show and Conference, MEOS, Proceedings, p. 551–565, doi:10.2118/93419-ms.
27. SPE-38575-MS.pdf, n.d.
28. Warpinski, N.R., Engler, B.P., Young, C.J., Sandia Natl. Labs; Peterson, R., CER Corp. Inc.; Branagan, P.T., Branagan & Assoc.; Fix, J.E., J. E. F. & A., 1995, Microseismic Mapping of Hydraulic Fractures Using Multi-Level Wireline Receivers: SPE Annual Technical Conference and Exhibition, p. 579–589.
29. Warpinski, N. R., P. T. Branagan, R. E. Peterson, and S. L. Wolhart, 1998, An interpretation of M-Site hydraulic fracture diagnostic results: SPE Rocky Mountain Regional / Low Permeability Reservoirs Symposium and Exhibition, v. 39950, p. 1–14, doi:10.2523/39950-MS.
30. Warpinski, N. R., S. N. Laboratories, R. Wilmer, and B. Engler, n.d., SPE 36451 Measuring the Hydraulic Fracture-Induced Deformation of Reservoirs and Adjacent Rocks Employing: p. 1–13.
31. Warpinski, N. R., S. N. Labs, T. B. Wright, R. E. Systems, J. E. Uhl, P. M. Drozda, S. N. Labs, R. E. Peterson, and P. T. Branagan, 1996, at the DOE/GRl: p. 327–335.
32. Wong, D. W., A. G. Harrington, and H. Cinco-Ley, 1986, Application of the pressure derivative function in the pressure-transient testing of fractured wells: Spe, v. 1, no. 5, p. 470–480, doi:10.2118/13056-PA.

Nomenclature

Chapter 2:

P = Pressure, [bar, kPa (a)]
r = position, m
t= time, [minute, sec]
P_{th}= Tubing Head Pressure, [bar, kPa (a)]
P_{bh}= Bottomhole pressure, [bar, kPa (a)]

Chapter 3:

F_{CD}= Dimensionless Fracture Conductivity
$P_{w,d}$ = Dimensionless wellbore pressure
k_{fD}= Dimensionless fracture permeability
w_D= Dimensionless fracture width
q = flow rate (m^3/min, m^3/sec)
B = Formation volume factor, m^3/ m^3
μ= Viscosity, Pa.s
h = fracture height, m
∅= porosity
c_t= total compressibility, 1/Pa
T = Temperature,°C
t_{debf}= Dimensionless end of bilinear flow
P_D= Dimensionless pressure
t_D= Dimensionless time
p_i= Initial Reservoir pressure, [bar, kPa (a)]
p_{wf}= wellbore pressure
L = Fracture half-length, m
t_{Dblf}= Dimensionless beginning of linear flow
t_{Delf}= Dimensionless end of linear flow
s_f= geometrical skin
r_w= wellbore radius, m
t_{Dbrf}= Dimensionless beginning of radial flow
v_{frac}= Fracture propagation velocity, m/s
v_{fluid}= Fluid propagation velocity, m/s
Q_l= rate of fluid injection, (m^3/min, m^3/sec)
$Q_{leakoff}$= rate of fluid Leakoff, (m^3/min, m^3/sec)
C_D= Dimensionless compliance
S = fracture face skin

Chapter 4

t_{pump}= t_{inj}= pump/ injection time, minute
t_{shutin}= time of shut in, minute
G = G-function time
$t_{D,pump}$= Dimensionless pump time
C_{fD} = Dimensionless fracture compliance
$p_{o,D}$= Dimensionless pressure at which length –wise shrinkage starts

Chapter 5:

Ψ= Pseudo pressure, [bar or kPa (a)]
S_g= Gas saturation
c_g= Gas compressibility, 1/Pa
z = Gad compressibility factor
Δt= shut-in time [minute or seconds]
t_c= closure time, [minute or seconds]
P_{shutin}= Shut-in pressure, [bar, kPa (a)]
P_{fo}= Pressure during fall-off (after shut-in), [bar, kPa (a)]
B_{gl}= Gas Formation volume factor
z_i= Gas compressibility Factor (Deviation Factor)
ρ_{gl}= Gas viscosity, Pa.s
c_{fl}= Formation Compressibility, 1/Pa
c_{tl} = Initial total compressibility, 1/Pa
ISIP = Instantaneous Shut-In pressure, [bar or kPa (a)]
D_{datum}= Depth of datum, m
C_f= fracture compliance, m^3/Pa
A = Surface are of the fracture, m^2
s_f = fracture stiffness, Pa/ m^3
V_{wl}= wellbore volume, m^3
c_f= Fluid compressibility, 1/Pa
ΔP_{net}= net fracture pressure, [bar or kPa (a)]
V_{inj}= volume of injection, m^3
c_{pl}= constant term in linear flow expression
c_{pr}= constant term in radial flow expression
Δt_a= pseudo/adjusted time, minute
$F_{L1} = F_{L2}$= Nolte Linear Time function
F_R= Nolte Radial Time function
C_R= Reservoir Fluid Loss coefficient, m/$\sqrt{min}$
C_T= Total Fluid Loss coefficient, m/$\sqrt{min}$
E = Young's Modulus, GPa
$k_{filtercake}$= filter cake permeability, m^2
d = filter cake thickness of the fracture face
X_w = well location in X-direction measured from boundary (semi-infinite reservoir) or origin (finite reservoir), m
Y_w = well location in Y-direction measured from boundary (semi-infinite reservoir) or origin (finite reservoir), m
X_e= Reservoir length, m
Y_e = Reservoir width, m
$P_i(syn)$= Synthetic initial pressure, kPa (a)
$P_{wo}(syn)$= Synthetic initial cushion pressure, kPa (a)
Δt_a= pseudo/adjusted time, minute
$\mu_{g,} OR\ \mu_{gl,}$ = Gas viscosity, Pa.s
S_W= water saturation

Symbols

η= Efficiency

σ = Fracture growth regime factor

τ= exposure time of fracture face to fluid, min

ξ, η = Confocal Elliptical system coordinates

Super-Script

Cr = constant terminal rate solution

i, k = time steps

Note: Nomenclature of Chapter6, Appendix section is not included. Explanation of all parameters is explained in the same paragraphs.

APPENDIX

APPENDIX A –

(A.1.) Concepts and Definitions

For addressing the full range of fracture growth (from very fast in case of MiniFrac / DFIT to slow fracture growth in long injection period cases), the results are presented in terms of dimensionless parameters groups, all of which are based on conventional reservoir engineering theory. They are given by:

$$t_{D,pump} = \frac{k}{\emptyset \mu c_t L^2}\, t_{pump} \;\; ; \quad t_D = \frac{k}{\emptyset \mu c_t L^2}\left(t - t_{pump}\right) \;\; ; \quad p_D = \frac{2\pi kh}{\mu Q_l\left(t_{pump}\right)}\left(p_{shut-in} - p\right) \tag{50}$$

Where, K = reservoir permeability; $\emptyset$= reservoir porosity; μ = viscosity of the reservoir fluid; c_t = total reservoir compressibility (reservoir fluid + formation rock); L = Fracture Half length; h is reservoir height and Q_l is the leak-off rate at the end of pumping i.e. t_{pump}

A.1.1. Compliance (Storage)

There are two kinds of Compliance (Storage) in pressure transient analysis:

(1) Well bore Compliance (Storage) - more renowned and well researched
(2) Fracture Compliance (Storage) – much higher magnitude than WBS, hence more impact on PTA results. Less understood

Wellbore Storage (WBS)

At the very beginning of starting up or shutting in oil or a gas well, the wellhead flow rate is not equal to the sand face flow rate. Wellbore Storage can occur at: (1) Well shut-in (2) Re-opening of wells

(1) Fig.91 During shut-in, the well can be shut in at the sand face/bottomhole or at the surface. If the well is equipped to shut at the sand face/bottomhole, little to no wellbore storage occurs. But the wells are generally shut at the surface; thereby wellbore storage factor is always present. For latter cases, the well is shut in at the surface by closing valve on the Christmas tree which reduces the surface flow rate to zero almost immediately however the sand face/bottomhole rate is active for some time. More natural fluid is needed for compression of the fluid in the wellbore due to the existing pressure differential. This pressure difference causes flow of fluid from formation to the wellbore and stops when the sand face (bottomhole) pressure and formation pressure equalizes. At this point, the wellbore storage effect is over

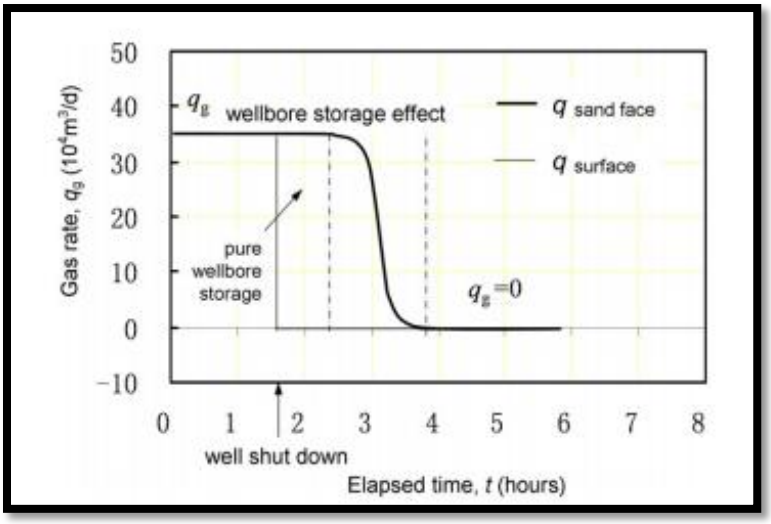

Figure 91 WBS during closing of the gas well

(2) Fig.92 The situation is just opposite during well reopening. During re-opening of the well to start production, the initial production is from the fluid accumulated in the wellbore and NOT from the formation. Initial production happens due to expansion of wellbore fluid. The surface rate increases gradually however the sand face rate (bottomhole rate) is still zero. As production progresses, bottom hole pressure keeps on decreasing until a pressure differential occurs between formation and bottom hole so that the sand face flowrate increases from zero gradually to the level of well head (surface) flow rate.

Storage effect remains until there is 'potential difference' between sand face rate and surface rate. Once they equalize, WBS effect is over and the production then is only from the reservoir.

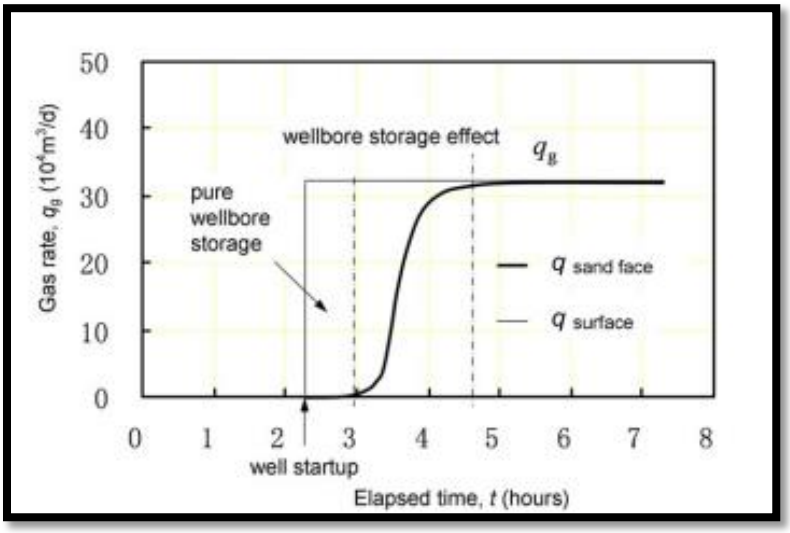

Figure 92 WBS during starting of the well

Reason for WBS: Two main reasons for WBS in a well are:

(1) Fluid compressibility and
(2) By changing fluid level (fluid volume) inside the well bore.

"A higher fluid compressibility or fluid volume will increase the wellbore storage coefficient making the unit slope straight lines longer towards later times as illustrated in fig.93 below"

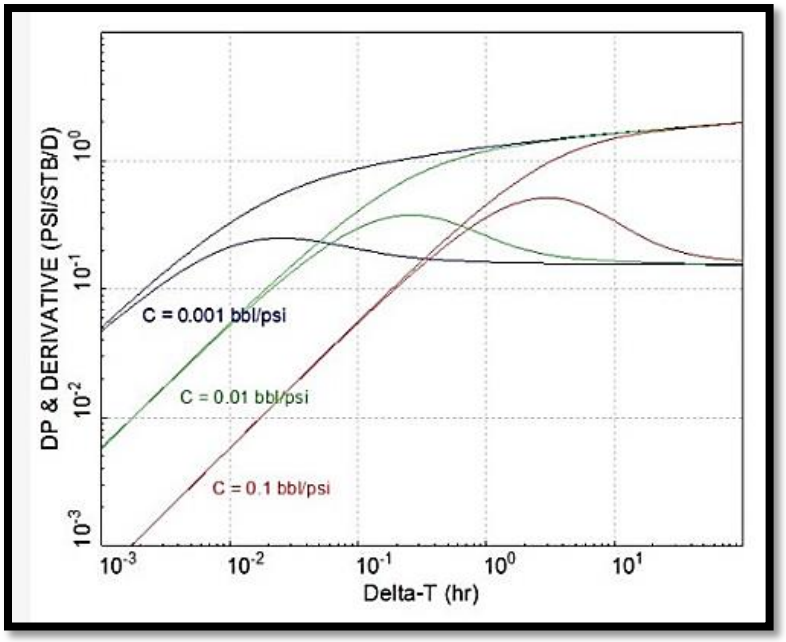

Figure 93 Effect of wellbore storage magnitude on log-log pressure plot

Wellbore storage affects well pressure response at the initial stages of pressure transient analysis of drawdown, buildup, minifrac and IFO tests.

Physically, it refers to the increased fluid volume (the surface volume) in the wellbore to increase one unit of bottom-hole pressure during the fluid compression process after shutting in.

During wellbore storage regime, the pressure change (ΔP) and pressure derivative (ΔP') are identical and overlap on a single linearly increasing line characterized by Slope=1. It is technically followed by 'Linear flow' (slope =1/2) in case of infinite conductivity fracture or 'Bilinear flow' (slope=1/4) in case of finite conductivity fracture before ultimately reaching the Radial flow stage, but as will be discussed in detail later, the linear or bilinear flow regime is often masked by the wellbore storage effect especially in the presence of fracture face skin.

For non-fractured wells, wellbore storage is a big source of problem leading more than often to wrong interpretations. It can be useful though only in few cases such as comparing wellbore storage coefficient in various pressure build up tests which could help to detect some changes in fluid properties and connected volume. On the other hand, as much as wellbore storage is a nuisance during well testing, recent research work by (van den Hoek, 2005) shows that wellbore storage period is a reliable stage to determine the dimensions of closing fracture in a vertically fractured well whereas parameters obtained during linear, bilinear flow period can be misleading during an Injection Fall-Off test.

In order to reduce or eliminate the influence of wellbore storage, tools and methods for downhole shut in have been proposed and developed. When such tools are used, however, special requirements are imposed on the wellbore structure and operation procedure.

(Van Everdingen and Hurst, 1949) were first to propose a mathematical expression for wellbore storage coefficient

$$C_{WBS} = \frac{\mathrm{dV_w}}{\mathrm{dP}} = \frac{\Delta \mathrm{Vw}}{\Delta \mathrm{P}} = c_f V_w \qquad (51)$$

Where, C_{WBS} = wellbore storage coefficient (unit); ΔVw = change in wellbore volume (unit); ΔP = change in bottom-hole (sand face) pressure (unit); V_w = Wellbore volume; c_f = Compressibility of the wellbore fluid

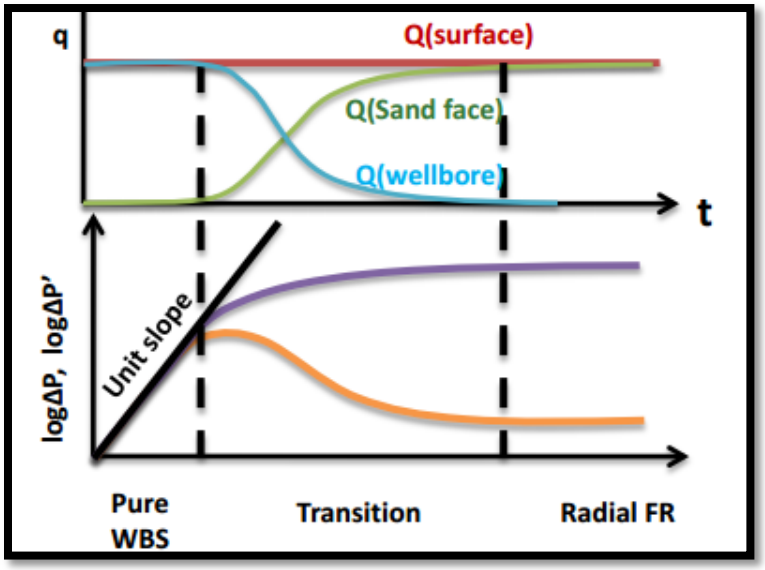

Figure 94Wellbore storage period on Cartesian and log-log plot of pressure w.r.t time

The dimensionless wellbore storage coefficient was defined by Agarwal et al (1970) (Gilles_Bourdarot, 1998)(Pg.36):

$$C_{D_{WBS}} = \left(\frac{1}{2\pi}\right) \frac{C}{\phi h c_t r_w^2} \tag{52}$$

Dimensionless wellbore storage coefficient was defined by (Gringarten et al., 1974)(Gilles_Bourdarot, 1998):

$$C_{D_{WBS}} = \left(\frac{1}{2\pi}\right) \frac{C}{\phi h c_t L} \tag{53}$$

The wellbore storage coefficient is easily calculated by a Cartesian plot between change in pressure (Δp) versus change in time (Δt). At early time, the slope follows a straight line with slope value, m=1, intercepting the origin. Everdingen and Hurst gave a formula for change in pressure response as:

$$\Delta p = \frac{\Delta Q}{C} \Delta t \tag{54}$$

The wellbore coefficient can be calculated from eq. (54) from the analogy of straight line equation, $y=mx + c$. Since the slope passes through origin, the intercept is zero and the equation reduces to, $y=mx$.

Fracture Storage

It was considered in this work that the fracture shape is elliptical in nature. Fracture Compliance (also called as "Fracture Storage") C_f for a fully open elliptical fracture is given by:

$$C_f = \frac{2}{3}\pi \frac{(1-v^2)}{E} hl * \frac{\min(h, 2L)}{E(m)} \quad where\ m = 1 - \left[\min\left(\frac{h}{2L}, \frac{2L}{h}\right)\right]^2 \tag{55}$$

Where E and ϑ are Young's modulus and Poisson's ratio respectively for the formation rock and $E(m)$ is the complete elliptical integral of the second kind.

Total compliance (storage) = wellbore compliance + fracture compliance. It is also expressed in dimensionless terms as (Van Den Hoek, 2016)

$$C_{tD} = c_f V_w + \frac{C_f}{2\pi h L^2 \emptyset c_t} \tag{56}$$

Value range of dimensionless fracture compliance varies between:

(i) Very elongated fracture, high formation fluid compressibility, high formation Young's modulus ~ 0

(ii) Radial to short fractures $\sim \frac{1}{3}$

Difference in Magnitude between Wellbore and Fracture Compliance

Generally, fracture compliance is several orders of magnitude higher than wellbore compliance; subsequently often this dominates early-time storage-dominated flow. Once the fracture closes, only 'true' wellbore storage remains. To demonstrate the difference, the values calculated for the field case examples used in this report are shown in table 20:

Table 20 Difference in magnitude - Wellbore compliance vs. Fracture compliance

SI No.	Well Data Name	Wellbore Compliance ($c_f V_w$) (m³/Pa)	Fracture Compliance (Eq. 55) (m³/Pa)
1	Injection – 2B	2E-08	6.2E-07
2	Injection – 5B	2E-08	4.7E-06
3	Injection – 6B	2E-08	3.0 E-06
4	Example 1	1E-08	4.1 E-06
5	Example 2	2E-08	9.2 E-07
6	Example 3	2E-08	3.0 E-06

It is evident from table 20 that the difference in values between wellbore compliance and fracture compliance for an elliptical shape fracture differs mostly by 2 orders of magnitude, emphasizing the point made that fracture storage is much more prominent in an Injection Fall-Off test.

Another example to validate the same idea was done by (McClure et al., 2016) which demarcates the magnitude difference between: compressibility of the fluid in the wellbore vs. compressibility of the fluid in the fracture vs. changes in fracture volume. For details, please refer to the Appendix (C)

A.1.2. Skin Effect

The skin effect reflects the degree of damage caused around immediate vicinity of wellbore area due to drilling, cementing, mud or stimulation work. The value of skin factor can be both positive (damage) and negative (stimulation). Permeability around skin zone, Ks is of lower value than of the original formation permeability, K. The reduced permeability around wellbore zone causes pressure drop in case of formation damage or pressure enhancement in case of well stimulation.

A.1.3. Liquid Drop in the Wellbore

This phenomenon occurs often in depleted reservoirs and is identified as "change in storage", shown in fig.95. The physics behind is that the fluid in the wellbore upon approaching the atmospheric pressure i.e. nearing the surface small air bubbles comes out of the liquid which increases the total compressibility of the liquid column. After a while, the slowly accumulating gas bubbles as the liquid nears the surface leads to formation of constant gas phase above liquid column and the pressure starts dropping. Below mentioned semi-log plot (fig.95) from an injector well in Oman highlights the phenomenon.

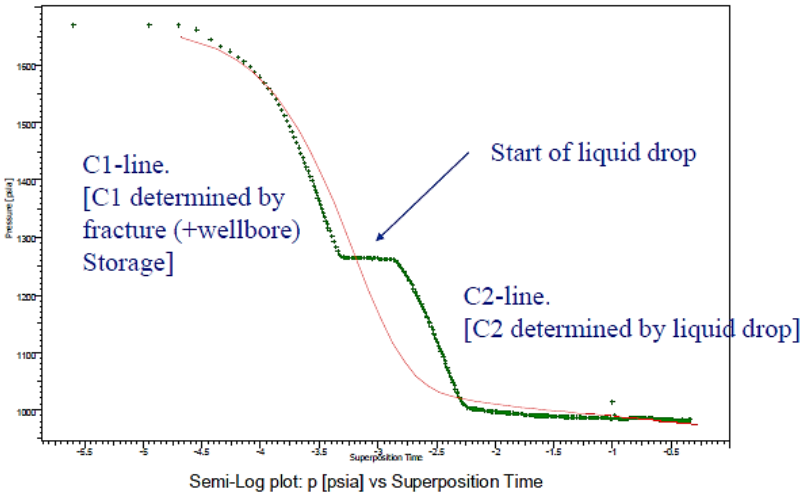

Figure 95 Liquid Drop in the wellbore

The data during the liquid drop is usually unanalyzable; hence one can only analyze the data before its commencement or only after the end of transition towards liquid drop

A.1.4. Diffusivity

This ratio gives the relationship between diffusivity inside the fracture and diffusivity around the formation. Expressed as(Gilles_Bourdarot, 1998),

$$\eta = \left(\frac{k_f}{\mu(\Phi c_t)_f}\right) \Big/ \frac{k}{\mu \Phi c_t} \qquad (57)$$

Where, k_f = fracture permeability, μ = fluid viscosity; Φ = porosity; c_t = total compressibility; k = reservoir / formation permeability

Relative Conductivity

The relative conductivity expressed as C_r expresses the relation between:

$$C_r = \frac{wk_f}{Lk} \qquad (58)$$

- The factors governing emptying of the fracture (w and k_f): the wider (w) and more permeable the fracture is, circulation of fluid is better
- The factors governing supply to the fracture (L and k): the longer the fracture and more permeable the formation is, the better supplied it is.

From equation (58), it can be concluded that lower the permeability of the formation or lower the fracture half-length, higher the value of relative conductivity and subsequently higher the fracture effectiveness. A fracture with C_r > 100 behaves like an infinite conductivity fracture

A.1.5. Reservoir Boundaries

Once the fluid flow crosses the fracture and enters formation, it moves further away resulting in formation linear flow and later to radial flow behaving as if the reservoir is infinite in nature, but sooner or later depending on the formation geology and characteristics, a boundary is encountered. When it happens, it is uniquely perceived as a characteristic change in the pressure at the well.

Some typical boundaries encountered are:

- Linear sealing fault
- Channel
- Intersecting linear fault
- Constant pressure boundary
- Closed Reservoir

In our case, we will discuss the most common ones which are:

A.1.5.(i.) Constant Pressure Boundary

A constant pressure boundary effect during a well test can be seen in following cases:

- When the compressible zone reaches the gas cap laterally
- When the compressible zone reaches the water aquifer with the water mobility much higher than that of oil

Fig.96 illustrates the above mentioned cases

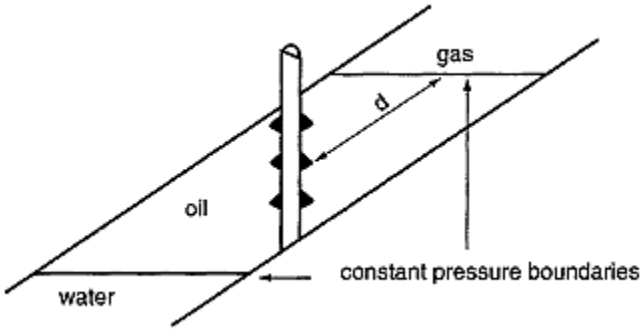

Figure 96 Constant pressure boundaries

In short, when the reservoir pressure is supported by fluid (gas or liquid) encroachment (either due to natural influx from an aquifer or gas cap, or by fluid injection), then a constant pressure boundary may be present. Such a boundary may completely close the well (for example, for a production well surrounded by injectors) or may be open boundary to one side of the well (for example, in case of an isolated producer/injector well pair).

The ultimate effect of any constant pressure boundary is to cause the well pressure response to achieve steady state, at which the well pressure will be the same constant pressure as the boundary

A constant pressure boundary on a log-log plot is shown in fig.97:

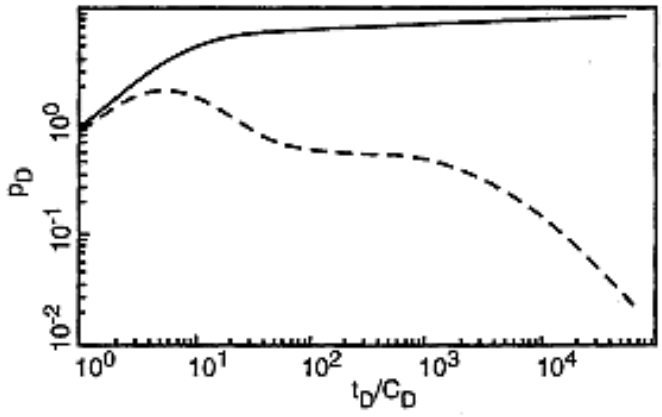

Figure 97 Typical Log-log plot curve with constant pressure boundaries

Pressure curve: characterized by pressure stabilization
Pressure derivative curve: characterized by sharp decrease corresponding to the pressure stabilization

A.1.5.(ii). Closed Boundary

When the reservoir is limited by no-flow boundaries, two cases can be distinguished when the compressible zone reaches the limits:

(a) When the well is producing: when pressure transient reaches the closed/no flow boundaries, the flow regimes becomes pseudo-steady state. In this state, pressure in the reservoir will decline at the same rate everywhere in the reservoir. It should be noted here that pseudo-steady state is not at all steady, and rather corresponds to the kind of pressure response that would be seen in a closed tank from which fluid is slowly being removed. Pressure drop here is due to the decompression of the reservoir fluid as fluid is produced from the well.

Once the boundary of the drainage area has reached, the pressure at well decrease linear with time. This pressure loss is simply given by the definition of compressibility

$$\Delta p = \frac{1}{V}\frac{q\Delta t}{c_t} \qquad (59)$$

From eq. (59), it is evident that pressure decrease is:

- Directly proportional to time. Hence identifiable as straight line on the plot
- Inversely proportional to the compressible volume of the drainage area

It is important to note that the pseudo-steady state response does not appear until a certain value of t_{DA} (dimensionless time which depends on the shape of reservoir).Recognition of this fact is helpful in to prevent wrong analysis.

A typical plot of closed reservoir is shown in the following figure 98 assuming a circular boundary reservoir, characterized by an end line slope of 1 on pressure derivative line:

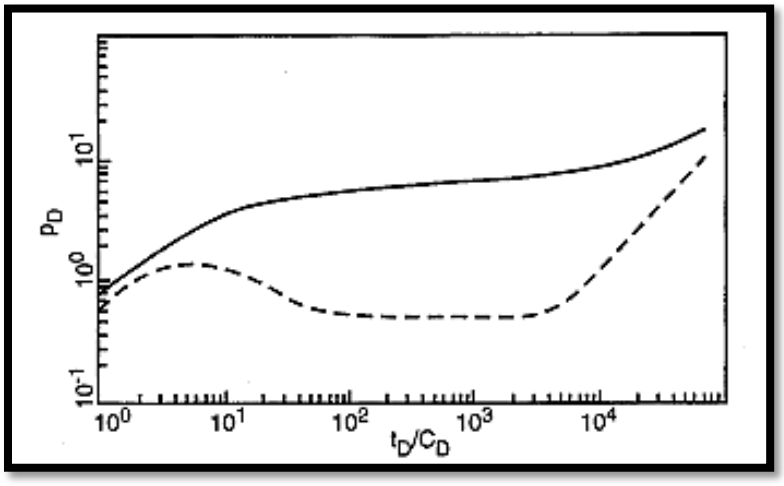

Figure 98 Typical Log-log plot curve with closed boundaries

(b) When the well is shut-in: when closed/no-flow boundaries are reached, the pressure stabilizes at a value called average pressure in the whole area defined by the no-flow boundaries.

APPENDIX B

B.1. Methodology of VdHoek analytical model's working

For practical field applications, a simple analytical model was developed by generalization of previous work designed for IFO of fractured waterflood injectors (van den Hoek, 2005)
Assumption:

1) Simple bi-wing planar fractures that were created during one preceding pump cycle with constant injection rate in one formation layer
2) Power Law of Fracture Propagation
3) Linear (Carter Leak-off) model

Analytical model designed for IFO of fractured water flood injectors is based on approximate solution to the elliptical diffusivity equation for transient fluid flow around a static hydraulic fracture. A quick summary of basic concepts used is as follows before we proceed with the actual derivation:

$$t_{D,pump} = \frac{k}{\emptyset \mu c_t L^2}\, t_{pump}\,; t_D = \frac{k}{\emptyset \mu c_t L^2}\,(t - t_{pump});\; p_D = \frac{2\pi kh}{\mu Q_l(t_{pump})}(p_{shut-in} - p) = \frac{2\pi kh}{\mu Q_\ell(t_{pump})}\Delta p \qquad (60)$$

where k is reservoir permeability, ϕ is reservoir porosity, μ is viscosity of the reservoir fluid, c_t is total reservoir compressibility (reservoir fluid + formation rock), L is fracture half length, h is reservoir height and Q_ℓ is the leak-off rate at time t_{pump}, i.e. at the end of pumping

Wellbore and fracture compliance (storage)

On top of the three dimensionless parameters given in (60), the following quantities are essential inputs for studying trends ('type curves') in the post-shut-in pressure transient:

- Fracture face skin S, given by $S=(k/k_{filtercake})*(d/L)$, where d is filtercake thickness on the fracture face
- Wellbore compliance ("wellbore storage"), given by $c_f V_w$ where c_f is the compressibility of the wellbore fluid and V_w is the wellbore volume.
- Fracture compliance ("fracture storage") C_f which for a fully open elliptical fracture is given by (van den Hoek, 2005)

$$C_f = \frac{2}{3}\pi \frac{1-v^2}{E} \frac{hL * min(h, 2L)}{E(m)} \;;\; = 1 - \left[\min\left(\frac{h}{2L}, \frac{2L}{h}\right)\right] \qquad (61)$$

where E and v are Young's modulus and Poisson's ratio, respectively, of the formation rock, and E*(m)* is the complete elliptical integral of the second kind. *In most cases, fracture compliance is several orders of magnitude higher than wellbore compliance, and therefore often this dominates early-time storage-dominated flow. Once the fracture is closed, only 'true' wellbore storage remains.*
Fracture and wellbore compliance (storage) are coupled by introduction of the total compliance, which is the sum of wellbore and fracture compliance. Its expression in dimensionless terms is

$$C_{tD} = \frac{c_f V_w + C_f}{2\pi h L^2 \emptyset c_t} \qquad (62)$$

Values of dimensionless fracture compliance C_{fD} vary between ~0 (very elongated fractures, high formation fluid compressibility, high formation rock Young's modulus) and ~⅓ (radial to short fractures).

Fracture growth

Simple bi-wing planar fractures that were created during one preceding pump cycle with constant injection rate in one formation layer. For such a case, conventional MF analysis theory (Nolte, 1986) applies, in which it is well-accepted that fracture growth can be (approximately) described by

$$\frac{A(t_2)}{A(t_1)} = \left(\frac{t_2}{t_1}\right)^{\left(\frac{1}{\sigma}\right)} \qquad 1 \le \sigma \le 2 \tag{63}$$

where A is the fracture surface area and the exponent σ indicates the fracture growth regime. In the limit of low leak-off and approximately constant fracture width (e.g. long contained fractures), almost all the injected volume is used to create fracture surface area and therefore we have $\sigma \approx 1$. This is called 'storage-dominated' fracture growth. On the other hand, if most of the injected fluid leaks off in the formation, it can be shown that $\sigma \approx 2$, see for example (Gringarten et al., 1974). The latter situation applies for cases ranging from medium- / high-permeability fracture stimulation to waterflooding.

In our numerical simulations, we addressed both the extremes of 'leak-off dominated' ($\sigma \approx 2$) and 'storage-dominated' ($\sigma \approx 1$) fracture growth during pumping. For linear (Carter) leak-off during pumping one can write

$$Q_l(t) = C_T \int_0^{A(t)} \frac{dA'}{\sqrt{t - \tau(A')}} \tag{64}$$

In combination with (49), one obtains for the leak-off rates during pumping ($t < t_p$)

$Q_\ell(t) = const = Q_{inj}$ leakoff dominated growth

$Q_\ell(t) \propto \sqrt{t} < Q_{inj}$ storage dominated growth

$Q_\ell(t) \propto t^{\frac{1}{\sigma}-\frac{1}{2}}$ general case

Fracture closure

Even for simple bi-wing planar fractures in one formation layer, the exact way in which fracture closure takes place is unknown. The simplest imaginable way is that after shut-in, the fracture is assumed to close like a "hinge" until at the point of complete closure, its compliance becomes equal to zero at once. However, as was pointed out already in (van den Hoek, 2005) , this would result in post shut-in pressure transient profiles with abrupt changes upon fracture closure, a feature that we never observed in injection fall-off tests in the field. Therefore, in (van den Hoek, 2005) a gradual post shut-in length recession was proposed based qualitatively on laboratory measurement results (Pater et al., 1996) (De, Van Dam et al., 2000). These results are captured phenomenologically as

$$[\, L(p_D) = L \;;\; p_D \le p_D^0 \,];\; [\; L(p_D) = L * \left(1 - \frac{p_D - p_D^0}{delpat}\right) \;\; p_D \ge p_D^0 \;] \tag{65}$$

where $p_D{}^o$ is the (dimensionless) pressure change after shut-in at which lengthwise shrinkage starts, and the parameter "*delpat*" is a measure of how fast lengthwise shrinkage takes place- i.e. in the limit $delpat \to 0$, fracture closure will be abrupt as soon as p_D exceeds $p_D{}^o$.

Equation (65) presents a mix of "hinge" closure and "zipper" closure: for a (dimensionless) post shut-in pressure change smaller than $p_D{}^o$, the fracture will close like a hinge (i.e. its length stays constant). Once the pressure change starts to exceed $p_D{}^o$, fracture length recession ("zipper closure") will take place until complete closure.

Pressure profile around the fracture is given by the exact solution to the transient diffusivity equation around a static, non-shrinking fracture at first. The obtained solution will then be generalized for changing fracture compliance i.e. for shrinking fracture.

The dimensionless transient diffusivity equation is given by

$$\nabla^2 p_D = \frac{\partial p_D}{\partial t_D} \tag{66}$$

$$c = c_{fluid} + \frac{3(1-2v)}{\emptyset E} \tag{67}$$

where E and v are Young's modulus and Poisson's ratio, respectively, of the formation rock.

Using a confocal elliptical coordinate system,

$$x = Lcosh\xi cos\eta\ , y = Lsinh\xi sins\eta \tag{68}$$

The diffusivity equation becomes

$$\frac{\partial^2 p_D}{\partial \xi^2} + \frac{\partial^2 p_D}{\partial \eta^2} = \frac{1}{2}(cosh2\xi - cos2\eta)\left(\frac{\partial p_D}{\partial t_D}\right) \tag{69}$$

The solution to Eq. 69 can be expressed as an infinite sum of Mathieu function products. The solution as developed characterizes the pressure profile:

- Around finite-conductivity fractures.
- Around fractures with fracture face skin.
- For multiple mobility zones.

Closing Fracture. The discussion above focused on computing the transient pressure around static fractures. However, in reality, after shutting in a fractured water injector, the fracture will gradually close, which by itself will generate a "fracture-closure-induced" flow rate. The corresponding bottomhole pressure is given by

$$\Delta p_D(t_D) = \int_0^{t_D} d\tau_D \left\{1 - C_{tD}[\Delta p_D\ (\tau_D)]\frac{\partial \Delta p_D\ (\tau_D)}{\partial \tau_D}\right\} x \left(\frac{\partial \Delta p_D^{cr}(t_D - \tau_D)}{\partial t_D}\right) \qquad t_D < t_D^{closure} \tag{70}$$

$$\begin{aligned}\Delta p_D(t_D) = &\int_0^{t_{Dclosure}} d\tau_D \left\{1 - C_{tD}[\Delta p_D\ (\tau_D)]\frac{\partial \Delta p_D\ (\tau_D)}{\partial \tau_D}\right\} x\ \frac{\partial \Delta p_D^{cr}(t_D - \tau_{D)}}{\partial t_D} + \Delta p_D^{cr}\left(t_D - t_D^{closure}\right) \\ &- C_{wD}\int_{t_D^{closure}}^{t_D} d\tau_D\ \frac{\partial \Delta p_D(\tau_D)}{\partial \tau_D}\ \ \frac{\partial \Delta p_D^{cr}(t_D - \tau_D)}{\partial \tau_D}\ ;\ t_D > t_D^{closure}\end{aligned} \tag{71}$$

where $\Delta p_D^{cr}(t_D)$ is the constant terminal rate solution to Eq. 69, and the time t_D has been defined so that t_D=0 corresponds to the moment of shut-in.

In Eq. 70 and 71, the dimensionless total compliance C_{tD} is defined by

$$C_{tD} = \frac{C_t}{2\pi h L^2 \emptyset c} \tag{72}$$

where C_t (units $\frac{m^3}{kPa}$) is the sum of wellbore and fracture compliances:

$$C_t = C_w + C_f = c_{fluid} V_w + C_f \tag{73}$$

In Eq. 73, V_w is the wellbore volume, and C_f is the fracture compliance, which for an elliptical fracture is given by Eq.61

It is important to note that Eq. 70 and 71 is obtained under the assumption that the conductivity of the fracture [which is captured by the constant terminal rate solution$\Delta p_D^{cr}(t_D)$] does not change as a result of fracture closure. This assumption appears to be in line with most field observations on hydraulic-fracture closure. Thus, the only fact by which fracture closure is exhibited in Eq. 70, 71 is by a reduction of the fracture compliance C_f to zero (see Eq. 71—i.e., we have mechanical closure but not hydraulic closure).

The period before fracture closure will, in general, be characterized by a *mixture* of storage and (non-)linear formation flow. Therefore, both flow regimes need to be captured simultaneously.

The above point is most clearly illustrated with a simplified description of post-shut-in pressure decline. For a non-shrinking fracture, the behavior of bottomhole pressure before fracture closure (Eq. 70) can be simplified to

$$\Delta \bar{p}_D(s) = \frac{\Delta \bar{p}_D^{cr}(s)}{\left(1 + s^2 C_{fD}\, \Delta \bar{p}_D^{cr}(s)\right)} \tag{74}$$

where $\Delta \bar{p}_D^{cr}(s)$ is the Laplace transform of the constant terminal rate solution of Eq. 69. At early times (s>>1), simplified expressions for $\Delta \bar{p}_D^{cr}(s)$ are readily available in the literature (for example, as presented by Raghavan).

$$\Delta \bar{p}_D^{cr}(s) = \pi/(sF_{CD}\alpha \tanh\alpha) \tag{75}$$

$$\alpha^2 = \frac{s}{\eta_{f_D}} + 2\sqrt{s}/F_{CD} \tag{76}$$

where the first term on the right side of Eq. 76 can be neglected except at very short times t_D (s>10^6).

Eqs. 74 and 75, 76 can be used readily to combine the storage and linear formation flow analyses into one, and standard curve-fitting techniques can be used to estimate fracture dimensions. One last important point that deserves emphasis here is that in the analysis, the formation compressibility as given by Eq. 67 should be consistent with the fracture compliance as given in Eq. 61 (i.e., both should contain the same values for Young's modulus and Poisson's ratio).

Changing Fracture Compliance as a Result of Shrinkage. *General Solution.* To solve for pressure in the case of changing fracture compliance during closure (e.g., receding fracture from a higher-stress zone), we rewrite Eq. 70 as

$$\begin{aligned} \Delta p_D(t_D) &= \int_0^{t_D} d\tau_D \left\{1 - c_{tD}[\Delta p_D(\tau_D)] \frac{\partial \Delta p_D(\tau_D)}{\partial \tau_D}\right\} x \left(\frac{\partial \Delta p_D^{cr}(t_D - \tau_D)}{\partial t_D}\right) \\ &= \Delta p_D^{cr}(t_D) - \int_0^{t_D} d\tau_D C_{tD}[\Delta p_D(\tau_D)] * \frac{\partial \Delta p_D(\tau_d)}{\partial \tau_D} \quad \frac{\partial \Delta p_D^{cr}(t_D - \tau_D)}{\partial t_D} \end{aligned} \tag{77}$$

$$\Delta p_D(t_D^i) = \Delta p_D^{cr}(t_D^i) - \sum_{k=1}^{i} C_{tD}\{\Delta p_D[\frac{1}{2}(t_D^{k-1}+t_D^k)]\} * \Delta p_D(t_D^k) - \Delta p_D(t_D^{k-1})/(t_D^k - t_D^{k-1}) * [\Delta p_D^{cr}(t_D^i - t_D^{k-1}) - \Delta p_D^{cr}(t_D^i - t_D^k)] \quad (78)$$

Splitting the *i*th term out of this sum and rearranging yields

$$\Delta p_D(t_D^i) = \left[1 + (C_{tD})^i \frac{\Delta p_D^{cr}(t_D^i - t_D^{i-1})}{(t_D^i - t_D^{i-1})}\right]^{-1} * \{\Delta p_D^{cr}(t_D^i) + (C_{tD})^i \Delta p_D(t_D^{i-1}) \frac{\Delta p_D^{cr}(t_D^i - t_D^{i-1})}{(t_D^i - t_D^{i-1})} - \sum_{k=1}^{i-1}(C_{tD})^k [\Delta p_D(t_D^i - t_D^{k-1}) - \Delta p_D^{cr}(t_D^i - t_D^k)] * \frac{\Delta p_D^{cr}(t_D^i - t_D^{k-1}) - \Delta p_D^{cr}(t_D^i - t_D^k)}{(t_D^k - t_D^{k-1})} \quad (79)$$

Where,

$$(C_{tD})^j \equiv C_{tD}\left\{\Delta p_D\left[\frac{1}{2}(t_D^{j-1}+t_D^j)\right]\right\} \quad j = i \text{ or } k \quad (80)$$

and the indices have been defined so that $t_D^{k=0} = t_D^{\text{shut-in}}$ and $t_D^{k=i} = t_D$.

One problem with Eq. 79 is that for low *i*, $\Delta p_D(t_D^i)$ is only a very rough approximation of the integral. This is, of course, a consequence of the fact that in that case, the integral is approximated by a sum with only a very low number of terms. The obvious way to reduce this problem is to compute $\Delta p_D(t_D^i)$ by means of the "exact" Laplace transform for the first few time steps when the total compliance $(C_{tD})^i$ is still approximately equal to its initial value.

B.2. Generalization to Include DFIT/Minifrac Phenomenon

In this paragraph, we propose a generalization to the analytical IFO model in order to make it suited for DFIT/Minifrac analysis as well.

The starting point of such a generalization is to incorporate the impact of the fact that shut-in time can be of the same order of magnitude as the pump time or even (much) larger. By virtue of the Duhamel superposition principle, for a static (i.e. non-propagating) fracture one can add up the transient pressures generated by the start of pumping and by the shut-in as follows

$$p(t) = p_{CR}(t_{pump}) - \Delta p(t) = p_{CR}(t + t_{pump}) - p_{CR}(t) \quad (81)$$

where t is the shut-in time, p_{CR} is the constant terminal rate solution to the transient diffusivity equation, t_{pump} is the pump time, and $\Delta p(t)$ is the pressure drop after shut-in (see also Equation (60)). The well-known constant terminal rate solution $p_{CR}(t)$ has been presented for a radial reservoir by, for example,. For an elliptical reservoir around a fracture, an approximate analytical solution is provided e.g. in (van den Hoek, 2005). *It should be noted that for cases of long pump time (e.g. waterflood with constant injection rate), we have* $t \ll t_{pump}$ *and the pressure drop after shut-in is essentially given by* p_{CR} *as presented in* (van den Hoek, 2005).

The impact of non-zero dimensionless total compliance C_{tD} is incorporated by replacing the constant terminal rate solution $p_{CR}(t)$ by the pressure $p_{IFO}(t)$ given by (van den Hoek, 2005)

$$P_{IFO,D}(s) = \frac{p_{CR,D}\ (s)}{1 + s^2 C_{tD}\ p_{CR,D}(s)} \tag{82}$$

where s is the Laplace transform of the dimensionless time t_D (see (Eq.60)) and the subscript "D" indicates dimensionless values. For cases of long pump time, replacing the constant terminal rate solution p_{CR} in (81) by the pressure p_{IFO} as given in (82) works well (Van den Hoek, 2005), but for shorter pump times it breaks down. Although for high dimensionless pump time, the agreement between numerical and analytical results is still good, for lower values of pump time, pronounced differences arise between numerical and analytical results, which increase with decreasing pump time. However, but it appeared that the differences between numerical and analytical results for low pump time are mainly a *translation* in the log-log plot, i.e. it appears that numerical and analytical results differ by a constant factor over the entire shut-in time period. These differences can be straightforwardly explained by the fact that short dimensionless pump times can be below the (dimensionless) period during which post shut-in reservoir flow is dominated by the storage of the open fracture. This period is approximately equal to the value at which the pressure derivative for an open fracture reaches its peak. In the paper SPE-181593 (Van Den Hoek, 2016), it has been shown through a figure where when $t_D, pump$ time is significantly higher than the fracture storage time, the agreement between numerical and analytical results is good.

The fact that the shapes of the pressure decline and derivative curves for the numerical and analytical results are the same, leads us to propose a modification to Eq. (68) as follows (with p_{CR} replaced by p_{IFO}) :

$$\Delta p(t) = \left[\, p_{IFO}(t) - p_{IFO}\left(t + t_{pump}\right) + p_{IFO}\left(t_{pump}\right)\right] * \frac{p_{IFO}(t_1)}{p_{IFO}\ (t_1) - p_{IFO(t_1 + t_{pump})} + p_{IFO}(t_{pump})} \tag{83}$$

In (83), the second factor on the RHS represents the translation in the log-log plot mentioned above. When this factor is equal to one, (83) reduces back to (81) (with p_{CR} replaced by p_{IFO}). The time t_1 in (83) can be any time after shut-in provided it is small enough such that the pressure $p_{IFO}(t_1)$ is still dominated by fracture storage.

APPENDIX C

C.1. Derivation of the Equations governing Pressure –Transient Behavior during a DFIT

The equations governing the pressure transient behavior during a DFIT shown here are derived and taken from (McClure et al., 2016).
Following key assumptions are made:

1) It is assumed that the entire fracture and wellbore system behaves like a "lumped parameter model" i.e. change of pressure with respect to time dp/dt is uniform throughout the entire system
2) The entire system remains isothermal
3) Implicitly neglects pressure gradient caused by flow in the well, perforation, near wellbore region and along the fracture.
4) Carter Leak Off
5) Fluid is slightly compressible and has constant compressibility, c_f

Using Chain Rule, Pressure derivative w.r.t time is broken into [change of pressure w.r.t total mass of the fluid in the wellbore and in the fracture] * [change of total mass of fluid w.r.t time], given by

$$\frac{\mathrm{d}P}{\mathrm{d}t} = \frac{\mathrm{d}P}{\mathrm{d}m} * \frac{\mathrm{d}m}{\mathrm{d}t} \tag{84}$$

Where, m= mass of the fluid in the well bore + mass of the fluid in the fracture = total mass of the fluid
P = pressure measured either at the bottom of the well or calculated from the surface pressure measurements.
dm/dt roughly speaking is, incoming/injecting liquid – outgoing/leak-off liquid. Given by the expression as,

$$\frac{\mathrm{d}m}{\mathrm{d}t} = q_{m,inj} - q_{m,leakoff} \tag{85}$$

$q_{m,inj}$ = surface mass injection rate
$q_{m,leakoff}$ = rate at which fluid mass flows out of the well and fracture into the matrix

Since density (ρ) = mass (m)/volume (V), the above fluid mass can be expressed in terms volume and density

$$\frac{\mathrm{d}m}{\mathrm{d}t} = q_{m,inj} - q_{m,leakoff} = q_{inj}.\rho_{inj} - q_{leakoff}.\rho_{leakoff} \tag{86}$$

q_{inj} = volumetric surface injection rate
ρ_{inj} = density of the injected fluid
$q_{leakoff}$ = volumetric rate of leak off in the matrix
$\rho_{leakoff}$ = average density of the fluid leak off into the matrix

Total mass of the fluid, 'm' can be expressed as,

$$m = \rho_{wl}.V_{wl} + \rho_{fr}.V_{fr} \tag{87}$$

Where, ρ_{wl} = average density of the fluid in the wellbore; V_{wl} = Volume of the wellbore; ρ_{fr}= average density of the fluid in the fracture; V_{fr} = Volume of the fracture
With assumption (5), density (ρ) in general can be expressed as,

$$\rho = \rho_0 \exp[P(P - P_0)c_f] \tag{88}$$

Where, P_o = reference pressure
ρ_0 = density of the fluid at the reference pressure

Expanding eq.(88) by Taylor series expansion and discarding higher-order terms provides the approximated linearized equation,

$$\rho = \rho_0[1 + c_f(P - P_0)] \tag{89}$$

Equation (89) can be differentiated w.r.t to pressure:

$$\frac{\mathrm{d}\rho}{\mathrm{d}P} = \rho_o . c_f \tag{90}$$

Equation (87) is differentiated w.r.t Pressure:

$$\frac{\mathrm{d}m}{\mathrm{d}P} = \frac{\mathrm{d}\rho_{wl}}{\mathrm{d}P}.\mathrm{V_{wl}} + \rho_{wl}.\frac{\mathrm{dV_{wl}}}{\mathrm{d}P} + \frac{\mathrm{d}\rho_{fr}}{\mathrm{d}P} + \rho_{fr}\frac{\mathrm{dV_{fr}}}{\mathrm{d}P} \tag{91}$$

Substituting eq. (85), eq. (91) in eq. (84) gives the following expanded form:

$$\frac{dP}{dt} = \frac{dP}{dm}.\frac{dm}{dt} = (q_{inj}.\rho_{inj} - q_{leakoff}.\rho_{leakoff}) \,/\, (\frac{\mathrm{d}\rho_{wl}}{\mathrm{d}P}.\mathrm{V_{wl}} + \rho_{wl}.\frac{\mathrm{dV_{wl}}}{\mathrm{d}P} + \frac{\mathrm{d}\rho_{fr}}{\mathrm{d}P}.V_{fr} + \rho_{fr}\frac{\mathrm{dV_{fr}}}{\mathrm{d}P}) \tag{92}$$

Since we assumed fluids to be slightly compressible in assumption (5), eq. (92) can be further simplified taking values for$\rho_{inj}, \rho_{leakoff}, \rho_{wl}, \rho_{fr}$ approximately equal (since for isothermal fresh water, their values would be within a few percentage of each other). The values for these quantities are also equal to the ρ_0 value used to calculate the derivatives of fluid density w.r.t pressure in the wellbore and the fracture. Cancelling out these terms in eq. (92), it further simplifies to,

$$\frac{dP}{dt} = \frac{(q_{inj}.\rho_{inj} - q_{leakoff}.\rho_{leakoff})}{c_{f_1}.V_{wl} + \frac{dV_{wl}}{dP} + c_{f_2}.V_{fr} + \frac{dV_{fr}}{dP}} = \frac{q_{inj}.\rho_{inj} - q_{leakoff}.\rho_{leakoff}}{C_t} \tag{93}$$

Where,

c_{f_1} = change of wellbore fluid average density w.r.t pressure
c_{f_2} = change of fracture fluid average density w.r.t pressure
C_t = total storage-coefficient of the entire system

The definition of total storage coefficient, C_t used here is more general and inclusive than one used by Raaen et al (2001) and by Craig and Blasingame (2006).Their postulated C_t expressions raises major questions about their validity but it is out of scope of the current work.

Eq. (93) can be applied during all phases of a fracturing test: during injection, the before-closure shut-in period, during closure, and the after-closure shut-in period. However in reality, during injection the pressure gradient

caused by the flow through well, perforations, near wellbore region and fractures causes $\frac{dP}{dt}$ to vary spatially throughout the system but after early shut-in period, these pressure gradients are minimal.

As shown above, the total storage coefficient has four parts:

(a) Compressibility of the fluid in the wellbore
(b) Changes in the wellbore volume
(c) Compressibility of the fluid in the fracture
(d) Changes in the fracture volume

Conventionally changes in the wellbore volume $\frac{dV_{wl}}{dP}$ is considered negligible compared to the $c_{f_1}.V_{wl}$ term (Horne 1995)

$\frac{dV_{fr}}{dP}$ can be written as $\frac{A}{S_f}$ where A is the surface area of the fracture and S_f is the fracture stiffness, obtained as the derivative of effective normal stress w.r.t aperture (Jaeger et al. 2007). $\frac{dV_{fr}}{dP}$ depends on fracture geometry and rock characteristics of the formation.

Two limiting cases of fracture geometry are discussed below: Radial; PKN (Perkins and Kern 1961, Nordgren 1972). If the fracture is not constrained by height due to layering, then the fracture propagates freely in all possible direction ultimately leading to an approximately circular shape. Reason it is approximately circular and not exact is the trends in stress with depth decides the preferential movement of fracture in the direction of least resisting stress.

For a radial fracture, the stiffness of the fracture (when open), $S_{f,o}$ can be written as (Sneddon 1946):

$$S_{f,r} = 3\pi G_m/(\,8(1-\vartheta)R_f \tag{94}$$

Where G_m is the shear modulus, ϑ is the Poisson's ratio and R_f is the radius.
However if the reservoir geometry is surrounded by much higher stressed layers above and below the pay zone, the fracture is generally confined within it giving rise to a condition where the fracture length will be much greater than its height, and the stiffness can be approximated from the 2D plane-strain solution which forms the key assumptions of the PKN model. The stiffness of the fracture for the PKN model can be estimated from the work done by Sneddon 1946; Perkins and Kern 1961 and Nordgren 1972):

$$S_{f,PKN} = \frac{4G_m}{\pi(1-\vartheta)h_f} \tag{95}$$

After shut-in, assuming 'constant wellbore volume and $c_{f_2}.V_{fr}{}'$ the pressure derivative can be written as,

$$\frac{dP}{dt} = -\frac{q_{leakoff}}{(c_f.V_{wl} + \frac{A}{S_f})} \tag{96}$$

One point to make here regarding eq. (96) is if the fracture continues propagating, value of 'A' may change significantly and S_f may change depending on the fracture geometry. But if the fracture is no longer propagating, fracture stiffness S_f remains constant before closure but will change during the process of fracture closure.

Using the Carter Leak-off model to calculate $q_{leakoff}$, the calculated value is such that it is inversely proportional to the square root of time. This is why the plot of Pressure versus sqrt of time is linear in nature before fracture closure. Evidently from eq. (96), if the denominator term on right hand side of the expression remains constant, then change of pressure with respect to time is directly proportional to the leak off rate. But if the value of parameters changes as is the case with fracture closing then area of the fracture, fracture stiffness etc changes and the straight line deviates from linearity indicating fracture closure phenomenon. The deviation of pressure

from the straight line when closure forms a benchmark technique to identify fracture closure in the industry (Castillo 1987,Zoback 2007). Fracture closure also reduces the 'transmissivity' and in some cases, can lead to the fracture from infinite conductive to finite conductive.

In addition, G*dP/dG vs. G is often plotted {equivalent to dP/d[ln(G)] vs. G}, where P is pressure. As long as pressure forms a straight line, G*dP/dG should also form a straight line, and hence closure can be picked at the deviation from the straight line (Barree and Mukherjee 1996). In many cases, the G-function is approximately equal to $\Delta t^{0.5}$ and the plots can also be made with $\Delta t^{0.5}$ substituted for G.

C.1.1. Pressure Trend after Fracture Closure

To understand pressure trend after closure, it is important to understand how stiffness is affected by closure. The stiffness after closure $S_{f,C}$ includes the effect of the elastic response of the formation as shown in eq. (94 and 95), BUT , also includes contribution from the contacting fracture walls(section 12.3 from Jaeger et al.2007).

To give a working conceptual explanation, a simplifying assumption is made that both the stress and aperture are constant along the fracture. This is strictly not correct but helps in giving an intuitive feeling of the physics involved. With this assumption, it can be written

$$\sigma_n' = \sigma_n^r + E\, S_{f,o} - P \tag{97}$$

Since the initial aperture of the fracture is zero, backstress is created by its entire aperture, E.

To determine fracture stiffness, eq. (97) can be solved for P and differentiated w.r.t E:

$$S_{f,C} = \left(\frac{dE}{dP}\right)^{-1} = \frac{dP}{dE} = S_{f,o} - \frac{d\sigma'}{dE} = S_{f,o} - \left(\frac{dE}{d\sigma_n'}\right)^{-1} \tag{98}$$

$$= S_{f,o} + \left(\frac{dE}{dP}\right)^{-1} = S_{f,o} + S_{f,cont} \tag{99}$$

Where $S_{f,cont}$ is the contribution to the stiffness from the contact stress. $S_{f,cont}$ can be calculated from any constitutive equation that specifies E as a function of effective normal stress.

Couple of key observation and 'cook – book' conclusions coming out of the above discussions are (McClure et al., 2014):

(a) The value of $S_{f,cont}$ increases as the fracture closes.
(b) Closure causes a sharp increase in S_f from $S_{f,o}$ to $S_{f,c}$ (eq.99) which causes an increase in the pressure derivative. The derivative increases very sharply because stiffness increases so much with closure, increasing generally roughly by a factor of 4. It continues to increase as the aperture value falls below residual aperture value ' E_o' . This is directly reflected in the Pressure versus Sqrt. of shut-in time or G-function time plot where 'first derivative of pressure w.r.t time' is also plotted. Point of maximum inflection in first derivative pressure plot also serves as technique for identifying 'fracture closure moment' in cases where it is not easily evident from G-function plot or can also be used as verification tool.

APPENDIX D

D.1. Minifrac Test: Principle and Methodology

D.1.1. Principle of Minifrac or DFIT Tests

A MiniFrac test is an injection-falloff diagnostic test performed without proppant before the main fracture stimulation treatment. One of the main physical processes which happen under a MF, DFIT is:

(1) Fracture Propagation velocity (v_frac) >> Fluid Propagation velocity (v_fluid)
(2) The Fluid leak-off rate is inversely proportional to the " square root of shut-in time"

The intent is to break down the formation to create a short fracture during the injection period, and then to observe closure of the fracture system during the ensuing falloff period. During the injection phase, a controlled volume of water is injected into the well to create a short fracture in the formation. Due to stress concentration at the edge of the fracture, the created fracture penetrates/propagates to the near-wellbore damaged area and exposes the undamaged formation to the flow transients. The fracture directly connects the undamaged formation with the wellbore and forms an efficient flow passage for the pressure response of the true formation to the injection. Once the fracture is open and has propagated a short distance, the pumps are shut down. There is a rapid pressure drop since there is no friction pressure loss when the fluids slow down and eventually stop moving. The pressure at this instance, when the frictional pressure drop stops, is called the ISIP, or the instantaneous shut-in pressure. Fluid begins to leak from the fracture into the formation immediately before closure happens. Since the pressure at which a fracture closes corresponds to the least pressure required to keep that fracture open, the fracture closure pressure represents the smallest compression against the rock. Therefore, it is equivalent to the smallest principal stress (also called as minimum horizontal stress) acting on it. After fracture closure, the pressure transient established around the wellbore propagates into the reservoir, transitioning into linear and radial flow periods.
Figure 99 shows typical pressure response during a minifrac test.

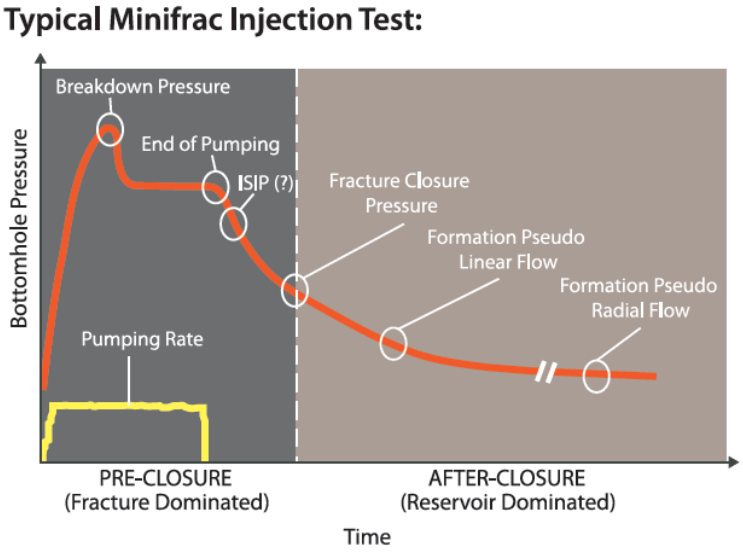

Figure 99 A typical Minifrac Injection Test process flow

D.1.2. DFIT Test and Minifrac Test

Diagnostic fracture injection tests (DFITs) are small pump-in treatments performed to gather data to help design follow-up main hydraulic-fracturing treatments, as well as to characterize the subject reservoir. DFITs have their basis in conventional minifracture treatments; however they are subtly different and are intended to acquire significantly more data for treatment design and reservoir description. DFITs use Newtonian non-wall building injection fluids (often water), intending to expand that role and acquire additional data such as reservoir pore pressure, closure and fracture gradients, transmissibility values that can give reservoir- permeability values and leak off mechanisms.

Conventional minifracture treatments have historically been focused on acquiring treatment-design parameters such as fluid efficiencies and leak off values. They use Non-Newtonian wall building injection fluid.

In unconventional reservoirs, DFITs have gained more value because most of the information gained is comparable with traditional pressure transient analysis tests, which are impractical to run in tight-sand and shale systems since the time to analyze pseudo radial flow can be months.

DFIT's involve injection of water and are frequently done in hydrocarbon bearing formations. The G- analysis is dependent on the assumptions that leak-off scales with square root of time. This scaling relationship is based on a single-phase, one dimensional solution to the diffusivity equation. Non-linear multi-phase flow effects may have an unpredictable effect on the scaling of leak-off rate with time, affecting the shut-in transient especially in the shale formations where the leak-off behavior is not well understood.

D.1.3. Key Results from Minifrac tests

The analysis of Pressure Fall-off data is done using specialized techniques to derive following key information:

- Fracture Closure Pressure (P_c)
- Instantaneous Shut-In Pressure (ISIP)
- ISIP gradient
- Net Fracture Pressure (Δp_{net}) = ISIP - P_c
- Fluid Efficiency
- Formation Leak-off characteristics and fluid loss coefficients
- Formation Permeability (k)
- Reservoir Pressure (p_i)

D.1.4.MiniFrac Analysis Techniques

Due to the nature of minifrac test, the analysis is performed in two parts:

(i) Before Closure Analysis (BCA)
(ii) After Closure Analysis (ACA)

Similar to traditional pressure transient analysis (PTA), specialized time and derivative functions are used to perform BCA and ACA.

D.1.4.1(i) Before Closure Analysis (BCA)

Before Closure Analysis consists of identifying closure and analyzing the early pressure fall off period while the induced fracture is closing. One of the most crucial parameters in fracture treatment design is the fracture closure pressure (P_c). In general the following parameters are obtained from the BCA:

- Fracture Closure Pressure (P_c)
- Instantaneous Shut-In Pressure (ISIP) = Final injection pressure - Pressure drop due to friction
- ISIP Gradient = ISIP / Formation Depth

- Closure Gradient = Closure Pressure / Formation Depth
- Net Fracture Pressure (Δp_{net}) = ISIP - P_c
- Fluid efficiency = (Stored volume in the fracture) / (Total Volume Injected)
- Formation leak off characteristics and fluid leak loss coefficients

G-Function

One important method that minimizes ambiguity and provides useful in-situ stress and leak-off information is the G-function analysis. It is derived so that the "cumulative fluid leaked-off volume from the fracture after shut-in" is linearly proportional to the G-function. In other words, at a G-time =4, twice as much fluid has leaked-off aftr shut-in as at G-time=2.

The G-function is a dimensionless time function that relates shut-in time to total pumping time. This process uses derivative curves to identify leak-off mechanisms and fracture closure point through the characteristic shapes of the curves. The G-function plot features a pressure and semi log derivative of pressure vs. G-time curve. In many cases, the expected signature of the semi log curve is a straight line that passes through the origin, representing normal fluid leak-off behavior. Fracture closure point is identified at the point when the G-function semi-log derivative curve starts to deviate from its straight tangent line in a normal leak-off (most ideal) case – Tangent Method.

An illustrative plot is shown in fig. 100

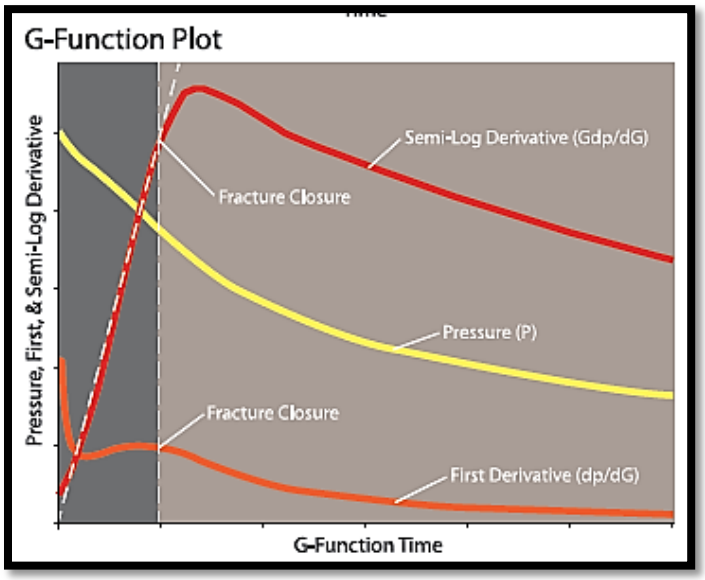

Figure 100 Typical G-function plot for normal fluid leak-off type

This technique was introduced by Kenneth G. Nolte in 1979, and has been widely used in the industry. G-function does not assume a single planar fracture and will show the effects of multiple fracture planes propagating against different closure stresses. One important assumption in G-function derivation is that the fluid pressure is constant during shut-in. Obviously, fluid pressure is not constant and decreases over time after shut-in. But during early shut-in period, it is approximately valid to assume that the fracture pressure is constant. The normal leak-off model is applied to the sole case of perfectly linear pressure decay on the P vs. G plot. However, deviation from this ideal behavior is generally expected. The other pressure fall-off scenarios are pressure dependent leak-off, fracture height extension and transverse storage, fracture tip extension. The G-function curves for each of these scenarios display a different signature; therefore, analysis and interpretation for each case are also handled differently.

The Log-Log Plot of Derivative

The log-log plot is a plot of the change in pressure with change in time after shut-in. This plot is extremely powerful in that it can be used to determine fracture closure, leak-off mechanism, and transient flow regimes, and after-closure transient flow regimes in the reservoir. This is also a common tool used to interpret well pressure transient test results. This plot features a pressure difference and its semi log derivative vs. change in time curve. It is common for the pressure difference and derivative curves to be parallel immediately before closure. It is also typical for the derivative curve to change from a positive slope to a negative slope when closure occurs.

The time used to calculate the derivative can be simple shut-in time (Δt) or specially calculated equivalent time t_{eq} called as Bourdet Derivative illustrated in fig.101

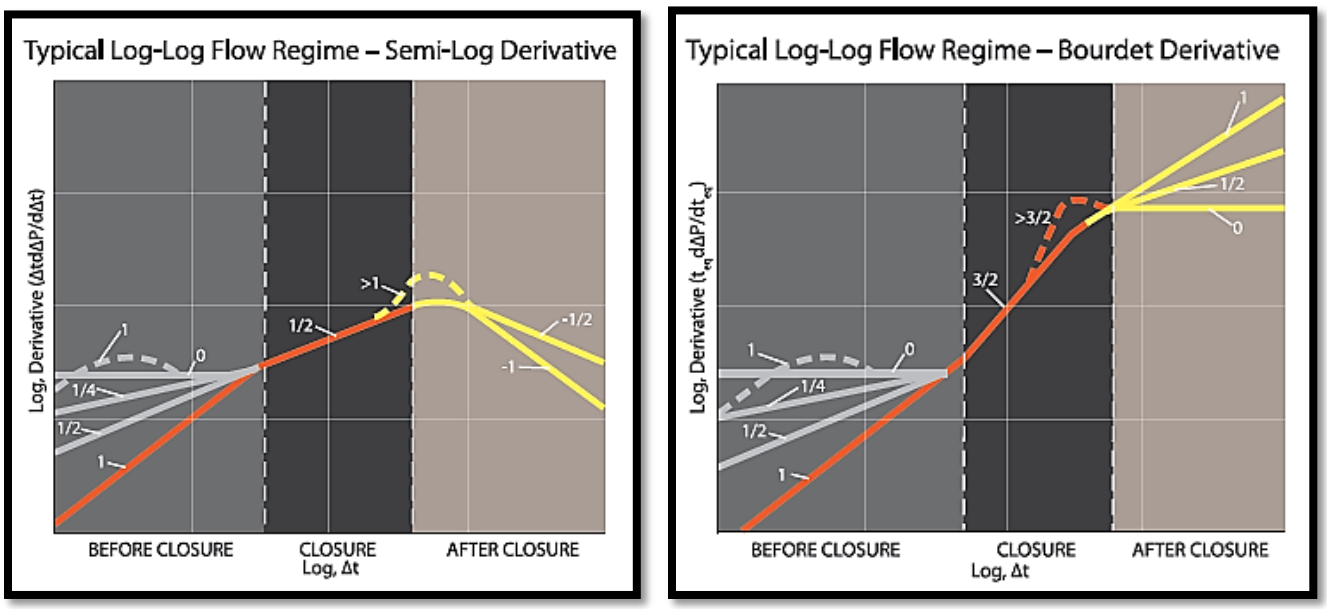

Figure 101 Log-log plot – Semi-Log Derivative and Bourdet Derivative

Table of flow regime and the characteristic slope to identify each regime can be summed in a concise table 21 as below(Barree et al., 2007):

Table 21 Flow regime with characteristic slopes to identify each regime

Flow Regime	**Derivative Function**		
	Delta time ($\Delta t\ d\Delta P/d\Delta t$)	Equivalent time[1] ($t_{eq}\ d\Delta P/d\ t_{eq}$)	
BEFORE CLOSURE			
Carter Leak-off[2] Early time	1	1	
Carter Leak-Off Late time	½	3/2	
Fracture Linear	½	½	

Fracture Bilinear	¼	¼	
Radial	0	0	
AFTER CLOSURE			
Fracture Linear	- ½	½	
Fracture Bilinear[3]	- ¾	¼	
Radial	-1	0	

1- **With Bourdet derivative**
2- **For low permeability reservoir**
3- **Bilinear flow regimes are not shown on type curves**

Because this plot lacks a distinct and clearly identifiable signature for closure, it is used only as a verification tool in this analysis. It is, on the other hand, a powerful tool in determining the transient flow regime. The slopes of the derivative curve are diagnostic of the flow regimes before and after fracture closure. For instance, a slope of 0.5 before closure indicates a period of fracture linear flow coupled with changing fracture or wellbore storage. A slope of 0.5 around the closure event indicates a period of formation linear flow. After closure, a slope of -1 indicates a fully developed pseudo-radial flow.

Table 22 Log-Log Graph Characteristic slopes

LOG – LOG GRAPH CHARACTERISTIC SLOPES					
	BEFORE CLOSURE		**AFTER CLOSURE**		
Log-Log Graph	**Bilinear**	**Linear**	**Bilinear**	**Linear**	**Pseudo radial**
Δp_{wf} vs. Δt Δp_{awf} vs. Δt_a	1/4	1/2	-	-	-
$\partial\Delta p_{wf}/\partial\Delta t$ vs. Δt $\partial\Delta p_{wfa}/\partial\Delta t$ vs. Δt_a	-3/4	-1/2	-7/4	-3/2	-2
$\Delta t\ \partial\Delta p_{wf}/\partial\Delta t$ vs. Δt $\Delta t_a\ \partial\Delta p_{wfa}/\partial\Delta t$ vs. Δt_a	1/4	1/2	-3/4	-1/2	-1
$\Delta t^2\ \partial\Delta p_{wf}/\partial\Delta t$ vs. Δt $\Delta t_a^2\ \partial\Delta p_{wfa}/\partial\Delta t$ vs. Δt_a	5/4	3/2	1/4	1/2	0

Square Root Time Analysis

The Primary P vs. sqrt (t) curve should form a straight line during fracture closure, as with the G-function plot. Barree, et al. emphasized that the indication of the closure is the inflection point on the P vs. sqrt (t) plot which can be found by plotting the first derivative of P vs. sqrt (t), $\frac{dP}{d(\sqrt{t})}$ and find the point of maximum amplitude of the derivative. The semi log derivative of the pressure curve is also shown on the sqrt (t) plot. This curve is

equivalent to the semi log derivative of the G-function. The closure pick falls at the departure from the straight line through the origin on the semi-log derivative of the P vs. sqrt (t) curve (Barree, Barree and Craig, 2009).

Other than validating the analysis and interpretation done by G-function plot and Log-Log plot, this analysis technique comes in use to identify leak-off mechanism associated with the pressure transient, which otherwise often go misinterpreted if other analysis method is used.

Few Other Methods to Identify Fracture Closure Pressure

- BHP vs. rate plot
- Square root of time vs. pressure plot
- Inclinometer tests

Type of Leak-offs – Please refer to (Barree et al., 2007)

D.1.4.(ii). After-Closure Analysis (ACA)

After-closure analysis is performed on the portion of the falloff data collected after the induced fracture has closed.
In general, the ACA is divided into two categories:

1. After-closure Diagnostic (Nolte) based on the work of K.G. Nolte.
2. After-closure Diagnostic (Soliman - Craig) based on the work of M.Y. Soliman and the work of D. Craig.

It is possible to obtain reasonable estimates of reservoir pressure and formation permeability from diagnostic analyses if the pressure falloff is recorded long enough to achieve radial flow. Brief introduction with associated equations for each flow regime for both types of ACA diagnostic is covered in "ACA subsection of Example 1 field data"

Table 23 highlights the similarities and difference between Nolte approach vs. Soliman & Craig approach (IHS, FEKETE, 2017)(Nolte et al., 1997; Soliman et al., 2005):

Table 23 Nolte vs. Soliman ACA method

SI No.	Nolte ACA Approach	Soliman & Craig ACA Approach
1	Based on work by Nolte. Later expanded by R.D.Barree	Based on work by M.Y.Soliman's solution for short tests. Later improvised by D.Craig
	Assumptions	
2	Based on solution of "constant pressure injection" followed by a fall-off	Based on "constant rate injection" and fall-off sequence
3	Assumes injection continues until fracture closure	Assumes injection stops at shut-in
	Technique	
4	Impulse test approach is considered here which assumes negligible injection period compared to shut-in period, assuming injection of fluid occurred instantaneously. Injected volume is assumed as the impulse volume	This technique considers both the injection (or production) period and the shut-in period.
	Nolte ACA Derivative	**Soliman & Craig Derivative**
5	Used to identify flow regimes: Impulse Linear (-1/2) , Radial (-1)	Used to identify: Impulse Bilinear(1/4), Linear (1/2), Radial (0)

6	Semi-log derivative against F_L (Nolte Linear time function) on log-log derivative plot	Impulse derivative plotted against $(t_p + \Delta t)$ on log – log derivative plot
7	This diagnostic may be used to help fine-tune the initial reservoir (Pi) estimate	This diagnostic may be used to help fine-tune the initial reservoir (Pi) estimate
		Soliman & Craig Bilinear Analysis
8	Not identifiable from Nolte ACA approach	If Bilinear flow is identified, fracture conductivity (k_f) can be estimated. It shows up as a straight line on a plot of pressure vs. $\frac{1}{(t_p+\Delta t)}^{\frac{3}{4}}$
9		The equation governing Bilinear flow is: $p_{fo} - p_i = \left(0.000135\frac{\pi}{2}\right)\frac{V_{inj}}{h}\,\mu^{0.75}\left(\frac{1}{\emptyset\, c_t k}\right)^{0.25}\frac{1}{\sqrt{k_f . w_f}}\left(\frac{1}{(t_p + \Delta t)}\right)^{0.75}$
	Nolte ACA Linear Analysis	**Soliman & Craig Linear Analysis**
10	Equation governing impulse linear flow is: $\Delta p_R = m_{lf} F_L\left(\frac{t}{t_c}\right)$ (100) $F_L\left(\frac{t}{t_c}\right)$ is the linear flow time function $F_{L1} = \frac{2}{\pi}\sin^{-1}\left(\frac{\sqrt{t_c}}{\sqrt{t}}\right)$ (101) m_{lf} is the corresponding slope on a Cartesian plot $m_{lf} = C_L\frac{\sqrt{(\pi\mu)}}{(k\emptyset c_t)}$ (102) ∀, t=shut-in time ; t_c = closure time ; C_L = leak-off or fluid-loss coefficient ; c_t = total compressibility	Equation governing is: $p_{fo} - p_i = (0.00424\frac{\sqrt{\pi}}{2})\frac{V_{inj}}{h}\left(\frac{\mu}{\emptyset c_t k\, L^2}\right)^{0.5}.\left(\frac{1}{t_p + \Delta t}\right)^{0.5}$
11	Impulse Linear flow shows up as straight line on a plot of pressure vs. Nolte linear time function (F_L)	It shows up as straight line on a plot of pressure vs. $\frac{1}{(t_p+\Delta t)}^{\frac{1}{2}}$
12	If linear flow is identified, fluid loss coefficients $C_T and\ C_R$ (Total and Reservoir) can be estimated.	If linear flow is identified, Fracture half-length "L" can be estimated
	Nolte ACA Radial Flow Analysis	**Soliman & Craig Radial Flow Analysis**

13	p* (extrapolated pressure which gives first value of initial reservoir pressure) and formation permeability can be estimated	p* (extrapolated pressure which gives first value of initial reservoir pressure) and formation permeability can be estimated
14	Equation governing radial flow are: $\Delta p(t) = m_{rf} \left\{F_L\left(\frac{t}{t_C}\right)\right\}^2$ $F_L\left(\frac{t}{t_c}\right)$ is the linear flow time function $F_{L1} = \frac{2}{\pi}\sin^{-1}(\frac{\sqrt{t_c}}{\sqrt{t}}$ (104) m_{rf} is the corresponding slope on the Cartesian plot given by: $m_{rf} = \frac{\pi}{16}\frac{V_i \mu}{kht_c}$	Equation governing radial flow is: $p_{fo} - p_i = \frac{(0.000014\frac{\pi}{2})V_{inj}\,\mu}{kh} \cdot \frac{1}{(t_p + \Delta t)}$
15	Radial flow portion of the data will have a straight line on a plot of P vs $\{F_L(\frac{t}{t_c})\}$^2	Radial flow portion of the data will have a straight line on a plot of P vs $\frac{1}{(t_p+\Delta t)}$

The key parameters as obtained by BCA and ACA using 'Standard' interpretation method practiced in industry can be summarized in Table 24:

Table 24 Parameters obtained from BCA and ACA using "standard method"

SI No.	Before Closure Analysis	After Closure Analysis
1	Shut in time	Loss Coefficient (C_R *and* C_T) – (Reservoir and Total fluid coefficients)
2	Fracture Closure Time, t_c	Extrapolated Pressure (p*) reflecting (Reservoir Pressure)
3	Fracture Closure Pressure , P_c	Permeability (k)
4	G function time	Fracture half-length (L)
5	Fluid Efficiency	Reservoir Boundaries / Geological features
6	Net Fracture Pressure ΔP_{net}	